OPTIMIZATION OF BIOETHANOL PRODUCTION, ENGINE PERFORMANCE AND EXHAUST EMISSIONS FROM *MANIHOT GLAZIOVII* AND SWEET SORGHUM IN A SPARK IGNITION ENGINE

ABDI HANRA SEBAYANG

FACULTY OF ENGINEERING
UNIVERSITY OF MALAYA
KUALA LUMPUR

2020

OPTIMIZATION OF BIOETHANOL PRODUCTION, ENGINE PERFORMANCE AND EXHAUST EMISSIONS FROM *MANIHOT GLAZIOVII* AND SWEET SORGHUM IN A SPARK IGNITION ENGINE

ABDI HANRA SEBAYANG

THESIS SUBMITTED IN FULFILMENT
OF THE REQUIREMENTS
FOR THE DEGREE OF DOCTOR OF PHILOSOPHY

FACULTY OF ENGINEERING
UNIVERSITY OF MALAYA
KUALA LUMPUR

2020

UNIVERSITI MALAYA

ORIGINAL LITERARY WORK DECLARATION

Name of Candidate : **Abdi Hanra Sebayang**

Registration/Matric No : **KHA140113**

Name of Degree : **Doctor of Philosophy (Ph.D)**

Title of Project/Research Report/Dissertation/Thesis ("This Work")

OPTIMIZATION OF BIOETHANOL PRODUCTION, ENGINE PERFORMANCE AND EXHAUST EMISSIONS FROM *MANIHOT GLAZIOVII* AND SWEET SORGHUM IN A SPARK IGNITION ENGINE

Field of Study : **Energy (Alternative Fuel)**

I do solemnly and sincerely declare that:

(1) I am the sole author/writer of the work;
(2) This work is original;
(3) Any use of any work in which copyright exists was done by way of fair dealings and any expert or extract from or reference to or reproduction of any copyright work has been disclosed expressly and sufficiently and the title of the work and tis authorship has been acknowledged in this work;
(4) I do not have any actual knowledge nor do I ought to reasonably to know that the making of this work constitutes an infringement of any copyright work;
(5) I hereby assign all and every rights in the copyright to this work to the University of Malaya (UM), who henceforth shall be the owner of the copyright in this work and that any reproduction or use in any form or by any means whatsoever is prohibited without the written consent of UM having been first had and obtained actual knowledge;
(6) I am fully aware that if in the course of making this work I have infringed any copyright whether internationally or otherwise, I may be subject to legal action or any other action as may be determined by UM.

Candidate's Signature Date: 4 August 2020

Subscribed and solemnly declared before,

Witness Signature Date: 5 August 2020

Name:

Designation

OPTIMIZATION OF BIOETHANOL PRODUCTION, ENGINE PERFORMANCE AND EXHAUST EMISSIONS FROM *MANIHOT GLAZIOVII* AND SWEET SORGHUM IN A SPARK IGNITION ENGINE

ABSTRACT

The ever-increasing fossil fuel consumption over the years is attributable to economic and population growth, which in turn, increases greenhouse gas emissions. Bioethanol is one of the promising solutions to address the depletion of fossil fuels as well as environmental problems. *Manihot glaziovii* tubers and sweet sorghum grains are inedible feedstocks that can be used for bioethanol production. The carbohydrate content (70%) of these biomasses makes them suitable as feedstocks for bioethanol production. In this study, enzymatic hydrolysis (liquefaction and saccharification) was used to obtain the reduction of sugars. The enzymes α-amylase from *Bacillus licheniformis* Type XII-A and amyloglucosidase from *Aspergillus niger* were used as the catalysts for liquefaction and saccharification. The reduced sugars were converted into ethanol during the fermentation process by the yeast *Saccharomyces cerevisiae*. Distillation was carried out to remove water from the bioethanols. Box-Behnken design was used to optimize the enzymatic hydrolysis and fermentation process parameters. The hydrolysis process parameters (substrate loading, α-amylase concentration, amyloglucosidase concentration, and stroke speed) were optimized to maximize the reduction sugar yield. The fermentation process parameters (yeast concentration, reaction temperature, and agitation speed) were optimized to maximize the bioethanol yield. The optimum reduced sugar yields were 196.15 and 170.26 g/L for *Manihot glaziovii* and sweet sorghum, respectively. The optimum yeast concentration, reaction temperature, and agitation speed were 1.18 g/L, 36.48°C and 217 rpm, respectively, for *Manihot glaziovii*, and the values were 1.29 g/L, 35.36°C and 188.97 rpm, respectively, for sweet sorghum. The corresponding bioethanol yields were 94.45 and 82.13 g/L for

Manihot glaziovii and sweet sorghum, respectively. The physicochemical properties of both the bioethanols fulfilled the specifications of the ASTM D4806 standard. Engine tests were carried out using a single-cylinder four-stroke spark ignition engine to determine the engine performance (engine torque, brake power, brake specific fuel consumption, brake thermal efficiency) and exhaust emissions (carbon monoxide, unburned hydrocarbons, and nitrogen oxides) of the *Manihot glaziovii* bioethanol-gasoline blends (ME5, ME10, ME15, and ME20) and sweet sorghum bioethanol-gasoline blends (SE5, SE10, SE15, and SE20). In general, the engine performance parameters were better and the exhaust emissions were lower for the bioethanol-gasoline blends compared with those for gasoline. For the ME20 and SE20 blends, the brake specific fuel consumption decreased while the brake thermal efficiency increased at an engine speed of 3200 rpm. The corrosive behavior of copper coupons immersed in the bioethanol-gasoline blends was also investigated in this study. The surface morphological changes of the copper coupons were analyzed using scanning electron microscopy. The rate of copper corrosion was faster for the ME20 and SE20 blends compared with that for gasoline. These blends also had the fastest rate of copper corrosion compared with the all blends tested in this study. Based on the results, it can be concluded that the *Manihot glaziovii* tubers and sweet sorghum grains have great potential as bioethanol feedstocks and the bioethanol-gasoline blends produced from these biomasses can be used in the spark ignition engine without modifications.

Keywords: *Manihot glaziovii*; sweet sorghum; bioethanol; engine performance; exhaust emissions.

PENGOPTIMUMAN PENGELUARAN BIOETANOL, PRESTASI ENJIN DAN PELEPASAN EKZOS DARIPADA *MANIHOT GLAZIOVII* DAN SORGUM MANIS DALAM ENJIN *SPARK IGNITION*

ABSTRAK

Penggunaan bahan api fosil yang semakin meningkat adalah disebabkan oleh pertumbuhan ekonomi dan penduduk yang semakin pesat dan ini menyumbang kepada pelepasan gas rumah hijau. Bioetanol merupakan salah satu penyelesaian yang berpotensi untuk menangani masalah kekurangan bahan api fosil dan masalah alam sekitar. Tuber *Manihot glaziovii* dan bijirin sorgum manis ialah stok suapan yang tidak boleh dimakan dan boleh digunakan untuk pembuatan bioetanol. Kedua-dua bahan mentah ini berpotensi sebagai stok suapan pembuatan bioetanol disebabkan kandungan karbohidrat yang tinggi (70%). Dalam kajian ini, proses hidrolisis enzim (pencecairan dan pensakaridaan) telah digunakan untuk menghasilkan gula penurunan dan enzim α-amilase dari *Bacillus licheniformis* Jenis XII-A dan enzim amiloglukosidase dari *Aspergillus niger* telah digunakan sebagai pemangkin pencecairan dan pensakaridaan. Proses penapaian oleh yis *Saccharomyces cerevisiae* telah digunakan untuk menukar gula penurunan kepada etanol. Proses penyulingan telah dilakukan untuk menyingkirkan air daripada bioetanol yang terhasil. Kaedah reka bentuk eksperimen Box-Behnken telah digunakan untuk mengoptimumkan parameter proses hidrolisis enzim (iaitu pemuatan substrat, kepekatan α-amilase, kepekatan amiloglukosidase, dan kelajuan strok) untuk memaksimumkan keluaran gula penurunan. Kaedah ini juga digunakan untuk mengoptimumkan parameter proses penapaian (iaitu kepekatan yis, suhu tindak balas, dan kelajuan agitasi) untuk memaksimumkan keluaran bioetanol. Keluaran gula penurunan untuk *Manihot glaziovii* dan sorgum manis pada keadaan optimum masing-masing ialah 196.15 and 170.26 g/L. Sementara itu, kepekatan yis, suhu tindak balas dan kelajuan agitasi optimum masing-masing ialah 1.18 g/L, 36.48°C,

dan 217 rpm, untuk *Manihot glaziovii*, dan 1.29 g/L, 35.36°C dan 188.97 rpm untuk sorgum manis. Keluaran etanol yang diperolehi daripada proses penapaian dalam keadaan optimum untuk *Manihot glaziovii* dan sorgum manis masing-masing ialah 94.45 dan 82.13 g/L. Sifat-sifat fizikokimia bioetanol yang telah dihasilkan didapati mematuhi spesifikasi piawaian ASTM D4806. Ujian enjin telah dijalankan denagan menggunakan enjin pencucuhan bunga api silinder tunggal empat lejang untuk menentukan prestasi enjin (kilas enjin, kuasa brek, penggunaan bahan api tentu brek, dan kecekapan haba brek) dan pelepasan gas ekzos (karbon monoksida, hidrokarbon tak terbakar, dan nitrogen oksida) apabila campuran bahan api bioetanol *Manihot glaziovii*-petrol (ME5, ME10, ME15, dan ME20) dan bioetanol sorgum manis-petrol (SE5, SE10, SE15, dan SE20) digunakan. Secara keseluruhannya, terdapat peningkatan dari segi prestasi enjin manakala pelepasan gas ekzos menunjukkan pengurangan. Untuk campuran bahan api ME20 dan SE20, penggunaan bahan api tentu brek berkurang manakala kecekapan haba brek meningkat pada kelajuan enjin 3200 rpm. Di samping itu, kelakuan kakisan spesimen kuprum yang direndam di dalam campuran bahan api bioetanol-petrol telah disiasat. Perubahan morfologi permukaan spesimen kuprum tersebut diperhatikan dengan menggunakan mikroskop elektron pengimbas. Kadar kakisan kuprum didapati lebih cepat untuk campuran bahan api ME20 and SE20 berbanding dengan kadar kakisan kuprum untuk petrol. Kedua-dua campuran ini juga mempunyai kadar kakisan yang paling cepat berbanding dengan campuran lain. Berdasarkan keputusan kajian, dapat disimpulkan bahawa *Manihot glaziovii* dan sorgum manis mempunyai potensi yang tinggi sebagai stok suapan bioetanol dan campuran bahan api bioetanol-petrol yang terhasil daripada bahan mentah ini boleh digunakan dalam enjin pencucuhan bunga api tanpa sebarang pengubahsuaian.

Kata kunci: *Manihot glaziovii*; sorgum manis; bioetanol; prestasi enjin; pelepasan gas ekzos.

ACKNOWLEDGEMENTS

First and foremost, all praise be to Allah S.W.T., the Almighty, for giving me the strength, patience, and perseverance to complete this thesis. I wish to express my deepest appreciation to my supervisors, Prof. Dr. Masjuki Haji Hassan and Dr. Ong Hwai Chyuan, for their constructive criticisms, patience, guidance, and support during the course of my study. All of these have contributed significantly towards the completion of this thesis. I also wish to express my gratitude to University of Malaya, Malaysia, for funding this research under the PPP research fund and High Impact Research (HIR) grant. I wish to express my warm appreciation to the technical and administration staff in the Dean Office and Department of Mechanical Engineering, Faculty of Engineering, for their kind assistance.

My sincere appreciation goes to Dr. Arridina Susan Silitonga, and friends (especially Surya Dharma, Fitranto Kusumo, and Jassinnee Milano) for their continuous support and encouragement throughout this research. It would have been impossible for me to finish this work without their moral support.

Lastly, I am eternally grateful to my family for their endless prayers and support that have spurred me to complete this research. May Allah S.W.T. bless of all you.

TABLE OF CONTENTS

LIST OF FIGURES

LIST OF TABLES

LIST OF SYMBOLS and ABBREVIATIONS

Symbol	Description	Unit
BSFC	Brake specific fuel consumption	g/kWh
BTE	Brake thermal efficiency	%
BP	Brake power	kW
CO	Carbon monoxide	%(v/v)
HC	Unburned hydrocarbons	ppm
NO_x	Nitrogen oxides	ppm
N	Engine speed	rpm
LHV	Lower heating value	MJ/kg
—	Reaction time	h
—	Reaction temperature	°C
V	Volume	L
$\dot{m}$	Mass flow rate	kg/s
	Viscosity	mm^2/s
	Density	kg/m^3
	Constant pi	
TAN	Total acid number	mg KOH/g
, ET	Engine torque	Nm
—	Yeast concentration	g/L
—	Ethanol concentration	g/L
—	Substrate loading	%(w/v)
—	α-amylase	unit/g
—	Amyloglucosidase	unit/mL
—	Agitation speed	rpm
—	Strokes speed	strokes/min
—	Reducing sugar concentration	g/L
CR	Corrosion rate	mm/year
A	Area	cm^2
t	Time	h
w	Weight	g
—	Wavelength	cm^{-1}
ASTM	American Society for Testing and Materials	
ANN	Artificial neural network	
AFEX	Ammonia fiber explosion	
BEA	Bosch emissions analysis	
BBD	Box-Behnken design	
Ca	Calcium	
$CaCl_2$	Calcium chloride	
CBP	Consolidated bioprocessing	
DNS	Dinitrosalicylic acid	
E5	5% ethanol + 95% gasoline	
E10	10% ethanol + 90% gasoline	
E15	15% ethanol + 85% gasoline	

E20	20% ethanol + 80% gasoline
EDX	Energy-dispersive X-ray
FTIR	Fourier transform infrared
GA	Genetic algorithm
GDP	Gross domestic product
GHG	Greenhouse gas
H_2SO_4	Sulfuric acid
H_3PO_4	Phosphoric acid
HBA	Hydroxyl benzaldehyde
HCN	Hydrogen cyanide
NH_4Cl	Ammonium chloride
HNO_3	Nitric acid
ISO	International Organization for Standardization
IgT	Ignition timing
$K_2Cr_2O_7$	Potassium dichromate
LHW	Liquid hot water
MAPE	Mean absolute percentage error
ME5	5% *Manihot glaziovii* bioethanol + 95% gasoline
ME10	10% *Manihot glaziovii* bioethanol + 90% gasoline
ME15	15% *Manihot glaziovii* bioethanol + 85% gasoline
ME20	20% *Manihot glaziovii* bioethanol + 80% gasoline
MON	Motor octane number
MSE	Mean square error
MWP	Microwave process
Na	Sodium
Na_2SO_4	Sodium sulfate or thenardite
$NaHCO_3$	Sodium bicarbonate
NaOH	Sodium hydroxide
OECD	Organisation for Economic Co-operation and Development
RMSE	Root mean square error
RON	Research octane number
SE5	5% sweet sorghum bioethanol + 95% gasoline
SE10	10% sweet sorghum bioethanol + 90% gasoline
SE15	15% sweet sorghum bioethanol + 85% gasoline
SE20	20% sweet sorghum bioethanol + 80% gasoline
SEM	Scanning electron microscope
SHF	Separate hydrolysis and fermentation
SPORL	Sulfite process to overcome recalcitrance of lignocellulose
SSF	Simultaneous saccharification and fermentation
SSCF	Simultaneous saccharification and co-fermentation
STEX	Steam explosion
WO	Wet oxidation

CHAPTER 1: INTRODUCTION

1.1. Background

Ever since the Industrial Revolution (the period in which hand production methods were replaced with the use of machines for chemical and manufacturing processes), fossil fuel-derived energy consumption has become more widespread, and recently natural gas and nuclear power have been used to supplement the ever-increasing energy demands. Driven by global economic growth, especially in developing countries, the global energy consumption is expected to rise by 70% from 2018 to 2050, as reported by the United States Energy Information Administration (EIA, 2019b). Also, reported by British Petroleum (BP, 2019), energy consumption grew at rate of 2.9% in 2018, which is almost doubled from its 10-year average of 1.5% per year, and is the fastest since 2010. Non-members of the Organization of Economic Cooperation and Development (OECD) were projected to have an increase in energy demand in transportation sector of 77% from 2018 to 2050. In fact, transportation energy consumption in non-OECD countries has been greater than that of the OECD countries since 2017, and by 2050 non-OECD countries are estimated to account for almost 65% of the world‘s transportation-related energy use (EIA, 2019b).

In determining oil prices, oil demand is one of the important factors, along with socioeconomics and political factors (Chen et al., 2016). **Figure 1.1** shows the average annual crude oil prices of the members of the Organization of the Petroleum Exporting Countries (OPEC) (measured in US$/barrel) versus the global oil consumption (measured in barrels/day). There is a notable drop from US$ 109.45/barrel in 2012 to US$ 65.09/barrel in 2020, and the extreme jumps or drops in the crude oil price here are closely affected by the on-going sociopolitical occurrences. In 2017, the decrease in crude oil price is due to the high crude oil production while the global oil demands were

lowered. This resulted in the decrease of oil price in 2017 (US$ 52.51/barrel). Further, as OPEC agreed to reduce the production of crude oil, this resulted to the reduced oil supplies, which leads to a greater oil price.

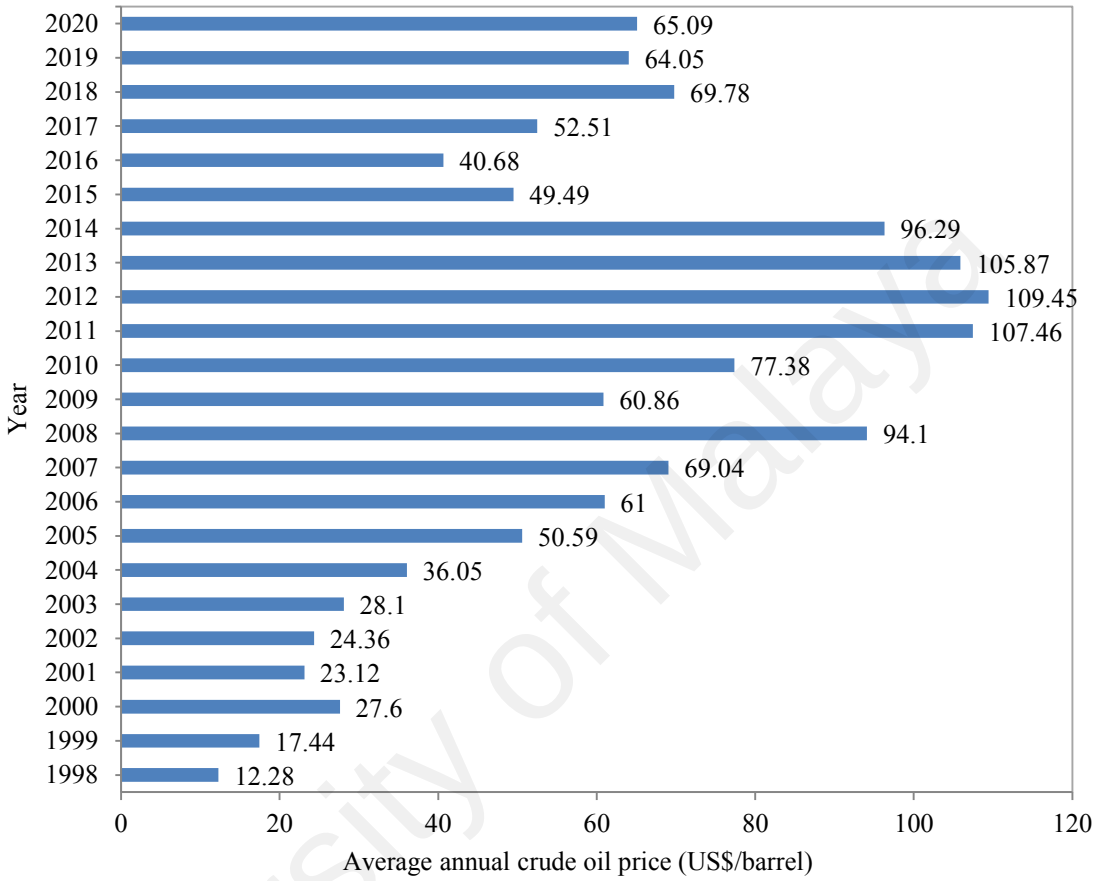

Figure 1.1: Average annual crude oil prices of the members of OPEC from 1998 to 2020 (in US$ per barrel) (Statista, 2020b)

Besides the unstable oil prices, the fossil fuel reserves are another concerning issue. Due to the non-sustainable and non-renewable nature, there is a possibility of fossil fuel depletion, which will create a massive problem in energy security. The fossil fuel depletion has been predicted to get worsen in the next 50 to 100 years, under assumption of constant productivity and fuel substitution. Through analysis of fuel price and consumption history, the price of fossil fuel is fluctuation which is due to the market have gradually shifted toward natural gas. Another concern is that, the fossil fuel consumption rate counterbalances the fossil fuel reserves over the last few decades. This

disrupts the stability of the worldwide fossil fuel reserves, as well as the stability of oil prices. The effect is inevitable, since in the purpose of social, economic development, health and welfare, people‘s energy demand must be satisfied in the long term, of which keeps increasing annually. Because of this reason, there is a need for development of alternative fuels that are sustainable which is the feasible solution to fulfill the energy demand sustainably. The use of alternative fuels also helps in alleviating greenhouse gas (GHG) emissions, which have been majorly produced from the emission of fossil fuel combustion. The development of alternative fuels is not problem-free, as different challenges appear with it. The availability and sustainability of the raw material must be ensured, the technological means must be met, the suitable knowledge must be improved, public awareness of the benefits and application of alternative fuels must be widely promoted. Also, carbon footprint must be measured regularly, in order to prepare the suitable climate change mitigation plan with a more sustainable development. The carbon footprint is a measure of the exclusive total amount of carbon dioxide emissions that are directly and indirectly caused by an activity or is accumulated over the life stages of a product (2013). These carbon footprints have become the ‗currency‘ of debate in a climate-constrained world. The overall carbon footprint due to the production of global biofuels was estimated in the present study to be 0.248 billion (bn) gha for 2010; rising to 0.449 bn gha by 2019 (Hammond & Seth, 2013). Biofuels may be carbon-neutral because the plants that are used to make biofuels (such as corn and sugarcane for bioethanol) absorb CO_2 as they grow and may offset the CO_2 emissions when biofuels are produced and burned (EIA, 2019a). For biofuels to gain more carbon credit values, prices of such products should remain as low as possible (Eshton & Katima, 2015). Though biofuels may not be able to completely mitigate GHG, they are good alternatives to fossil fuels since they may reduce GHG emissions while guaranteeing the energy security of the country (Crutzen et al., 2007). Though they may

ensure energy security while minimizing fossil fuel imports, bioenergy policy should discourage the production of bioenergy crops in land suitable for the production of food crops since this may interfere with food security (Cerri et al., 2011). This is very important in informing the government, policymakers, and bioenergy stakeholders on the type of biofuel to be given priority when a decision is to be made based on their carbon credit potential.

Carbon footprints, or the amount of greenhouse gas emissions linked to particular activities, are associated with climate change and its impacts. Globally, calls have been intensified to reduce the carbon footprint of energy use, including the use of alternative fuels. Besides CO_2-based fuels, biofuel is another alternative that has been extensively investigated, and vehicles running on biofuel reduce fossil carbon emissions. Increasing feedstock scarcity (e.g. due to deforestation) coupled with the negative socio-economic and environmental outcomes of inefficient production and consumption technologies (Iiyama et al., 2014) make it imperative to identify alternative energy solutions that benefit people without harming the environment.

The type of feedstock cultivated for ethanol production is crucial to define the level of the environmental impact from the agricultural phase. Among the tested crops, sugarcane and corn were the most sustainable feedstocks for ethanol production, while sugar beet presented the higher CO_2 emissions (Machado et al., 2017). It was assigned, in part, due the amount of soil carbon added by residue plants and the mineralization rate of each crop (Muñoz et al., 2014). In a temporal scale, was observed that the carbon removal from soil is more intensive in the first five years of cultivation. After that, the CO_2 emission tends to reduce over time. Considering the high demand for ethanol (currently and in the future), the differences in the CO_2 emission among the tested crops may result in the reduction of large amounts of carbon into the atmosphere depending of the crop type cultivated (Machado et al., 2017; Wu et al., 2018). Alternative fuel can

mitigate the climate change by discovering potential challenges and the feasibilities to tackle environmental and climate change issues.

Fossil fuel use in industry and transportation sector is responsible for the great GHG emissions production. There are numerous negative impacts as the results of combustion process in a large scale, where greenhouse gas (GHG) emissions are the main contribution to global warming. Release of harmful gases to the environment have been increasing over the years, namely carbon dioxide (CO_2), methane (CH_4), sulfur dioxide (SO_2), nitrogen oxides (NO_x), and fluorine-based gases (perfluorocarbons, hydrofluorocarbons, sulfur hexafluoride). When those gases are concentrated in the atmosphere, it hinders the sun radiation and traps it on the earth‘s surface, thus rises the global temperature or global warming. According to United States Energy Information Administration (EIA, 2019b), it is predicted that the global CO_2 emissions alone is going to rise from 32.3 billion metric tons in 2012 to 35.6 billion metric tons in 2020. It is further expected that the number will go higher in 2040 to 43.2 billion metric tons. In other words, there will be an increase up to 34% over a period of 28 years. Acid rain is another side-effect of the increase in GHG emission, in which emissions and pollutant gases such as sulfur dioxide (SO_2) and NO_x contribute to the acid rain formation (Grennfelt et al., 2020). Acid rain is formed through the reaction between NO_x and SO_2 emissions with water and oxygen in the clouds, and this produces nitric acid (HNO_3) and sulfuric acid (H_2SO_4) respectively, both of them cause damage to the building structures (Bergin et al., 2005). The exhaust gases released by power stations as well as the passenger engine vehicles are the main sources of these sulfur gases emission. There is a scientific consensus that climate change is occurring, which besides the rise in the earth‘s surface temperature (global warming), there is an increased evaporation in the air, and changes in rainfall and air pressure patterns, all of which affect the world‘s climate. When ethanol is involved as alternative fuel, there is an offset of CO_2 as it is

captured back by the crops that are cultivated as the feedstock in bioethanol production. By this, GHG emissions can be lowered as high as 34% when using dried milled corn-based feedstock, and can reach higher up to 108% when cellulosic feedstock is incorporated (Demirbas, 2008). Because of that, many are in the path to develop bioethanol as fuel substitute, as it is closely relevant to industrial and transportation sectors. It carries great impact to the environment following the sustainable principle in reducing GHG emissions. As a gasoline substitute or additive, bioethanol can be possible produced from household wastes, straw and woods, which makes it economically attractive. Despite, the adverse effect the gasoline-ethanol blend of 90:10 blending ratio would result to a more volatile fuel than gasoline (which can contribute to the ozone issue), there is limited information on the relationship between ethanol content and fuel volatility and pure ethanol (100% ethanol) is less volatile than gasoline (Sadeghinezhad et al., 2014a).

One distinct characteristic of bioethanol, as one attractive alternative fuel, is the blends of 5-25% ethanol in gasoline (E5 to E25) does not require engine modification or alternation (Ruan et al., 2019). This is due to bioethanol addition to gasoline leads to leaner operation and improves engine performance. (Zhai et al., 2011). (Tibaquirá et al., 2018). In addition, heat of evaporation of ethanol is about 3 times higher than that of gasoline, cold start would be difficult. Also ethanol has high octane number of about 107, the advance ignition timing shall be considered. Therefore, It was stated that the blended ethanol into gasoline shall not be over 25% (E25) considered without engine modification.

Ethanol is a hydrocarbon compound consisting of hydroxyl bonds (OH) with two carbon atoms (C). The chemical formula of ethanol is C_2H_5OH. In general, ethanol (ethyl alcohol) is produced from plant materials. The formation of ethanol is due to microbial activity in converting the simple sugars into ethanol, which process is called

fermentation (Brownstein, 2014). The development of bioethanol production is orbited around the utilization of various types of feedstock, as well as the technology improvement. This development starts from the traditional conversion of sugar-bearing crops and feedstock (i.e. corn, cassava, sugarcane, and agricultural biomass) through fermentation to the conversion system with a high-complexity, multi-stage bioethanol production (Sarkar et al., 2012).

According to Balat at al. (2008), there are 3 classifications of feedstock used for bioethanol production: (1) starchy materials, (2) lignocellulosic materials, and (3) sucrose-containing feedstocks. Bioethanol is regarded environmentally friendly due to the renewable nature of the resource. In comparison with gasoline combustion, bioethanol produces a cleaner emissions (Guido et al., 2013; Masum et al., 2013). It is considered as one feasible energy source that is sustainable in terms of socio-economic and environmental aspects (Ghazikhani et al., 2013; Manzetti & Andersen, 2015).

Bioethanol is not only a promising substitute for gasoline, but it can also be blended with gasoline to produce gasohol. Compared with conventional gasoline, bioethanol has greater resistivity to engine knocking from its high octane number. Also, it carries higher heat of vaporization, flame speed and broader flammability limits (Hansdah et al., 2013; Hassan & Kalam, 2013). As the result, bioethanol as fuel would allow higher compression ratio with leaner combustions. On this premise, ethanol is superior to gasoline for spark ignition engines.

1.2. Problem statement

Owing to the depletion of fossil fuel reserves, it is important to develop safe and reliable alternative fuels from renewable and sustainable sources, and the fuel production process should be efficient and cost-effective. Currently, first-generation feedstocks such as corn, sweet potatoes, cassava, sago, and sugarcane are typically used for bioethanol production. Nevertheless, the use of edible feedstock and converting

these feedstocks to bioethanol is not sustainable in the long term because these feedstocks are primarily for human and animal consumption. The main disadvantage of first-generation feedstocks is that these raw materials are the staple foods in some countries and using these feedstocks for bioethanol production will drive the food prices up.

Second-generation feedstocks are the feasible substitutes for edible feedstocks because these feedstocks does not compete with food and typically possess good quality source of carbohydrates to yield high amount of sugar for bioethanol production. *Manihot glaziovii* tubers contain more than 80% of starch (dry weight basis) that can be hydrolyzed for fermentation (Moshi et al., 2014). Meanwhile, the sweet sorghum plant (Sorghum bicolor L.) is more resistant to temperature change and droughts as it requires less water (Almodares & Hadi, 2009; Davila-Gomez et al., 2011). The *Manihot glaziovii* and sweet sorghum are attractive because these feedstocks are inexpensive and a sustainable means for bioethanol production. However, due to the uncommonness of these materials in second generation bioethanol production, the use of both feedstocks poses a significant challenge, since it requires a thorough investigations of the capability and the quality of feedstock (sugar content and ethanol yield) in bioethanol production. To date there is no significant attention given to these materials in bioethanol production.

Besides, the material itself, with mathematical approach used to interactive the statistical analysis on conversion of bioethanol is equally important. The production without optimization will consume more time and produce low sugar reducing (hydrolysis) and low ethanol yield (fermentation). Therefore, optimization should be implemented to tackle these issues in order to produce high quality bioethanol with shorter time and lower energy consumption. In this study, effective pre-treatment will improve the hydrolysis and fermentation of carbohydrates present in the feedstock,

which will boost the bioethanol yield as well as minimize the presence of inhibitors during the fermentation process. This can be achieved by optimizing the parameters of the enzymatic hydrolysis and fermentation processes. Optimization of parameters such as reagents, enzymes, yeast concentration, and temperature can be achieved by developing an artificial neural network (ANN) model.

Relating to the energy consumption, economic evaluation of bioethanol production from *Manihot glaziovii* and sweet sorghum need to be investigated. The approach is only meaningful when full, industrial scale is considered, where operating cost, industrial equipment requirement, productivity and feasibility can be determined and concluded for a realistic scenario. Moreover, the evaluating the economic feasibility of bioethanol production from non-edible sources would result to a more substantial outcome, especially when the outcome is more favorable than that of bioethanol production from edible sources. The energy analysis of bioethanol production from non-edible sources will further confirm the sustainability in the long term, aside from the economical values.

In addition, bioethanol is claimed to be able to replace gasoline in future due to the higher octane number, broader flammability limit, higher flame speed and higher heat of vaporization. However, according to the physicochemical properties of bioethanol, bioethanol carries lower LHV (21.2 MJ/L) than that of gasoline (30-33 MJ/L), and this results to a greater amount of bioethanol needed to obtain the same energy output as gasoline (Ruan et al., 2019). Researchers found that bioethanol–gasoline fuel blends improve the engine performance and reduce exhaust emissions without the need for major design modifications in spark-ignition engines. However, there are no studies on the performance and exhaust emissions of a spark-ignition engine with *Manihot glaziovii* and sweet sorghum bioethanol blends at different blending ratio.

In this study, therefore, *Manihot glaziovii* and sweet sorghum bioethanol is developed to investigate and identify the suitable bioethanol-gasoline blends that, which will be further analyzed for their performance in a spark-ignition engine.

Besides, researchers found that corrosion issue tends to occur on bioethanol and bioethanol with gasoline fuels. The compatibility issues of the bioethanol with certain materials as bioethanol are inherently instable and highly corrosive in nature which is not thoroughly investigated. Researcher also found that blending bioethanol and gasoline will lead to corrosion in the engine components and fuel storage. In this study, the effect of *Manihot glaziovii* and sweet sorghum bioethanol-gasoline blends on the corrosive characteristic of *Manihot glaziovii* and sweet sorghum bioethanol are investigated. Copper was immersed in different *Manihot glaziovii* and sweet sorghum bioethanol–gasoline concentrations with time of immersion up to 3 months to observe their corrosion rate with degradation of bioethanol. Copper were selected for this study due to following reason, copper is a construction material that commonly used for gasoline engine such as fuel lines and fuel pump. This material is a common metallic material that has contact with bioethanol which is why this study need to be performed to observe the rate of corrosion.

1.3. Objectives

The following sub-objectives were set in order to achieve the main objective of this study:

1. To study the reducing glucose and bioethanol production from second-generation feedstocks *Manihot glaziovii* tubers and sweet sorghum grains.
2. To optimize the parameters of the enzymatic hydrolysis and fermentation processes using ANN models. Then, calculate energy consumption of the bioethanol production parameters optimum from *Manihot glaziovii* and sweet sorghum

3. To analyze the physicochemical properties of *Manihot glaziovii* and sweet sorghum bioethanols and its blends.
4. To investigate the effect of *Manihot glaziovii* and sweet sorghum bioethanol-gasoline blends on the engine performance and exhaust emission characteristics of a single-cylinder four-stroke spark ignition engine.
5. To investigate the effect of bioethanol-gasoline blends (ME5-ME20 and SE5-SE20) at room temperature on the corrosion of copper coupons by static immersion tests.

1.4. Significant contributions of the study

The main contribution of this study is the optimization of the bioethanol production process parameters in order to maximize the yield bioethanols produced from second-generation feedstocks (*Manihot glaziovii* tubers and sweet sorghum grains) by using ANN models and investigating the physicochemical properties, engine performance, and exhaust emissions of a spark ignition engine fueled with these bioethanol-gasoline blends. This study provides insight on the bioethanol production, energy consumption, engine performance, and exhaust emissions of a single-cylinder four-stroke spark ignition engine fueled with *Manihot glaziovii* and sweet sorghum bioethanol-gasoline blends. In this study, alternative feedstocks are explored to produce bioethanol fuels whose properties will improve the engine performance and exhaust emission characteristics. Although only two second-generation feedstocks are considered, the methodology adopted in this study can be used to optimize the bioethanol production process parameters for other types of feedstocks, with only minor modifications to the ANN models.

The contributions of this study are summarized as follows:

1. Explore the potential of *Manihot glaziovii* and sweet sorghum feedstocks as nonedible feedstock for bioethanol production.

2. Propose a method to produce reducing sugars and bioethanols from the *Manihot glaziovii* and sweet sorghum feedstocks, and analyze the physicochemical properties of the *Manihot glaziovii* and sweet sorghum bioethanols according to the ASTM D4806 standard.
3. The production of *Manihot glaziovii* and sweet sorghum bioethanols by enzymatic hydrolysis followed by fermentation and perform comparative analysis. The novelty of this study lies in the optimization of the process parameters for bioethanol production and calculate energy consumption from the process parameters. It is aimed to investigate the energy consumption, duration of processing and obtained bioethanol yield can be used in industrial feasibility
4. The utilization of *Manihot glaziovii* and sweet sorghum nonedible feedstock can provide solutions to reduce exposure to the vulnerability of supply and price volatility of edible feedstock. This approach also creates the possibility of innovations development in the production and processing industry which would contribute to the society economic activity.
5. Production of bioethanol technology from *Manihot glaziovii* and sweet sorghum nonedible feedstock as a local technology can create linkages between Research & Development in universities and industry players, which contributes to the increase the labours skills, improvement training of experts and expansion of job opportunities.

The results obtained in this study can serve as a reference for other researchers in this field, with emphasis on bioethanol production, optimization of enzymatic hydrolysis and fermentation process parameters using an artificial intelligence tool, and characterization of the engine performance and exhaust emissions of the bioethanol-gasoline blends produced from non-edible feedstocks. The outcomes of this study have been published recently in many international journals and conference proceedings.

1.5. Organization of the thesis

This thesis consists of five chapters and six appendixes. The scope of each chapter is briefly described as follows:

Chapter 1 : This chapter presents a brief background on the concept of fuels and the current global scenario regarding fuel production and consumption. In addition, this chapter presents a general review on biofuels, specifically the production of bioethanols from second-generation feedstocks.

Chapter 2 : This chapter is focused on general review of biofuels, with emphasis on the production of bioethanols from second-generation feedstocks. A review on the state-of-the-art production of bioethanol and the different processes involved are also presented. The literature survey includes the technologies, production methods, pre-treatment techniques, energy consumption, engine performance, physicochemical properties of the produced bioethanol, and exhaust gases characterization. The corrosion behavior of metals immersed in bioethanol-gasoline blends is also covered in this chapter.

Chapter 3 : The optimization of bioethanol production using mathematical models is presented in this chapter, along with the procedure used to validate the models. Besides, energy consumption has been calculated to assess the energy analysis in bioethanol production. The procedure used to evaluate the physicochemical properties, engine performance, and exhaust emissions of the *Manihot glaziovii* and sweet sorghum bioethanol-gasoline blends is also described in detail. The procedure used to assess the effect of the corrosion rate of copper immersed in the *Manihot glaziovii* and sweet sorghum bioethanol-gasoline blends such as total acid number, density, viscosity, and color changes were evaluated.

Chapter 4 : This chapter presents the key findings of this study, including the optimum enzymatic hydrolysis and fermentation process parameters, optimum *Manihot glaziovii* and sweet sorghum bioethanol yields, energy consumption from optimum parameters, physicochemical properties, engine performance (brake specific fuel consumption (BSFC), engine torque (ET), brake thermal efficiency (BTE), brake power (BP), and air-fuel ratio), and exhaust emissions (HC, NO_x, CO) of the *Manihot glaziovii* and sweet sorghum bioethanol-gasoline blends. The results of effect of metals on degradation of fuel properties in static immersion tests such as total acid number, density, viscosity, and color changes also presented and discussed. The results obtained in this study are also compared with those of other researchers.

Chapter 5 : The conclusions deduced from the findings and observations in this study are presented in this chapter, followed by the recommendations for future work.

Appendixes: Sample calculations of engine performance parameters, corrosion rate, % Uncertainty and Air-fuel ratio are provided in Appendix A, B, C and D, respectively. The standard operating procedures for exhaust emission, and engine performance tests are presented in Appendix E. Photographs of the bioethanol production process, instruments and equipment used for the engine tests, and the instruments for characterization of the reducing sugars and bioethanols are provided in Appendixes F, G, and H, respectively.

CHAPTER 2: LITERATURE REVIEW

2.1. Introduction

The rapid development of technology along with the escalating economic and population growth increases energy demands in all sectors. Fuel plays a vital role in our daily lives as source of power for industrial processes as well as an export commodity since it is a source of national revenue. The primary sources of energy used today are fossil fuels such as petroleum, natural gas, and coal, which are non-renewable and non-sustainable. Thus, fossil fuel reserves will continue to decline in line with the ever-increasing energy demands.

At present, fossil fuels provide most of the world‘s energy demand. Finished petroleum products such as motor gasoline, diesel, and jet fuel have been consumed massively, especially in the transportation sector. Globally, the transportation industry consumes the liquid fuel consumption and contributed to the increment of the fuel consumption. As reported by British Petroleum (BP, 2019), 1.4 million barrels of oil per day (b/d) are consumed globally, with China and United States as the top consumers at 680,000 and 500,000 b/d respectively. Due to this, oil production has significantly inclined by 2.2 million b/d, of which United States is the biggest net producer. Besides, oil production by Saudi Arabia and Canada have cover the fuel production decline by Iran and Venezuela. According to the United States Energy Information Administration (EIA, 2019b), the demand for liquid fuels up to 50% in OECD and non-OECD countries originated from the transportation sector. The growth, however, is mainly developed in the non-OECD countries, with the consumption increase is predicted from 56 quadrillion Btu in 2018 to 85 quadrillion Btu in 2050.

As the world population continues to grow and the amount of fossil fuels becomes more limited, there is a need to explore alternative sources of energy such as biofuels as

well as solar, wind, and geothermal energy. In addition, there is growing concern on improving energy security, mitigating the effects of fossil fuel combustion on the environment, and stabilizing fuel prices in the long term. With growth rate at an annual average rate of 3%, this indicates an acceleration in the utilization of renewable energy technologies (EIA, 2019b). Further, according to British Petroleum (BP, 2019), there was an increase of 9.7% in the production of biofuel globally in 2018. Despite being lower than the 10-year average of 11.4%, the recent growth is the fastest within 3-year period (**Figure 2.1**). In 2018, the growth of biofuel was accounted by Brazil and Indonesia with 3.1 and 2.2 mtoe, respectively, and those combined contributed to about two-thirds of the global growth of 8.5 mtoe. Bioethanol production in North America reached 60.4 mtoe or 56% of the global production, while Europe produced 34.9 mtoe biodiesel or 37% of the global biodiesel production (BP, 2019).

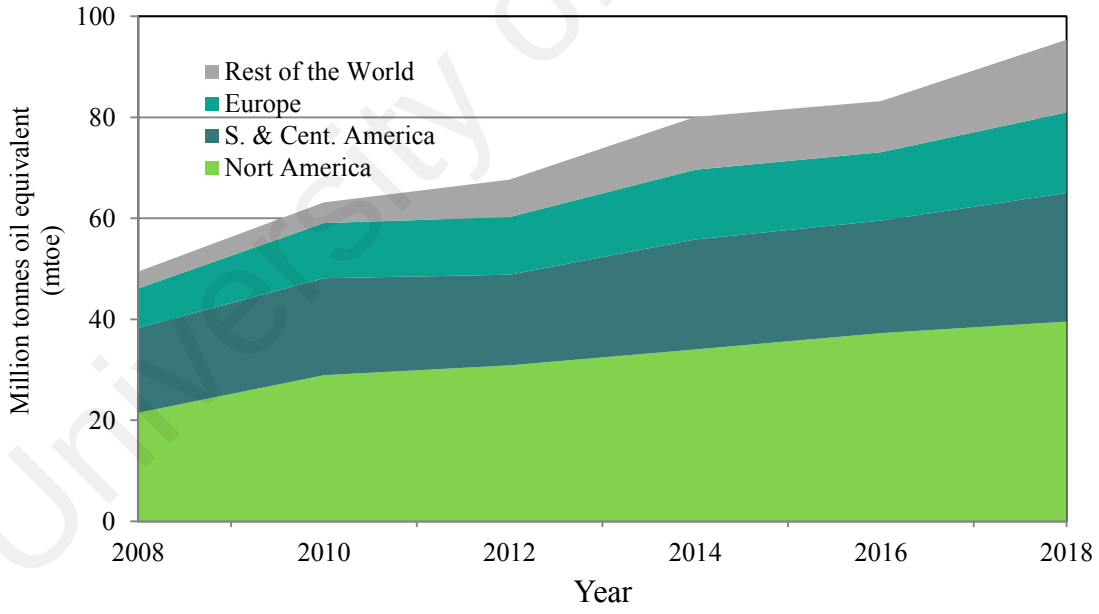

Figure 2.1: Global biofuel production (BP, 2019)

2.2. Exhaust emissions

Exhaust emissions are waste products of fuel combustion in internal combustion engines, external combustion engines, and jet engines. These waste products are released through the engine exhaust system. Undesirable exhaust emissions are released

when there is incomplete combustion, which can be due to lack of oxygen and non-ideal air-fuel ratios. This leads to the release of toxic gases such as CO, NO_x, and HC. The release of CO_2 emissions into the atmosphere generated from fuel combustion has a significant impact on global warming. One of the ways to reduce the causes of global warming is to develop renewable energy technologies (e.g., solar, wind, and wave energy systems) and formulate alternative fuels, which will produce lower carbon emissions.

Figure 2.2 shows that world energy-related CO_2 emissions according to fuel type. The United States Energy Information Administration (EIA, 2019b) estimated an increase in CO_2 emissions at an annual average in between 0.4-0.6% from 2018 to 2050 with respect to the nature of fuel used (coal, liquids, and natural gas) which can be seen in **Figure 2.2 (a)**. This projected CO_2 emission growth, however, is considered lower in comparison to the annual growth from year 1990-2018 which is due to the advancement of coal power plants that work with higher efficiency with invented carbon capture ability device and it is expected that coal-fired power generations is gradually decline in future. Besides, the advancement in the transportation sector, especially in India and China, where liquid fuels was their main fuel sources have shown relatively lower projected CO_2 emission with annual average of 0.6%. From **Figure 2.2 (b)**, it shown that China and US will have similar emission levels by 2050, this is due to the growth in the country‘s population are at a slower pace. From natural gas, it was projected an annual rise of CO_2 emission of 1.1% in between 2018 to 2050 which is still lower than annual average of 2.2% per year from 1990 to 2018. There is a great decline in CO_2 emission in near future for all fossil fuel sources, compare to the emission occurred from 1990 to 2018. It is forecasted that electric power sector will experience a decrease in coal consumption while natural gas will be come the leading fuel for the generation of electricity. This scenario can be seen from a few leading countries such as United

States and China that implemented cleaner energy to generate electricity that eventually reduce the rate of annual growth of CO_2 emission.

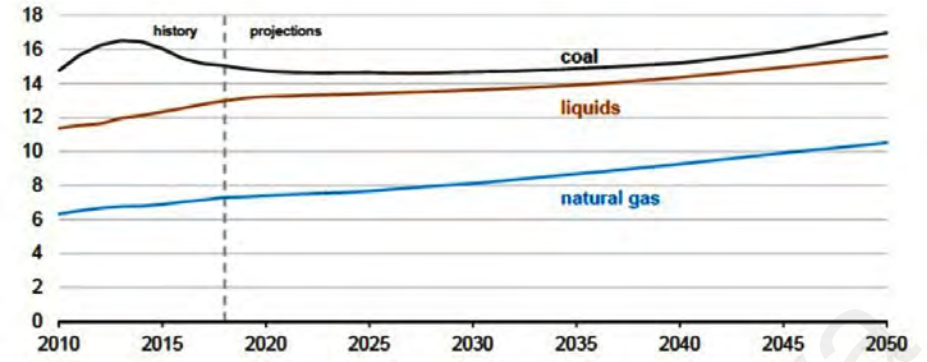

(a)

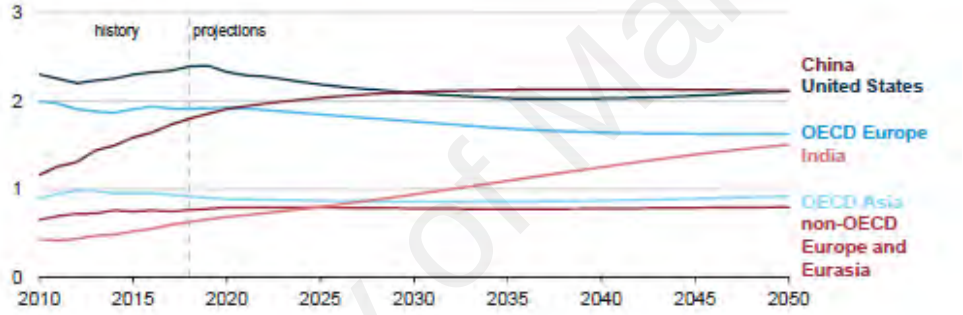

(b)

Figure 2.2: World energy-related CO_2 emissions according to fuel type from 2018 to 2050 (EIA, 2019b)

However, according to the data from British Petroleum (BP, 2019), the average growth rate of CO_2 emissions in India is 5.4%/year from 2008 to 2018, spanning a period of 10 years. The global CO_2 emissions from the consumption of oil, gas, and coal increase by 2% in 2018.

Figure 2.3 depicts the increase of CO_2 emissions from the burning of oil, natural gas, and coal in China at an annual average of 2.5% from 2008 to 2018. As observed, in comparison with China's CO_2 emission growth, India emitted a greater CO_2 emission, despite a greater total CO_2 emission that China emitted (BP, 2019).

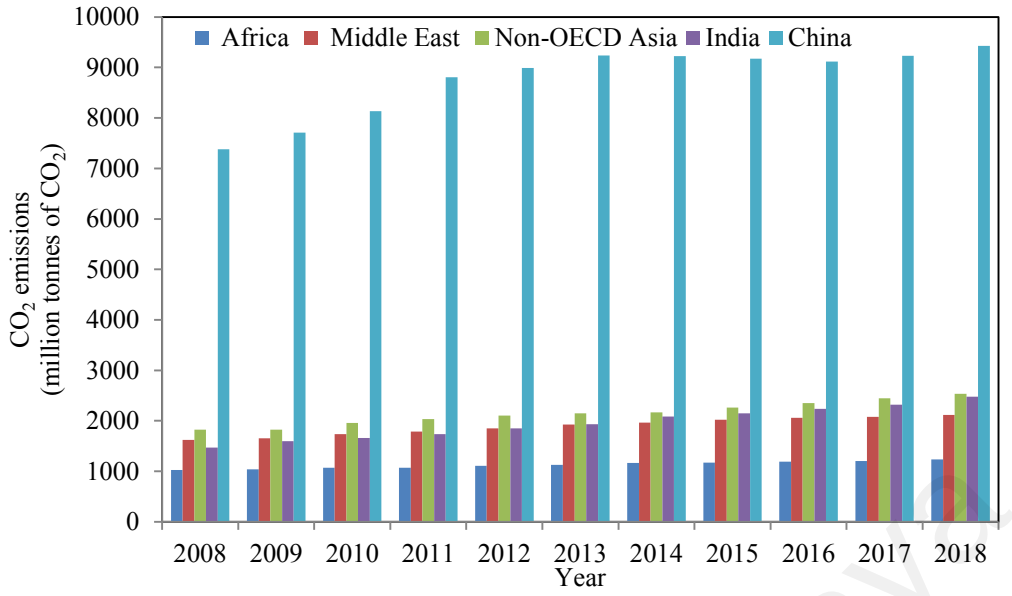

Figure 2.3: The trend of CO_2 emissions from 2008 to 2018 (BP, 2019)

2.3. Bioethanol policy, and economic and environmental impact

The global bioethanol production continues to increase rapidly in recent years. In Brazil, the share of renewable energy in total energy consumption is at the level of 42%, making it a world leader in the use of energy from RES (renewable energy sources). From the total RES, 18% consists of sugarcane bioenergy (bioethanol). Currently, bioethanol in Brazil is still consumed within the domestic market, in which ethyl alcohol is marketed as pure bioethanol or additive to gasoline (Mączyńska et al., 2019). In 2014 bioethanol was responsible for 32.3% of the total energy consumed in light vehicles in Brazil (de Carvalho et al., 2016). In the same year, United.States. generated 14.31 billion gallons of bioethanol as biofuel, and in the recent production, it increased to 15.8 billion gallons in 2019. This corresponds to an average increase of 1.9% per year over a five-year period (2014–2019) (RFA, 2020).

Selection of the main feedstock in bioethanol production varies in one country to another. In the United States, corn is the primary source in bioethanol production. On the other hand, Brazil utilizes sugarcane as the feedstock in producing its national bioethanol (Gnansounou et al., 2015; RFA, 2020). Many countries such as Europe, Asia, and Latin America have exploited the bioethanol production on industrial scale for

feedstock such as sugar beet, cassava, wheat, and other first-generation materials. In fact, in Europe, sugar bioethanol from beets accounts for more than 30% of the total bioethanol demand (Alonso-Gómez et al., 2020).

China is diversifying the feedstock used in bioethanol production, to non-grain materials. This includes sweet sorghum, cassava, and sweet potato. While wheat and corn-based bioethanol production continues in practice, the expansion of bioethanol production from these material types is halted (Ge & Lei, 2017). This is primarily due to the side effects of using first-generation materials (i.e. sugarcane, beets, cassava, corn, etc.), which include the requirement of land and water use to sustain the feedstock regular cultivation. In addition to that, there is a debate on biofuel versus food security, where food prices may inevitably soaring as crops are massively diverted into the sector of fuel production (Chao et al., 2017; Correa et al., 2017; Koizumi, 2015).

The production of bioethanol in several countries shows that the usage of biofuel to improve energy security and reduce dependency on imported oil will decrease the oil import bill and promote sustainable development (Osei et al., 2013). However, the current increasing trend in bioethanol production from first-generation feedstocks may lead to an increase in ethanol price, which brings about the fuel versus food issue. In addition, the lack of crop cultivation owing to the limited availability of lands makes it impractical to produce bioethanol merely from first-generation feedstocks (Demirbas, 2011). Therefore, it is crucial to explore the production of bioethanol from second-generation feedstocks through innovation and policy support instruments (Gnansounou, 2010). **Figure 2.4** shows the bioethanol production in 2019 from selected countries. The **Figure** illustrates that the United States are the premier in bioethanol production, at the total of 15.8 billion gallons. Brazil ranked the second with nearly 8.6 billion gallons of bioethanol production.

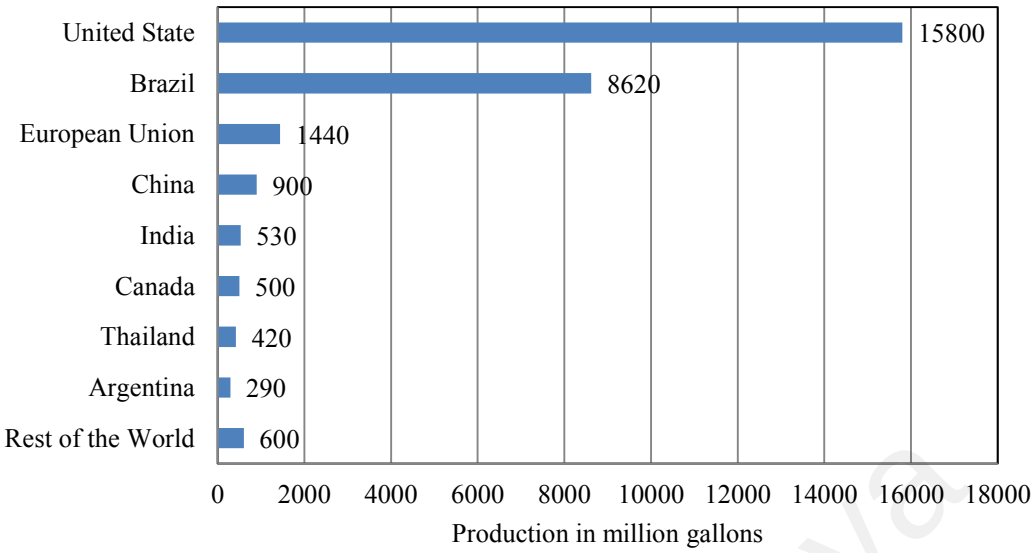

Figure 2.4: Bioethanol fuel production in 2019 (Statista, 2020a).

The economic assessment for bioethanol production involves several elements such as feedstock costs, by-product revenues, cost of process energy, investment costs (related to the type of feedstock), plant location, transportation costs, and financing costs (Balat, 2011). At the same time, the uncertainties related to the economic performance are highly influenced by several factors such as labor and capital, product and infrastructure, lack of knowledge concerning how the feedstock market will behave in the long term (e.g., unexpected surge in feedstock demands), and lack of knowledge concerning the market prices of ethanol. The lack of knowledge concerning the existence or inexistence of a correlation with the price of gasoline when the share of bioethanol for road transport is significant and the willingness of investors to be involved in the production of second-generation bioethanol are also factors that influence the economic performance (Gnansounou, 2010). The cost of bioethanol is considered higher compared with gasoline because bioethanol is derived from first-generation feedstocks (edible biomass) such as corn and sugarcane, which creates competition between the use of crops for food and biofuel production (Pimentel & Patzek, 2005). Bioethanol production from lignocellulosic biomass has made slower

progress compared with that from conventional sugar/starch plants owing to the complexity of the former process, where pre-treatment is required to convert the biomass into ethanol (Girard & Fallot, 2006). Pre-treatment is required to degrade the lignocellulosic biomass, remove lignin, partial or total hydrolysis of hemicellulose, and reduce the fraction of crystalline cellulose related to amorphous cellulose. Amorphous cellulose is the most suitable form for the hydrolysis process. In the enzymatic hydrolysis process, the cellulose is hydrolyzed to obtain glucose, which is then transformed into ethanol by microorganisms (Mood et al., 2013). Consequently, bioethanol production from lignocellulosic materials is more complex, which leads to higher production costs compared with that from molasses or starch feedstocks. The pre-treatment of lignocellulosic biomass is perceived as one of the costliest processing steps in the conversion of lignocellulosic biomass into fermentable sugars. Therefore, the growth of the bioethanol industry is largely dependent on the development of new processes in order to convert lignocellulosic biomass from non-edible crops and waste materials into bioethanol (Woodson & Jablonowski, 2008). In 2012, the cost of bioethanol production from different types of feedstocks is shown in **Table 2.1.**

Table 2.1: Cost of bioethanol production from different types of feedstocks (IRENA, 2012)

Feedstock	Production cost (US$/L)
Sugarcane	0.7–0.9
Corn	0.9–1.1
Lignocellulose	1.04–1.45

For a more recent price, and as shown in **Figure 2.5**, the average price of global ethanol is USD 0.95 per liter in 2020. Despite this, there is a substantial difference in these prices among countries. The difference is visible from the status of the economy of the country, which means countries with higher economic status or wealth would implement higher prices. Meanwhile, poor countries, which are also typically the

producers and exporters, would have cheaper fuel prices. United States is one apparent exception here, as it possesses the capability to produce and export with an advanced economy, yet it has low fuel prices. The phenomenon is mainly driven by subsidies and various taxation schemes imposed on the fuel, regardless of the raw fuel price that is priced at a universal rate prior to the imposition of those schemes locally. This results in different retail prices for ethanol.

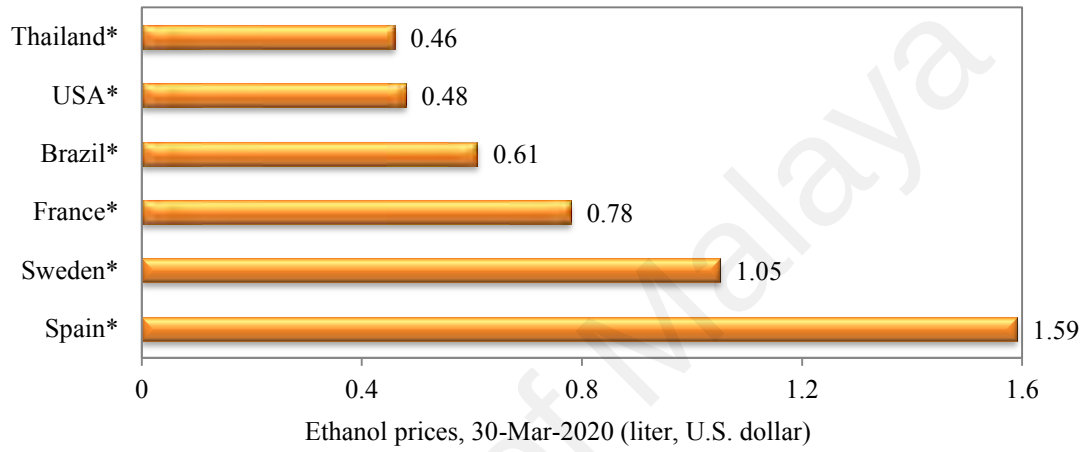

Figure 2.5: Ethanol prices in several countries (Prices, 2020)

Note: The prices for the countries with a * are updated weekly. The data for the remaining countries are updated monthly.

Net energy is defined as the energy produced from an energy resource after subtracting the energy investment to develop that source. The net energy yield of a fully developed resource measures the true value of an energy resource to the society (Prakash et al., 1998). From a biofuel economy viewpoint, to reduce the reliance on fossil fuels, reduce GHG emissions, and enhance rural economies, it is important to ensure that the net energy in bioethanol production is positive. The net energy production has been used to evaluate the energy efficiency of ethanol and it is the ratio of the total energy output to the total energy input from the biomass feedstock (Saga et al., 2010; Schmer et al., 2008). The net energy value (NEV), net energy ratio (NER), and net energy yield (NEY) of the biofuel output have been studied and compared with the petroleum energy ratio (PER) to measure the sustainability of a biofuel. Switchgrass

is estimated to have a net energy balance of 343% if it is used to produce ethanol (McLaughlin & Walsh, 1998).

More of the recent energy models that simulated biomass yields and estimated agricultural inputs have shown that switchgrass can produce more than 700% of output energy than input energy. In contrast, GHG emissions were assumed to be near zero or estimated to be slightly positive for switchgrass-derived ethanol (Schmer et al., 2008). In Brazil, the NER of sugarcane ethanol is positive because of the by-product bagasse, which is used to produce heat and power needed for ethanol conversion plants. The NER of sugarcane has been reported to be 8.3–10.2 (Saga et al., 2010). The NERs of corn ethanol in the United States of America have also been evaluated and the values were found to be 0.71 (Pimentel & Patzek, 2005) and 1.67 (Shapouri, 2004). In Malaysia, net energy balance (NEB) and life cycle assessment (LCA) have been proven to be suitable to evaluate the environmental sustainability of biofuels and identify opportunities to improve environmental efficiency. NEB can also be used to measure the energy effectiveness and efficiency of bioethanol production systems. Even though both of these methods have been widely used to assess bioethanol production systems, the results tend to vary (Hanif et al., 2017). According to (Shapouri, 2004), the NEB of corn bioethanol was greater than 1. In general, positive NEB values indicate that the process is energy-efficient. Other feedstocks such as sugarcane, cane molasses, and cassava have also been studied in terms of their NEB and LCA (Dai et al., 2006; Farrell et al., 2006; Kim & Dale, 2006; Leng et al., 2008). In terms of emission reduction, a recent study conducted in Belgium showed that the production of bioethanol from wheat could reduce GHG emissions by 91% compared with conventional gasoline (Belboom et al., 2015). For cassava bioethanol, the emissions reduced by ~58% without any energy allocations (Numjuncharoen et al., 2015).

Concerns over the depletion of fossil fuels and environmental problems such as global warming have driven the need to produce alternative fuels such as bioethanol. However, there are also concerns on the local impact of bioethanol production on soil, water, air, direct land use, and biodiversity (Gnansounou, 2010; Soccol et al., 2010). One of the benefits of bioethanol is that it allows CO_2 to be run in a closed cycle. Once ethanol is burned, the CO_2 released is recycled back into the plant material because plants use CO_2 to synthesize cellulose during photosynthesis (Chan et al., 2007). In addition, the toxicity of exhaust emissions from the burning of bioethanol is lower compared with that from the burning of gasoline (Masum et al., 2013). Indeed, the interesting fundamental carbon neutrality of combusted biomass is based on the fact that the emitted CO_2 from the plant originates from the atmosphere where it eventually goes back to. If land conversion to biomass production implies additional CO_2 emission through soil organic carbon losses, it may offset this carbon neutrality which is shown in **Figure 2.6.** (Bessou et al., 2011).

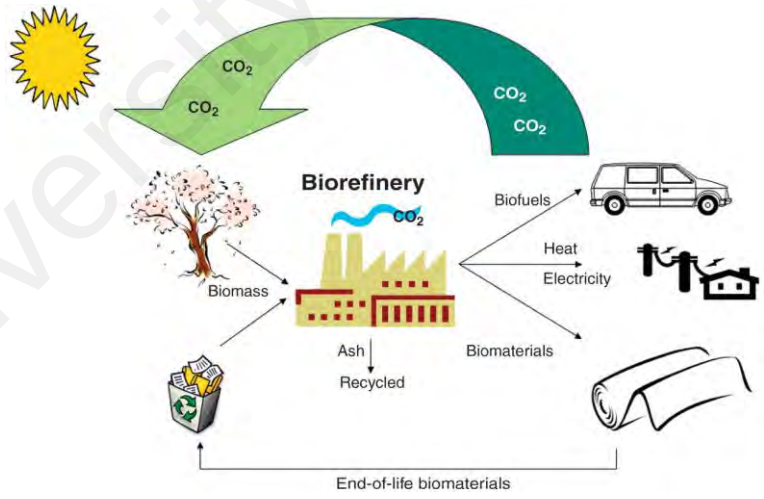

Figure 2.6: Biofuel cycle for sustanaible technologies (Bessou et al., 2011)

Bioethanol is of plant origin and it can be used as transportation fuel. The CO_2 emitted from the burning of bioethanol-gasoline blends is not counted as GHG because it is recaptured as a nutrient for crops used for their production (Luo, 2010). Therefore, the reduction of GHG emissions is the main advantage of bioethanol since bioethanol

consists of 35% of oxygen, which can enhance combustion and reduce exhaust emissions, which are detrimental to people's health (Balat et al., 2008). However, the main disadvantage of bioethanol is the food versus fuel issue, where there are concerns on the lucrative business of bioethanol production because some farmers may sacrifice food crops for biofuel production, which will increase global food prices. In addition, bioethanol has lower energy density than gasoline, higher corrosivity owing to the presence of alcohol, lower flame luminosity, and lower vapor pressure (making cold starts difficult). Bioethanol is also miscible with water and toxic to ecosystems (Balat et al., 2008).

2.4. Energy assessment for bioethanol production

Bioethanol can be produced from various agricultural and industrial activities, and biomass can also be found in nature. Forestry and agricultural materials, as well as their wastes, are the popular feedstock in biofuel production. Bioethanol production from non-edible feedstock is one of the key areas in bioethanol production that aims for the sustainability of both cost and environment, which are the main primary concerns in the modern fuel industry (Robak & Balcerek, 2018). In this regard, non-edible feedstock can be obtained directly from local farmers. This consequently helps the economy issue in the society, and further minimizes the controversial impact of food conversion into fuel (Jambo et al., 2016). More importantly, the non-edible feedstock can be used continuously in bioethanol production process, and the products will contribute to fulfil the ever-increasing global energy demands (Thompson & Meyer, 2013).

The general cycle of bioethanol production is shown in **Figure 2.7**, in which also depicts the flow of carbon capture of CO_2 emission after bioethanol combustion back to the crops. For bioethanol production from starch-based biomass, saccharification stage is important to yield the useful sugars for the subsequent fermentation stage. Prior to that, the feedstock is pulverized and steamed to accelerate the saccharification process.

Each stage consumes certain amount of energy, and the intensity depends on the treatments at each stage. Energy consumption analysis of starch-based bioethanol is then critical, as it will determine the productivity and energy cost characteristics based on the selected crops.

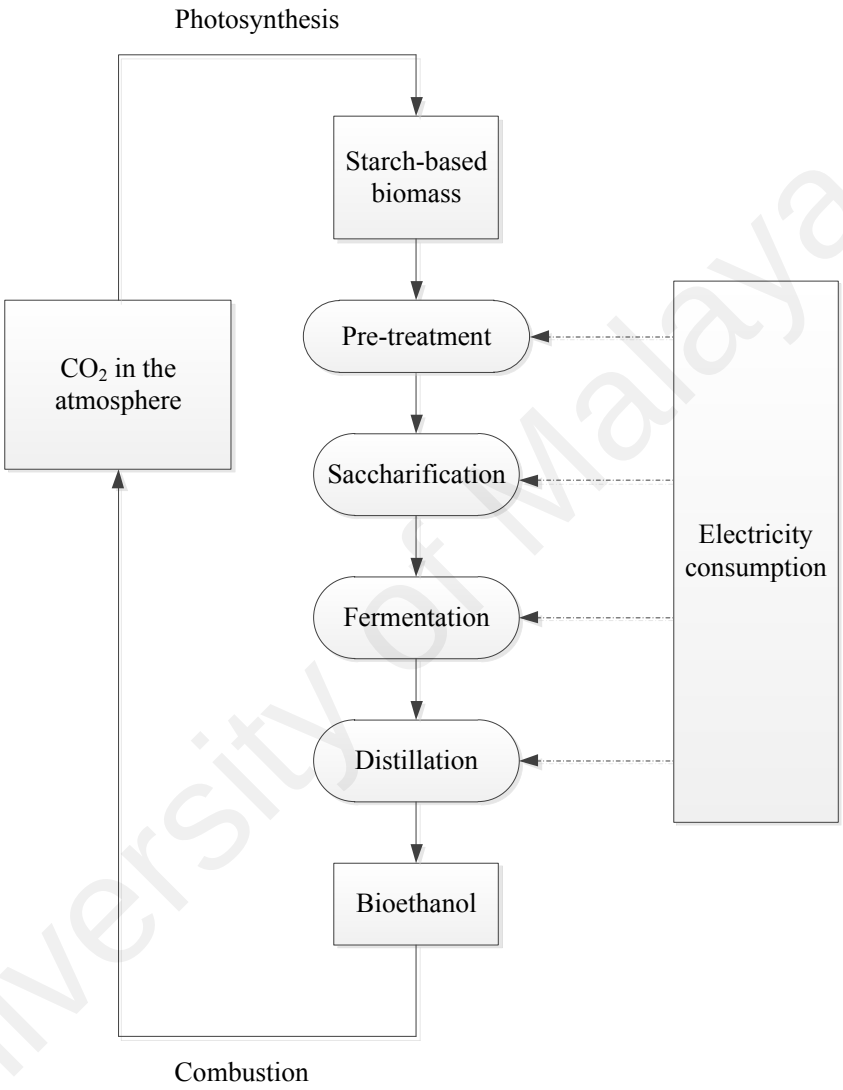

Figure 2.7: Production processes of bioethanol from starch

To fit into the qualification as a suitable fossil fuel substitute, an alternative fuel should have remarkable economic and environmental benefits. Further, it must carry the net energy gain characteristic according to the selected feedstock (Hill et al., 2006). Alternative fuel should have the potential of offsetting the extraction and burning cost of fossil fuels. In calculating the net energy benefit of bioethanol as a replacement of

fossil fuel, it is should be assessed by accounting the net energy contained in the biomass as well as the energy required in feedstock and during the entire process of bioethanol production (Bansal et al., 2016). Analyzing energy consumption is a widely common approach to determine the bioethanol production efficiency, and this can be achieved by taking the ratio of energy output from the produced bioethanol to the total of consumed energy in the bioethanol production (Schmer et al., 2008). A study in Poland reported energy consumption of bioethanol production in agricultural distillers with various performance coefficients from the employed equipment. The study analyzed energy consumption in bioethanol production using 20% of starch-based feedstock, boiler with heating performance coefficient of 0.7, and chemical reaction coefficient of 0.9 with steamer consuming 550 kg/h of steam (Trajer et al., 2015). Another study developed Energy and resource group biofuel analysis meta-model (EBAMM), and from this model, it estimated an energy gain of 23 MJ/L of produced ethanol from production based on cellulosic (Bansal et al., 2016). A similar result has been reported by Schmer et al. (2008), as they studied bioethanol production from ten switchgrass farms established on marginal lands ranging from 3 to 9 ha, resulting in net energy of 21.5 M J/L of ethanol. Swana et al. (2011) compared the energy yield of 2G ethanol and corn-derived bioethanol using life cycle assessment (LCA). They found a significantly higher energy gain in cellulosic ethanol (15.9 MJ/L) than corn-based ethanol. Net energy value (NEV) of cellulosic feedstocks like switchgrass (8.80 MJ/L of ethanol) and *Miscanthus* (11.99 MJ/L of ethanol) were also determined (Bansal et al., 2016). The difference in biomass yield might be the reason for variation in the net energy gains among different studies.

In this study, *Manihot glaziovii* and sweet sorghum are selected for nonfood crops, and they can be planted on marginal land. The advantages of *Manihot glaziovii* and sweet sorghum are tolerant to poor environmental conditions, the possibility of all year

long planting and harvesting, high root productivity, continuous improvements of high yield varieties, fewer input requirements for planting and harvesting, high quantity and quality of carbohydrates, highest energy content per acre among starchy crops, and high ethanol yield per acre (Almodares & Hadi, 2009). Therefore, energy assessment has been proven to be suitable methods to evaluate the energy sustainability of biofuels to identify opportunities for energy efficiency improvements. Energy assesment could also be used to measure the energy effectiveness and efficiency of bioethanol production systems.

2.5. Bioethanol

Bioethanol is also known as ethyl alcohol (EtOH), pure alcohol, or grain alcohol. It has a chemical formula of C_2H_5OH, empirical formula of C_2H_6O, and group formula of $CH_3–CH_2–OH$. For bioethanols, the methyl group ($CH_3–$) is coupled to the methylene group ($–CH_2–$) and hydroxyl group (–OH). Bioethanol is colorless and tasteless, with a distinctive odor (Balat, 2011).

Bioethanol is a renewable energy source, which is derived from plants and it has great potential as a gasoline substitute in spark ignition engines (Ghazikhani et al., 2013). Bioethanol is also a viable alternative to unleaded gasoline, and it can be used without engine modifications. A higher compression ratio can be achieved with fuel blends above 20% bioethanol, and this improves the indicated thermal efficiency (Park et al., 2016). Anu Nair et al. (2018) reported that gasoline with bioethanol content up to 25 vol% enhances the engine thermal efficiency by 10.37%. By raising the intake air temperature to 60°C, the gasoline blend can attain a 40% bioethanol content, but the engine thermal efficiency reduces by 7.59% compared to that of pure gasoline fuel. Abdel-Rahman and Osman (1997) conducted an investigation on varying the compression ratio of spark ignition engines working under different ethanol-gasoline fuel blends. They reported that 10% ethanol gasoline fuel blends increase the maximum

pressure over that of pure unleaded gasoline. Ruan et al. (2019) reported that bioethanol carries lower LHV (21.2 MJ/L) than that of gasoline (30-33 MJ/L), and this results to a greater amount of bioethanol needed to obtain the same energy output as gasoline. Although the energy content of bioethanol is 32% lower compared with that of gasoline, bioethanol has higher oxygen content, which will improve the combustion characteristics and produce lower exhaust emissions. Bioethanol has a high octane number of 108 with a high oxygen content of 34.7%(w/w), and this will improve the combustion characteristics with the production of lower exhaust emissions. Because of this, bioethanol prevents engine knocking and early ignition in spark ignition engines (Aditiya et al., 2016).

The use of bioethanol in gasoline has become the worldwide interest as it is regarded as an alternative to mitigate greenhouse gas emissions from the transportation sector. United States Department of Agriculture (USDA, 2017) reported that corn bioethanol has the potential to reduce greenhouse gas emissions by up to 76% along with the production advancements, efficient techniques, and sustainable agricultural practices. In a hindsight, with the ethanol industry, it allows engines to perform better, gives consumer a great save, and improves the air quality. The latter effect is due to the combustion products of gasoline-ethanol blend that contain less HC and CO emissions. The cleaner combustion is possible considering that the carbon chains in the blend are lesser than that of pure gasoline, and those carbon-based emissions would be lower as the ethanol content is increased (Tutunea & Dumitru, 2017). Further, improvement in the combustion products of gasoline-ethanol blend is owing to the oxygen compound in the blend and this enhances the combustion process. The formation of CO is mainly introduced in the exhaust gases when the fuel is not combusted completely, and HC is formed when there is an excess of unburned fuel (Yusaf et al., 2009). Elfasakhany (2015) also supported that the oxygen in the blend enhances the combustion, and this

leads to an improved exhaust emissions and combustion efficiency. On the other hand, the blending of bioethanol in gasoline can increase CO_2 concentration in the emission. This is due to the oxygen content that enhances the combustion, which then allows to burn more fuel and forming more CO_2 as the product (Doğan et al., 2017). NO_x is generally produced during the combustion of both gases and fuel oils. When the combustion is under fuel-lean conditions with a rise in temperature, this will lead to an increase of NO_x emissions due to increased oxygen radicals forming with the help of high temperatures in the combustion process. However, when the combustion is under the fuel-rich condition the oxidation reaction will involve the OH and H radicals (Szczepanski, 1998). High activation energies are required for the dissociation of oxygen molecules and the disengagement of the triple bond of nitrogen. This phenomenon causes the formation of thermal NO_x to be largely dependent on the temperature, the degree of air to fuel mixing, the concentration of oxygen and nitrogen in the flame, and the duration of the reaction occurred (Hermann et al., 2004). NO_x emissions also dependent on the engine operating condition when using bioethanol gasoline blends in a spark ignition engine. NO_x concentrations can be adversely affected because of the increasing cylinder temperature as the ethanol percentage is also increased (Bayraktar, 2005). An increase in NO_x emission can also occur due to advanced ignition timing for hydrous ethanol, therefore, higher peak temperature during burning and thereby increase the formation of NO_x (Costa & Sodré, 2010). The higher aromatic content of gasoline leads to lower phase separation temperatures. It is worth pointing out that increasing the aromatic content in gasoline may increase the total emissions of NO_x (Schifter et al., 2004).

In fact, the use of bioethanol as an automotive fuel has been long known. In the 1880s, Henry Ford invented the quadricycle and since 1908, bioethanol was used for Ford Model T. However, bioethanol was given little attention when fuel was cheap and

abundant (Aditiya et al., 2016). However, in recent years, with the depletion of fossil fuel reserves and the fluctuations in oil prices, much effort is made to develop bioethanols.

Bioethanol is gradually gaining acceptance as an alternative fuel because of the depletion of fossil fuel reserves as well as environmental concerns. At present, bioethanol blends are already available at many service stations across the United States of America and Europe. The demand for bioethanols is increasing worldwide because of concerns on the detrimental effects of fossil fuel combustion on the environment. According to the Renewable Fuels Association (RFA, 2020) the total production of bioethanols worldwide increased from 25.7 billion gallons in 2015 to 29.1 billion gallons in 2019, which corresponds to an increase of 11.4%.

Figure 2.8 shows that the production of bioethanol in the United States of America was nearly 16 billion gallons in 2019, making this country the leading ethanol producer in the world. Brazil produced about 8 billion gallons in the same year. Both of these countries produced 84% of the world's ethanol. Most of the ethanol in the United States of America is produced from corn whereas sugarcane is the main feedstock for bioethanol production in Brazil.

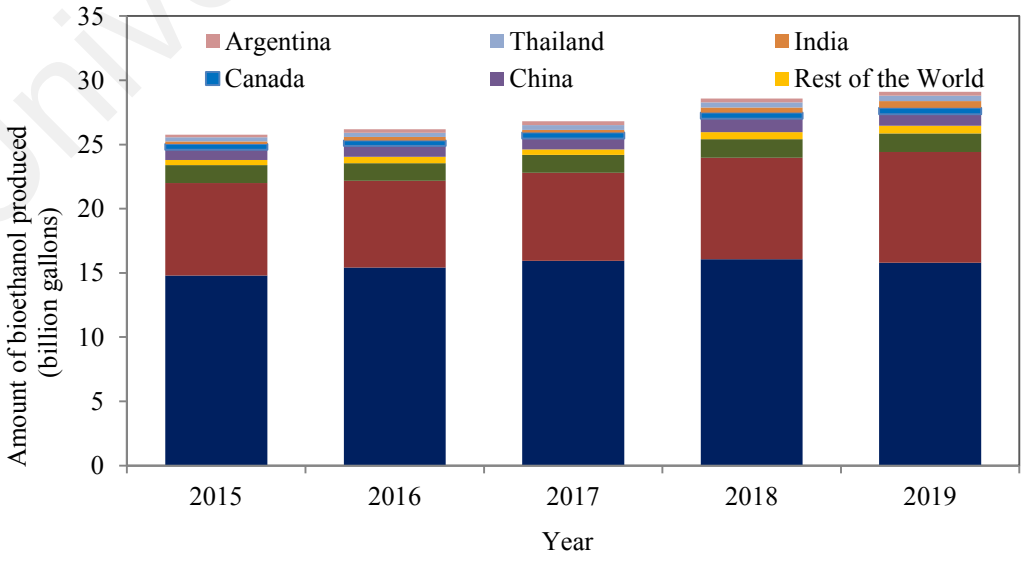

Figure 2.8: Global ethanol production from 2015 to 2019 (RFA, 2020)

2.6. Non-edible feedstocks for bioethanol production

Non-edible feedstocks have become more attractive recently owing to their environmental benefits and the fact that they renewable. As the name implies, non-edible feedstocks are not fit for human consumption because of the toxic components in the feedstocks. In order to choose a suitable non-edible feedstock for bioethanol production, it is necessary to review the current scientific literature. The production of bioethanol from non-edible feedstocks can help address the food versus fuel issue, environmental problems, and the related economic conundrums (Saravanan et al., 2018)

Non-edible plants typically grow on marginal lands as well as in poor areas and damaged forests. These plants can also be planted on the boundaries of arable and fallow lands, as well as on public lands such as along railways, roads, and irrigation canals. The production of bioethanol from non-edible feedstocks can be a part of poverty alleviation programs in poor areas while at the same time promote energy security. Many researchers have concluded that bioethanols from non-edible feedstocks have great potential as alternative fuels.

2.6.1. Botanic description of *Manihot glaziovii*

Various species of cassava are widely cultivated in tropical regions, especially in the tropical areas of Africa, Latin America, and Asia. One of these species is *Manihot glaziovii,* which is native to Brazil, but is now widely grown in Southeast Asia (Joseph et al., 2000). The trees grow rapidly, reaching a maximum height of about 10 m in only a few years (Joseph et al., 2000). *Manihot glaziovii* is a plant that contains linamarin, which is a cyanogenic glucoside (Joseph et al., 2000; Phambu et al., 2007). The leaves and tubers of *Manihot glaziovii* contain cyanogenic glycosides, which can produce a highly toxic compound, hydrogen cyanide (HCN), that can cause poisoning to humans and animals. *Manihot glaziovii* has enzymes that can break down cyanogenic glycosides to produce HCN.

Manihot glaziovii has been cultivated as a crop with finger-shaped leaves, and can reach a height of 2.75 m (Nassar, 2007). This plant grows well in areas with an elevation of up to 2,500 m above sea level. *Manihot glaziovii* is a promising feedstock for bioethanol production because of its high starch yield (36.3 ton/(ha·year)) and the raw materials are available throughout the year (Muktham et al., 2016). *Manihot glaziovii* has tubers or roots with a diameter and length that varies according to the variety. Taxonomically, *Manihot glaziovii* is in the family *Euphorbiaceae,* and its classification is as follows:

Kingdom : *Plantae*
Division : *Magnoliophyta*
Class : *Magnoliopsida*
Family : *Euphorbiaceae*
Genus : *Manihot*
Species : *Manihot glaziovii Muell*.

Manihot glaziovii plant can be cultivated through generative (seeds) and vegetative (stem cuttings) methods (Nguyen et al., 2007). Stem cutting is the preferable method to produce *Manihot glaziovii* plants with characteristics identical to the parent plants because the rooting will be quicker and easier (Department of Agriculture, 2010). The main advantage of *Manihot glaziovii* compared with other crops is that it can be grown in dry and less fertile lands. In addition, it is more resistant to diseases compared with other plants.

2.6.2. Botanic description of sweet sorghum

Sweet sorghum (*Sorghum bicolor* (L.) Moench) is one of the non-edible feedstocks used to produce bioethanol (Fedenko et al., 2015). It is one of the plants that originate from Africa, but it is now cultivated in Asia (Elhassan et al., 2015; Mehboob et al., 2015). Sweet sorghum is a highly adaptable plant because it can be grown on lowlands and highlands, as well as dry and humid climatic regions (Deesuth et al.,

2015). Sweet sorghum can also be grown on marginal lands (mainly arid lands) where other plants are unable to thrive (Elhassan et al., 2015; Wang et al., 2016). For this reason, marginal lands can be used to cultivate sweet sorghum, which is an advantage because this eliminates competition with the lands used for food production (Matsakas & Christakopoulos, 2013).

In addition, sweet sorghum has other advantages such as high grain production and high biomass. Sweet sorghum has high biomass yield (~3–6 t/hm^2 of grains and 45–75 t/hm^2 of sugar-rich stalks (Jiang et al., 2019). Moreover, it is resistant to droughts (Marx et al., 2014; Mehboob et al., 2015; Zhang et al., 2010) and it has short regeneration time (3–5 months), low fertilization needs, and higher photosynthetic rate compared with sugarcane and corn (Deesuth et al., 2015; Houx & Fritschi, 2015; Sjöblom et al., 2015). The starch content of sweet sorghum grains is high (65–71%) and therefore, this starch can be hydrolyzed into simple sugars (Dyartanti et al., 2015). For these reasons, sweet sorghum has attracted much attention as a promising non-edible feedstock for bioethanol production.

2.7. Optimization of bioethanol production using artificial neural networks

The concept of artificial neural networks (ANN) is influenced by the complex system of human nervous. In artificial intelligence field ANN is a method that is popular to model and optimize convoluted processes or phenomena that typically involve a large number of variables (Siswantoro et al., 2016). Since ANN is designed based on the workings of the human brain, the programming is assumed to be simple, such as that shown in **Figure 2.9**. Here, the input signal x is multiplied by the corresponding weight P. Next, the products of x_n and P_n are added and used as the transfer function to obtain the output $F(x, P)$.

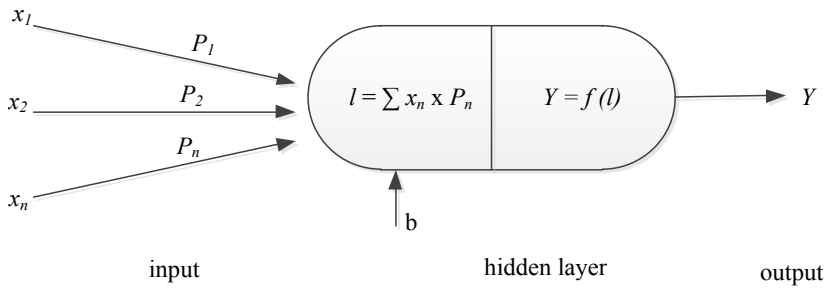

Figure 2.9: Structure of a neuron, where $x_1, x_2, \ldots, x_n$ are the inputs, $p_1, p_2, \ldots, p_n$ are the weights, b is the bias, f is the transfer function, and Y is the output (Siswantoro et al., 2016)

Through trained ANNs models for optimization and prediction are possible to be implemented in diverse, numerous applications. In ANN experimental data is essential which will be used to assess the prediction capability, while through independent data the validation is performed (Kiani et al., 2010). Further, through parameters relationship evaluation of the input and output ANN is effective in solving non-linear problems. This also applies for the data that are incomplete or complex (Ismail et al., 2012). ANN has the ability to relearn when new data are available in order to improve its performance (Najafi et al., 2009). Because of this reason and coupled with the efficiency and reliability, ANN is deemed as a suitable alternative to be implemented in optimizing production and operation parameters in a bioethanol production. The advancement in the use of the technique is in line with the betterment of technology. As the result, ANN can be adapted in wide range of scientific applications, including chemical, mechanical engineering and in renewable energy studies (Ayodele & Cheng, 2015; Pelletier et al., 2016).

Optimization is essential as the effort to elevate the efficiency, which leads to the maximization of the production. To increase efficiency and maximize bioethanol production with good quality, it is necessary to optimize the process conditions. With the suitable optimization method, the optimal process conditions can be determined within a shorter period. ANN is a combination of mathematical modeling and statistical

techniques, which can be used to optimize the response variable due to changes in several independent variables. With ANN, the process parameters and response variable can be optimized simultaneously. For instance, in bioethanol production where in different production phase many parameters are possibly involved, ANN can be utilized to evaluate the optimum parameters that are critical and carry the highest influence throughout the production process (e.g. in hydrolysis and fermentation production phases).

Many studies involving ANN have been carried out in optimizing production parameters in bioethanol production. For example, Grahovac et al. (2016) investigated the production of bioethanol from feedstocks made of the intermediates and by-products of sugar beet. They predicted the bioethanol yield using ANN. Trajer et al. (2015) used ANN to investigate the energy consumption of bioethanol production in agricultural distilleries. Moradi et al. (2013) used ANN to optimize the operating conditions of biodiesel production from soybean oil.

2.8. Bioethanol production technologies

Handling the biomass feedstocks is the preliminary step in bioethanol production, which involves cleaning and preliminary cutting to reduce their physical size prior to the pre-treatment process (Chiaramonti, 2007). Proper storage of the feedstocks is equally important to maintain their quality for bioethanol production. A large, cool, dry storage is recommended to store biomass feedstocks in order to protect them from humidity, rodents, and microbial growth. Drying under the sun as well as thermal or mechanical drying techniques are the common methods used to dry the feedstocks prior to storage (Chohnan et al., 2011). It has been proposed that bioethanol production using separate hydrolysis and fermentation (SHF) offers more advantages such as low cost of chemicals, short residence time, simple equipment, and the possibility of optimizing the hydrolysis and fermentation protocols independently (Maslova et al., 2019; Tavva et al.,

2016). **Figure 2.10** shows the conversion of biomass into bioethanol using SHF (Zhang, 1999).

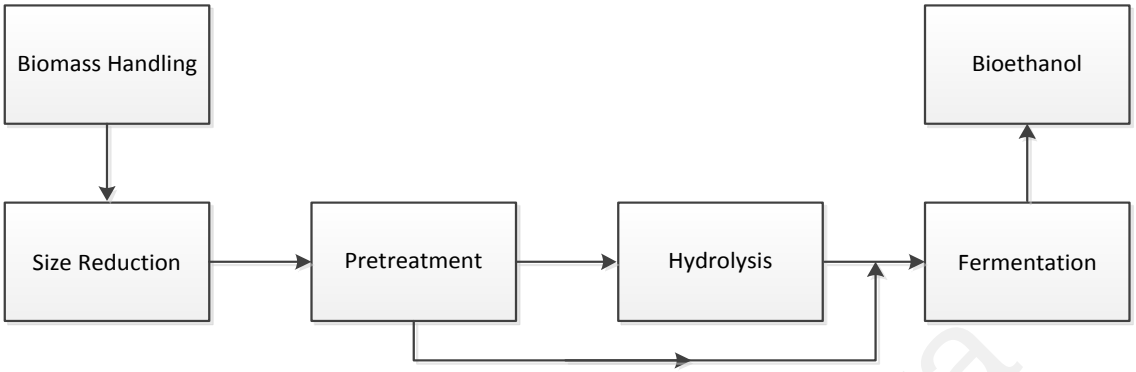

Figure 2.10: Conversion of biomass into bioethanol using separate hydrolysis and fermentation (Zhang, 1999)

2.8.1. Pre-treatment of biomass feedstock

In bioethanol production, biomass has complex structures that need to be broken down into oligomeric subunits by pre-treatment (Alvira et al., 2010). Pre-treatment is needed to remove hemicellulose, remove, or redistribute lignin (for lignocellulose biomass), increase the mean pore size, and provide better access for enzymes during enzymatic hydrolysis (Jain & Chaurasia, 2014). There are four types of pre-treatment methods, which will be described in the following sub-sections.

2.8.1.1.Physical pre-treatment

Physical pre-treatment reduces the particle size of the feedstock to increase the surface-volume ratio and facilitate the subsequent biodiesel production processes (Harmsen et al., 2010; Tanthapanichakoon & Jian, 2012). Mechanical pre-treatment reduces the particle size of the feedstock by breaking its physical structure. Pre-treatment typically involves washing, reducing the particle size of the feedstock by grinding, extracting the essence, and separating the solid fractions (Eufrozina, 2009; Mahalaxmi & Williford, 2012). Size reduction is particularly important for lignocellulose materials in order to increase their exposure during the hydrolysis process

(Alvira et al., 2010). However, it has been reported that a particle size of less than ± 40 mesh is not effective for bioethanol production (Mahalaxmi & Williford, 2012). The biomass feedstock is usually ground into a more compact form (3–8 mm particles) with higher density such as pellets or briquettes (Rupar & Sanati, 2005). Therefore, particle size is an important property because it affects the power required for the equipment (e.g., knife mill, hammer mill) and the economic feasibility of the selected method (Soccol et al., 2011). According to Zheng, Pan, and Zhang (2009b), mechanical process such as attrition milling, ball milling, compression milling, and steam treatment can be used to destruct lignin, which provides better access for the enzymes to attack the cellulose and hemicellulose during enzymatic hydrolysis.

2.8.1.2.Chemical pre-treatment

Chemical pre-treatment involves destructing the structure of the biomass through chemical reactions. Similar to mechanical pre-treatment, chemical pre-treatment removes lignin, which reduces the crystallinity of the cellulose and enhances the biodegradability of the biomass (Sudiyani et al., 2014). Chemical pre-treatment is most widely used pre-treatment method. The common chemical pre-treatment methods are briefly described as follows:

(a) Acidic pre-treatment

Acidic pre-treatment involves the use of acidic substances (typically H_2SO_4 or hydrochloric acid (HCl)) for lignocellulosic feedstocks because of its powerful ability to rupture the components into simpler form (Harmsen et al., 2010; Soccol et al., 2011). The low temperature of this process makes it a low-cost pre-treatment method, and it can loosen the cell wall matrix by means of hemicellulose degradation (Alvira et al., 2010). Even though acidic pre-treatment does not affect the lignin content of the feedstock, the cellulose microfibrils are sufficient to produce a high yield of monomeric sugars for fermentation (Taherzadeh & Karimi, 2008; Vohra et al., 2014). However, the

use of acidic pre-treatment increases the tendency of corrosion to the production equipment and therefore, it is important to overcome this problem, especially for large-scale bioethanol production where high amounts of acidic reagents are used (Harmsen et al., 2010; Mahalaxmi & Williford, 2012; Sun & Cheng, 2002; Taherzadeh & Karimi, 2008). For this reason, many acidic pre-treatment methods have been modified to improve the downstream processes and boost the bioethanol yield and price of bioethanol (Vohra et al., 2014). Tang, Chen, Huang, Xu, and Li (2013) performed acidic pre-treatment on *Eulaliopsis binata* using dilute 0.5% H_2SO_4 at 160°C for 30 min with a solid-to-liquor ratio of 1:5, resulting in total sugar content of 21.02% with a low inhibitor level after pre-treatment. Marzialetti et al. (2008) performed acidic hydrolysis on loblolly pine using various acids, including trifluoroacetic acid (CF_3CO_2H), HCl, H_2SO_4, HNO_3, and phosphoric acid (H_3PO_4). The results showed that CF_3CO_2H yielded the highest sugar monomers (70%) from hemicellulose at a temperature of 150°C and pH of 1.65. In addition, it was stated that CF_3CO_2H was the mildest acid among the acids employed in their work.

(b) Alkaline pre-treatment

This method involves the use of alkaline chemicals to pre-treat the feedstock. Alkaline pre-treatment is normally performed at room temperatures and pressures compared with other types of pre-treatment methods (Alvira et al., 2010; Mahalaxmi & Williford, 2012; Taherzadeh & Karimi, 2008). The main advantage of alkaline pre-treatment is its simplicity and it gives high conversion yields within a short period (Harmsen et al., 2010). Alkaline pre-treatment also results in less sugar degradation, though the presence of inhibitors should be eliminated in order to optimize the pre-treatment conditions (Canilha et al., 2012). For these reasons, this pre-treatment method is more effective for bioethanol production compared with acidic pre-treatment (Bensah & Mensah, 2013). The suitable alkaline reagents are sodium hydroxide (NaOH) and

lime, which are employed to break intercellular bonds between crosslinking hemicellulose and other components (lignin and cellulose) (Sun & Cheng, 2002). Moreover, alkaline pre-treatment can cause swelling of the structure, as well as increase the porosity, decrease the crystallinity and degree of polymerization, promote the separation of lignin, hemicellulose, and cellulose, and disrupt the lignin structure (Soccol et al., 2011). According to Sun and Cheng (2002), alkaline pre-treatment is capable of delignifying lignocellulose and enhancing the reactivity of carbohydrates. In addition, the use of NaOH in alkaline pre-treatment improves lignocellulose digestibility in typical lignocellulose feedstocks such as wheat straw and thus, it is suitable to pre-treat second-generation biomass feedstocks (Bjerre et al., 1996; Chang & Holtzapple, 2000). Chang, Nagwani, Kim, and Holtzapple (2001) used oxidative lime pre-treatment to pre-treat poplar wood feedstock. The results showed that 78% of lignin was removed and the glucose yield was improved by 71% during enzymatic hydrolysis. Sun, Sun, Fowler, and Baird (2004) conducted alkaline pre-treatment on wheat straw using different alkaline solutions. The results showed that 80% of hemicellulose and 60% of lignin were released using 1.5% NaOH at 20°C for 144 h of pre-treatment. In addition, they observed that a significant amount of xylose was formed during the hydrolysis process compared with glucose and galactose, since hemicellulose was the main focus of their study. Park, Shiroma, et al. (2010b) conducted alkaline pre-treatment and the results showed that the ethanol yield was 74% ethanol after 79 h of fermentation by a combination of yeasts *Saccharomyces cerevisae* and *Pichia stipitis* as the fermentation agents. Other alkaline substances, including potassium hydroxide (KOH), NaOH, hydrazine (N_2H_4), anhydrous ammonia (NH_3), and calcium hydroxide ($Ca(OH)_2$), are also typically used in alkaline pre-treatments of biomass. Other typical alkaline substances cause biomass swelling, which exposes the internal surface area as

well as decrease the crystallinity and degree of polymerization (Chang & Holtzapple, 2000; Mosier et al., 2005).

2.8.1.3.Biological pre-treatment

In biological pre-treatment, microorganisms (e.g., fungi) are employed to degrade the biomass structure (Han et al., 2013b; Mahalaxmi & Williford, 2012). The typical microorganisms employed for this technique are white, brown, and soft-rot fungi (Mahalaxmi & Williford, 2012). Several white-rot fungi, namely, *Ceriporia lacerata*, *Phanerochaete chrysosporium*, *Pleurotus ostreaus,* and *Cyathus stercolerus*, have been evaluated for delignification of various lignocellulosic biomasses and the results showed that these fungi resulted in high delignification efficiency (Alvira et al., 2010; Zhao et al., 2011). In general, brown-rot fungi degrade the hemicellulose and cellulose components of the biomass, white-rot fungi degrade the cellulose and lignin components, and soft-rot fungi are useful to release cellulose from degradation of the lignocellulose complexes (Kumar & Wyman, 2009; Sarkar et al., 2012). Biological pre-treatment is very well-known for its environmental friendliness, although it tends to work on a slow rate compared with other pre-treatment methods (Saini et al., 2015; Sarkar et al., 2012). The low process cost and low energy consumption are the major advantages of biological pre-treatment because this method does not require additional chemicals and applied pressure owing to the less mechanical assistance. Furthermore, biological pre-treatment does not cause corrosion to the equipment and it does not produce a high amount of inhibitors (Alvira et al., 2010; Brownstein, 2014). However, the main disadvantage of biological pre-treatment is its supremely low degradation rate to attain a high degree of lignin degradation (as long as a few months). This leads to delays in the subsequent processes (hydrolysis and fermentation), which leads to delays in obtaining the final product (bioethanol) (Zhao et al., 2011). Therefore, there is a need to develop efficient biological pre-treatment methods, considering that it is one of the

most economical techniques to pre-treat biomass in the bioethanol industry (Canilha et al., 2012; Chiaramonti, 2007).

Studies have shown the favorability of biological pre-treatment. Studies (Emtiazi et al., 2001; Pérez et al., 2002; Shide et al., 2004) have shown that the use of *Aspergillus terreus*, *Trichoderma* spp., *Cyathus stercoreus*, and *Lentinus squarrosulus* successfully degraded lignin and holocellulose by 65–80% and 45–75% respectively, at a temperature of 25–35°C for 3–22 days. Sindhu et al. (2016) studied the effectiveness of white-rot fungi in decomposing lignocellulosic biomass and enhancing the subsequent enzymatic hydrolysis process. The results showed that *Irpex lacteus* (a white-rot fungus) was able to degrade lignin by 43.8% and the sugar yield from the subsequent enzymatic hydrolysis was found to increase sevenfold.

2.8.1.4.Thermochemical pre-treatment

Direct combustion is used in thermochemical pre-treatment, which is a simple pre-treatment for biomass. This pre-treatment generally depends on the biomass properties, including volatile content, moisture content, fixed carbon content, concentrations of impurities (S, N, Cl), and ash content, all of which influence the techno-economic factors of bioethanol production (Badger, 2002; Berg, 2013; Harmsen et al., 2010). The combination of low-cost feedstock and thermochemical pre-treatment for bioethanol production can promote future security in terms of energy, economy, and infrastructure (Naik et al., 2010). **Figure 2.11** shows the types of thermochemical processes used to convert lignocellulosic biomass into liquid, solid, and gaseous fuels (Peng et al., 2011). Several thermochemical pre-treatment methods commonly used for bioethanol production are also discussed below.

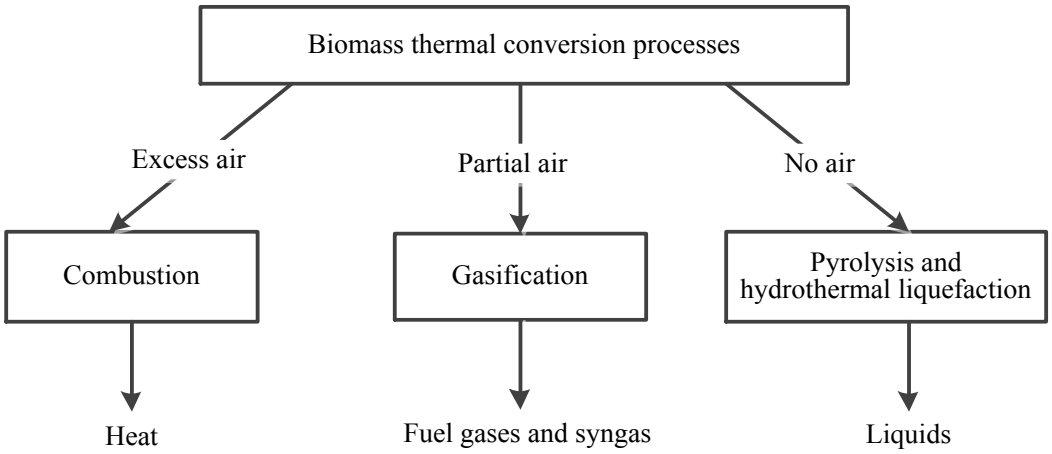

Figure 2.11: Thermochemical pre-treatment methods used to convert lignocellulosic into fuels (Peng et al., 2011)

2.8.2. Hydrolysis

Hydrolysis is a process that breaks down complex sugar structures in the biomass (e.g., polysaccharides in starch and lignocellulose) into the simplest sugar monomers such as xylose and glucose. In general, the main purpose of hydrolysis is to produce fermentable sugars suitable for the fermentation microbes in the fermentation process, which is carried out after the hydrolysis process. Hydrolysis is necessary because microbes are only able to convert the certain types of sugar monomers into ethanol (Mahalaxmi & Williford, 2012; Vohra et al., 2014). The common types of hydrolysis methods are described in the following sub-sections.

2.8.2.1. Dilute acid hydrolysis

Dilute acid is typically used to hydrolyze lignocellulosic biomass because acid is capable of degrading the lignocellulosic structure of the biomass into fermentable sugars. Dilute acid hydrolysis uses ~1% of the acid concentration to degrade the biomass and it yields around 50% of glucose as the final product (Badger, 2002; Graf & Koehler, 2000; Morikawa et al., 2014). Based on the composition of lignocellulosic biomass, dilute acid hydrolyzes hemicellulose and cellulose in different ways. In a mild hydrolysis environment, hemicellulose is degraded by the dilute acid, releasing xylose

monomers (5-carbon sugar). Cellulose requires a higher temperature for the dilute acid to degrade the complex structure of cellulose, resulting in glucose monomers (6-carbon sugar) (Balat et al., 2008). Dilute acid hydrolysis is a feasible method for a continuous-production bioethanol plant; however, prior size reduction of the feedstock is required. In general, dilute acid hydrolysis produces sugar monomers within a reasonable period. However, it is still a challenge to obtain high sugar yields using this method (Badger, 2002). In addition, this method produces inhibitors such as acetate, furfural, hydroxyl benzaldehyde (HBA), and 5-hydroxymethyl furfural as by-products, which are harmful for the fermentation microorganisms (Rao et al., 2006).

2.8.2.2. Concentrated acid hydrolysis

In this method, a concentrated acid (concentration of more than 10%) is used to hydrolyze lignocellulosic biomass at room temperature. Concentrated acid hydrolysis produces a higher sugar yield compared with dilute acid hydrolysis and it is a more cost-effective hydrolysis process. Despite the high sugar recovery and ability of the acid to be recovered and deconcentrated, concentrated acid hydrolysis requires extreme care especially during handling because concentrated acid is extremely hazardous to human health and the environment (Balat et al., 2008; Refaat, 2012).

The chemical reactions for the hydrolysis process of a carbohydrate to become glucose has two stages, namely the liquefaction and saccharification stages. The chemical reactions of hydrolysis can be seen in the equation below.

Liquefaction process used the catalyst α-amylase enzyme or acid

$$(C_6H_{10}O_5 5)_{1000} \quad \rightarrow \quad 100(C_6H_{10}O_5)_{10}$$

Carbohydrates Dextrin

Saccharification process used the catalyst amyloglucosidase or acid

$$(C_6H_{10}O_5)_{10} + 5H_2O \rightarrow 5(C_{12}H_{22}O_{11})$$

Dextrin water Maltosa

A high glucose yield can be obtained from acid hydrolysis of wood fibers, whose cellulose has been soaked at room temperature in high concentration sulfuric acid of 72% (w/w), with aqueous sulfuric acid under reflux at 6% (w/w) concentration (**Figure 2.12**). The hydrolysis with the presence of a high concentration of acid (e.g. 20% sulfuric acid) at high hydrolysis temperature will break polysaccharides into monosaccharides. Decomposition reactions follow next, in which furfural formation can occur. Furfural can be separated through distillation, and its formation from pentose or pentosans can be quite significant. 5-(hydroxymethyl)-2-furfural is non-volatile furfural formed as the result of hexoses and polymers of hexoses, including glucomannans, starch, and cellulose. It can be further decomposed to levulinic acid and other compounds (Bajpai, 2018). These reactions are summarized in **Figure 2.13**.

In addition, the use of concentrated acid can corrode the production equipment, which can lead to financial losses in the long term. This method is claimed to have shorter processing times (Iranmahboob et al., 2002) although others have argued that the hydrolysis period is longer compared with that for dilute acid hydrolysis (Graf & Koehler, 2000).

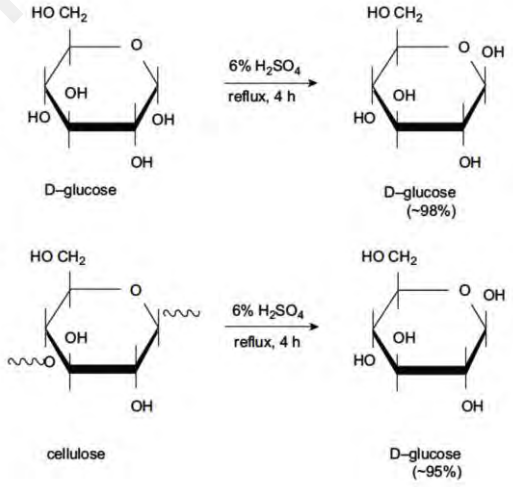

Figure 2.12: Dilute acid hydrolysis of glycosidic linkages (Bajpai, 2018).

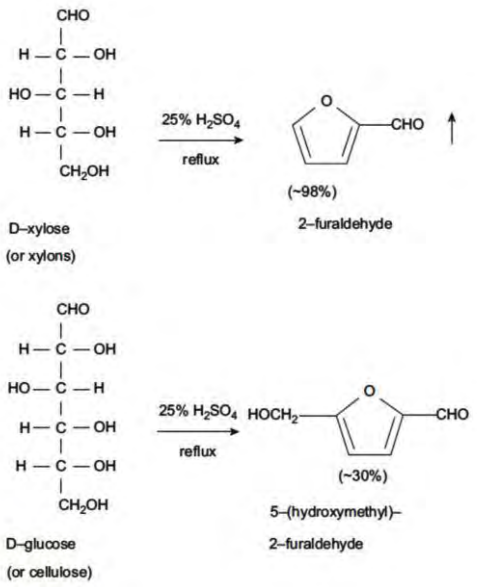

Figure 2.13: Decomposition of carbohydrates by strong acids (Bajpai, 2018).

2.8.2.3. Enzymatic hydrolysis

Enzymatic hydrolysis is another common method used for bioethanol production. In this process, a specific type of enzyme is used, depending on the component of the biomass. For example, cellulase is used to hydrolyze cellulose whereas amylase is used to hydrolyze amylose. This hydrolysis method is a complex degradation process (especially for lignocellulosic materials) in order to release the simplest, fermentable sugar monomers. For lignocellulosic biomass, enzymatic hydrolysis works in three ways: (1) The biomass is first deformed physically and chemically; (ii) The biomass surface degrades, releasing less-complex sugars in the solution; (3) The less-complex sugars released in the solution are hydrolyzed into sugar monomers (Mosier et al., 2002).

In general, enzymatic hydrolysis is highly favorable for bioethanol production. Enzymatic hydrolysis can be operated in a mild hydrolysis environment (pH: ~4.8, temperature: ~318–323 K). Enzymatic hydrolysis produces higher sugar yields compared with acidic hydrolysis and it does not tend to corrode the processing equipment (Sun, 2002). The high cost of enzymes indeed drives the cost of enzymatic

hydrolysis and ultimately, the overall bioethanol production cost. However, the rapid development of enzymes (triggered by the favorability of enzymatic hydrolysis) coupled with the advancement of technologies has made the use of enzymes economically viable for hydrolysis, which in turn, will promote bioethanol production (Pan et al., 2005). Enzymes such as cellulase can be extracted from fungi and bacteria. *Trichoderma reesei, Trichoderma longibrachiatum,* and *Trichoderma viride* have been recorded as cellulase-producing fungi, where cellulose and hemicellulose are used as the food source (Gusakov et al., 2007) Meanwhile, the typical cellulase-producing bacteria are *Acetovibrio*, *Bacteriodes*, *Bacillus*, *Cellulomonas*, *Clostridium*, *Erwinia*, *Microbispora*, *Ruminococcus*, *Streptomyces*, and *Thermomonospora* (Sun, 2002).

Tye, Lee, Wan Abdullah, and Leh (2012) used kapok fibers (*Ceiba pentandra*) as the feedstock and commercial cellulase enzymes in order to obtain a high yield of fermentable sugars. They observed that the cellulase altered the complex structure of the kapok fibers, producing a reducing sugar yield of 85.2% with prior acidic pre-treatment. In an attempt to produce third-generation bioethanol, Tan and Lee (2014) performed enzymatic hydrolysis on seaweed solid wastes. The results showed that enzymatic hydrolysis produced very high glucose content of 99.8% for very mild hydrolysis conditions (pH: 4.8, temperature: 50°C). Following this, they performed fermentation on the produced glucose, resulting in an ethanol yield of 55.9%. However, with small modifications (i.e., simultaneous saccharification and fermentation (SSF), a higher ethanol yield (90.0%) was obtained from the seaweed wastes. This shows that enzymatic hydrolysis can be enhanced using a suitable pre-treatment and biomass feedstock.

2.8.3. Fermentation

Fermentation is a process where the biomass feedstock is converted into bioethanol by bacteria, yeast, or fungi. By digesting fermentable sugars, these

organisms produce ethyl alcohol and other by-products (Balat et al., 2008; Mahalaxmi & Williford, 2012; Vohra et al., 2014). *Saccharomyces* spp. and *Pichia* spp. are the most common yeasts used for bioethanol production, whereas *Zymomonas* spp. and *Escherichia* spp. are the most commonly used bacteria for this purpose. *Aspergillus* spp. are the most common fungi employed in the fermentation process in order to produce bioethanol (Brownstein, 2014). Fermentation microorganisms are able to convert specific types of sugar monomers into ethanol, namely, hexoses (C6 sugars), and pentoses (C5 sugars). Hexoses are the fermentable sugars in first- and second-generation bioethanol production whereas pentoses (C5) are the fermentable sugars in second-generation bioethanol production (Kang et al., 2014). As one of the most employed yeasts, *Saccharomyces cerevisiae* is able to theoretically produce 90% of ethanol from glucose (Wyman & Yang, (2009). According to Abbi et al.(1996), *Saccharomyces cerevisiae* is able to ferment hexose, while the yeasts *Pichia stipitis*, *Pachysolen tannophilus*, and *Candida shehatae* can be used to ferment xylose into ethanol efficiently. The yeast *Kluyveromyces marxianus* is able to withstand a high temperature range of 45–52°C and it is capable of digesting a wide variety of sugar monomers such as xylose, mannose, arabinose, and galactose (Martin et al., 2007; Sarkar et al., 2012). With technological advancements, engineering microbes are now being used to enhance the conversion of sugar monomers into bioethanol. The use of engineering microbes enables more substrates to be digested, producing higher ethanol yields.

Fermentation is the last step in conventional bioethanol production and it is carried out after the biomass has been pre-treated and completely hydrolyzed. However, with technological advancements, efforts have been made to improve the fermentation process in order to boost the ethanol yield and improve the efficiency of the production process.

2.8.3.1. Simultaneous saccharification and fermentation

The SSF technique only requires a fermentation reactor to minimize the production of inhibitors by combining the saccharification and fermentation processes simultaneously, which will reduce the overall bioethanol production cost (Korzen et al., 2015; Sarkar et al., 2012; Soccol et al., 2011). Enzymatic hydrolysis of the biomass is carried out in a single reactor and once the process is complete, the fermentation agent converts the released sugar monomers into ethanol. In terms of the process stream, SSF shortens the production period, which enhances the production efficiency. In addition, the accumulation of ethanol in the reactor does not inhibit the hydrolysis activity, which makes SSF a favorable method for bioethanol production (Kura, 2014; Soccol et al., 2010). However, this fermentation method is limited by the respective operating conditions of the hydrolysis and fermentation processes, and it can be quite challenging to ensure that the conditions are optimum for both processes (Olofsson et al., 2008). In standard practice, hydrolysis is best to be carried out at ~50°C, but fermentation requires warm, mild temperatures (28–37°C) to sustain the fermentation microbes. Hence, it is challenging to fulfill the desired conditions for both hydrolysis and fermentation processes. **Figure 2.14** shows the flow chart of the SSF process (Wingren et al., 2003).

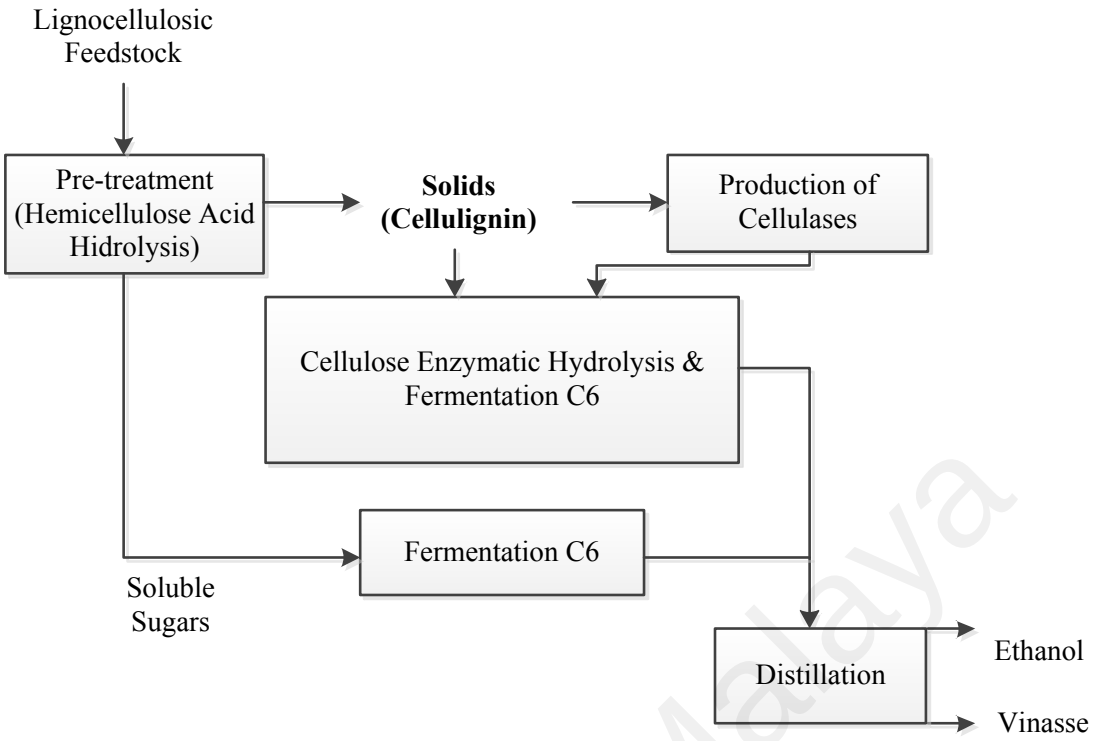

Figure 2.14: Flow chart of the simultaneous saccharification and fermentation process (Wingren et al., 2003)

2.8.3.2. Separate hydrolysis and fermentation

Unlike SSF, SHF is carried out in different vessels, where each one performs a specific task (Sarkar et al., 2012; Soccol et al., 2010). SHF allows the hydrolysis and fermentation processes to be carried out at their respective optimum conditions, which maximizes the reducing sugar yield and ethanol yield. For instance, with SHF, hydrolysis can be performed at the optimum temperature range of 45–50°C while fermentation can be performed ~30°C without any hassle. SHF also allows fermentation of sugars according to type. The hydrolysate first flows into the first vessel to ferment the glucose content of the hydrolysate by glucose-fermenting microbes. The process then continues, where the solution is distilled and flows into the second fermentation vessel to ferment the next sugar type by specific fermentation microbes (Vohra et al., 2014). The SHF technique is considerably cost-effective in terms of the substrates and the high ethanol yield, although it may not be cost-effective in terms of the installation,

operation, and maintenance of equipment (Liu et al., 2014; Sarkar et al., 2012). **Figure 2.15** shows the flow chart of the SHF process (Wingren et al., 2003).

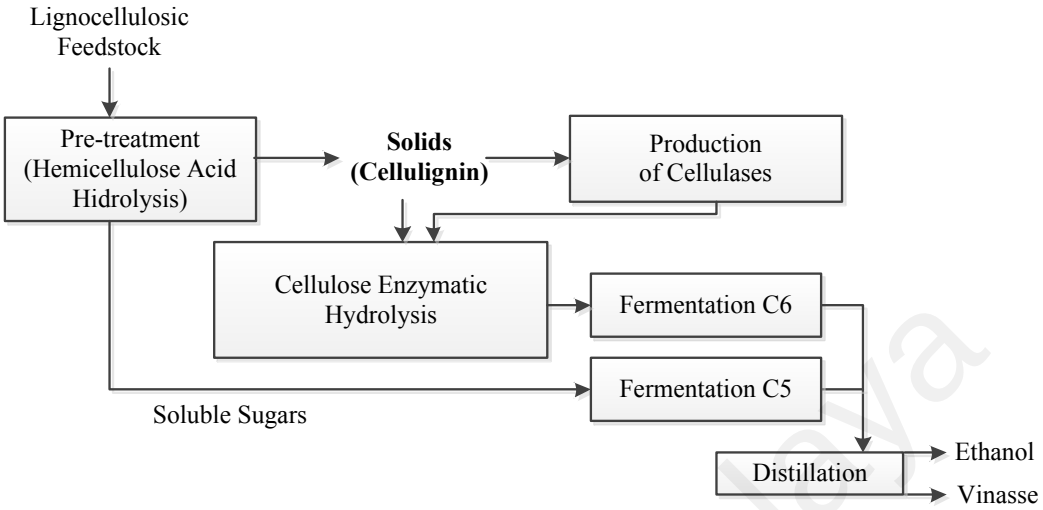

Figure 2.15: Flow chart of the separate hydrolysis and fermentation process (Wingren et al., 2003)

2.8.3.3. Simultaneous saccharification and co-fermentation

This fermentation technique is based on the integration principle, where mixed microbes are used to ferment more than one type of sugar (e.g., pentoses and hexoses) obtained from the pre-treatment and hydrolysis processes (Buruiana et al., 2013; Sarkar et al., 2012). The use of mixed microbes is limited by the ability of each fermentation microbe. For example, hexose-fermenting microbes usually grow faster than pentose-fermenting microbes, which leads to a higher rate of ethanol conversion from hexose (Brownstein, 2014). SSCF offers a number of benefits such as lower enzyme requirement, faster production rate, and lower production cost because the process is performed in a single reactor (Soccol et al., 2010). However, SSFC requires stringent control because each fermentation microbe in the mixed microbes may require a different optimum temperature. In addition, there is a need to control the conditions of the hydrolysis and fermentation processes because these processes are carried out in the same reactor (Balat & Balat, 2009). *Candida shehatae*, *Saccharomyces cerevisiae*,

Escherichia coli KO11, and *Escherichia coli* FBR5 are some of the microbes that are used together in the SSCF technique to produce bioethanol from various biomasses such as barley hull and wheat straw (Gupta & Verma, 2015; Karagöz et al., 2012; Kim et al., 2008; Saha & Cotta, 2006). **Figure 2.16** shows the flow chart of the SSCF process (Wingren et al., 2003).

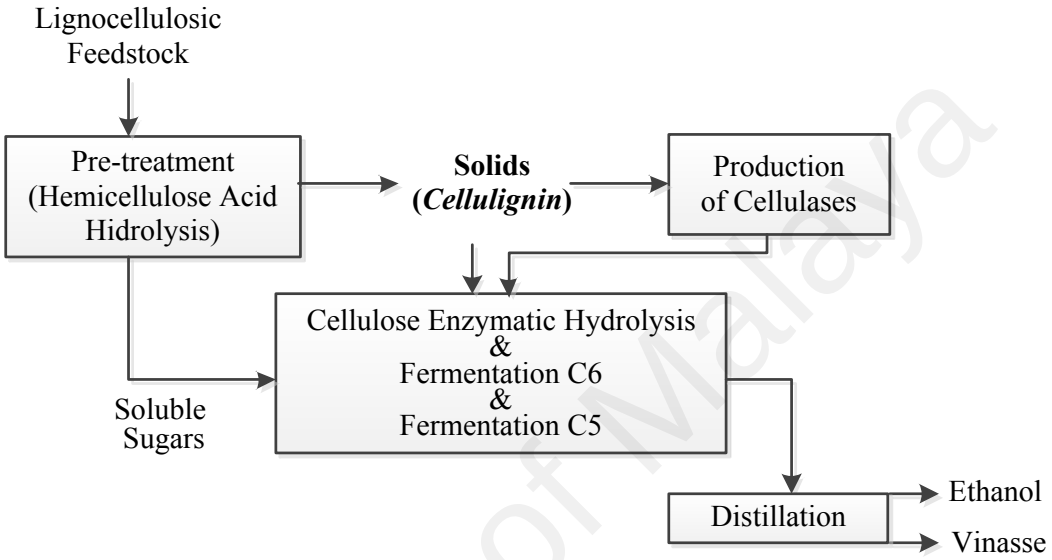

Figure 2.16: Flow chart of the simultaneous saccharification and co-fermentation process (Wingren et al., 2003)

2.8.3.4. Consolidated bioprocessing

Consolidated bioprocessing (CBP) is a bioethanol production method where the production of enzymes, enzymatic hydrolysis, and biomass fermentation are carried out in the same reactor. This method is also known as direct microbial conversion (DMC) (Taherzadeh & Karimi, 2008). In general, a specific microorganism species is used in the CBP technique. This microorganism species is able to perform an array of tasks, which eliminates the need for additional flowing or removal process to another reactor. For example, in order to convert lignocellulosic biomass into bioethanol, the production of cellulose enzymes, hydrolysis of cellulose, and fermentation of the sugars produced from the hydrolysis process are performed by one type of microorganism. This method is a low-cost route to convert cellulosic biomass into bioethanol with high rates and

acceptable yields (Gupta & Verma, 2015; Limayem & Ricke, 2012; Vohra et al., 2014); however, others have reported that CBP is disadvantageous because of its long processing times and low ethanol yields (Gupta & Verma, 2015; Vohra et al., 2014). With CBP, it is not necessary to add external cellulose enzymes into the pre-treatment and hydrolysis processes (Baeyens et al., 2015; Sarkar et al., 2012; Vohra et al., 2014). The common microorganisms used for the CBP method are *Thermoanaerobacter ethanolicus*, *Clostridium thermohydrosulfuricum*, *Thermoanaerobacter mathranii*, *Thermoanaerobium brockii*, and *Clostridium thermosaccharolyticum.* The ability of these microorganisms to perform multiple tasks (enzyme production, enzymatic hydrolysis, and fermentation) and their ability to withstand extreme temperatures render them favorable for low-cost lignocellulosic biomass-to-ethanol conversions (Sarkar et al., 2012). One study (Cardona & Sánchez, 2007) has reported a potential yeast strain (*Kluyveromyces marxianus*) for the CBP method. This yeast strain resulted in a good growth of endoglucanase and β-glucosidase enzymes on the cell surface even at a high temperature of 48°C. The ethanol was produced from β-glucan (which is a cellulosic material), with a yield of 0.47 g ethanol/g consumed carbohydrate. However, the microorganisms typically used for the CBP method are not recommended for large-scale bioethanol production (i.e., high ethanol yields) and therefore, engineering microbes are needed to promote the applicability of this method (Chan et al., 2007; Goel et al., 2013). **Figure 2.17** shows the flow chart of the CBP process (Wingren et al., 2003).

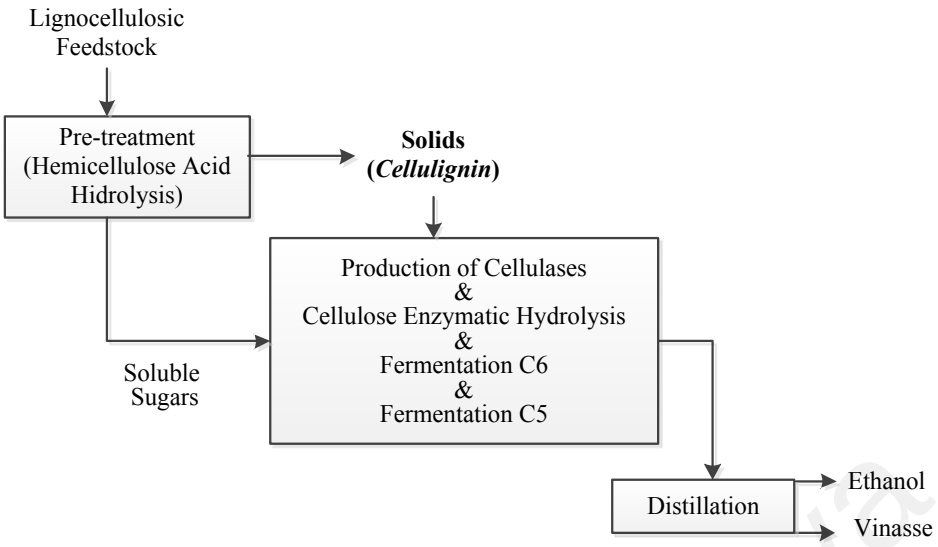

Figure 2.17: Flow chart of the consolidated bioprocessing process (Wingren et al., 2003)

2.8.4. Distillation and dehydration

Distillation is required in bioethanol production to separate the ethanol content from the product of the fermentation process based on the boiling point of ethanol (78.3°C). In water-ethanol distillation, ethanol will vaporize before water because of its lower boiling point (Balat et al., 2008; Onuki, 2006). In a typical bioethanol refinery, the fermentation product flows to the distillation column for distillation, and the product from this process flows into the rectifier and concentrated to below the azeotropic point (Tanthapanichakoon & Jian, 2012; Wooley et al., 1999). Meanwhile, the remaining undistilled fermentation product flows into the stripping column to remove water. Afterwards, the product of this process is combined with the ethanol produced from the previous process (Gabriel & El-Halwagi, 2013). Consequently, the bioethanol recovery process produces bioethanol with a purity of ~99.6% (Balat, 2011). The solid compounds of the product are separated using a centrifuge (McAloon et al., 2000). Distillation (bioethanol recovery) is an energy-intensive process, which requires high volumes of cooling water and the average water consumption is 4 gal water/gal ethanol produced (Jain & Chaurasia, 2014).

Dehydration is advantageous to remove the remaining water in the azeotropic phase (Madson & Monceaux, 1995; Zhang, 1999). Dehydration is quite similar to extractive distillation because this process uses additional component, which lowers the heterogeneous boiling azeotrope (Kiss et al., 2012). Before the dehydration process, the ethanol is first distilled to achieve a purity of more than 96%, and then the ethanol is filtered through molecular sieves, which absorbs water from the mixture (Tanthapanichakoon & Jian, 2012). The result of this process is an upgraded ethanol product. The used molecular sieves can be recycled by heating the sieves to remove the absorbed water (Soccol et al., 2011).

2.9. Properties of bioethanol

The quality of an engine fuel can be assessed based on its physicochemical properties (Tutunea et al., 2014). The specifications of the bioethanol blending with gasoline are given in the ASTM D4806 standard (**Table 2.2**) while the comparison between the properties of bioethanol and gasoline are presented in **Table 2.3** (Masum et al., 2013).

Table 2.2: Specifications of the bioethanol blending with gasoline given in the ASTM D4806 standard (RFA, 2018)

Quality Parameter	Limits	ASTM Test Methods
Ethanol, % by volume, min	92.1	D5501
Methanol, % by volume, max	0.5	D5501
Solvent washed gum, mg/100mL, max	5	D381
Water content, % by volume, (% by mass), max	1.0 (1.26)	D7923, E1064 or E203
Inorganic Chloride, mg/kg (mg/L), max	6.7 (5)	D7319 or D7328
Copper, mg/kg, max	0.1	D1688
Acidity, as acetic acid, mg/kg, (% by mass) [mg/L], max	70 (0.0070) [56]	D7795
pHe	6.5 – 9.0	D6423
Sulfur, mg/kg, max	30**	D5453
Existent Sulfate, mg/kg, max	4	D7318, D7319 or D7328

** EPA Tier 3 Regulations reduced this parameter to 10. mg/kg, maximum

Table 2.3: Properties of bioethanol and gasoline (Masum et al., 2013)

Property	Unit	Gasoline	Ethanol
Chemical formula	—	C_5–C_{12}	$C_2H_5O_H$
Molecular weight	kg/kmol	114.15	46.07
C-fraction	%(m/m)	87.4	52.2
O-fraction	%(m/m)	0	34.7
H-fraction	%(m/m)	12.6	13
H/C	atom ratio	1.795	3
O/C	atom ratio	0	0.5
Specific gravity	–	0.70–0.78	0.794
Density at 15°C	kg/m^3	750–765	785.0–809.9
Stoichiometric air-fuel ratio	w/w	14.2–15.1	8.97
Kinematic viscosity	mm^2/s	0.5–0.6	1.2–1.5
Reid vapor pressure at 37.8°C	kPa	53–60	17
Research octane number	—	91–100	108.61–110.00
Motor octane number	—	82–92	92
Cetane number	—	8	5–20
Enthalpy of formation			
(a) Liquid	kJ/mol	−259.28	−224.1
(b) Gas	kJ/mol	−277	−234.6
Higher heating value	MJ/kg	47.3	29.7
Lower heating value	MJ/kg	44	26.9
Latent of vaporization	kJ/kg	380–400	900–920
Specific heat			
(a) Liquid	kJ/kgK	2.4	1.7
(b) Vapor	kJ/kgK	2.5	1.93
Freezing point	°C	−40	−114
Boiling point	°C	27–225	78
Flash point	°C	−45 to −13	12–20
Autoignition temperature	°C	257	425
Vapor Flammability Limits	%(v/v)	0.6–8.0	3.5–15.0
Laminar flame speed at 100 kPa, 325 K	cm/s	~33	~39
Distillation			
(a) Initial boiling point	%	45	78
(b) 10	%	54	78
(c) 50	%	96	78
(d) 90	%	168	79
(e) End boiling point	%	207	79
Water solubility	%	0	100
Aromatics volume	%	27.6	0
Vapor toxicity	—	Moderate irritant	Toxic in large doses
Smoke characteristic	—	Black	Slight to none
Conductivity	—	None	Yes
Color	—	Colorless to light amber glass	Colorless

Some of the properties related to bioethanol and gasoline are discussed below.

2.9.1. Ethanol yield and content

Ethanol yield is a parameter used to evaluate the performance of the bioethanol production (González-García et al., 2010). Ethanol yield can be described in terms of the theoretical and actual/experimental ethanol yields. The theoretical ethanol yield is obtained through stoichiometric calculation of the fermentable sugars and it is usually used as a comparison factor. Meanwhile, the actual ethanol yield is obtained from the actual sugar fermentation process, where the sugar is derived from the hydrolyzed biomass feedstock. The actual ethanol yield depends on the fermentation conditions, particularly the fermentation agents used for the process (Ademiluyi & Mepba, 2013). Therefore, in addition to the selection of the biomass feedstock, the selection of microorganisms also plays a vital role in obtaining a high ethanol yield. The resultant ethanol concentration can be detected by checking the corresponding refractive indexes obtained from the refractometer readings (Han et al., 2013a). The ASTM D4806 standard is used to assess the ethanol yield or content of bioethanols (Küüt et al., 2011).

2.9.2. Acidity or alkalinity

The acidity or alkalinity of a bioethanol is tested by reacting it with phenolphthalein to determine whether the solution is alkaline or acidic. The acidity is expressed as the percentage by mass of acetic acid (International Standard Organization, 2001). The acidity can be determined from the following equation:

$$\text{Acidity} = \frac{0.0006 \times V}{\rho} \tag{2.1}$$

where:

V = Volume of the NaOH solution in milliliters (mL)

ρ = Density of the sample at 20°C in grams per milliliter (g/mL)

0.0006 = Mass in grams of CH_3COOH, which corresponds to 1 mL of NaOH

The acidity or alkalinity of bioethanol describes the concentration of acid-type compounds present in the untested solution, and it is usually regarded as the total acid number (Bates et al., 1950). A high acid content can lead to the formation of gums and lacquers on metal surfaces, which will increase the fuel viscosity. This will impair the fuel circulation in the engine and also cause engine corrosion (Yue, 2009). ASTM D1613 is the standard used to measure the acidity or alkalinity of bioethanols. According to this standard, the acidity or alkalinity of bioethanols should not exceed the permissible limit of 0.007 (% by mass) (RFA, 2018).

2.9.3. Water content

The stability of a bioethanol is dependent on its chemical composition, water content, and temperature (Lapuerta et al., 2007). There are two types of bioethanol based on purity: (1) anhydrous bioethanol, where the water content is less than 1% and (2) hydrous bioethanol, where the water content is within a range of 5−10% (Larsen et al., 2009). Water contamination is possible because of the hydroscopic nature of bioethanol, where the bioethanol tends to absorb water from the atmosphere if it is stored in an open container (Dominik & Rainer, 2007). The water content of bioethanols can be measured according to the ASTM E203 method, where it is specified that the water content should not exceed the permissible limit of 1.0 %(v/v) (McCormick & Parish, 2001).

2.9.4. Denatured content

Denatured ethanol contains added denaturants, rendering the ethanol inconsumable and toxic. These additives also give ethanol an unpleasant taste and foul smell (Reynolds, 2002). These additives are added to the ethanol at a concentration of ~10% after distillation. Denatured ethanol also can be blended with gasoline to improve the octane number of gasoline (Larsen et al., 2009). According to the ASTM D4806

standard, the denatured ethanol content should be within a range of 1.960–4.760 %(v/v) (McCormick & Parish, 2001).

2.9.5. pHe

pHe is the pH of denatured ethanol. In general, it is quite difficult to measure this property because high-quality denatured ethanol is not an aqueous solution (Brown et al., 2010). pHe tests are typically conducted after the denaturing process and the addition of corrosion inhibitors (Spitzer et al., 2009). The procedure of the pHe test is provided in the ASTM D6423 standard method, which also covers the rehydration specifications of the probe in between readings and the repeatability of the results. Here, repeatability refers to the difference between the successive test results obtained by the same operator using the same apparatus under constant operating conditions on identical test materials (Reynolds, 2002). The pHe of bioethanol is within a range of 6.5–9.0 with a confidence factor of 90% and reproducibility of 0.52 (Brown et al., 2010; Dominik & Rainer, 2007).

2.9.6. Octane number

The octane number is a measure of the fuel resistivity towards detonation and self-ignition (Cernat & Elescu, 2013). The octane number can be rated as the motor octane number (MON) or the research octane number (RON), where both of these parameters describe the combustion behavior in the engine high or steady loads (Chiaramonti, 2007; Social & Estratégicos, 2008). As an excellent anti-detonating additive, bioethanol can improve the octane number of gasoline (Sadeghinezhad et al., 2014b; Social & Estratégicos, 2008). According to the ASTM D2700 standard, the MON and RON of ethanol are 92 and 108, respectively, whereas the MONs and RONs of bioethanol-gasoline blends (E5–E60) are within a range of 81–90 and 90–100, respectively (Larsen et al., 2009; Masum et al., 2013).

The physicochemical properties of bioethanols produced from various biomass feedstocks are summarized in **Table 2.4** (Adelekan, 2010; Ademiluyi & Mepba, 2013; Ghanim, 2013; Kheiralla et al., 2011; Küüt et al., 2011; Matuszewska et al., 2013; Prasad et al., 2007). The physcochemical properties of various bioethanol-gasoline blends are summarized in **Table 2.5** (Ghazikhani et al., 2013; Kheiralla et al., 2011; Küüt et al., 2011; Schifter et al., 2011; Siddegowda & Venkatesh, 2013; Tutunea et al., 2014).

Table 2.4: Comparison between the physicochemical properties of bioethanol produced from various biomass feedstocks (Adelekan, 2010; Ademiluyi & Mepba, 2013; Ghanim, 2013; Kheiralla et al., 2011; Küüt et al., 2011; Matuszewska et al., 2013; Prasad et al., 2007)

Property	Unit	Sugar molasses	Sugarcane	Low-quality grains	Cassava tubers	Cassava flour	Palm juice	Sweet sorghum syrup
Boiling point	°C	78.5	78.4	—	78.5	—	—	78
Heat of combustion	MJ/L	23.625	—	—	—	—	—	—
Heat of vaporization	kJ/mol	33.74	—	—	—	—	—	—
Lower heating value	kJ/kg	—	—	—	—	—	—	21.09
Octane rating	—	106–108	—	—	—	—	—	—
Stoichiometric air-fuel ratio	—	9:1	—	—	—	—	—	—
Concentration	—	99.6–99.8	—	—	—	98	96	—
pH	—	—	—	—	5–6	6.78	3-4	5.0
Acidity	mg/L	≤30	—	—	—	—	≤36	—
Water content	%(v/v)	≤0.3	0.378	6.94	—	—	—	—
Viscosity at 40°C	mm^2/s	—	—	—	—	2.2	—	—
Density at 15°C	kg/m^3	789.0 at 20°C	791 at 20°C	816.2	791.0 at 20°C	—	795.0 at 25°C	785.0
Flammability limit	°C	—	—	—	—	—	—	13-42
Flash point	°C	—	13-14	24.5	—	23	—	13
Vapor pressure at 37.5°C	kPa	—	—	14.5	—	—	—	17 at 37.8°C
Autoignition temperature	°C	—	—	—	—	—	—	366
Distillation range	°C	—	—	—	—	78–100	—	—

Table 2.5: Comparison between the physicochemical properties of bioethanol-gasoline blends

Property	Unit	Test method	Gasoline	Low-quality grains (Küüt et al., 2011)		Sugar molasses (Kheiralla et al., 2011)					Sugarcane (Tutunea et al., 2014)	Cassava (Ghazikhani et al., 2013)		
				E58.9	E60	E10	E15	E20	E25	E30	E20	E5	E10	E15
Density at 20°C	kg/cm^3	ASTM D1298	745.4	917.0	908.0	739.6	749.5	754.1	757.1	761.3	759.7	740.8	743.9	746.9
Flash point	°C	ASTM D93	—	24.5	24.5	—	—	29.2	30.0	29.2	—	—	—	—
Lower heating value	MJ/kg	ASTM D240	42.54	—	—	—	—	—	—	—	39.47	43.45	42.51	41.58
Autoignition temperature	°C	—	246.0	—	—	—	—	—	—	—	—	—	—	—
Research octane number	—	ASTM D2699	91.3	—	—	97.1	98.6	100.4	99.5	102.5	93	—	—	—
Motor octane number	—	ASTM D2700	84.0	—	—	—	—	—	—	—	83.4	—	—	—
Distillation temperature		ASTM D86		—										
Initial boiling point	°C		38.8	—	—	—	—	—	—	—	40.5	—	—	—
10% evaporated	°C		68.5	—	—	—	—	—	—	—	62.4	—	—	—
50% evaporated	°C		109.6	—	—	—	—	—	—	—	79.2	—	—	—
99% evaporated	°C		161.5	—	—	—	—	—	—	—	201.4	—	—	—

Table 2.5: (continued 1)

Property	Unit	Test method	Gasoline	Cassava (Siddegowda & Venkatesh, 2013)									
				E10	**E20**	**E30**	**E40**	**E50**	**E60**	**E70**	**E80**	**E90**	**E100**
Density at 20°C	kg/cm^3	ASTM D1298	745.4	750.8	760.5	778.2	779.2	780.5	781.2	782.3	783.4	784.0	789.0
Flash point	°C	ASTM D93	—	−40	−20	−15	−13.5	−5.0	−1.0	0.0	5.0	8.5	12.5
Heating value	MJ/kg	ASTM D240	42.54	—	—	—	—	—	—	—	—	—	—
Auto ignition temperature	°C	—	246.0	260	279	281	294	320	345	350	362	360	365
Research octane number	—	ASTM D2699	91.3	93	94	95	97	99	100	103	104	106	129
Motor octane number	—	ASTM D2700	84.0	—	—	—	—	—	—	—	—	—	—
Distillation temperature		ASTM D86	—	—	—	—	—	—	—	—	—	—	—
Initial boiling point	°C		38.8	—	—	—	—	—	—	—	—	—	—
10% evaporated	°C		68.5	—	—	—	—	—	—	—	—	—	—
50% evaporated	°C		109.6	—	—	—	—	—	—	—	—	—	—
99% evaporated	°C		161.5	—	—	—	—	—	—	—	—	—	—

Table 2.5: (continued 2)

Property	Unit	Test method	Gasoline	Potato waste (Najafi et al., 2009)				Cassava (Schifter et al., 2011)			
				E5	E10	E15	E20	E6	E10	E15	E20
Density at 20°C	kg/cm^3	ASTM D1298	745.4	—	—	—	—	754	757.6	758.6	759.7
Flash point	°C	ASTM D93	—	—	—	—	—	—	—	—	—
Heating value	MJ/kg	ASTM D240	42.54	—	—	—	—	41.41	40.8	40.08	39.47
Autoignition temperature	°C	—	246.0	—	—	—	—	—	—	—	—
Research octane number	—	ASTM D2699	91.3	89.7	92.3	94	99.4	92.8	93.0	92.4	93.0
Motor octane number	—	ASTM D2700	84.0	—	—	—	—	84	83.8	82.8	83.4
Distillation temperature		ASTM D86	—	—	—	—	—	—	—	—	—
Initial boiling point	°C		38.8	40.9	38.9	44	40.8	42.6	47.1	43.2	40.5
10% evaporated	°C		68.5	54.3	53.1	57.2	55.4	61.3	65.1	62.7	62.4
50% evaporated	°C		109.6	93.5	71.9	71.4	71.6	111.4	98.3	87.6	79.2
99% evaporated	°C		161.5	184.1	175.1	182.4	176.6	206.1	191.6	203.6	201.4

2.10. Engine performance and exhaust emissions of bioethanol and bioethanol-gasoline blends

As biomass-derived alternative fuels, the performance of bioethanol used in internal combustion engines has been studied extensively. Parameters of engine performance, namely engine power, BSFC and BTE, have been widely assessed with bioethanol as the alternative fuel. Bioethanol can also be blended with gasoline at different concentrations to enhance the physicochemical properties and combustion performance of the fuels. Several studies support the concept of bioethanol-gasoline blend through extensive investigations, including the engine performance by various compositions of blending. Yücesu et al. (2006) focused on the engine performance of a four-stroke, single-cylinder SI engine and its exhaust emission affected by various blend compositions and engine compression ratio. The experiments were conducted under the following conditions: (1) minimum advanced timing, (2) full load, and (3) stoichiometric air-fuel ratio. The results showed that the engine torque increased by 8% with an increase in compression ratio up to 11:1 relative to 8:1 compression ratio. The highest increase in engine torque (14%) was obtained at a compression ratio of 13:1 using E40 and E60 fuels, relative to a compression ratio of 8:1. The study recorded a low BSFC value for gasoline (E0) at a compression ratio of 11:1 and further decrease of 10% at compression ratio of 8:1. However, when E40 was employed and the largest BSFC decrease of 15% was recorded at engine speed of 2000 rpm. Moreover, for the fuel blending of E60, the BSFC was further decrease by 14.5% and 17% at 3500 and 5000 rpm engine speeds, respectively.

Ghazikhani et al. (2013) investigated engine performance using bioethanol-gasoline blend fuel (ethanol concentration: 5, 10, and 15%) in a two-stroke spark ignition engine at an engine speed range of 2500 to 4500 rpm. From the experiment, they found that employing ethanol in the engine test increases the delivery ratio of mass

fuel and scavenging efficiency due to the rapid ethanol evaporation. Further, this ethanol has properties of rapid evaporation results to a reduction in trapping efficiency, which is possible as this rapid evaporation hinders the inlet path of the air and lowers the air pressure in the intake manifold. The lower ignition delay and a low flash point of bioethanol are the encouraging characteristics, despite its drawback in the lower heating value. Another drawback of blending ethanol in gasoline (e.g. 10 and 15% for half and 75% of full engine load) is increases the BSFC. However, 5% of ethanol content in the blend at high engine speed range (2500, 3000 and 4500 rpm) recorded for a reduction of BSFC.

Delivery ratio is a parameter for describing the scavenging process in two stroke engines. It can be defined as :

$$= \frac{\text{mass of delivered mixture per cycle}}{\text{reference mass}} \tag{2.2}$$

$$= \frac{\text{mass of delivered mixture per cycle}}{\text{displacement} \times \text{ambientdensity}} \tag{2.3}$$

Scavenging efficiency indicates to what extent the residual gases in the cylinder have been replaced with fresh air as follows definition

$$_{sc} = \frac{\text{mass of delivered mixture retained}}{\text{mass of trapped cylinder charge}} \tag{2.4}$$

useful and applicable equation for experimental purposes for scavenging efficiency is presented by Ganesan (2012)

$$_{\text{sc}} = \frac{\dot{m}_a \ (\text{kg/min})}{\text{N (rpm)} \times \rho_{\text{sc}} \times V_{\text{total}}} = \frac{\dot{m}_a \ (\text{kg/min})}{N(rpm) \times \frac{p}{287 \times T_0} \times V_d \times \frac{r}{r-1}} \tag{2.5}$$

There was a significant reduction in the CO emissions (35%) for the blend with an ethanol concentration of 15%. Schifter et al. (2011) performed an engine performance test and analysis (parameters BSFC and BP) as well as exhaust emissions (CO, HC, and NO_x) of ethanol-gasoline blends at different lambda values. The engine test was

conducted by varying blending composition, minimum load, and 2000 rpm engine speed. CO and HC were found reduced by 52 and 19% respectively using 20% ethanol concentration in the blend, while 60% of NO_x increased. The results showed that due to the higher heat release rate the NO_x emissions were higher for the fuel blends compared with those for gasoline. Topgül et al. (2006) studied the engine performance using various ethanol-gasoline blends (E0 to E60), as well as their effect on the emissions and ignition timing. The experiments were performed under the following conditions: (1) variable compression ratio: 8:1, 9:1, and 10:1, (2) constant engine speed: 2000 rpm, and (3) fully opened throttle. For the E0 fuel, engine knock was occurred at 10:1 compression ratio and by advancing the ignition timing to 24° crank angle (CA). However, knocking phenomenon disappeared using E40 and E60 at ignition timing of 36° CA. Yüksel and Yüksel, (2004) tested bioethanol-gasoline blend in a four-cylinder spark ignition engine of 60% ethanol + 40% gasoline by modifying the throttle valve opening of the carburetor (25, 50, 75, and 100%). The experimental results shows 20% increase of CO_2 emissions whereas the NO_x emissions decreased under certain operating conditions. In addition, CO and HC emissions decreased by 80 and 50% respectively using the blend, whereas 20% increase of CO_2 was recorded depending on the engine conditions. Yusaf et al. (2009) performed experiments on a four-stroke, four-cylinder KIA 1.3 single overhead camshaft spark ignition engine. The results indicated that as the ethanol percentage in the blend increased the BTE increased accordingly. The maximum BTE was ~35% at 3500 rpm for the blend with an ethanol concentration of 20%. The volumetric efficiency reached by 95% for 20% ethanol in the gasoline ethanol blend at 3500 rpm. The BSFC was the lowest (0.25 kg/kWh) at 3500 rpm for the blend with an ethanol concentration of 20%. The CO_2 emissions increased (13.8 %(v/v)) at 3000 rpm owing to the improved chemical properties of the ethanol. In contrast, the CO emissions decreased (45.42%) at 3000 rpm. The main reason is the increase of oxygen

in the ethanol-gasoline blend, despite the fuel-rich combustion. As a product of an inadequate combustion, the production of HC as ethanol is introduced to the fuel reduced the HC emissions (125 ppm) at 3000 rpm owing to the greater oxygen load in the fuel blend, and this promotes a more complete combustion. When combustion occurs at the air-fuel ratio near stoichiometric, the flame temperature increases. From here it can be expected that the formation of NO_x will increase. This is mainly because the slightly increased in excess air ratio (air-fuel ratio, λ=1.25) contributes to the improved mixing homogeneity and more complete combustion has achieved, which consequently avails the enhancement of the indicated thermal efficiency (ITE). The addition of dimethyl ether (DME) with ethanol could reduce HC emissions from all SI engine operations, and could reduce CO emission at the combustion condition of $\lambda >$ 1.00. However, NOx emissions increase averagely by 10% with the addition of DME (Liang et al., 2012). Saleh and Al-Zubaidi (2018) conducted experiments on a spark ignition engine at 8:1 compression ratio. Bioethanol was blended with gasoline at a concentration of 10%. At that blend level, they found an improvement in the volumetric efficiency, which can be attributed to the –OH molecules in the chemical structure of ethanol. Volumetric efficiency increased from 85% to 90%. In addition, increasing amount of oxygen in the combustion chamber improved the combustion quality. Moreover, the high heat of evaporation of ethanol prolongs the time for the fuel mixture to evaporate. Because of this more air can be added into the combustion chamber, which improves the volumetric efficiency of the engine.

In a diesel engine, ethanol is also a favorable fuel additional to diesel fuel since it is a low-cost oxygenated compound. Another reason for adding ethanol in diesel fuel blend is due to ability to be produced from renewable sources and low toxicity (Pang et al., 2008). Can et al. (2004) studied compression ignition engine performance and exhaust emissions using ethanol-diesel fuel blends. The engine test was conducted at

various fuel injection pressures, turbocharged at full load. The results revealed that ethanol added to diesel fuel will reduce CO and SO_2 emissions and soot. However, it increased the NO_x emissions.

Based on the literature survey, it can be deduced that much effort has been made to investigate the engine performance and exhaust emission under influence of various composition of ethanol-gasoline blends in spark ignition engines. Broadly, by adding ethanol into gasoline fuel increases BSFC in spark ignition engines, thanks to the lower heating value and the ethanol-gasoline fuel blend stoichiometric air-fuel ratio. The latter indicates the requirement of supplying more fuel to achieve a desired equivalence ratio and to gain the same power level produced as that of gasoline-fueled spark ignition engine (Koç et al., 2009). The increase in BSFC is also due to the lower energy content in the blends. Furthermore, there are differences in the BSFC between gasoline and ethanol-gasoline blends, where the BSFC tends to decrease with an increase in engine speed until it reaches a minimum value. The BSFC tends to decrease with an increase in the percentage of ethanol in the ethanol-gasoline blend at all engine speeds because of the oxygen content of ethanol, which improves combustion and enhances the power output compared with gasoline. Oxygenates (organic oxygen-containing compounds) are one of the most important fuel additives to improve fuel efficiency (Eyidogan et al., 2010). The use of oxygenates makes more oxygen available during the combustion process, which has great potential to reduce the exhaust emissions of spark ignition engines (Iliev, 2018). The BSFC is lower for ethanol-gasoline blends compared with that for gasoline, which enables higher compression ratios and increases the engine power output, as well as increases the resistance to engine knocking (Stein et al., 2013).

BP is one of the parameters that is used to assess the engine performance. In general, as the engine speed increases the BP increases accordingly for all fuel blends (El-Faroug et al., 2016). However, owing to the improved combustion quality and lower

temperature in the intake manifold, the engine power is higher for ethanol-gasoline blends (Pikunas et al., 2003). In general, ethanol will ignite faster than gasoline and therefore, an engine burning ethanol will produce more power. In addition, the higher octane rating of ethanol will help improve the efficiency of converting the combustion energy into mechanical power (Iliev, 2018).

The BTE for ethanol-gasoline fuel blends increases respectively with the increase in engine speed it reaches a maximum value, and then it decreases as the engine speed increases further. However, such is not the case for pure gasoline, where the effect of mechanical loss is more significant. Ethanol-gasoline blends have higher BTE compared with gasoline, which will provide more BP for the same amount of fuel consumed. In addition, since compared with gasoline the higher octane number in ethanol makes it possible to achieve higher compression ratios, which will boost the BTE of the engine (Wang et al., 2017).

To date, there are numerous studies on ethanol-gasoline blends. Ethanol offers a number of advantages compared with gasoline, which include reducing HC and CO emissions, and minimizing the possibility of engine knocking (Canakci et al., 2013; Iodice et al., 2016). The reduction in CO emissions is resulted from the low carbon content in ethanol fuel than that in gasoline. In addition, under assumption of similar fuel dispersion characteristics as gasoline, the higher oxygen content in ethanol-gasoline promotes the oxygen-to-fuel ratio, especially during rich combustion. This enhances the combustion quality (Yusaf et al., 2009). However, even though ethanol enhances combustion efficiency of the spark ignition engine, it results in higher CO emissions compared with gasoline because it is an oxygenated fuel (Masum et al., 2013).

Ethanol can reduce HC emissions because of its higher oxygen content and relatively higher relative air-fuel ratio, which improves the combustion characteristics (Elfasakhany, 2015). As the engine speed increases, the combustion temperature

increases, which when combined with the high level of excess oxygen contributed by ethanol in ethanol-gasoline blends, leads to lower HC emissions compared with gasoline (Özsezen, 2016). However, it is worth noting that with ethanol content in the blend it reduces flame temperature, which consequently produces higher HC emissions (Al-Hasan, 2003). Moreover, it has been shown that ethanol-gasoline blends with higher ethanol concentrations produced higher HC emissions, which may be due to misfiring or flame quenching with more mass of cold air-fuel mixtures (Raja et al., 2015).

Studies have shown that the burning of ethanol or ethanol-gasoline blends may produce higher or lower NO_x emissions. Through studies of physicochemical properties between gasoline and the blends of ethanol-gasoline engine performances parameters that are influenced can be observed, including combustion speed, mass burn fraction, combustion temperature, combustion speed and NO_x emission. Schifter et al. (2011) investigated the influence of ethanol-gasoline fuel blends (ethanol concentration: 0–20%) in a single-cylinder spark ignition engine. The results showed that due to the higher heat release rate, the NO_x emissions were higher for the fuel blends compared with those for gasoline. Najafi et al. (2009) found that the NO_x emissions were higher as the ethanol content was increased in the blend. This can be attributed to the higher oxygen-to-fuel ratio during rich combustion due to the higher oxygen content. Air-fuel ratio is the most significant parameter that affects the NO_x emissions. The oxygen increases in the gasoline bioethanol blends, which is lateral to the increase in ethanol content, rises lambda (air-fuel ratio) to a maximum value of 0.925 for 20% ethanol fuel. As a consequence, the increase in ethanol content leads to an increase in NO_x emission (Schifter et al., 2011). Zhuang and Hong (2013) observed that the NO_x emissions increased for ethanol-gasoline blends (EER 60%) compared with gasoline because of the improved combustion as ethanol is added, which increased the in-cylinder temperature. The effect of higher NO_x emission is due to the higher combustion

temperatures, hence generated higher NO_x fractions in the exhaust emissions. The NO_x emissions increase as the engine compression ratio increases, especially at high engine loads. Furthermore, the increase in NO_x emission is due to the high burning rate of ethanol blend with oxygen-rich mixture, which eventually leads to the high combustion temperature at high engine loads and compression ratio (Zheng et al., 2009a). However, some researchers have observed a different trend for NO_x emissions, where the NO_x emissions decreased in spark ignition engines under influence of ethanol-gasoline blends because of leaner air-fuel mixtures. Saikrishnan et al. (2018) found that the peak pressure decreased and the peak cycle temperature reduced NO_x emissions for ethanol-gasoline blends. Tibaquirá et al. (2018) found that the greater ethanol percentage in ethanol-gasoline blends decreases the air-fuel mixture temperature at the end of intake stroke as it increases the latent heat of vaporization of the blends. Also, the increases in ethanol concentration reduces the energy content of the ethanol-gasoline blends, which reduces the combustion temperature. Because of this, the ethanol-gasoline blends with higher concentrations of ethanol can reduce NO_x emissions due to the lower combustion temperatures, leaner air-fuel mixtures, and ethanol cooling effect (Renzi et al., 2016). The exhaust emissions and engine performance parameters under various types of ethanol blends reported by other researchers are summarized in **Table 2.6**.

Table 2.6: Summary of engine performance parameters and exhaust emissions of internal combustion engines fueled with various types of ethanol blends

No.	Researchers	Ethanol blend(s)	Engine specifications	Operating conditions	Engine performance parameters			Exhaust emissions			
					BSFC	BTE	BP	CO	CO_2	HC	NO_x
1	(Al-Hasan, 2003)	E0–E25 (percentage of ethanol was increased by 2.5%)	Four-cylinder four-stroke spark ignition engine, swept volume: 1452 cm^3	Compression ratio: 9:1, maximum power: 52/5600 (kW/rpm), engine speed: 1000–4000 rpm	Decreased by ~2.4%	Increased by 9.0%	Increased by 8.3%	Decreased by ~46.5%	Increased by 7.5%	Decreased by 24.3%	—
2	(Ceviz & Yüksel, 2005)	E0, E5, E10, E15, and E20	Four-cylinder four-stroke spark ignition engine, bore: 86.4 mm, stroke: 67.4 mm, displacement volume: 1.581 dm^3, type of cooling: water cooling	Compression ratio: 9.2:1, engine speed: 2000 rpm, maximum power: 62/5800(kW/rpm), maximum torque: 13/2900 (Nm/rpm)	—	—	—	Decreased by ~30.1%	—	Decreased by ~20.2%	—
3	(Yücesu et al., 2006)	E0, E40, and E60	Single-cylinder engine, bore: 80.26 mm, stroke: 88.9 mm, compression ratio: 5:1–13:1	Engine speed: 2000, 3500, and 5000 rpm, compression ratio: 8:1–13:1, petrol injection, ignition timing: 70°BTDC[a]–20°ATDC[b], maximum power: 15 kW, maximum engine speed: 5400 rpm	▪ Decreased by 10% for E0 ▪ Decreased by 15% for E40 at 2000 rpm ▪ Increased by 14.5 and 17% at 3500 and 5000 rpm, respectively for E60	—	—	▪ Decreased by 11% for E40 ▪ Decreased by 10.8% for E60	—	▪Decreased by 9.9% for E40 ▪Decreased by 16.45% for E60	—
4	(Yücesu et al., 2007)	E0, E10, E20, E40, and E60	Single-cylinder four-stroke spark ignition engine, bore: 80.26 mm, stroke: 88.9 mm, Tappet clearance: 0.3–0.4 mm, overhead camshaft, no. of vertical valves: 2, type of cooling: water cooling	Compression ratio: 5:1–13:1, engine speed: 2000 rpm, relative air-fuel ratio: 0.8–1.2, ignition timing: 70°BTDC–20°ATDC	▪ BSFC was minimum at a relative air-fuel ratio of 1.05 and compression ratio of 11:1 ▪ Maximum decrease of 15% obtained for E40	—	—	—	—	—	—

Table 2.6: (continued 1)

No	Researchers	Ethanol blend(s)	Engine specifications	Operating conditions	Engine performance parameters			Exhaust emissions			
					BSFC	BTE	BP	CO	CO_2	HC	NO_x
5	(Celik, 2008)	E0, E25, E50, E75, and E100	Single-cylinder four-stroke spark ignition engine, displacement volume: 250 cm^3, compression ratio: 6:1–10:1, type of ignition system: transistorized coil ignition system, type of cooling: air and water cooling	Compression ratio: 6:1, 8:1, and 10:1, engine speed: 1500–4000 rpm	▪ At a compression ratio of 6:1 and engine speed of 2000 rpm, BSFC increased by 10, 19, 37, and 56% for E25, E50, E75, and E100, respectively ▪ Minimum specific fuel consumption (411 g/kWh) was achieved for E0 at a compression ratio of 6:1 and engine speed of 2500 rpm. ▪ At compression ratio of 10:1, BSFC decreased by 3% for E50.	—	▪ At a compression ratio of 6:1 and engine speed of 2000 rpm, BP increased by 3, 6, and 2% for E25, E50, and E75, respectively. ▪ At compression ratio of 10:1, BP increased by 29% for E50.	Decreased by 53% for E50	Decreased by 10% for E50	Decreased by 12% for E50	Decreased by 19% for E50
6	(Al-Baghdadi, 2008)	E0, E5, E10, E15, E20, E25, and E30	Single-cylinder, four-stroke spark ignition engine, bore: 76.2 mm, stroke: 110.0 mm, length of connecting rod: 241.3 mm	Compression ratio: 8:1–9.2:1, engine speed: 1500 rpm, ignition timing: variable	Increased by 4.3% for E30 at a compression ratio of 8:1	Increased by 3.5% at a compression ratio of 8:1 for E30	Increased by 4% at a compression ratio of 8:1 for E30	Decreased by 16% for E30 at a compression ratio of 8:1	Decreased by 10% for E30 at a compression ratio of 8:1	—	Decreased by 56% for E30 at a compression ratio of 8:1

Table 2.6: (continued 2)

No.	Researchers	Ethanol blend(s)	Engine specifications	Operating conditions	Engine performance parameters			Exhaust emissions			
					BSFC	BTE	BP	CO	CO_2	HC	NO_x
7	(Seshaiah, 2010)	E0, E10, E15, E25, E35, K15, K25, K35, and LPG	Single-cylinder spark ignition engine, power: 2.5 BHP[c], bore: 70 mm, stroke: 66.7 mm, compression ratio: 2.5:1–10:1, maximum engine speed: 3000 rpm, type of starter: cranking starter, type of cooling: air cooling	Engine speed: 2400 rpm, compression ratio: 4.6:1, 6:1, 8:1, and 9:1, type of instrument used for load measurements: eddy current dynamometer	—	▪ BTE was highest for E0 and E35 ▪ BTE was lowest for K35	—				
8	(Srinivasan & Saravanan, 2010)	E69.5+0.5, E64.6+0.4, E59.7+0.3, E49.8+0.2[d]	Three-cylinder four-stroke engine, bore: 86.5 mm, stroke: 72 mm, displacement volume: 796 cm^3, compression ratio: 8.7:1, ignition timing: 10°BTDC	Engine speed: 2000–2800 rpm		Increased		Decreased by 0.08 %(v/v)	Decreased by 8 %(v/v)	Increased	Decreased
9	(Eyidogan et al., 2010)	E5, E10, M5, and M10	Four-cylinder four-stroke spark ignition engine, no. of valves: 16, cylinder volume: 1396 cm^3, type of cooling: water cooling	Compression ratio: 10.4:1, wheel power: 5, 10, 15, and 20 kW, vehicle speed: 80 and 100 km/h, maximum torque: 130/4300 (Nm/rpm), maximum power: 66/5600 (kW/rpm)	▪ BSFC increased by 2.8, 3.6, 0.6%, and 3.3% for E5, E10, M5, and M10, respectively, at a vehicle speed of 80 km/h. ▪ BSFC increased by 0.2, 1.5, 1.1, and 1.2% for E5, E10, M5, and M10, respectively, at a vehicle speed of 100 km/h.	▪ BTE increased by 1.9, 2.5, 1.8, and 4.7% for E5, E10, M5, and M10, respectively, at a vehicle speed of 100 km/h. ▪ BTE increased by 0.4, 2.2, and 2.5% for E10, M5, and M10, respectively. ▪ BTE decreased by 0.8% for E5.	—	—	—	—	—

Table 2.6: (continued 3)

No.	Researchers	Ethanol blend(s)	Engine specifications	Operating conditions	Engine performance parameters			Exhaust emissions			
					BSFC	BTE	BP	CO	CO_2	HC	NOx
10	(Park et al., 2010a)	E0, E85, and E0+SRG[e]	Bore: 82 mm, stroke: 93.5 mm, displacement volume: 0.494 L	Engine speed: 1500–2000 rpm, compression ratio: 10.1:1, brake mean effective pressure: 0.4 MPa, idle speed: 700 ± 100 rpm, ignition timing: 3–13 CAD BTDC[f], intake valve open: 9°BTDC, intake valve close: 43°ABDC[g], exhaust valve open: 50°BBDC[h], exhaust valve close: 10°ATDC		▪ Remained unchanged for E85 ▪ Increased for E0+SRG	—	—	Decreased	Decreased	Decreased
11	(Schifter et al., 2011)	E0, E6, E10, E15, and E20	Single-cylinder spark ignition engine, displacement volume: 0.5 L, bore: 86 mm, stroke: 86 mm, compression ratio: 10.5:1	Engine speed: 2000 rpm	Increased	—	—	Decreased by 13.6%	—	Increased by 5%	Increased by 5%
12	(Costa & Sodré, 2011)	E22 and E100	Four-cylinder, eight-valve engine, bore: 70.0 mm, stroke: 64.9 mm, swept volume: 999.057 cm^3	Compression ratio: 10:1–12:1, engine speed: 1500–6500 rpm, ignition timing: 15–35°BTDC, fuel-air mixture equivalence ratio: 1.11	BSFC was higher for E100 compared with that for E22 at all engine speeds	BTE was higher for E100 compared with E22 at all engine speeds	Increased with an increase in compression ratio	—	—	—	—

Table 2.6: (continued 4)

No.	Researchers	Ethanol blend(s)	Engine specifications	Operating conditions	Engine performance parameters			Exhaust emissions			
					BSFC	BTE	BP	CO	CO_2	HC	NO_x
13	(Kumbhar et al., 2012)	E0, E5, E10, and E20	Single-cylinder four-stroke spark ignition engine, displacement volume:100 cm^3, bore: 50 mm, stroke: 50.6 mm	Engine speed: 4000–8000 rpm	Increased	—	At 6000 rpm, the BP increased by 2.31, 2.77, and 4.16% for E5, E10, and E20, respectively, compared with gasoline.	Decreased	—	Decreased	Increased
14	(Liang et al., 2012)	DME0, DME1, and DME2[1]	Four-cylinder spark ignition engine, displacement volume: 1.6 L, bore: 85 mm, compression ratio: 10:1	Engine speed: 1400 rpm, λ: 1.00–1.45	—	—	—	Decreased	—	Decreased by 45% for DME2	Increased by 10%
15	(Datta et al., 2012)	E0, E10, E20, E30, and E40	Single-cylinder four-stroke spark ignition engine, bore: 76.2 mm, stroke: 82.84 mm, type of cooling: air cooling	Compression ratio: 5.3:1	Increased by 20% for E30	Increased by more than 6% for E40	Increased	—	—	—	—
16	(Ghazikhani et al., 2013)	E0, E5, E10, and E15	Single-cylinder two-stroke spark ignition engine, displacement volume: 34 mL, bore: 35 mm, stroke: 35 mm, compression ratio: 6:1	Engine speed: 2500–4500 rpm	Decreased	—	—	Decreased by 71%	Decreased by 6.3%	Decreased by 6%	Decreased by 38%

Table 2.6: (continued 5)

No.	Researchers	Ethanol blend(s)	Engine specifications	Operating conditions	Engine performance parameters			Exhaust emissions			
					BSFC	BTE	BP	CO	CO_2	HC	NO_x
17	(Srinivasan & Saravanan, 2013)	E0, E50+5, and E60+10[j]	Three-cylinder four-stroke multipoint fuel injection engine, bore: 86.5 mm, stroke: 72 mm, no. of engine valves: 6, displacement volume: 796 cm^3	Compression ratio: 8.7:1, engine speed: 2200, 2400, 2600, 2800, and 3000 rpm, maximum power: 35.0/5000 (bhp/rpm), maximum torque: 6.1/3000 (kgm/rpm), water cooling	—	At 2800 rpm, the BTE was higher by 23.24% for the E60+10 blend compared with that for E0.	—	Decreased to 0.08 %(v/v) at 2600 and 3000 rpm	Decreased to 7.9 %(v/v) at 2800 rpm	Decreased to 15 ppm at 2800 and 3000 rpm	Decreased to 224 ppm at 3,000 rpm
18	(Türköz et al., 2014)	E85	Four-cylinder four-stroke spark ignition engine, displacement volume: 1581 cm^3, type of cooling: water cooling	Compression ratio: 9.2:1, engine speed: 2000–4000 rpm, ignition timing: 2–6°, maximum BP: 64.1 kW at 5800 rpm, maximum brake torque: 130 Nm at 2900 rpm, brake torque: 105.6 Nm at 5800 rpm, maximum power: 185 kW	—	—	BP increased for an ignition timing of 4°.	Relatively invariant	Relatively invariant	—	Increased
19	(Masum et al., 2014)	M20, E20, P20, and B20	Four-cylinder spark ignition engine, displacement volume: 1596 cm^3, bore: 78 mm, stroke: 84 mm, length of connecting rod: 131 mm	Compression ratio: 10:1, engine speed: 1000–6000 rpm, Fuel system: multipoint electric port fuel system, maximum output: 78 kW at 6000 rpm, maximum torque: 135 Nm at 4000 rpm, maximum power:150 kW at full load	BSFC was higher for M20, E20, P20, and B20 compared with that for unleaded gasoline by 7.58, 5.17, 4.43, and 1.95%, respectively.	BTE was higher for M20, E20, P20 and B20 compared with that for gasoline by 3.60, 2.15, 0.70, and 1.86%, respectively.		Decreased for M20	Increased for M20	Decreased for E20	Increased for E20

Table 2.6: (continued 6)

No.	Researchers	Ethanol blend(s)	Engine specifications	Operating conditions	Engine performance parameters			Exhaust emissions			
					BSFC	BTE	BP	CO	CO_2	HC	NO_x
20	(Elfasakhany, 2014)	E0, E3, E7, and E10	Single-cylinder four-stroke spark ignition engine, weight: ~17 kg, length × width × height: 515 × 345 × 370 mm, bore: 65.1 mm, stroke: 44.4 mm, length of connecting rod: 79.55 mm	Output power: ~1.5 kW, oil volume: 0.6 L, magnetic ignition voltage, compression ratio: 7:1, air cooling, engine speed: 2600–3500 rpm	Decreased		Increased	Decreased for E10	Increased for E10	Decreased for E10	—
21	(Najafi et al., 2015)	E5, E7.5, E10, E12.5, and E15	Four-cylinder four-stroke spark ignition engine, bore: 71 mm, stroke: 83.6 mm, displacement volume: 1323 cm^3	Compression ratio: 9.7:1, engine speed: 1500–4000 rpm, maximum torque: 103/2750 (Nm/rpm), maximum power: 47/5200 (kW/rpm), combustion order: 1-3-4-2	Decreased	—	Increased	Decreased	Increased	Decreased	Increased
22	(Elfasakhany, 2015)	E0, E3, E7, E10, M3, M7, M10, EM3, EM7, and EM10	Single-cylinder, four-stroke spark ignition engine, bore: 65.1 mm, stroke: 44.4 mm, type of cooling: air cooling	Compression ratio: 7:1, engine speed: 2600–3450 rpm	—	—	BP was highest for E0, E3, E7, and E10	Decreased	Increased by 9.2% for M10	Decreased by 26% for M10	

[a] °BTDC: number of degrees before top dead center
[b] °ATDC : number of degrees after top dead center
[c] BHP : brake horsepower
[d] Additives added: cycloheptanol and cyclooctanol
[e] SGR : Simulated reformed gas
[f] CAD BTDC : crank angle degree before top dead center
[g] °ABDC : number of degrees after bottom dead center
[h] °BBDC : number of degrees before bottom dead center
[i] DME : dimethyl ether
[j] Additives added into ethanol: toluene (50%), methanol (15%), isopropyl alcohol (15%), acetone (10%), and xylene (10%)

2.11. Corrosion

Corrosion is the degradation of metal due to electrochemical reactions between the metal and the environment (Liu et al., 2015). Corrosion is one of the important problems in engineering because it can cause serious detriment to metallic components, resulting in significant maintenance, repair, and replacement costs (Hu et al., 2015). According to De Baere et al. (2013), in 2002, the United States of America spent US$ 275.7 billion/year to deal with corrosion problems, which include disruptions in production because of corrosion incidents and repairs. According to Biezma and San Cristóbal (2005), countries such as Japan, the United Kingdom, and the United States of America have suffered national economic losses because of corrosion, amounting to 5% of their gross domestic product (GDP). Even though corrosion is inevitable, it can be controlled. Most petrol engine parts are made from copper, such as bearing, washer, and bushing, and are directly affected by the fuels (Haseeb et al., 2011). The long term exposing the fuel to those metallic surfaces may lead to potential problems, such as corrosion and it will damage the crucial engine parts. Moreover, corrosion can be further impact negatively on engine performance by causing engine damage (Ambrozin et al., 2010). Ethanol has the nature properties of being hydrous, and in consequence, blending bioethanol with gasoline will promote degradation and interrupt the stability of the blended fuels. These effects adversely influence engine performance and emissions. Hence, it is of interest to observe the corrosive behavior of bioethanol fuel on metal surfaces. Knowing the corrosiveness of bioethanol on metals, helps the manufacturer to choose better materials for making engine parts, fuel storage, and distribution system. Therefore, corrosion inhibitors for the bioethanol fuel need to be conducted at room temperature.

2.12. Corrosion behavior of metals immersed in ethanol-gasoline blends

The behavior of metal corrosion by bioethanol and bioethanol-gasoline blends have been studied by many researchers. Kannan et al. (2014) investigated the corrosion characteristics in copper as frequently observed in spark ignition engines using bioethanol-gasoline blends. They performed static immersion tests at room temperature using gasoline and the bioethanol-gasoline blends (E10 and E85) for 1320 hours. The bioethanol used in this study is an 80:20 mixture of laboratory-grade ethanol with sago bark bioethanol. The sample used in the test is a pure copper flat plate (99.99%) as in **Figure 2.18**.

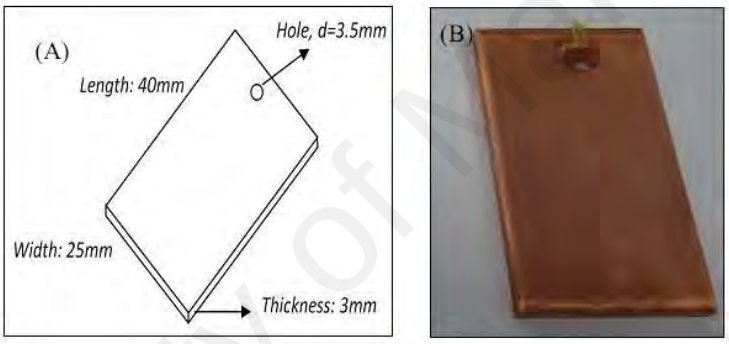

Figure 2.18: Copper test specimen preparation for static immersion test (Kannan et al., 2014)

The corrosion rate at E85 is higher than the corrosion rate of E10 and E0. Copper corrosion rate after 1320 hours immersion is 0.720 mm/year for E85 mixed fuel. Increasing the concentration of water in a mixture of gasoline-bioethanol is essential in contributing the increasing copper corrosion rate. Besides that, from the observation that the surface morphology of copper in a mixture of gasoline-bioethanol (E85) experienced more localized pitting corrosion than that of E10 and gasoline (E0) fuels. In other words, as ethanol content gets higher the size and distribution of the pits increases. They also concluded that the corrosion rate was linear to the bioethanol content in the fuel blend. From the study it was also suggested that copper is a strong catalyst for

bioethanol oxidation, indicated by the acid concentration found increasing in the bioethanol-gasoline blends.

In addition, Thangavelu et al. (2016a) has also conducted the copper immersion experiment in E25 blend (25% bioethanol + 75% gasoline) and E50 (50% bioethanol + 50% gasoline) for a duration of 700 h and 1400 h at room temperature. At 1400 h, the rate of copper corrosion in the mixture of E50 and E25 fuels is 0.441 and 0.285 mm/year, respectively. Copper corrosion rate decreases with increasing immersion time. The occurrence is due to the presence of oxide formation in such aggressive condition, and it responds as corrosion barriers.

Figure 2.19 displays the morphology of metal surfaces corroded by gasoline and blends of bioethanol-gasoline fuels (Thangavelu et al., 2016a). There is little damage to the metal surface exposed to gasoline (E0) compared to the bioethanol mixture (E25 and E50). It can be observed that the severity of surface damage and formation of pits are greater due to E25 and E50 than that of E0. At specimen exposed to E50 more visible pits are observed, compared to that by E25 blend. The corrosion in copper begins with the reaction with oxygen, which leads to formation of CuO. Further, as CuO is exposed to ethanol this causes the formation of the corrosion product: cuprite (Cu_2O).

(a) (b) (c)

Figure 2.19: Photographs of copper coupons immersed in (a) gasoline (b) mixture of gasoline-bioethanol (E25) and (c) mixture of gasoline-bioethanol (E50) for 1400 h at room temperature (Thangavelu et al., 2016a)

Matějovský et al. (2017) investigated copper corrosion immersed in several blends of bioethanol-gasoline (E40, E60, E85, and E100) at room temperature through electrochemical and surface analysis tests. The results showed that the polarization resistance of copper decreases with the increase of water content and ethanol up to 85 %vol. Besides, the highest corrosion rate was measured for copper in the contaminated E60 fuel. This is due to the most extensive pitting corrosion that occurred for E60, and this can be associated with the water content and acidic substances along with the solubility of oxygen in the fuel, which decreases with increasing content of ethanol. Abel and Virtanen (2015) investigated the corrosion behavior due to bioethanol-gasoline blends of DIN 1.4035 stainless steel as a function of water, chloride, and acetic acid concentrations. The results showed that the DIN 1.4035 stainless steel was subjected to a strong pitting corrosion or uniform corrosion when the material was immersed in the ethanol-gasoline blends at room temperature. They concluded that water and chloride concentrations are the primary corrosion precipitating factors in ethanol-gasoline blends.

2.13. Summary

A review of the recent studies pertaining to bioethanol production from second-generation feedstocks has been presented in this chapter. The availability of bioethanol feedstocks is crucial to ensure the sustainability of bioethanol and its blends as fossil fuel substitutes. Second-generation feedstocks (non-edible feedstocks) are attractive for bioethanol production because they help overcome the food versus fuel issue, which is serious concern especially in developing countries. Although these feedstocks are promising for sustainable production of bioethanol and its blends, more research is needed to produce commercially viable and environmentally friendly methods.

The production of bioethanol from second-generation feedstocks consists of three stages: (1) pre-treatment, (2) hydrolysis of carbohydrates into sugars, and (3)

production of ethanol by fermentation of sugars. Much effort has been made in recent years to optimize the biodiesel production processes with promising results. Ideally, the pre-treatment method should be cost-effective, and it should minimize energy consumption, minimize the use of chemicals, and reduce or remove the maximum amount of extractives and inhibitors. The pre-treatment method should also be environmentally friendly such that it does not pollute the environment. It is also crucial to perform optimization to the parameters in hydrolysis and fermentation processes and more research is needed to improve each process in order to maximize the ethanol yield.

Even though second-generation bioethanol is more environmentally friendly compared with fossil fuels, it is important to determine the net energy balance in order to justify whether it is possible to sustain high yields of biomass needed for long-term bioethanol production. It is also important to assess whether the cultivation of non-edible plants (to be used as feedstocks) and bioethanol production processes will cause detriment to the environment. There will be variation on the results, which is influenced by the good management in utilizing the by-products and wastes, and configuration of the industrial system. Second-generation biofuels can solve these problems and can supply a larger proportion of biofuel sustainably and affordably with greater environmental benefits. The goal of second-generation biofuel processes is to extend the amount of biofuel that can be produced sustainably by using biomass (Tye et al., 2011). With growing concerns over the detrimental impact of large-scale fossil fuel use on the environment and climate change, the development of biofuels such as second-generation bioethanol has received considerable attention to deliver transportation energy without causing serious detriment to the environment. Second-generation bioethanol can also be blended with fossil fuels such as gasoline and diesel in order to improve engine performance and CO, CO_2, HC, and NO_x emissions.

CHAPTER 3: METHODOLOGY

3.1. Introduction

The methodology adopted in this study is presented in this section, beginning with a detailed literature survey on bioethanol production/optimization, bioethanol-gasoline blends, and the engine performance and exhaust emissions of bioethanol-gasoline blends obtained from journal articles, conference proceedings, theses, scholarly books, and technical reports.

The methodology used to optimize the enzymatic hydrolysis and fermentation process parameters for *Manihot glaziovii* and sweet sorghum is presented in this chapter. In this study, the performance of Subaru EX17D single-cylinder four-stroke air-cooled spark ignition engine fueled with bioethanol-gasoline blends are presented. The experiments were conducted at the Energy Efficiency and Engine Laboratory, Department of Mechanical Engineering, University of Malaya.

Manihot glaziovii and sweet sorghum are non-edible feedstocks composed of starch, proteins, fats, non-starch polysaccharides, phenolic compounds, and phytosterols . Because of their chemical compositions, *Manihot glaziovii* and sweet sorghum can be used as a substitute for agricultural distilling in bioethanol production. The bioethanol conversion process involves gelatinization and separate hydrolysis and fermentation (SHF). The SHF method was employed in this study, where enzymatic hydrolysis is performed separately from fermentation. First, the starch in the raw feedstock is gelatinized, followed by liquefaction. The addition of heat and enzymes accelerate the process. During the SHF process, the combined liquid flows from both hydrolysis reactors enter the glucose fermentation reactor. Next, the mixture is distilled (removal of bioethanol) and the uncovered xylose (C5 sugar) is left behind. The remaining xylose is fermented to form bioethanol in the second reactor, followed by distillation. The

advantage of the SHF process is that the hydrolysis and fermentation processes can be carried out at their optimum conditions. However, it is worth considering how to make use of the by-product of the bioethanol production process, which is known as stillage. Because enzymatic hydrolysis and fermentation are performed separately in the SHF method, this reduces the risk of contamination compared with simultaneous saccharification and fermentation (SFF) and simultaneous saccharification and co-fermentation (SSCF). In addition, the optimum conditions are used separately for the enzymes and yeast, which means that the operating conditions used in SHF are optimum for both the enzymes and yeast. The pre-treated hydrolysate has a significant effect on the yeast activity, and at optimum concentrations, it has a positive effect on the ethanol productivity and ethanol yield by stressing the yeast.

Based on the results of Moshi et al. (2014), SHF is the preferable method to produce bioethanol from the starch contained in the raw feedstocks. The separation of the pre-treated hydrolysate from fermentation seems to have a positive effect because it reduces the production of inhibitors during bioethanol production. Hence, in SHF, the enzymes can work at the optimum temperature. With the SHF method, the concentration of inhibitors is decreased prior to the fermentation process, which makes it possible to attain a high ethanol yield.

3.2. Materials and methods

3.2.1. Preparation of the *Manihot glaziovii* tubers and sweet sorghum grains

3.2.1.1. *Manihot glaziovii* tubers

Manihot glaziovii flour was sourced from north Sumatra, Indonesia. The *Manihot glaziovii* tubers were first peeled and washed to remove impurities, and then cut and shredded. The shredded *Manihot glaziovii* was added into water, transforming into wet starch. The wet starch was dried in an oven at a temperature of 50°C for 48 h. This

drying process is important for longer storage periods at 25°C. The dried starch was then milled and sifted to obtain starch with a homogeneous particle size.

3.2.1.2. Sweet sorghum grains

Sweet sorghum (*Sorghum bicolor* (L.) Moench) was sourced from Cilacap, Central Java, Indonesia. The sweet sorghum was washed and then dried in order to facilitate in peeling the skin off the sweet sorghum grains. Following this, the sweet sorghum grains were ground and sieved to obtain starch. The sweet sorghum was homogenized to obtain a particle size of 125–150 μm, in order to enhance the reducing sugar concentration during the hydrolysis process. According to Barcelos et al. (2011), a smaller particle size (< 1 mm) will enhance diffusion, which will boost the reducing sugar yield compared with larger particle sizes. The homogenized sweet sorghum was dried so that it can be stored over a longer period at 25°C.

3.2.2. Reagents and catalyst

The following reagents were used in this study, namely, sulfuric acid (H_2SO_4, purity: 95–97%), 3,5-dinitrosalicylic acid (DNS), potassium dichromate ($K_2Cr_2O_7$), potassium dihydrogen phosphate (KH_2PO_4), ammonium chloride (NH_4Cl), sodium hydroxide pellets (NaOH, purity: 99.9%), and sodium potassium tartrate. Enzyme α-amylase from *Bacillus licheniformis* Type XII-A, enzyme amyloglucosidase from *Aspergillus niger*, yeast *Saccharomyces cerevisiae*, yeast extract, bacteriological peptone, D-glucose, potato dextrose and distilled water were also used in the bioethanol production process. All of the reagents were used without purification.

3.3. Experimental setup

The bioethanol production process was carried out on a laboratory scale using a water bath shaker. The heater was used to maintain the water temperature up to 90°C during the reaction. The shaking motion (linear back and forth motion) of the water bath shaker was 35–160 strokes per minute (spm).

3.4. Preparation of the DNS solution

Solution A was prepared by dissolving 90 g of sodium potassium tartarate in ~150 mL of distilled water. Solution B was prepared by dissolving 3 g of DNS into 60 mL of NaOH solution composed of 80 g of NaOH mixed with 1 L of distilled water. The DNS solution was prepared by mixing Solutions A and B and the final volume was raised to 300 mL with distilled water. The mixture was mixed thoroughly and the container was covered with an aluminum foil. The DNS solution was prepared to check the reducing sugar concentration after the hydrolysis process.

3.5. Preparation of the dichromate solution

To prepare the dichromate solution, 2.72 g of potassium dichromate ($K_2Cr_2O_7$) and 22.21 mL of sulfuric acid (H_2SO_4) was added and mixed with 100 mL of distilled water. The dichromate solution was prepared to check the ethanol concentration after the fermentation process.

3.6. Preparation of the yeast culturing media

The yeast *Saccharomyces cerevisiae* Type II purchased from Sigma-Aldrich was used to ferment the *Manihot glaziovii* starch into bioethanol. The yeast peptone dextrose media was used to cultivate *Saccharomyces cerevisiae*. The yeast peptone dextrose media was prepared by mixing 2 g of yeast extract, 4 g of bacterial peptone, 4 g of glucose, and 12 g of agar in 200 mL of distilled water. Following this, the dry yeast was activated by adding 100 mL of distilled water into the flask. The solution was sterilized in an autoclave for 35 min and it was placed and maintained in a glass Petri dish. The yeast was stored in an incubator at 37°C for 48 h in order to inoculate the yeast before it was used for bioethanol production.

3.7. Determination of carbohydrates

Carbohydrates are a source of energy source, consisting of the elements carbon, oxygen and hydrogen, with the molecular formula $C_n(H_2O)_n$. Starch is a complex carbohydrate, which is insoluble in water, tasteless, and odorless, and available in the form of white powder. Starch is the main substance produced by plants to store excess glucose (which is one of the products of photosynthesis) in the long term.

Starch is composed of two types of carbohydrates (amylose and amylopectin) in different compositions (Aditiya et al., 2016). These fractions of carbohydrates can be separated by using hot water, where the soluble and insoluble fractions are amylose and amylopectin, respectively. Amylose has a straight structure whereas amylopectin has a branched structure (Ebnesajjad, 2012).

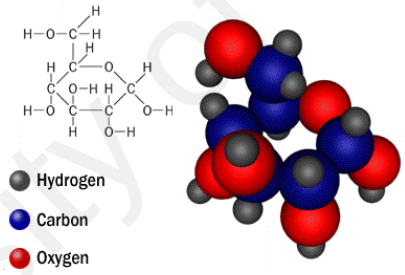

Figure 3.1: Chemical structure of carbohydrates

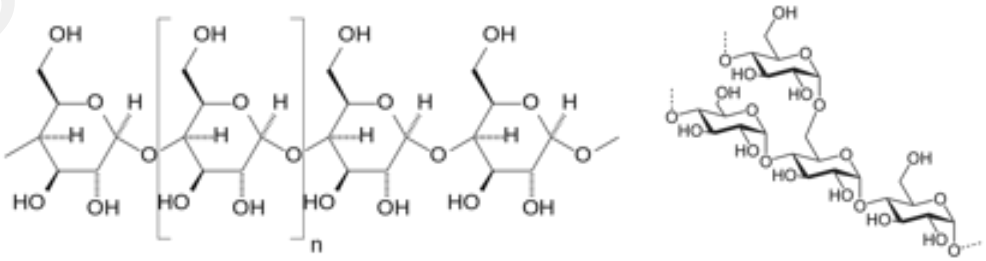

(a) (b)

Figure 3.2: Chemical structures of (a) amylose and (b) amylopectin

The carbohydrate content of *Manihot glaziovii* and sweet sorghum grains varies depending on the quality of the feedstock and the geographical location in which the plant is grown. In this study, the protein content was estimated based on the total nitrogen using the Kjeldahl method with the formula: $N \times 6.25$ (Chang, 2010). The Soxhlet extraction method was used to analyze the fat content. The moisture content was determined by gravimetric analysis where the weight of the sample was measured after the sample was dried in a laboratory oven at 105°C. The ash content was determined by gravimetric analysis, residue remaining after ignition in the oven at 600°C. The residue sample was oven dried to a constant weight. The fiber content was determined based on the loss in weight on ignition of dry residue remaining after digestion of the sample with 1.25% sulfuric acid and 1.25% NaOH solutions. The carbohydrate content was estimated using the fresh weight-derived data and the following equation (Merrill & Watt, 1973):

(% carbohydrate) = 100% − (%protein + %fat + %ash + %moisture + %fiber) (3.1)

3.8. Hydrolysis process

Hydrolysis is a chemical decomposition process using water to separate the chemical bonds of a substance. Hydrolysis is used to break down starch into its constituents such as dextrin, isomaltose, maltose, and glucose (Adewuyi & Deshmane, 2015). In the hydrolysis reaction, the reaction between water and starch is rather slow and therefore, it is necessary to use a catalyst to speed up the breakdown of starch (Aditiya et al., 2016). The enzymes that can be used as the catalysts of the hydrolysis process are α-amylase, β-amylase, amyloglucosidase, glucose isomerase, pullulanase, and isoamylase. The enzymes that are frequently used to produce glucose synergistically are α-amylase and glucoamylase. The enzyme α-amylase will quickly break down the amylose bonds in the starch during the liquefaction process. Following this, the enzyme glucoamylase will break down the starch completely into glucose

during the saccharification stage. The process of producing glucose by starch hydrolysis is shown below:

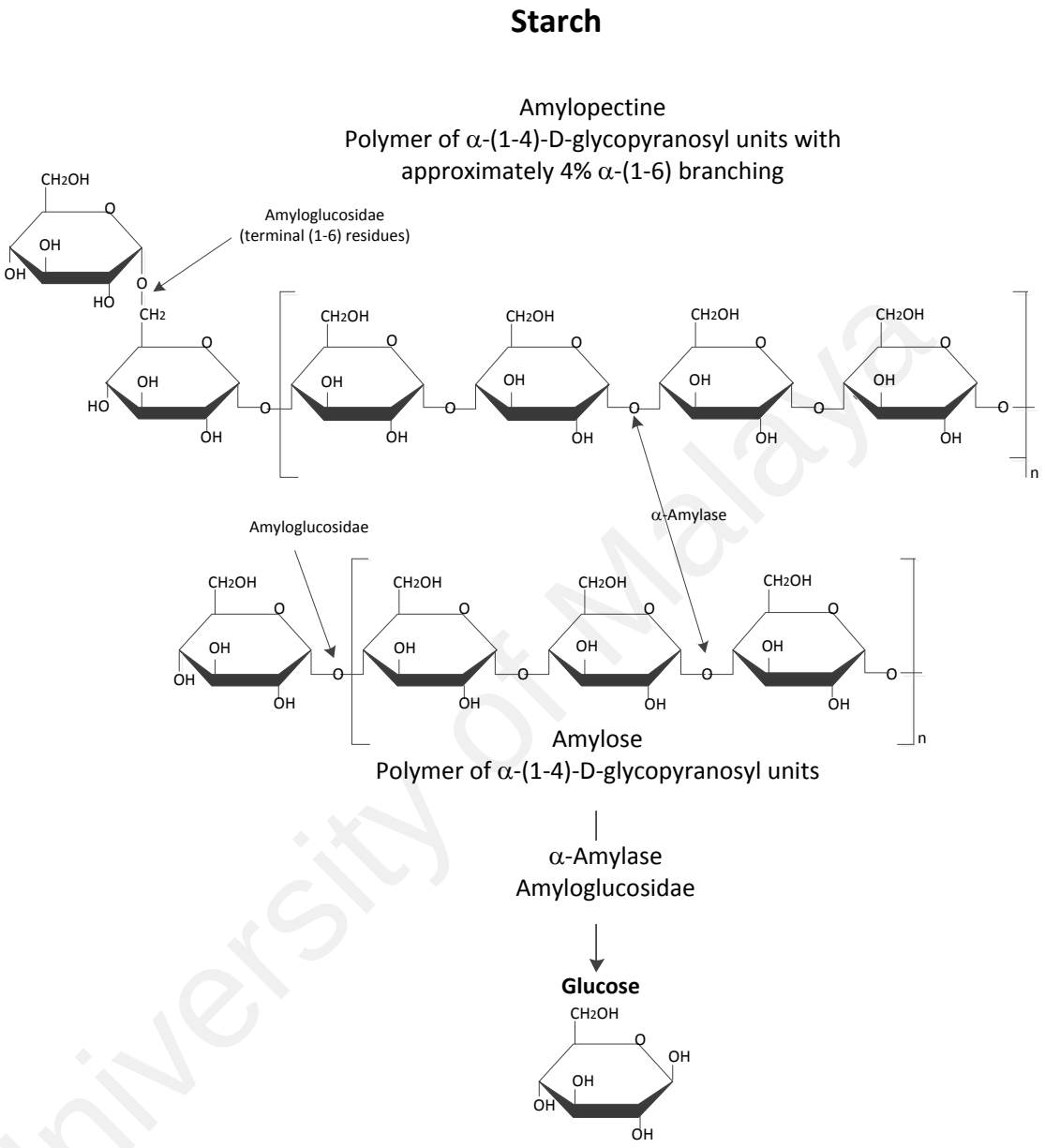

Figure 3.3: Formation of glucose by enzymatic hydrolysis of starch

In this study, enzymatic hydrolysis was first carried out by preparing the respective substrates in a flask filled with distilled water. For the liquefaction process, *Manihot glaziovii* starch (10 %(w/v)) and α-amylase (90 U/g) at 90°C with a stroke speed of 50 spm. The saccharification process was then carried out with 15 U/mL of amyloglucosidase at 70°C for 240 min. Each sample was then centrifuged at 10000 rpm

for 5 min to separate the solid residues. Following this, the DNS solution was used to determine the reducing sugar concentration in each hydrolysate.

3.9. Determination of the reducing sugar concentration

The reducing sugar concentration of each sample obtained from the enzymatic hydrolysis process was analyzed using the DNS solution. Glucose, which was used as the standard for the reducing sugar solution, was diluted with distilled water up to 1 mL in a test tube (Miller, 1959). Following this, 1 mL of the DNS solution was added into the reducing sugar solution and the mixture was boiled at 90°C for 5 min. Ultraviolet-visible (UV-VIS) spectrophotometer (SPEKOL® 1500, Germany) was used to measure the absorbance of each sample at a wavelength of 540 nm.

3.10. Fermentation process

Fermentation is a process of chemical changes in an organic substrate due to the biocatalyst activity of the fermentation agent such as yeast (Avilés Martínez et al., 2011). Fermentation microbes and fermentation medium containing nutrients were required to produce the cells. According to Ballesteros et al. (2004), in the fermentation process, one molecule of glucose produces two molecules of ethanol, two molecules of CO_2, and energy. Theoretically, 1 g of sugar will be converted into 0.51 g of ethanol (51% of ethanol) and 0.49 g of CO_2 (49% of CO_2) (Kumar & Singh, 2016).

$$\underset{\text{Glucose}}{C_6H_{12}O_6} \xrightarrow{\text{Yeast}} \underset{\text{Ethanol}}{2\ C_2H_5OH} + \underset{\text{Carbon dioxide}}{2\ CO_2}$$

In this study, the yeast *Saccharomyces cerevisiae* was used to convert sugar into ethanol in order to produce a high ethanol yield. The fermentation process was carried out using 250-mL Erlenmeyer flasks filled with the hydrolyzed *Manihot glaziovii* starch. The hydrolysed *Manihot glaziovii* starch was mixed the following fermentation nutrients: 1 g of yeast extract, 0.4 g of KH_2PO_4, and 0.2 g of NH_4Cl. Each flask was filled with 100 mL of hydrolyzed solution and sterilized at a temperature of 125°C and

pH of 6.0 for 35 min using an autoclave. The sterilized solutions were then inoculated with 1.0 g/L of yeast *Saccharomyces cerevisiae*. The chemicals were purchased from Sigma-Aldrich (Saint Louis, USA). The flasks were then placed into an incubator shaker for the fermentation process. The shaker was set at a temperature of 37°C and agitation speed of 120 rpm for the fermentation process.

3.11. Distillation process

Distillation or refining is a method of separating two or more components in a solution based on the difference in the volatility or boiling point (Huang et al., 2008). The separation of ethanol and water is the purification by distillation frequently encountered. The ethanol content after the fermentation process should not be more than 5–12 %(w/w) (Huang et al., 2008; Kiss et al., 2012). Distillation was carried out using a rotary evaporator at a temperature, pressure and rotary speed of 60°C, 175 mbar, and 100 rpm, respectively. The vaporized fermentation solution was vacuumed by a pump and flowed to the other end to be condensed, resulting in ethanol of higher quality.

3.12. Determination of the ethanol content

The ethanol concentration of each sample was determined using a gas chromatograph system (7890A, Agilent Technologies, USA) equipped with a thermal conductivity detector and DB-ALC2 analytical column (30 m × 0.00032 m). Hydrogen (H_2) was used as the carrier gas. The temperatures of the injector and detector were 150 and 200°C, respectively. Quantification was carried out by analyzing the corresponding peak areas based on the calibration curve prepared from various aqueous ethanol standards.

The schematic of bioethanol production process in this study is shown in **Figure 3.4**.

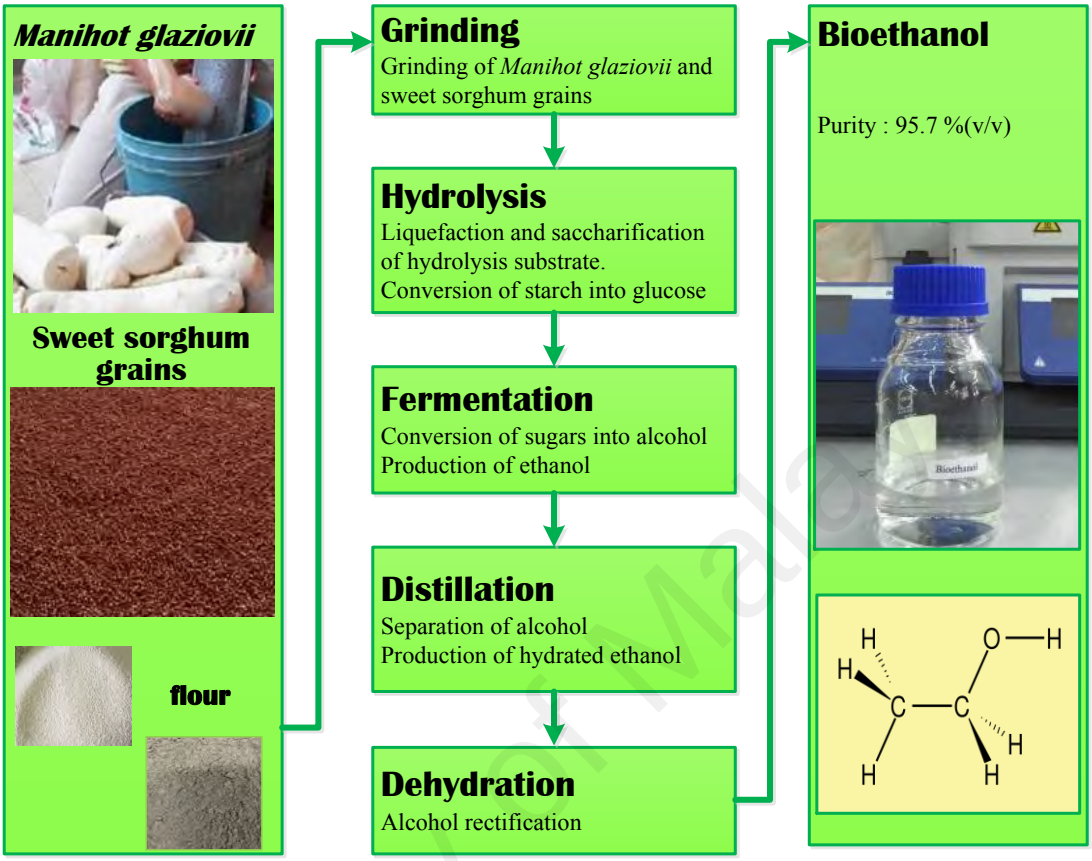

Figure 3.4: Schematic of the bioethanol production process in this study

3.13. Optimization of the bioethanol production process parameters

Enzymatic hydrolysis and fermentation were carried out on a laboratory scale using a water bath shaker and incubator shaker, respectively. Different values were used to obtain the optimum enzymatic hydrolysis and fermentation process parameters. Experiments were conducted to determine the optimum conditions for enzymatic hydrolysis in order to maximize the reducing sugar yield. The effects of the yeast concentration, reaction temperature, and agitation speed on the ethanol yield were also investigated. The purpose of optimizing the operating conditions of the enzymatic hydrolysis and fermentation processes was to maximize the reducing sugar yield and ethanol yield in order to fulfill the requirements of international standards. **Table 3.1**

shows the details of the optimization of the enzymatic hydrolysis and fermentation process parameters in this study.

Table 3.1: Details of the enzymatic hydrolysis and fermentation optimization

Process	Parameter	Uncoded levels		
Enzymatic hydrolysis	Substrate loading (%(w/v))	10	15	20
	α-Amylase concentration (U/g)	90	100	110
	Amyloglucosidase concentration (U/mL)	36	51	66
	Stroke speed (spm)	50	90	130
Fermentation	Yeast concentration (g/L)	0.5	1.0	1.5
	Reaction temperature (°C)	30	36	42
	Agitation speed (rpm)	50	150	250

An optimization experiment is a series of tests where changes are made to the input variables according to a given rule in order to identify the reasons for the changes in the output response (Cavazzuti, 2012). The Box-Behnken design (BBD) is a three-level factorial design, which is built by combining two-level factorial designs with an incomplete block design in a particular manner. The BBD was introduced to limit the sample size as the number of experimental parameters increases (Cavazzuti, 2012). In addition, the BBD is a non-factorial experimental design, where each experiment involves the midpoint value of each variable (Maran et al., 2013)

The BBD consists of three factors with three levels for each factor. Hence, there are three coded levels for each independent variable (factor): −1, 0, and +1. The independent variables are coded according to the following equation (Maran & Manikandan, 2012):

$$x_i = \frac{X_i - X_z}{\Delta X_i} \quad i = 1, 2, 3, \dots k \tag{3.2}$$

where x_i is the dimensionless value of the independent variable, X_i is the real value of the independent variable, X_z is the real value of the independent variable at the center point, and ΔX_i is the step change of the real value of the variable i corresponding to a variation of a unit for the dimensionless value of the variable i.

One of the advantages of the BBD is that it does not contain any combinations where all of the factors are at their highest or lowest levels. Therefore, this design prevents carrying out the experiments under extreme conditions, where the results may not be satisfactory. In addition, the BBD has a smaller number of experiments and therefore, this design is suitable for studies with limited samples or research materials.

In this study, the BBD was used for the experimental design. The number of experiments, N, required to develop the BBD is given by (Ferreira et al., 2007):

$$N = 2k(k-1) + Nc \qquad (3.3)$$

where k is the number of factors and Nc is the number of central points (Kundu et al., 2015). The BBD consisted of 29 experimental runs for the enzymatic hydrolysis process. Four parameters were investigated for the enzymatic hydrolysis process, namely: (1) substrate loading (%(w/v)), (2) α-amylase concentration (U/g), (3) amyloglucosidase concentration (U/mL), and (4) stroke speed (spm). The BBD consisted of 17 experimental runs for the fermentation process. Three parameters were investigated for the fermentation process, namely: (1) yeast concentration (g/L), (2) reaction temperature (°C), and (3) agitation speed (rpm). The coded levels of the independent variables used for enzymatic hydrolysis and fermentation of *Manihot glaziovii* and sweet sorghum are presented in **Table 3.2.**

Table 3.2: Box-Behnken design for enzymatic hydrolysis and fermentation of *Manihot glaziovii* and sweet sorghum

Process	Parameter	Coded level			
		Unit	−1	0	+1
Enzymatic hydrolysis	A: Substrate loading	%(w/v)	10	15	20
	B: α-amylase concentration	U/g	90	100	110
	C: amyloglucosidase concentration	U/mL	36	51	66
	D: Stroke speed	spm	50	90	130
Fermentation	A: Yeast concentration	g/L	0.5	1	1.5
	B: Reaction temperature	°C	30	36	42
	C: Agitation speed	rpm	50	150	250

3.13.1. Modeling and optimization using artificial neural networks and genetic algorithm

MATLAB 7.10.0 software (The MathWorks, Inc., USA) with the Neural Network toolbox and Global Optimization Toolbox was used in this study. A three-layer feedforward architecture with the Levenberg-Marquardt backpropagation algorithm was used for the ANN models. The ANN models consisted of four input variables for the hydrolysis process (substrate loading, α-amylase concentration, amyloglucosidase concentration, and stroke speed), three input variables for the fermentation process (yeast concentration, reaction temperature, and agitation speed), hidden layers with the optimum number of neurons, and one output variable (reducing sugar yield and ethanol yield for the hydrolysis and fermentation processes, respectively). The ANN models were trained until the mean square error (MSE) was minimized and the average correlation coefficient (R) was close or equal to 1. Genetic algorithm (GA) was then carried out on the well-trained and tested ANN models to optimize the reducing sugar and ethanol yield using different combinations of process parameters.

3.13.2. Statistical analysis

The performance and prediction capability of the ANN models were assessed based on the coefficient of determination (R^2), mean absolute percentage error ($MAPE$), and root mean square error ($RMSE$), which are given by the following equations:

$$R^2 = 1 - \sum_{i=1}^{n} \left(\frac{(x_{ia} - x_{ib})^2}{(x_m - x_{ib})^2} \right) \tag{3.4}$$

$$MAPE = \frac{100}{n} \sum_{i=1}^{n} \left| \frac{x_{ia} - x_{ib}}{x_{ia}} \right| \tag{3.5}$$

$$RMSE = \sqrt{\frac{\sum_{i=1}^{n} (x_{ib} - x_{ia})^2}{n}} \tag{3.6}$$

Here, n is the number of experimental points, x_{ia} denotes the experimental value, x_{ib} denotes the predicted value, and x_m denotes the mean experimental value. The accuracy of each ANN model was evaluated based on the R^2 value. In general, the higher the R^2 value, the better the accuracy of the model. It shall be noted that the R^2 value should not be less than 80% (Stamenković et al., 2013). The prediction capability of each model is indicated by the $MAPE$ and $RMSE$, where the lower the $MAPE$ and $RMSE$ values, the higher the prediction capability of the model.

3.13.3. Sensitivity analysis

In this study, the equation proposed by Garson was used to determine the relative significance of each input such as the yeast concentration, reaction temperature, and agitation speed based on the partitioning of the connection weights, which is expressed as:

$$Ij = \frac{\sum_{m=1}^{m=N_h}\left(\left(\left|W_{jm}^{ih}\right|/\sum_{k=1}^{N_i}\left|W_{km}^{ih}\right|\right)\times\left|W_{mn}^{ho}\right|\right)}{\sum_{k=1}^{k=N_i}\left\{\sum_{m=1}^{m=N_h}\left(\left|W_{km}^{ih}\right|/\sum_{k=1}^{N_i}\left|W_{km}^{ih}\right|\right)\times\left|W_{mn}^{ho}\right|\right\}} \quad (3.7)$$

where Ij is the relative significance of the j^{th} input variable on the output variable, N_i and N_h represent the number of input and hidden neurons, respectively, and W is the connection weight. The superscripts i, h, and o represent the input, hidden, and output layers, respectively, while the subscripts k, m, and n refer to the input, hidden, and output neurons, respectively.

3.14. Energy inputs into bioethanol production

The energy component of the model contains four stages as shown in **Figure 3.5**: *Manihot glaziovii* starch and sweet sorghum grain pretreatment, hydrolysis process, fermentation process, distillation into bioethanol for final use. The calculation of energy inputs for each stage is described as below:

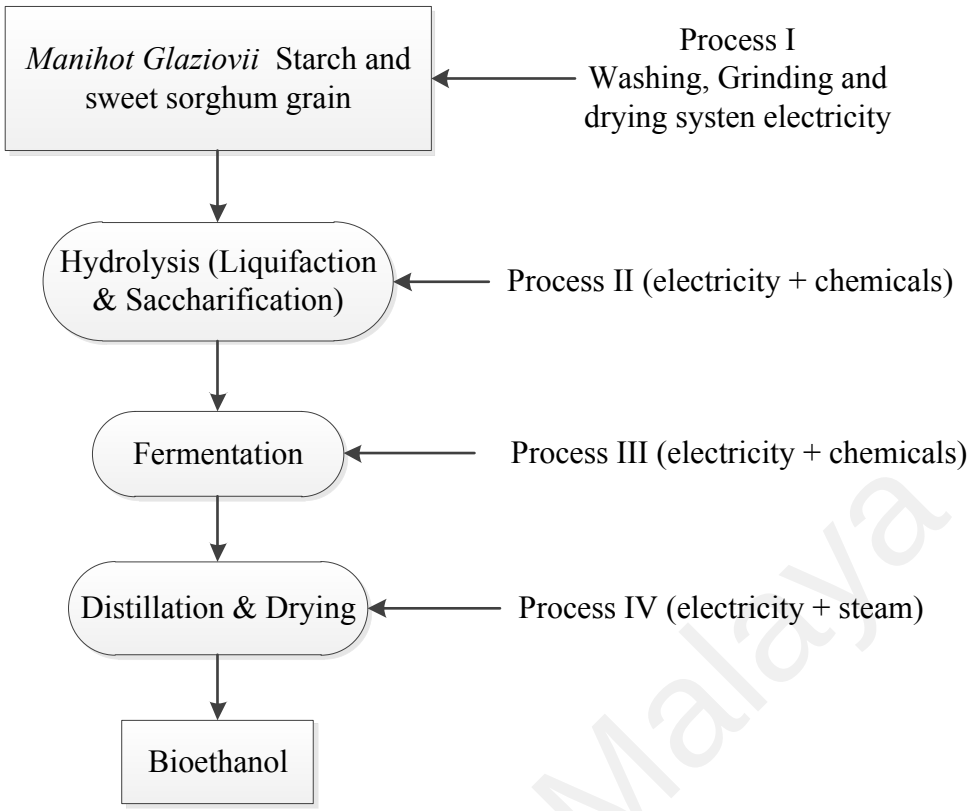

Figure 3.5: Energy inputs for *Manihot glaziovii* starch and sweet sorghum grain bioethanol production

3.14.1. Electricity

The electricity or heating used in the process is considered direct energy, which means that the energy contents of these items are directly used in the calculation. **Table 3.3** shows the domestic electricity tariff used as the reference for the bioethanol production in this study.

Table 3.3: The domestic electricity tariff in Malaysia (TNB, 2020)

No	Tariff Category	Current Rate (1 January 2014)
1	Tariff D-Low Voltage Industrial Tariff	
	For the first 200 kWh (1-200 kWh) per month	38.00 sen/kWh
	For the next kWh (201 kWh onwards) per month	44.10 sen/kWh
	The minimum monthly charge is RM 7.20	
2	Tariff E1-Medium Voltage General Industrial Tariff	
	For each kilowatt of maxium demand per month	29.60 RM/kW
	For all kWh	33.70 sen/kWh
	The minimum monthly charge is RM 600.00	
3	Tariff E2-Medium Voltage Peak/Off-Peak Industrial Tariff	
	For each kilowatt of maxium demand per month during the peak period	37.00 RM/kW
	For all kWh during the peak period	35.50 sen/kWh
	For all kWh during the off-peak period	21.90 sen/kWh
	The minimum monthly charge is RM 600.00	
4	Tariff E3-High Voltage Peak/Off-Peak Industrial Tariff	
	For each kilowatt of maximum demand per month during the peak period	35.50 RM/kW
	For all kWh during the peak period	33.70 sen/kWh
	For all kWh during the off-peak period	20.20 sen/kWh
	The minimum monthly charge is RM 600.00	

3.14.2. Machinery

Machines and equipment (bioreactors, reactors for hydrolysis, fermentation, evaporation, distillation, etc.) are used in ethanol production plants. As stated above, the manufacturing of machines requires steel and other metals along with some other materials to be produced, and ore extraction is also needed. All these operations consume energy. Therefore, total energy input in ethanol production from *Manihot glaziovii* and sweet sorghum are calculated as the following equation:

$$EC_{total} = EC_{electricity} + EC_{machinery} \quad (3.8)$$

Where: EC_{Total} = Total energy consumption during ethanol production

$EC_{Electricity}$ = Total energy input related to electricity consumption during ethanol production

$EC_{Machinery}$ = total energy input related to machinery use during ethanol production.

3.15. Energy output during ethanol production

During the production of bioethanol from *Manihot glaziovii* and sweet sorghum, starch and grain biomasses go through a series of processes, including liquefaction, saccharification, fermentation, distillation, and drying. Outputs from the conversion process of *Manihot glaziovii* and sweet sorghum into bioethanol are water-free bioethanol. Therefore, to calculate total energy output during ethanol production from *Manihot glaziovii* and sweet sorghum is by using equation below:

$$EC_{output} = EC_{EtOH} \quad (3.9)$$

Where: EC_{output} = Total energy generated during ethanol production

EC_{EtOH} = Total energy generated from ethanol

3.16. Characterization of the *Manihot glaziovii* and sweet sorghum bioethanols

The physicochemical properties of the reducing sugars and bioethanols obtained from the enzymatic hydrolysis and fermentation processes, respectively, were analyzed according to the ASTM International (formerly known as the American Society for Testing and Materials) standards. The reducing sugar concentrations were determined using a UV-VIS spectrophotometer (SPEKOL® 1500, Analytik Jena AG, Germany). The viscosity at 20°C, density at 15°C, and lower heating value of the samples were measured using Stabinger viscometer (SVM 3000, Anton Paar GmbH, Austria) (ASTM D445), density meter (DMA™ 4500, Anton Paar GmbH, Austria) (ASTM D1298), calorimeter system (IKA® C 2000 Basic, IKA Industrie- und Kraftfahrzeugausrüstung GmbH, Germany) (ASTM D240) and a digital chiller (IKA KV 6000, IKA Industrie- und Kraftfahrzeugausrüstung GmbH, Germany). Elemental analysis was performed to determine the carbon, hydrogen, and oxygen content of the samples using an elemental analyzer (CE440, Exeter Analytical, Inc., USA) (ASTM D5291). The ethanol concentrations was measured using a gas chromatography system (Agilent 7890A, Agilent Technologies, Inc., USA) (ASTM D4806).

3.16.1. Reducing sugar concentration

The reducing sugar concentration needs to be determined to measure the success of fermentation process. The reducing sugar concentration is also determined for wines in order to verify the reducing sugar content as well as for routine quality control. Batch analytical methods are used to determine the reducing sugar concentration and the process involves sample preparation and reflux in distillation to remove alcohol. Such method takes a long time to complete and it produces residue in large volume. Hence, a spectrophotometric batch assay was proposed by Başkan, (2016) to evaluate the amount of reducing sugar, following the reduction principle Cu(II) to Cu(I), with reducing sugars in the presence of neocuproine and in a medium of alkaline.

3.16.2. Viscosity and density

The viscosity and density are among the most important properties of bioethanol. It is important to regard fuel viscosity of a fuel notably when carburetor is used as the fuel delivery system. In general, viscosity tends to decrease as the temperature increases. The viscosity is measured using an instrument called a viscometer. In fuel characterization, viscosity of a fuel is important to be determined, since it is associated with the fuel flow from the fuel tank to the injector nozzle, which eventually to be injected into the combustion chamber. Low viscosity in fuel makes it run through easily and will not be able to maintain the lubrication of the surfaces between moving and stationary parts of the carburetor or fuel pump. However, too viscous of a fuel degrades the fuel atomization process, indicated by large fuel droplets formation that leads to poor combustion. In conclusion, the blends viscosities must be within an acceptable range for spark ignition engine operation (Kheiralla et al., 2011).

The density of the bioethanol gasoline blend is the major properties of the brake specific fuel consumption of a fuel blend. Increasing the density of bioethanol-gasoline blends as well as an increasing percentage of ethanol can enhance brake power in spark

ignition engines (Thakur et al., 2017). The addition of bioethanol in gasoline increases the charge density due to the evaporative cooling during injection in the intake manifold (Taylor et al., 1996). As fuel density increases, it reduces the required volume of the fuel to be aspirated from the carburetor, hence leading to a lesser fuel to be combusted in the spark ignition engines (Kheiralla et al., 2011). Low density in fuel characteristic results in an increase in volumetric fuel consumption, while high fuel density (attributable to less-volatile components) leads to oil dilution and excessive combustion chamber deposits (Kalghatgi & Stone, 2018).

3.16.3. Lower heating value

In fuel characteristic, lower heating value, LHV, is a property that describes the amount of heat energy released after combusting a specific amount of fuel (starting at 25^{o}C) and after returning the combustion products to 150^{o}C. One method in measuring this heating value is using bomb calorimeter. Water, as one of the combustion products, is vaporized in the bomb calorimeter using the heat energy from the fuel, and the value is assigned as net calorific value of the fuel or LHV. The lower heating value of ethanol is 21.1 MJ/L in comparison with 32 MJ/L for gasoline, which affects the fuel volatility (Kalghatgi & Stone, 2018). In the other hand, higher heating value (HHV) or gross calorific value of a fuel is measured with latent heat of vaporization of water as an additional component in the measurement. In general, heating value is associated with fuel consumption, as it determines the amount of fuel being combusted per unit time.

3.16.4. Elemental analysis

Elemental analysis is carried out to determine the primary elements, namely, carbon, hydrogen, nitrogen, and oxygen present in the sample. The chemical composition can affect the engine performance, exhaust emissions, and structural components of the engine system such as fuel storage tanks and pipelines. Bioethanol

may contain some chloride ions, acetic acid, and azeotropic water. In general, alcohol molecules are characterized by their polarity. Because of this property, the presence of alcohol in the fuel can have a corrosive effect on the engine components. Some metallic surfaces can oxidize upon contact with bioethanol blends.

3.17. Bioethanol-gasoline blends

In this study, the *Manihot glaziovii* and sweet sorghum bioethanol-gasoline blends were prepared in glass bottles on a volume basis. The blends were agitated at an agitation speed of 300 rpm for 30 min at room temperature to attain homogeneous blends. Even though bioethanol-gasoline blends can be prepared on a weight basis, it is not recommended to do so because the constituents of the blends in percent by weight do not change with temperature. Thus, bioethanol-gasoline blends are typically prepared by mixing the constituents on a volume basis and the properties are measured at ambient temperature (fuel storage temperature) used by the manufacturers. Therefore, in this study, the bioethanol-gasoline blends were prepared based on percent by volume.

In this study, the *Manihot glaziovii* and sweet sorghum bioethanols were blended with gasoline at a concentration 5, 10, 15, and 20 %(v/v). The *Manihot glaziovii* and sweet sorghum bioethanol-gasoline blends were designated as ME5, ME10, ME15, and ME20, and SE5, SE10, SE15, and SE20, respectively. The physicochemical properties of the bioethanol-gasoline blends were evaluated and compared with those of gasoline. Gasoline (Primax 95) with a research octane number of 95 and purchased from Petronas Malaysia was used in this study. The physicochemical properties of the gasoline and bioethanol-gasoline blends were measured based on ASTM standard test methods and the results were compared with those of other studies. The bioethanol-gasoline blends were prepared prior to the experiments and then mixed thoroughly to form homogeneous blends to prevent reaction between bioethanol and water.

3.18. Assessment of the engine performance and exhaust emissions

Experiments were carried out using a Subaru EX17 single-cylinder four-stroke spark ignition engine in the Heat Engine Laboratory, Department of Mechanical Engineering, University of Malaya. The engine was mounted on a test bed. **Figure 3.6** shows the schematic of the experimental setup while the technical specifications of the engine are listed in **Table 3.4**.

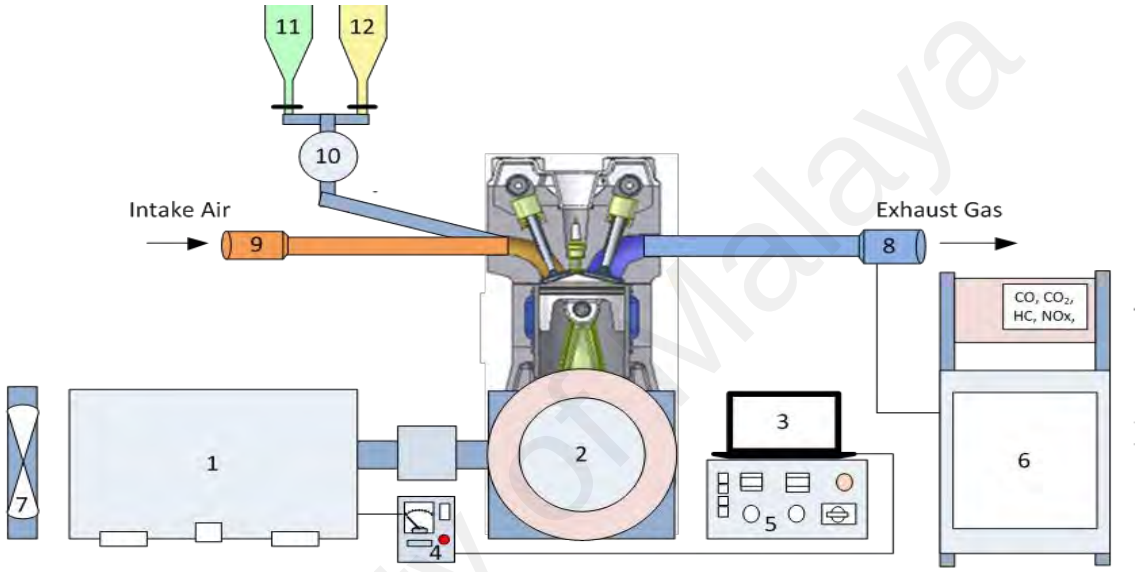

Figure 3.6: Schematic of the experimental setup

1 Dynamometer
2 Subaru E17 engine
3 Data acquisition system
4 Dynamometer controller
5 Controller/panel box
6 Gas analyzer
7 Dynamometer cooling system
8 Exhaust gas
9 Intake air
10 Fuel meter rate totalizer
11 Gasoline fuel tank
12 Bioethanol fuel tank

Table 3.4: Technical specifications of the spark ignition engine

Engine parameter	**Value**
Engine name	Subaru EX17
Engine type	Slant single cylinder, four-stroke, horizontal power takeoff shaft
Number of cylinders	1
Displacement volume	169 cm^3
Bore × stroke	67 mm × 48 mm
Compression ratio	8.5
Cooling system	Forced air cooling system
Maximum output	4.2 kW at 4000 rpm
Maximum torque	11.3 Nm at 2500 rpm

The engine was coupled to an eddy current dynamometer with a maximum absorption power of 20 kW to control the loads at different engine speeds (2450–10000 rpm). A dynamometer data acquisition software (Dyno-max Pro version 10.23 software) was used to operate the eddy current dynamometer during the engine tests. The technical specifications of the eddy current dynamometer are listed in **Table 3.5.**

Table 3.5: Technical specifications of the eddy current dynamometer and dynamometer auto-controller unit

Technical specifications of the eddy current dynamometer	
Type	DYNOmite #20 eddy current (air-cooled)
Manufacturer	Land & Sea, Inc., USA
Absorber load capacity	Maximum torque of 88.13 Nm at 3000 rpm (cold)
	Maximum torque of 40.67 Nm at 3000 rpm (warm)
	Maximum torque of 18.98 Nm at 3000 rpm (hot)
Technical specifications of the dynamometer auto-controller unit	
Model	Auto-ETS1 OM12C
Accuracy	0.10%
Precision	0.005% ± 1 digit
Weight measurement	Linear (load cell)
Speed measurement	Sensor
Screen type	7-segment, 5 LEDs, character height: 10 mm
Power	VDC ± 10% at maximum of 50 mA
Operation temperature	0–70°C
Operation voltage	230 VAC ± 10%, 50–60 Hz
Output	PC interface with Dyno2000× software

Note: LED: light emitting diode; VDC: direct current voltage; VAC: alternating current voltage; PC: personal computer.

The experiments were conducted at different engine speeds (1600–3400 rpm) and two fuel tanks (one for gasoline and the other for bioethanol-gasoline blends) were used to supply the fuels to the test engine. Gasoline was used as the baseline fuel in this study. The *Manihot glaziovii* and sweet sorghum bioethanol-gasoline blends were prepared by mixing gasoline with 5, 10, 15 and 20 %(v/v) of *Manihot glaziovii* and sweet sorghum bioethanols, respectively. Pure *Manihot glaziovii* and sweet sorghum bioethanols were also tested. For the engine tests, the engine was first switched on and operated for 5–10 min until the engine reached steady-state operating conditions. The required time to burn 25 mL of fuel in the combustion chamber was recorded based on

the fuel flow into the millimeter tube. When the engine was fueled with gasoline or bioethanol-gasoline blends, the engine ran satisfactorily without any starting difficulties during the engine tests, which were performed at room temperature. The engine tests were performed under steady-state conditions with sufficiently warm exhaust gas and air coolant temperature. The engine tests were conducted in triplicate to ensure that the results were consistent and the mean values of the engine performance and exhaust emission parameters were determined.

A four-component exhaust gas analyzer (BEA-350, Robert Bosch GmbH, Germany) was used to measure the concentrations of different exhaust gas species such as HC, CO, and NO_x. Measurements of the exhaust emissions were performed automatically by the exhaust gas analyzer with microprocessor control, which gives a higher degree of accuracy in analyzing low concentrations of gases in the exhaust emissions. The measurement range and accuracy of the instruments used are presented in **Table 3.6**. The exhaust emissions were tapped approximately 2 m from the exhaust valve.

Table 3.6: Technical specifications of the four-component exhaust gas analyser

Exhaust component	Measurement range	Resolution
Carbon monoxide, CO	0–10 %(v/v)	0.001 %(v/v)
Unburned hydrocarbons, HC	0–9999 ppm vol.	1 ppm vol.
Nitrogen oxide, NO_x	0–5000 ppm vol.	≤ 1 ppm vol.

Measurement uncertainties can arise from various sources such as uncertainties in the calibrated instruments, experimental conditions, as well as the experimental procedure. Therefore, uncertainty analysis was performed to determine the uncertainties in the measured engine performance parameters (BSFC, BP, BTE, and ET) and exhaust emissions (CO, HC, and NO_x). The percentage uncertainties of all measuring instruments used in this study are presented in **Table 3.7**. The uncertainty percentage

calculation follows the calculations performed by (Ruhul et al., 2016) and this can be seen in Appendix C.

Table 3.7: List of measuring instruments used in this study and their percentage uncertainties

Measured parameter	Measurement range	Accuracy	Measuring instrument	Percentage uncertainty (%)
Emissions				
CO	0–10 %(v/v)	± 0.001%	Non-dispersive infrared detector	± 0.95
HC	0–9999 ppm	± 1 ppm	Heated flame ionization detector	± 1.8
NO_x	0–5000 ppm	± 1 ppm	Electrochemical detector	± 1.5
Computed				
BP	—	± 0.03 kW	—	± 1.29
BSFC	—	± 5 g/kWh	—	± 1.5
BTE	—	± 0.2%	—	± 1.5

3.19. Corrosion tests

Static immersion tests were performed at room temperature of 25–30°C for 2400 h to assess the corrosion rate of copper coupons immersed in the bioethanol-gasoline blends. Teflon yarn was used to suspend the copper coupons during the immersion tests. The bioethanol-gasoline blends were stored in screw glass bottles with caps to prevent the blends from being exposed to moisture. The weight loss of the copper coupons during the corrosion test was determined using an analytical balance (resolution of four decimal places). The weight of the specimens before the corrosion test were measured, which later to be compared with the weight after the test. The measurements were performed after every 800 h of immersion to investigate the effect of immersion time on the corrosion rate.

Static immersion test to observe corrosion characteristics of metals due to the exposure of lignocellulosic bioethanol has been studied by Thangavelu et al. (2016a). They performed the immersion test for 700 and 1400 hours at room temperature (25–30°C). It was observed that metals exposed to E50 resulted higher oxidation products,

water content and metal elements than those exposed to E0 and E25. Further, as the immersion time was increased, the rate of corrosion was found low for copper and aluminum, which is due to passivation. No corrosion was observed at mild steel. Its can be concluded that ethanol concentration up to 10% is a feasible limit for the material compatibility (Hoai Vu et al., 2019).

In addition, Matějovský et al. (2017) employed an electrochemical method collaborating with the corrosion immersion test in bioethanol-gasoline fuel blends. Performed in a grounded Faraday cage, radiometer VoltaLab 40 PGZ 301 radiometer and potentiostat reference 600 (Gamry Instruments) were used as measurement tools, while two- and three-electrode arrangements were set during the electrochemical measurements. The results showed that both ferrous and nonferrous metals reacted significantly with gasoline with a higher bioethanol concentration. The highest corrosion rate was observed with higher bioethanol concentration (E60) especially for brass, copper and mild steel metals. Besides, they claimed that corrosion happened is due to oxygen, water and acidic substances content in the fuel. Electrochemical impedance spectroscopy (EIS) method was employed by Jafari et al. (2011) in an investigation of corrosion for metallic materials in gasoline and gasoline-ethanol blends with and without water contamination. In addition, scanning electron microscopy was used to determine the types of corrosion attack based on the specimens surface morphology. Ethanol content in the gasoline increases the corrosion rate owing to the decrease in the solution resistance and polarization resistance of the samples.

3.19.1. Fabrication of copper coupons for the corrosion tests

The copper coupons were prepared by cutting and grinding copper with the following dimensions: (1) diameter: 20 mm and (2) thickness: 2 mm. A wire cutter machine was used to cut the specimens to anticipate changes in the material due to heat effects. A hole (diameter: 2 mm) was drilled at the edge of the specimens for the

corrosion test. Prior to the static immersion tests, the specimens were polished with silicon carbide abrasive papers (grit size: 400–1500), and then washed and cleaned with acetone. Lastly, the specimens were rinsed with deionized water.

3.19.2. Corrosion analysis

The weight difference of each specimen was recorded and the corrosion rate was determined using the following equation:

$$\text{Corossion rate, } CR \text{ (mm/year)} = \frac{(8.76 \times 10^4 \times w)}{\rho \times A \times T} \quad (3.10)$$

where w is the weight loss in grams (g), ρ is the density of the metal in kilograms per cubic meters (kg/m^3), A is the cross-sectional area of the specimen in square meters (m^2), and T is the immersion time in hours (h).

In addition, the surface morphologies of the test specimens were observed using scanning electron microscope (SEM). Elemental analysis was carried out using energy dispersive X-ray (EDX) spectrometer to determine the compositions of the corrosion products for each specimen. The changes in the fuel properties such as the total acid number (TAN), viscosity, and density due to corrosion were also analyzed.

3.20. Summary

The methodology adopted in this study has been elaborated in this chapter, beginning from the selection of feedstocks, followed by the optimization of the enzymatic hydrolysis and fermentation process parameters using the ANN models. In addition, the procedure used to investigate the engine performance and exhaust emissions of the spark ignition engine fueled with gasoline, *Manihot glaziovii* and sweet sorghum bioethanols, as well as their blends, and the procedure used to investigate the corrosion behavior of copper coupons immersed in the bioethanol-gasoline blends are presented. The *Manihot glaziovii* and sweet sorghum feedstocks were sourced from

North Sumatra and Central Java in Indonesia. The bioethanols were produced from enzymatic hydrolysis, followed by the fermentation process. The enzymatic hydrolysis process parameters (substrate loading, α-amylase concentration, amyloglucosidase concentration, and stroke speed) and fermentation process parameters (yeast concentration, reaction temperature, and agitation speed) were optimized in order to maximize the bioethanol yield. Following this, engine tests were carried out using a single-cylinder four-stroke gasoline engine fueled with the bioethanol-gasoline blends in order to assess the engine performance (BSFC, BTE, ET, and BP) and exhaust emissions (NO_x, CO, and HC). Corrosion tests were also conducted, where copper coupons were immersed in the bioethanol-gasoline blends at room temperature (25–30°C) for 2400 h. The corrosion rate was calculated based on the weight loss of the specimens after the static immersion tests. SEM and EDX spectroscopy were carried out to analyze the surface morphologies and elemental compositions of the samples, respectively. In addition, the TAN, density, and viscosity of the samples were analyzed and FTIR spectroscopy was carried out to investigate the effect of corrosion on the properties of the bioethanol-gasoline blends.

CHAPTER 4: RESULTS AND DISCUSSION

4.1. Introduction

The key findings of this study are presented and discussed in this chapter, including the physicochemical properties of *Manihot glaziovii* and sweet sorghum bioethanols, optimization of the enzymatic hydrolysis and fermentation process parameters, physicochemical properties of the bioethanol-gasoline blends, engine performance and exhaust emissions of the single-cylinder four-stroke gasoline engine fueled with bioethanol-gasoline blends, and results of the corrosion tests.

4.2. Properties of the *Manihot glaziovii* and sweet sorghum feedstocks tuber and seed mass

The mean weight values of the *Manihot glaziovii* tubers and sweet sorghum seeds were found to be 2000 g/tuber and 0.021 g/seed, respectively. The measurement of a *Manihot glaziovii* tuber and sweet sorghum seed is shown in **Figure 4.1.**

(a) (b)

Figure 4.1: Measurement of a (a) *Manihot glaziovii* tuber and (b) sweet sorghum seed

4.3. Compositions of the *Manihot glaziovii* and sweet sorghum starches

The *Manihot glaziovii* and sweet sorghum starches were stored in a closed container in a refrigerator prior to the experiments. The *Manihot glaziovii* and sweet

sorghum starches consisted of particles (diameter: 125–150 μm), where 98% or more particles passed through a 150-μm sieve (United States Standard No. 100, Certifications ASTM E11-09). The compositions of the *Manihot glaziovii* and sweet sorghum starches were determined by chemical analysis and the results are presented in **Table 4.1.** The carbohydrate content was more than 70 %(w/w) for both *Manihot glaziovii* and sweet sorghum starches, rendering them potential substrates for bioethanol production.

Table 4.1: Compositions of the *Manihot glaziovii* and sweet sorghum starches

Parameter	Unit	*Manihot glaziovii* starch	Sweet sorghum starch
Carbohydrates	%(w/w)	74.8	73.1
Proteins	%(w/w)	6.62	10.3
Lipids	%(w/w)	3.12	3.14
Ash	%(w/w)	5.15	1.56
Fiber	%(w/w)	1.7	1.7
Moisture content	%(w/w)	8.61	10.2

4.4. Optimization of the biodiesel production process parameters

4.4.1. Optimization of the enzymatic hydrolysis process parameters

In this study, BBD was used to design the experiments for the enzymatic hydrolysis process, with a total of 29 experimental runs. Four input parameters of the hydrolysis process (substrate loading, α-amylase concentration, amyloglucosidase concentration, and stroke speed) were varied to determine the interaction effects of these parameters on the reducing sugar yield. The optimum number of hidden neurons of the ANN model was determined by testing different numbers of neurons until the mean square error (MSE) of the output data was minimized and the mean correlation coefficient (R value) was close or equal to 1.

4.4.1.1. Enzymatic hydrolysis of the *Manihot glaziovii* starch

The number of neurons in the hidden layer were varied at 2, 3, 4, 5, and 6, as shown in **Table 4.2**. The optimum number of hidden neurons for the ANN model were determined based on the MSE and R value. It can be observed from **Table 4.2** that the

optimum number of hidden neurons was 4 because this value resulted in the lowest MSE (8.1104) and highest R value (0.996). The results of the regression analysis for the ANN model are presented in **Figure 4.2**. Thus, the ANN architecture for the enzymatic hydrolysis of the *Manihot glaziovii* starch was 4-4-1 (**Figure 4.3**).

Table 4.2: Determination of the optimum number of neurons in the hidden layer of the ANN model for enzymatic hydrolysis of *Manihot glaziovii* starch

No. of neurons in the hidden layer	**2**	**3**	**4**	**5**	**6**
Mean square error, MSE	46.0300	30.7400	8.1104	10.3700	28.3150
Correlation coefficient, R	0.9790	0.9850	0.9960	0.9950	0.9870

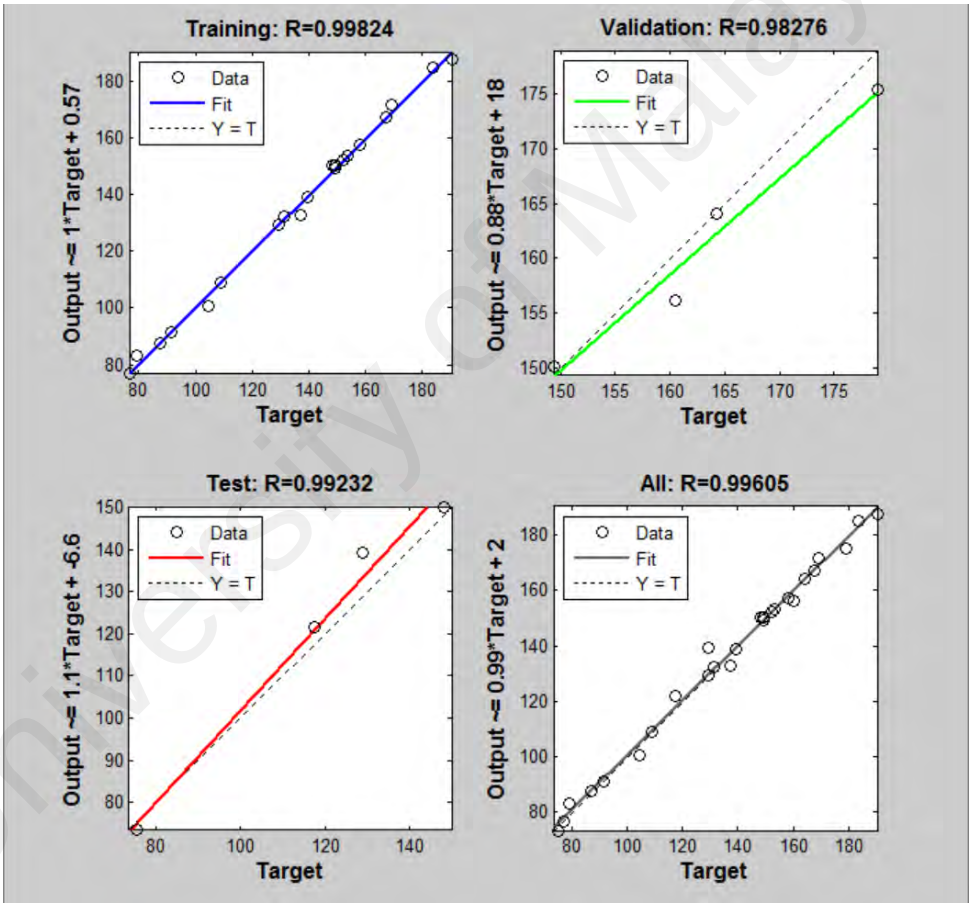

Figure 4.2: Results of the regression analysis for the ANN model for enzymatic hydrolysis of *Manihot glaziovii* starch

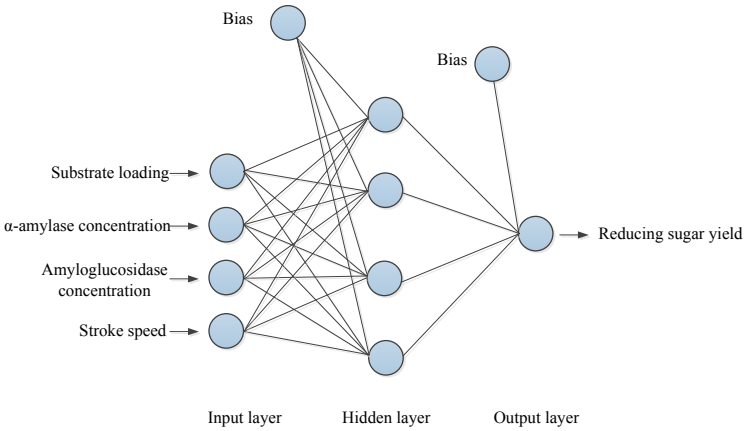

Figure 4.3: ANN architecture for enzymatic hydrolysis of *Manihot glaziovii* starch

The R^2 value was more than 80% (R^2 = 0.9921), indicating that the ANN model explains 99.21% of the variability in the response variable (reducing sugar yield) due to variations in the input variables (substrate loading, α-amylase concentration, amyloglucosidase concentration and stroke speed), as shown in **Figure 4.4**. The mean absolute percentage error ($MAPE$) and root mean square error ($RMSE$) of the ANN model were 1.46 and 2.85, respectively, as shown in **Table 4.3**. Based on the results, it can be deduced that the ANN model has good prediction capability and the model can be used to predict the reducing sugar yield for enzymatic hydrolysis of *Manihot glaziovii* starch.

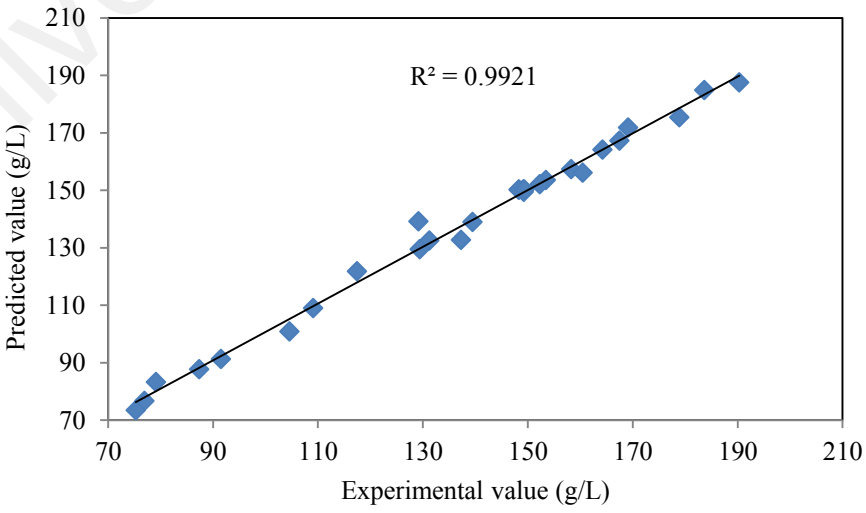

Figure 4.4: Comparison between the reducing sugar yield obtained from the Box-Behnken experiments (experimental values) and ANN model (predicted values) for enzymatic hydrolysis of *Manihot glaziovii* starch

Table 4.3: Box-Behnken experiment for enzymatic hydrolysis of *Manihot glaziovii* starch

Experimental run	Substrate loading %(w/v)	α-amylase concentration (U/g)	Amyloglucosidase concentration (U/mL)	Stroke speed (spm)	Reducing sugar yield (g/L)	
					Experimental value	Predicted value
1	10	100	66	90	104.56	100.78
2	10	100	36	90	76.96	76.62
3	15	100	66	50	149.25	149.38
4	15	100	36	130	129.39	129.47
5	20	100	51	50	169.12	171.82
6	20	110	51	90	183.67	184.89
7	10	100	51	130	87.35	87.67
8	15	100	51	90	149.1	150.13
9	15	90	51	130	131.26	132.44
10	15	110	66	90	167.47	167.23
11	15	110	51	130	153.45	153.52
12	10	110	51	90	91.54	91.29
13	15	100	51	90	148.28	150.13
14	20	100	51	130	178.9	175.37
15	10	90	51	90	75.27	73.47
16	15	90	51	50	117.45	121.78
17	20	90	51	90	152.31	152.07
18	10	100	51	50	79.11	83.24
19	15	110	36	90	129.16	139.20
20	15	100	51	90	148.34	150.13
21	15	100	51	90	149.25	150.13
22	15	90	36	90	109.08	108.95
23	15	90	66	90	139.46	138.91
24	15	100	36	50	137.25	132.65
25	20	100	36	90	158.25	157.36
26	15	110	51	50	160.44	156.10
27	20	100	66	90	190.32	187.56
28	15	100	51	90	149.35	150.13
29	15	100	66	130	164.24	164.08
Mean absolute percentage error, $MAPE$						1.46
Root mean square error, $RMSE$						2.85

GA was subsequently performed after ANN modeling to determine the optimum operating parameters for the enzymatic hydrolysis process. The optimum substrate loading, α-amylase concentration, amyloglucosidase concentration, and stroke speed were determined to be 19.99 %(w/v), 109.97 U/g, 65.98 U/mL, and 51.46 spm, respectively. The corresponding reducing sugar yield was 196.15 g/L. The ANN-GA

model was validated by performing independent experiments at these optimum process parameters and the mean reducing sugar yield was found to be 194.47 g/L, which was close to the predicted reducing sugar yield.

In general, the results indicate that the ANN-GA model adequately describes the enzymatic hydrolysis process. The weights of the input and output variables as well as the associated biases of the ANN model for the hydrolysis process are presented in **Table 4.4**. **Figure 4.5** shows the levels of significance of each input variable in the enzymatic hydrolysis process. The substrate loading, amyloglucosidase concentration, α-amylase concentration, and stroke speed had a level of significance of 53.90, 27.50, 13.79, and 4.8%, respectively.

Table 4.4: Weights of the input and output variables of the ANN model for enzymatic hydrolysis of *Manihot glaziovii* starch

Neuron	Input weight				Output weight	Bias to layer 1	Bias to layer 2
	X_1	X_2	X_3	X_4			
1	1.2222	0.3043	−2.4372	1.1716	−0.2188	−1.7361	−1.0699
2	−1.9446	0.05954	−0.1896	−1.0906	2.1478	0.4045	
3	−0.2227	0.1670	0.9469	0.6251	−0.3250	−1.4949	
4	−0.2884	−0.0127	−0.6202	−1.4279	0.0488	2.1914	

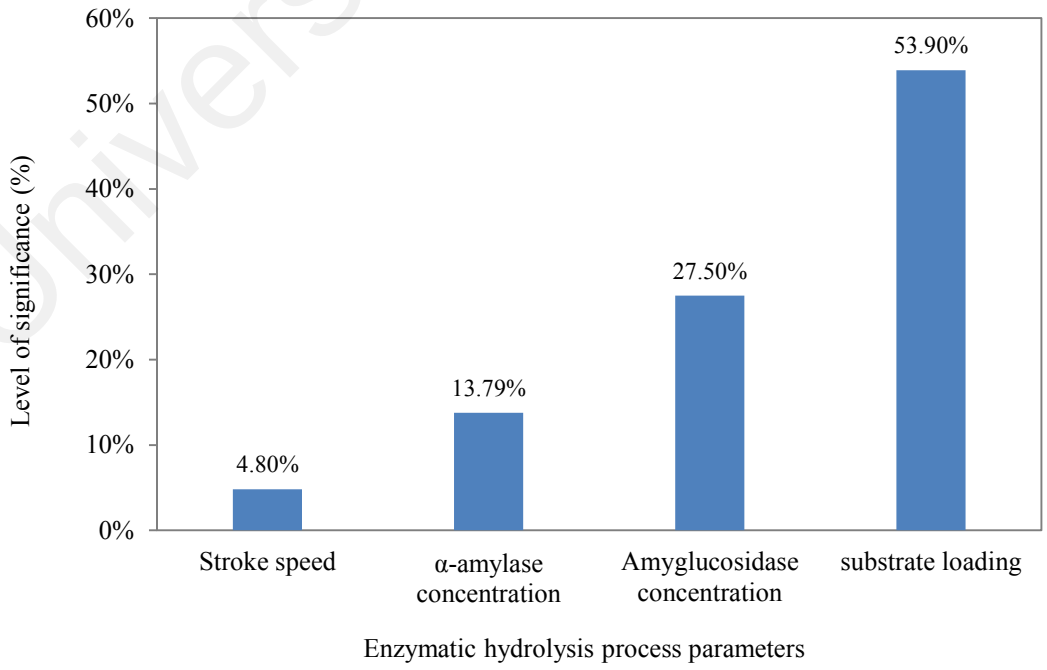

Figure 4.5: Levels of significance of the input variables for enzymatic hydrolysis of *Manihot glaziovii* starch

4.4.1.2. Enzymatic hydrolysis of sweet sorghum starch

The number of neurons in the hidden layer of the ANN model was varied from 2 to 8, as shown in **Table 4.5**. The optimum number of hidden neurons was determined based on the MSE and R value. The optimum number of hidden neurons was found to be 5 because this value produced the lowest MSE (3.069468) and highest R value (0.997), as shown in **Table 4.5**. The results obtained from the regression analysis for the ANN model are shown in **Figure 4.6**. Thus, the ANN architecture for enzymatic hydrolysis of sweet sorghum was 4-5-1, as shown in **Figure 4.7**.

Table 4.5: Determination of the optimum number of neurons in the hidden layer of the ANN model for enzymatic hydrolysis of sweet sorghum starch

No. of neurons in the hidden layer	**2**	**3**	**4**	**5**	**6**	**7**	**8**
Mean square error, MSE	25.5595	10.4071	5.4565	3.0695	5.0798	15.5051	16.1036
Correlation coefficient, R	0.9768	0.9904	0.9948	0.9971	0.9955	0.9870	0.9849

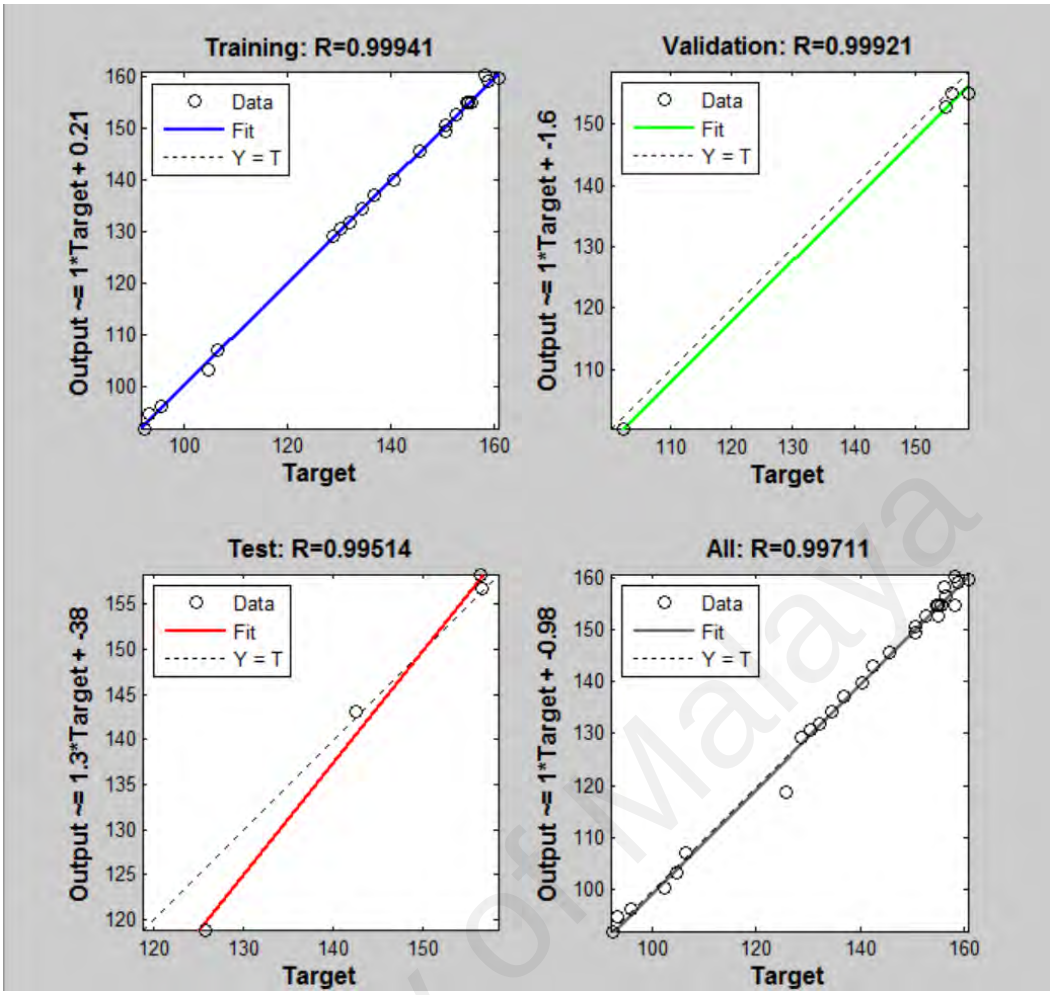

Figure 4.6: Results of the regression analysis for the ANN model for enzymatic hydrolysis of sweet sorghum starch

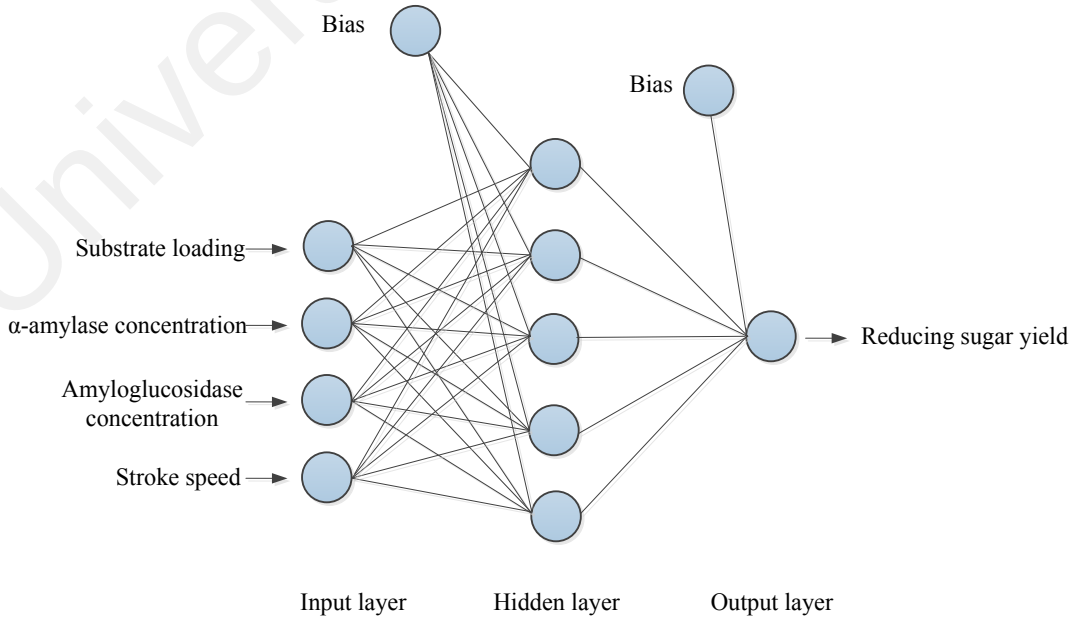

Figure 4.7: ANN architecture for enzymatic hydrolysis of sweet sorghum starch

The R^2 value of the ANN model was found to be more than 80% (R^2 = 99.42), indicating that the ANN model explains 99.42% of the variability in the response variable (reducing sugar yield) due to variations in the input variables (substrate loading, α-amylase concentration, amyloglucosidase concentration, and stroke speed), as shown in **Figure 4.8**. The $MAPE$ and $RMSE$ of the ANN model were determined to be 0.79 and 1.75, respectively, as shown in **Table 4.6**, indicating that the model is reliable to predict the reducing sugar yield for enzymatic hydrolysis of sweet sorghum starch.

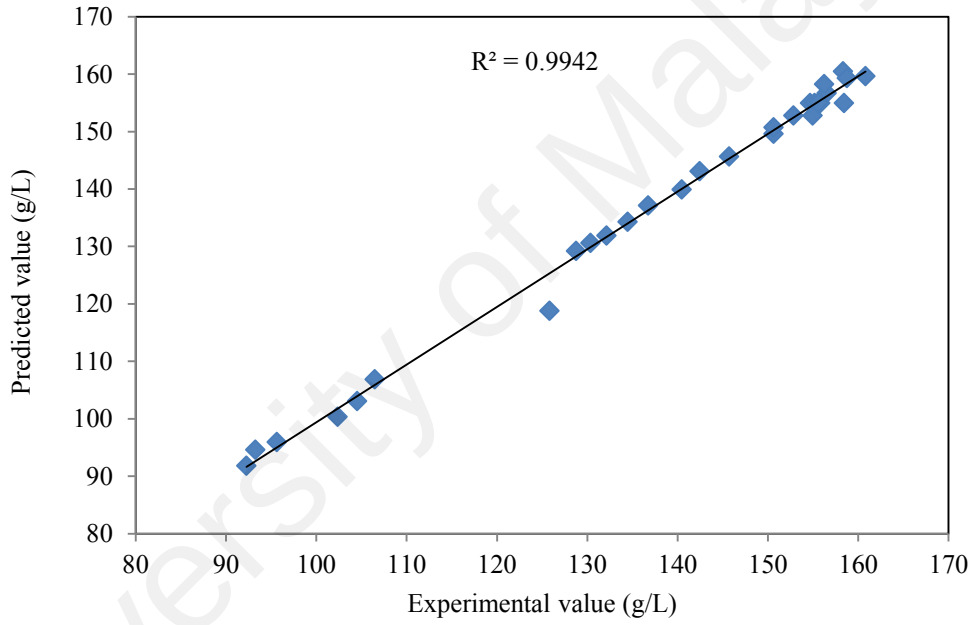

Figure 4.8: Comparison between the reducing sugar yield obtained from the Box-Behnken experiments (experimental values) and ANN model (predicted values) for enzymatic hydrolysis of sweet sorghum starch

Based on the results, it can be deduced that the ANN model has good prediction capability and the model can be used to optimize the enzymatic hydrolysis process parameters of sweet sorghum starch in order to maximize the reducing sugar yield.

Table 4.6: Box-Behnken design for enzymatic hydrolysis of sweet sorghum starch

Experimental run	Substrate loading (%(w/v))	α-amylase concentration (U/g)	Amyloglucosidase concentration (U/mL)	Stroke speed (spm)	Reducing sugar yield (g/L)	
					Experimental value	Predicted value
1	15	110	36	90	136.75	137.11
2	15	100	51	90	158.45	154.94
3	20	100	51	50	152.84	152.79
4	20	110	51	90	158.35	160.48
5	20	100	66	90	156.55	156.71
6	15	110	51	50	142.45	143.08
7	10	110	51	90	104.55	103.08
8	15	100	51	90	154.68	154.94
9	15	90	36	90	125.85	118.80
10	15	100	51	90	155.18	154.94
11	20	90	51	90	140.48	139.94
12	10	100	66	90	106.49	106.88
13	15	110	66	90	158.78	159.28
14	10	100	51	50	93.28	94.59
15	15	100	66	130	160.82	159.65
16	15	110	51	130	156.27	158.27
17	15	100	36	50	132.16	131.91
18	15	100	66	50	150.66	149.59
19	20	100	36	90	150.66	150.75
20	15	90	51	130	130.38	130.62
21	10	100	51	130	102.37	100.32
22	10	90	51	90	92.27	91.82
23	15	90	51	50	128.78	129.20
24	15	100	51	90	155.82	154.94
25	10	100	36	90	95.65	95.96
26	20	100	51	130	154.96	152.80
27	15	100	36	130	134.49	134.29
28	15	100	51	90	155.58	154.94
29	15	90	66	90	145.72	145.67
Mean absolute percentage error, $MAPE$						0.79
Root mean square error, $RMSE$						1.75

GA was executed after the ANN model to determine the optimum operating parameters for the enzymatic hydrolysis of sweet sorghum starch. The optimum substrate loading, α-amylase concentration, amyloglucosidase concentration, and stroke speed were determined to be 19.99 %(w/v), 109.59 U/g, 36 U/mL, and 63.19 spm, respectively. The corresponding reducing sugar yield was 170.26 g/L. Experiments were

carried out in duplicate using these optimum process parameters to validate the ANN-GA model. The mean reducing sugar yield was obtained to be 171.03 g/L, which was close to the predicted value.

Based on the results, it can be deduced that the ANN-GA model adequately describes the enzymatic hydrolysis process of sweet sorghum starch. The weights of the input and output variables as well as the associated biases of the ANN model for the enzymatic hydrolysis process are presented in **Table 4.7**. **Figure 4.9** shows the level of significance of each input variable involved in the enzymatic hydrolysis process. The levels of significance of the substrate loading, α-amylase concentration, amyloglucosidase concentration, and stroke speed were found to be 35.09, 27.23, 23.55, and 14.14%, respectively.

Table 4.7: Weights of the input and output variables of the ANN model for enzymatic hydrolysis of sweet sorghum

Neuron	Input weights				Output weight	Bias to layer 1	Bias to layer 2
	X_1	X_2	X_3	X_4			
1	−0.3533	0.0851	1.3516	−0.5084	−0.3925	3.1115	−0.4004
2	1.1241	3.8757	−2.2985	2.3100	0.1119	1.5886	
3	−2.7032	0.1208	−0.8937	−0.6568	−0.8680	−1.1954	
4	2.3528	−3.3691	0.0294	−1.1046	−0.1961	−2.3249	
5	0.7909	0.9825	1.2216	−1.5016	0.6059	2.8825	

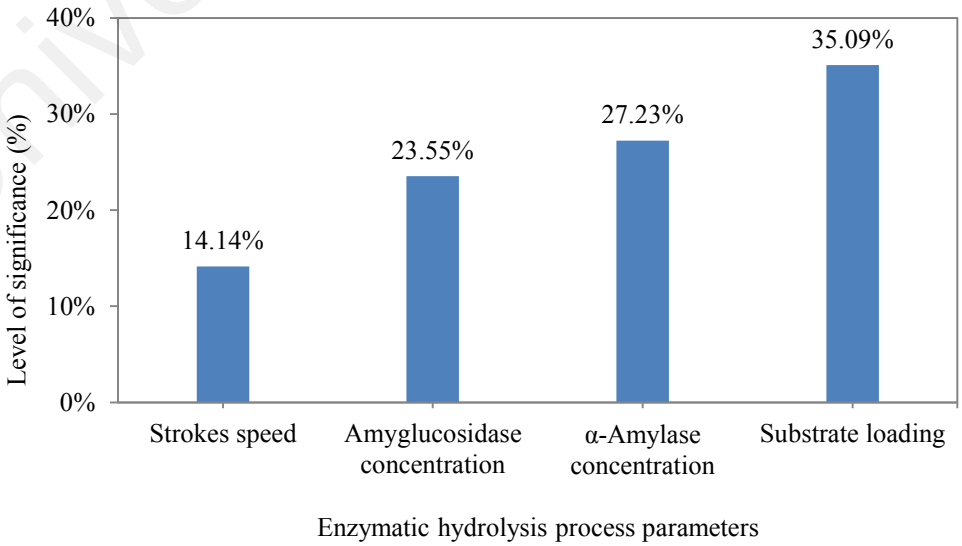

Figure 4.9: Levels of significance of the input variables for enzymatic hydrolysis of sweet sorghum starch

4.4.2. Optimization of the fermentation process parameters

The operating parameters of the fermentation process (i.e., yeast concentration, reaction temperature, and agitation speed) were varied to determine the interaction effects of these parameters on the bioethanol yield. The optimum number of neurons in the hidden layer of the ANN model was determined by testing different numbers of neurons until the MSE of the output data was minimized and the mean R value was close or equal to 1. GA was executed subsequent to the ANN model to determine the optimum operating parameters for the fermentation process.

4.4.2.1. Fermentation of reducing sugars obtained from enzymatic hydrolysis of *Manihot glaziovii* starch

The number of neurons in the hidden layer of the ANN model was varied from 2 to 6, as shown in **Table 4.8**. The optimum number of hidden neurons was determined based on the MSE and R value. It can be seen that the optimum number of hidden neurons was 4 because this value resulted in the lowest MSE (0.7241) and highest R value (0.998). The results of the regression analysis for the ANN model are shown in **Figure 4.10**. The ANN architecture for the fermentation of reducing sugars obtained from enzymatic hydrolysis of *Manihot glaziovii* starch was 3-4-1, as shown in **Figure 4.11**.

Table 4.8: Determination of the optimum number of neurons in the hidden layer of the ANN model for fermentation of reducing sugars obtained from enzymatic hydrolysis of *Manihot glaziovii* starch

No. of neurons in the hidden layer	2	3	4	5	6
Mean square error, MSE	6.5100	3.5350	0.7241	3.0880	12.1600
Correlation coefficient, R	0.9830	0.9900	0.9981	0.9920	0.9707

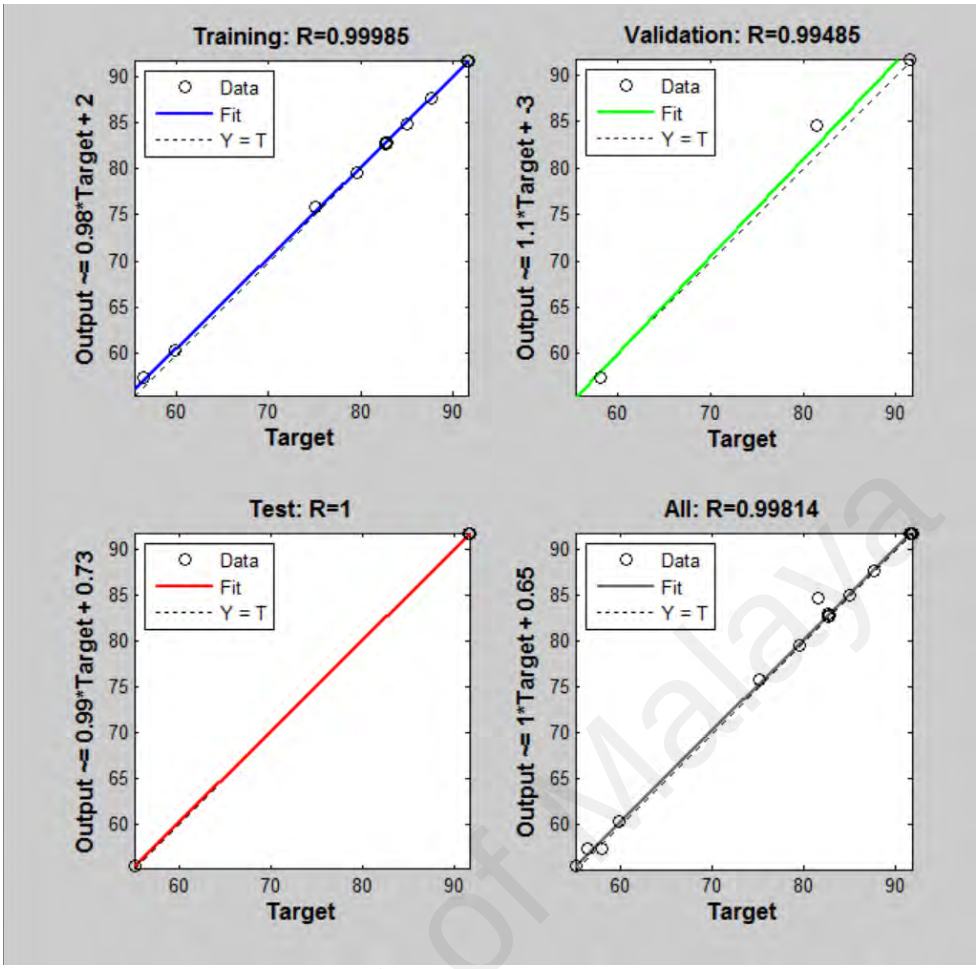

Figure 4.10: Results of the regression analysis for the ANN model for fermentation of reducing sugars obtained from enzymatic analysis of *Manihot glaziovii* starch

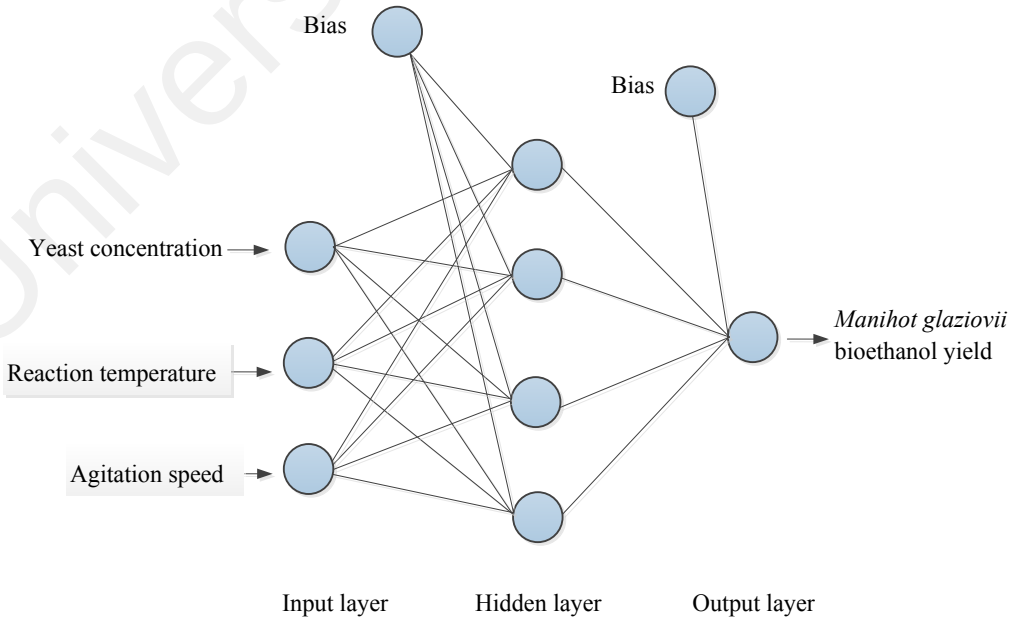

Figure 4.11: ANN architecture for fermentation of reducing sugars obtained from enzymatic hydrolysis of *Manihot glaziovii* starch

The R^2 value was 99.63, indicating that the ANN model describes 99.63% of the variability in the response variable (*Manihot glaziovii* bioethanol yield) due to variations in the independent variables (yeast concentration, reaction temperature, and agitation speed), as shown in **Figure 4.12**. The *MAPE* and *RMSE* were determined to be 0.58 and 0.85, respectively, as shown in **Table 4.10**, indicating that the ANN model has good prediction capability and the model can be used to determine the optimum parameters of the fermentation process.

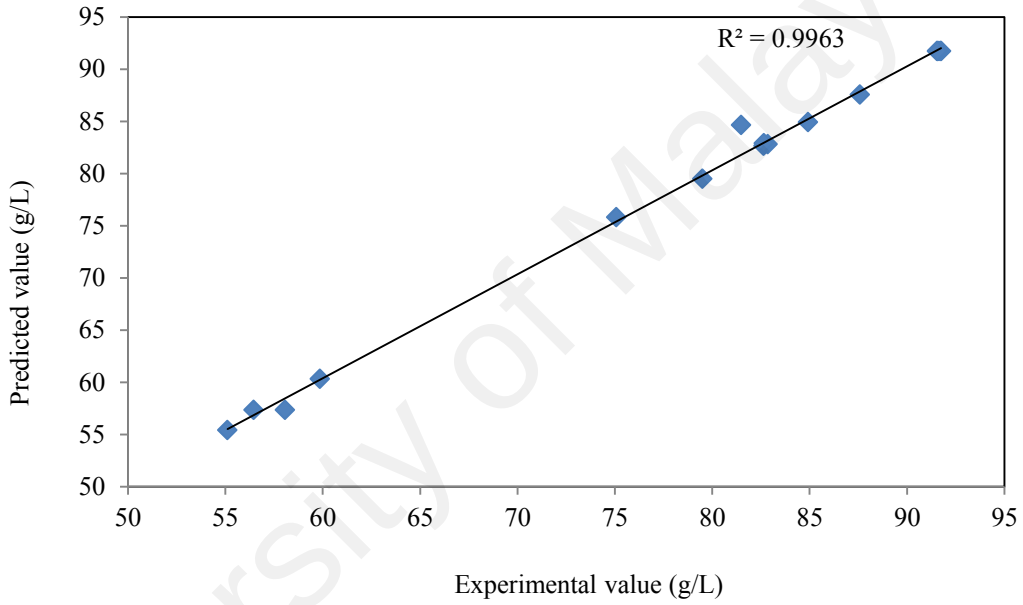

Figure 4.12: Comparison between the *Manihot glaziovii* ethanol yield obtained from the Box-Behnken experiments (experimental values) and ANN model (predicted values) for fermentation of the reducing sugars obtained from enzymatic hydrolysis of *Manihot glaziovii* starch

Table 4.9: Box-Behnken design for fermentation of the reducing sugars obtained from enzymatic hydrolysis of *Manihot glaziovii* starch

Experimental run	Yeast concentration (g/L)	Reaction temperature (°C)	Agitation speed (rpm)	*Manihot glaziovii* bioethanol yield (g/L)	
				Experimental value	Predicted value
1	0.5	42	150	56.45	57.34
2	1.5	42	150	82.64	82.64
3	1.5	30	150	79.49	79.49
4	1.5	36	250	87.58	87.56
5	1.0	36	150	91.64	91.71
6	1.5	36	50	81.48	84.65
7	1.0	36	150	91.75	91.71
8	1.0	42	50	82.84	82.80
9	1.0	36	150	91.72	91.71
10	0.5	36	50	58.07	57.36
11	0.5	30	150	55.11	55.42
12	1.0	42	250	84.92	84.92
13	0.5	36	250	59.85	60.33
14	1.0	30	250	82.65	82.89
15	1.0	30	50	75.08	75.80
16	1.0	36	150	91.55	91.71
17	1.0	36	150	91.56	91.71
Mean absolute percentage error, $MAPE$					0.58
Root mean square error, $RMSE$					0.85

The optimum yeast concentration, reaction temperature, and agitation speed were found to be 1.18 g/L, 36.48°C, and 217 rpm, respectively, and the corresponding *Manihot glaziovii* bioethanol yield was 94.45 g/L. Experiments were performed in duplicate under these optimum conditions to validate the ANN model and the mean *Manihot glaziovii* bioethanol yield was 94.02 g/L, which was close to the value predicted by the ANN model. Based on the results, it can be deduced that the ANN model adequately describes the fermentation process of reducing sugars obtained from enzymatic hydrolysis of *Manihot glaziovii* starch. The weights of the input and output variables as well as the associated biases of the ANN model for the fermentation process are summarized in **Table 4.10. Figure 4.13** shows the levels of significance of the three input variables involved in the fermentation process. The yeast concentration,

reaction temperature, and agitation speed had a level of significance of 48.08, 34.42, and 17.50%, respectively.

Table 4.10: Weights of the input and output variables of the ANN model for the fermentation of the reducing sugars obtained from enzymatic hydrolysis of *Manihot glaziovii* starch

Neuron	Input weights			Output weight	Bias to layer 1	Bias to layer 2
	X_1	X_2	X_3			
1	−2.3303	1.7475	0.1646	0.4705	2.1956	−0.2006
2	−0.2744	−2.3517	0.3528	0.4086	1.5251	
3	−2.1368	−0.6728	−0.1436	−1.1600	−1.1354	
4	−0.5195	−0.5078	1.4205	−0.5766	3.2475	

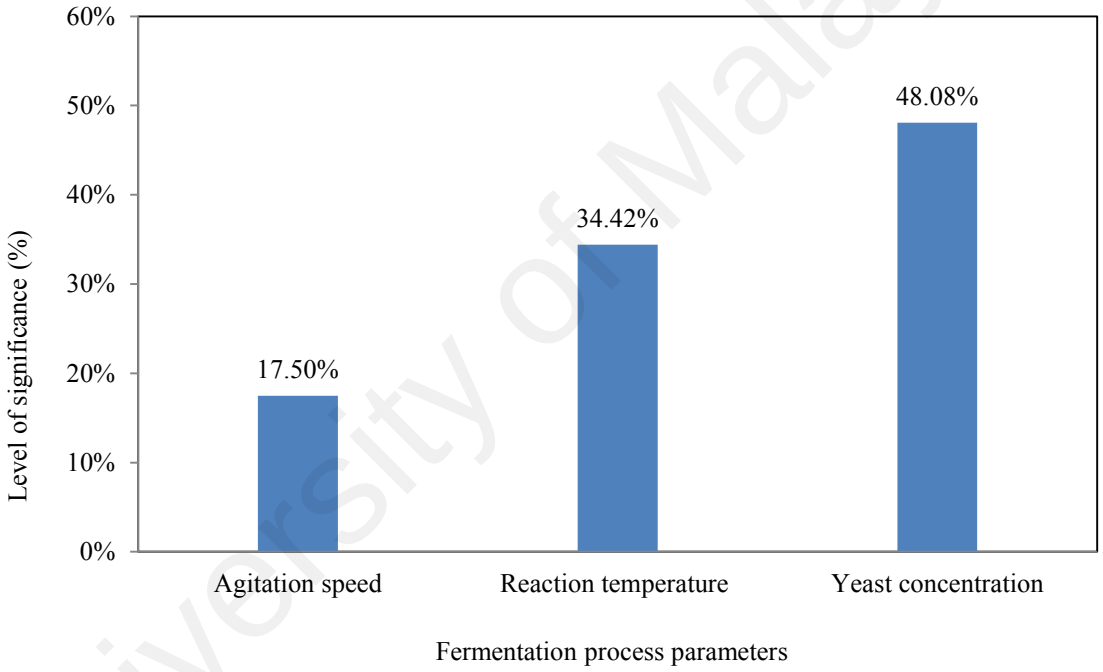

Figure 4.13: Levels of significance of the input variables for the fermentation of reducing sugars obtained from enzymatic hydrolysis of *Manihot glaziovii* starch

4.4.2.2. Fermentation of reducing sugars obtained from enzymatic hydrolysis of sweet sorghum starch

The number of neurons in the hidden layer was varied from 2 to 8, as shown in **Table 4.11**. The optimum number of hidden neurons was determined based on the MSE and R value. It can be seen that the optimum number of hidden neurons was 6, where this value yielded the lowest MSE (4.531) and the highest R value (0.993). **Figure 4.14**

shows the results of the regression analysis for the ANN model. The optimum ANN architecture for the fermentation of reducing sugars obtained from enzymatic hydrolysis of sweet sorghum starch was 3-6-1, as shown in **Figure 4.15**.

Table 4.11: Determination of the optimum number of neurons in the hidden layer of the ANN model for fermentation of reducing sugars obtained from enzymatic hydrolysis of sweet sorghum starch

No. of neurons in hidden layer	**2**	**3**	**4**	**5**	**6**	**7**	**8**
Mean square error, *MSE*	9.7012	7.0348	8.1521	4.5400	4.5319	5.8199	8.3755
Correlation coefficient, *R*	0.9735	0.9746	0.9809	0.9858	0.9933	0.9815	0.9765

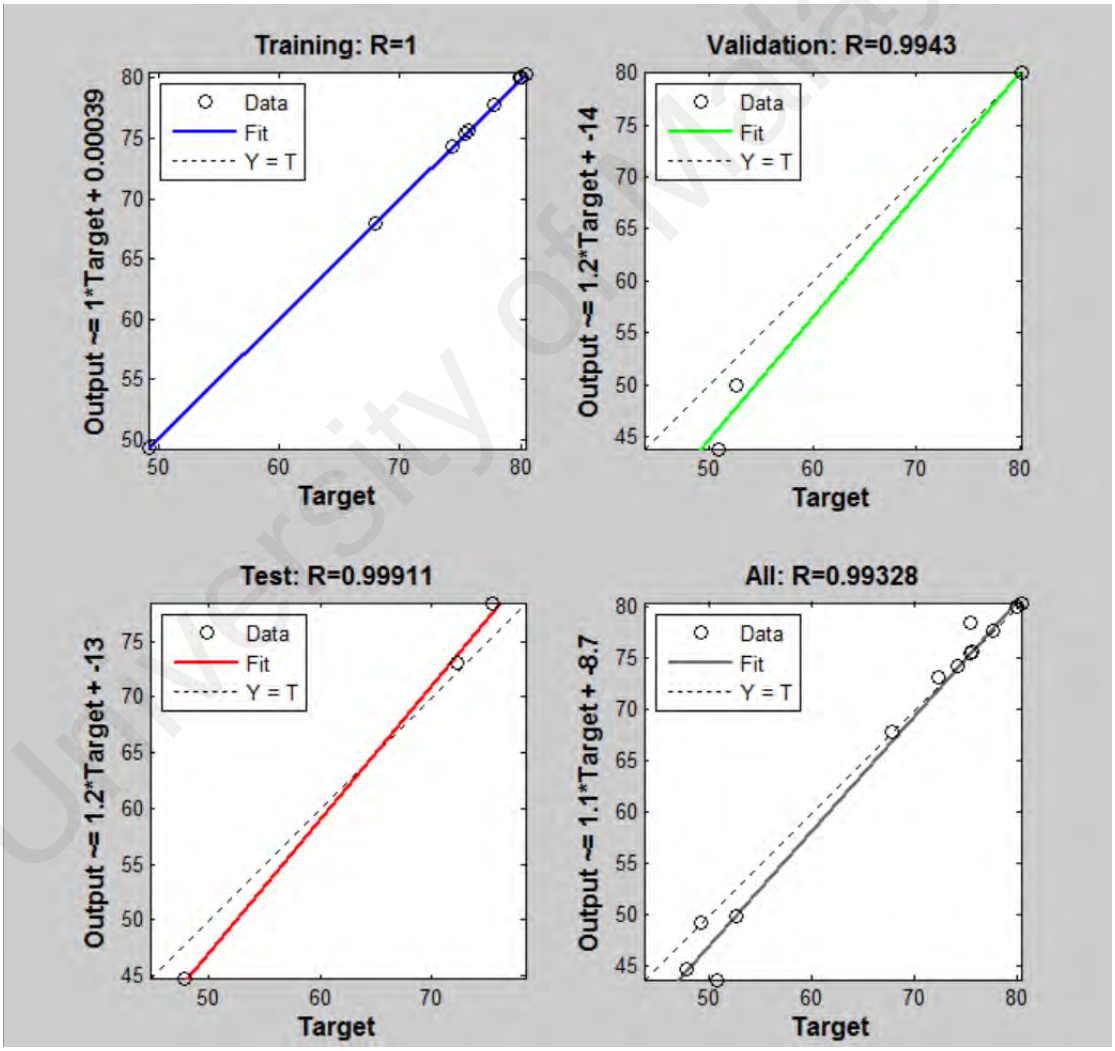

Figure 4.14: Results of the regression analysis for the ANN model for fermentation of reducing sugars obtained from enzymatic hydrolysis of sweet sorghum starch

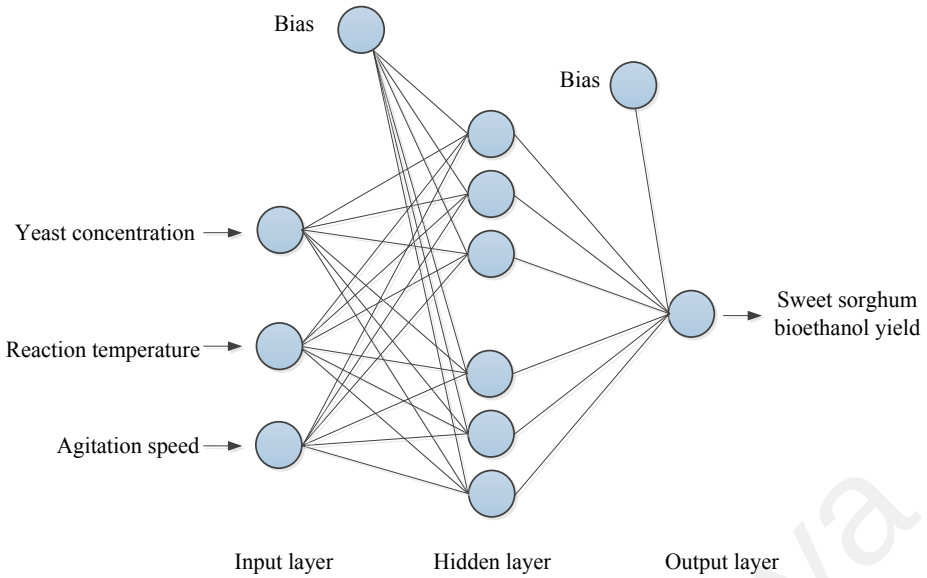

Figure 4.15: ANN architecture for fermentation of reducing sugars obtained from enzymatic hydrolysis of sweet sorghum starch

The R^2 value was 98.66, indicating that the ANN model explains 98.66% of the variability in the response variable (sweet sorghum bioethanol yield) due to variations in the independent variables (yeast concentration, reaction temperature, and agitation speed), as shown in **Figure 4.16**. The $MAPE$ and $RMSE$ were found to be 1.81 and 2.13, respectively (**Table 4.12**), indicating that the model has good prediction capability and the ANN model can be used to optimize the fermentation process parameters.

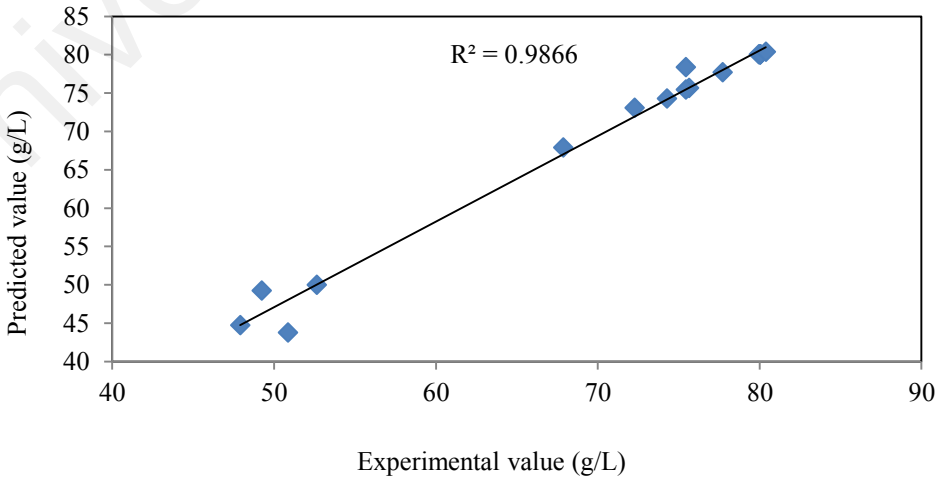

Figure 4.16: Comparison between the sweet sorghum bioethanol yield obtained from the Box-Behnken experiments (experimental values) and ANN model (predicted values) for fermentation of the reducing sugars obtained from enzymatic hydrolysis of sweet sorghum starch

Table 4.12: Box-Behnken design for the fermentation of reducing sugars obtained from enzymatic hydrolysis of sweet sorghum

Experimental run	Yeast concentration (g/L)	Reaction temperature (°C)	Agitation speed (rpm)	Sweet sorghum bioethanol yield (g/L)	
				Experimental value	Predicted value
1	0.5	36	250	52.65	49.98
2	0.5	42	150	49.25	49.25
3	1.0	36	150	80.034	80.02
4	1.0	36	150	80.035	80.02
5	1.0	42	50	75.64	75.64
6	0.5	36	50	50.87	43.75
7	0.5	30	150	47.91	44.75
8	1.0	36	150	80.04	80.02
9	1.5	30	150	72.29	73.09
10	1.0	30	50	67.88	67.88
11	1.0	42	250	77.72	77.72
12	1.5	36	50	74.28	74.28
13	1.5	42	150	75.44	78.38
14	1.0	36	150	79.95	80.02
15	1.0	36	150	80.06	80.02
16	1.5	36	250	80.38	80.38
17	1.0	30	250	75.45	75.45
Mean absolute percentage error, $MAPE$					1.81
Root mean square error, $RMSE$					2.13

The optimum yeast concentration, reaction temperature, and agitation speed were determined to be 1.29 g/L, 35.36°C, and 188.97 rpm, respectively, and the corresponding sweet sorghum bioethanol yield was 82.13 g/L. Experiments were performed in duplicate using these optimum process parameters in order to validate the ANN model and the mean sweet sorghum bioethanol yield was 81.28 g/L, which was close to the value predicted by the ANN model. Based on the results, it can be deduced that the ANN model adequately describes the fermentation of reducing sugars obtained from enzymatic hydrolysis of sweet sorghum starch. The weights of the input and output variables as well as the associated biases of the ANN model for the fermentation process are summarized in **Table 4.13. Figure 4.17** shows the levels of significance of the three input variables involved in the fermentation process. The yeast concentration,

reaction temperature, and agitation speed had a level of significance of 41.01, 31.47, and 27.51%, respectively.

Table 4.13: Weights of the input and output variables of the ANN model for fermentation of reducing sugars obtained from enzymatic hydrolysis of sweet sorghum starch

Neuron	Input weights			Output weight	Bias to layer 1	Bias to layer 2
	X_1	X_2	X_3			
1	−0.8278	1.8709	−1.4120	0.1446	2.7163	−0.2700
2	0.3452	−0.60345	−2.4092	−0.1063	−1.6780	
3	−0.3025	2.3888	0.90043	−0.1662	−1.0469	
4	−3.4609	−0.7405	−0.30641	−0.9585	−1.4650	
5	0.1351	−2.0354	−2.2070	−0.3323	−1.1208	
6	−0.1038	1.6695	2.1029	−0.2601	2.2353	

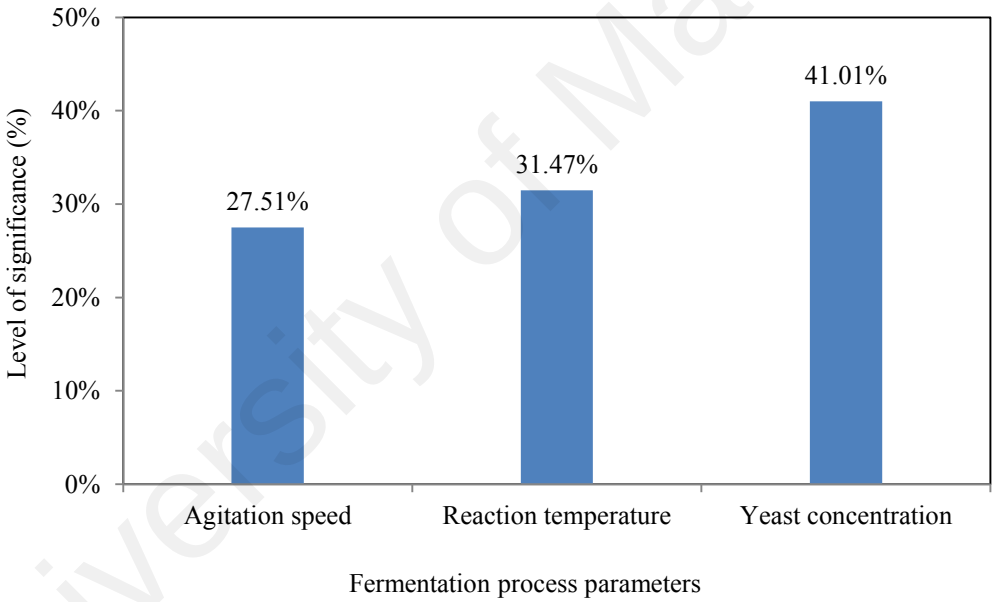

Figure 4.17: Levels of significance of the input variables for the fermentation of reducing sugars obtained from enzymatic hydrolysis of sweet sorghum starch

4.5. Energy consumption from optimum process parameters

Studies on the energy consumption of bioethanol production have been conducted for *Manihot glaziovii* and sweet sorghum. The optimum process parameters in bioethanol production can be shown in **Figure 4.18** below:

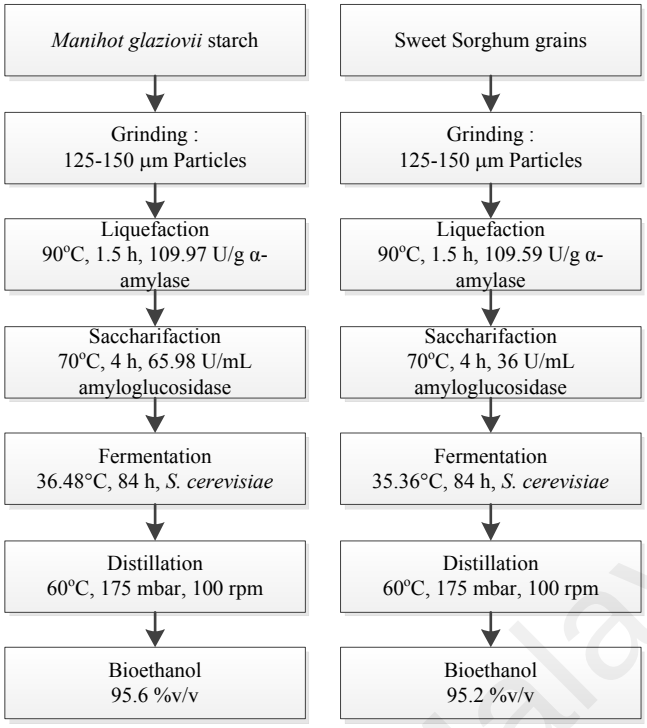

Figure 4.18: Comparison optimum parameters of bioethanol production from *Manihot glaziovii* and sweet sorghum

In this study, the bioethanol production is started by mixing *Manihot glaz*iovii starch or sweet sorghum grains with water. 2 kg of *Manihot glaziovii* starch or sweet sorghum grains was mixed with 10 liters of water and enzymes. Before entering the fermentation process, yeast was mixed with hydrolysates at 11.8 g/L for Manihot glaziovii starch and 12.9 g/L for sweet sorghum grains. After fermentation process, the solutions were filtered and purified, the concentration obtained from *Manihot glaziovii* starch or sweet sorghum grain were 95.6 %(v/v) and 95.2 %(v/v), respectively, in the distillation. Electricity consumption was calculated for bioethanol production in a laboratory scale as energy consumption is one of the key parameters that determine the variability of the bioethanol production.

4.5.1. Optimum hydrolysis process

Carbohydrates from *Manihot glaziovii* and sweet sorghum are mostly composed of glucose and some pentose-derived polymers that must be hydrolyzed to be efficiently used. When enzymatic hydrolysis takes place, a water bath shaker is required. A water

bath shaker is one machine that uses heating elements in the operation. In this study, the effect of strokes and enzyme concentration were validated, and the energy consumed in this process was calculated. Enzymatic hydrolysis is preferred over acid hydrolysis due to lower energy consumption (electricity), mild operating conditions, high sugar yields, and lower equipment and capital costs (Chen & Liu, 2017). For the process of liquefaction and saccharification, electricity is supplied to the heating element as well as the mechanical stroker. In the liquefaction process the heating water temperature is required at 90^{o}C and for 90 minutes, then proceed with the saccharification process by heating water of 70^{o}C for 240 minutes. Energy consumption of the optimal hydrolysis process (liquefaction and saccharification) in bioethanol production is presented in **Table 4.14**. It can be shown that *Manihot glaziovii* and sweet sorghum where the substrate and enzymes were added simultaneously consumed energy of 35,640 kJ (9.9 kWh).

4.5.2. Optimum fermentation process

The fermentation stage to produce ethanol consumes more electricity than in the hydrolysis stage. Energy input in this stage is in the form of heat and stirring. Yeast input of 11.8 g/L for *Manihot glaziovii* and 12.9 g/L for sweet sorghum was fed into the fermentation reactor, along with the sterilized hydrolysates. During the fermentation reaction, the glucose component in the hydrolysis liquid is converted into ethanol and carbon dioxide, as represented in Equation 4.1:

$$C_6H_{12}O_6 \rightarrow C_6H_{12}O_6 \rightarrow 2C_2H_6O + 2CO_2 \quad (4.1)$$

Another by-product generated as a result of fermentation process is protein. The fermented solution formed two layers, a protein layer and an ethanol-water layer in the upper layer. The ethanol-water layer is separated from its sediment (protein layer) with filter paper. In this study, fermentation was carried out at 36.48^{o}C and 35.36^{o}C for *Manihot galziovii* and sweet sorghum, respectively. Fermentation temperature is an

important component in ethanol production, because room temperature influences yeast activity, hence increases the ethanol yield (Kucharczyk & Tuszyński, 2018). Therefore, the use of energy in the fermentation process is influenced by temperature which indicates energy consumptions. Energy consumption for this fermentation stage can be seen in the **Table 4.14**.

4.5.3. Distillation process

To achieve technical-grade of bioethanol product, crude ethanol must be purified using distillation operations. Distillation is a method of separating the dissolved liquid mixture based on the difference in pure vapor pressure or the difference in the boiling points of each component contained in the mixture. Distillation is operated by using a heat separation force; hence it also requires energy input to operate. The fermented mixture, which consists of ethanol together with unfermented, dissolved and insoluble solids, is distilled in a series of steps. The energy input associated with distillation depends on the type of product desired and the use of energy saving techniques. **Table 4.14** shows the energy consumption of distiller RV 10 V IKA with a capacity of 500 mL *Manihot glaziovii* or sweet sorghum, which each at a rating of 10,800 kJ (3 kWh). The distillation took 60 minutes for each feedstock. These results indicate that it is economically feasible to produce ethanol from *Manihot glaziovii* and sweet sorghum using sustainable distillation technology. Energy consumption cost for the production of bioethanol from *Manihot glaziovi* and sweet sorghum are 38% of the total cost bioethanol production.

The use of chemicals is needed to produce reducing sugars in the hydrolysis process and the formation of bioethanol in the fermentation process. Chemical costs from these two processes constitute 62% of the total production costs. This finding is in line with the results by Cheng et al. (2019), where the cost of chemicals is 60% for bioethanol production. The operating conditions of the hydrolysis and fermentation

processes play an important role in determining the cost of production. Chemical costs for most of the variable operating costs are listed in **Table 4.15**. In addition, hydrolysis process and fermentation process occur in two additional, discrete process steps. This process has many advantages such as increased ethanol yield, decreased enzyme loading, decreased contamination, and lower capital cost.

Table 4.14: Energy consumption in the bioethanol production process

Process	Equipment	Time (h)	Power (kW)	Energy consumption (kWh)	Price (MYR)
Pre-treatment	Oven dryer	48	0.8	38.4	14.6
Hydrolysis Process					
- Liquefaction process	Water bath shaker	1.5	1.8	2.7	1.0
- Saccharifaction process	Water bath shaker	4	1.8	7.2	2.7
Sterilized	Autoclave	0.6	1.8	1.05	0.4
Fermentation process.	Incubator shaker	84	0.65	54.6	20.7
Distillation	Rotary evaporator	1	3	3	1.1
				Σ	40.6

Table 4.15: Chemical costs for hydrolysis and fermentation processes

Process	Chemical		Price (MYR)
Hydrolysis	Enzyme α-amylase	2.2 mL	14.8
	Enzyme amyloglucosidase	3.6 mL	39.3
Fermentation	Yeast extract	10.0 gr	9.3
	Potassium dihydrogen phosphate (KH_2PO_4)	4.0 gr	3.1
	Ammonium chloride (NH_4Cl)	2.0 gr	0.63
		Σ	67.13

4.6. Properties of the *Manihot glaziovii* and sweet sorghum bioethanols and bioethanol-gasoline blends

4.6.1. Physicochemical properties of the bioethanols

In general, the physicochemical properties indicate the fuel quality. In this study, the physicochemical properties of *Manihot glaziovii* and sweet sorghum bioethanols were determined according to the ASTM D4806 standard. The physicochemical

properties of these bioethanols were compared with those for gasoline and ethanol, as shown in **Table 4.16**.

Table 4.16: Comparison between the physicochemical properties of *Manihot glaziovii* bioethanol, sweet sorghum bioethanol, gasoline and ethanol

Property	*Manihot glaziovii* bioethanol	Sweet sorghum bioethanol	Gasoline (Masum et al., 2013)	Ethanol (Masum et al., 2013)
Chemical formula	C_2H_5OH	C_2H_5OH	C_5–C_{12}	C_2H_5OH
Carbon fraction (%(m/m))	56.1	55.7	85–88	52.2
Hydrogen fraction (%(m/m))	12.5	12.1	12–15	13
Oxygen fraction (%(m/m))	35.1	35.8	0	34.7
Carbon/hydrogen ratio (atomic ratio)	0.37	0.31	0.56	0.33
Viscosity at 20°C (mm^2/s)	1.28	1.40	0.5–0.6	1.2–1.5
Density at 15°C (kg/m^3)	803.7	807.9	750–765	785–809.9
Higher heating value, HHV (MJ/kg)	30.26	29.90	47.30	29.70
Lower heating value, LHV MJ/kg	27.3	26.9	44	26.9
Ethanol content (%(v/v)) min.	95.6	95.2	—	92.1

It can be seen from **Table 4.16** that the *Manihot glaziovii* and sweet sorghum bioethanols have an oxygen content of 35.1 and 35.8%, respectively, which can improve the combustion efficiency at high temperatures. In addition, lower carbon/hydrogen ratios of bioethanol (30–35%) in gasoline blends at the compression ratio of 11.5:1 lowers adiabatic flame temperature due to the lower energy content (Turner et al., 2011). One of the interesting findings of this work is that with the increase in oxygen content in the fuels adiabatic flame temperature decreases linearly consequently NO_x emission decreased linearly (Nabi, 2010).

The viscosity values at 20°C of the *Manihot glaziovii* and sweet sorghum bioethanols (1.28 and 1.40 mm^2/s, respectively) were within the range (1.2–1.5 mm^2/s) recommended for the properties of ethanol in **Table 4.16**. This indicates the effectiveness of the bioethanol production method and the viability of the *Manihot glaziovii* and sweet sorghum feedstocks. The density values at 15°C of the *Manihot glaziovii* and sweet sorghum bioethanols were found to be 803.7 and 807.9 kg/m^3,

respectively, which were also within the range specified the properties of ethanol in **Table 4.16** (785–809.9 kg/m^3). The carbon fractions of the *Manihot glaziovii* and sweet sorghum bioethanols were 56.1 and 55.7 %(m/m), which were higher than that in the properties of ethanol in **Table 4.16** (52.2 %(m/m)). However, the values were found to be lower than that for gasoline (85–88 %(m/m)). The hydrogen fractions of the *Manihot glaziovii* and sweet sorghum bioethanols were found to be 12.5 and 12.1 %(m/m), respectively, which were slightly lower than the maximum value specified the properties of ethanol in **Table 4.16** (13 %(m/m)). The oxygen fractions of the *Manihot glaziovii* and sweet sorghum bioethanols were measured to be 35.1 and 35.8 %(m/m), respectively, which were slightly higher than that specified in the properties of ethanol in **Table 4.16** (34.7 %(m/m)). The HHVs of the *Manihot glaziovii* and sweet sorghum bioethanols were 30.26 and 29.9 MJ/kg, respectively, which are greater than that given in the properties of ethanol in **Table 4.16** (29.7 MJ/kg); however, the values were lower than that for gasoline (47.3 MJ/kg). In general, the results indicate that the physicochemical properties of the *Manihot glaziovii* and sweet sorghum bioethanols are acceptable and fulfil most of the specifications stipulated in the properties of ethanol.

4.6.2. Density of the bioethanol-gasoline blends

Figure 4.19 shows the results of the density tests for the *Manihot glaziovii* and sweet sorghum bioethanol-gasoline blends. It can be seen that the blends with 20% of *Manihot glaziovii* and sweet sorghum bioethanols have the highest densities, with a value of 764.6 and 765.1 kg/m^3, respectively. In contrast, the blends with 5% of *Manihot glaziovii* and sweet sorghum bioethanols lead to the lowest densities, with a value of 753.7 and 754.4 kg/m^3, respectively. The results are in good agreement with those of Wu et al. (2004), where the density increase is less than 0.4%. Yücesu et al. (2006) performed experiments by blending ethanol with gasoline up to 60% and the density increase was found to be 0.93%. In general, density increases with the

increasing bioethanol content in the bioethanol-gasoline blends. This aspect lowers the intake manifold temperature, and this enhances the air-fuel mixture density (Tibaquirá et al., 2018). In addition, owing to the higher density of ethanol, more fuel is injected into the cylinder, which can increase the engine torque and power (Karaaslan et al., 2011).

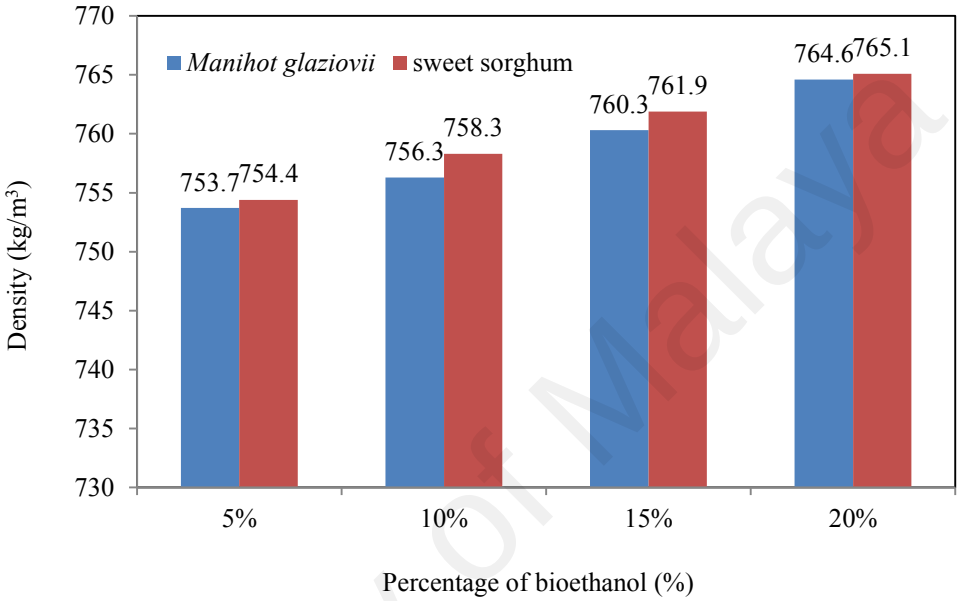

Figure 4.19: Density values of the *Manihot glaziovii* and sweet sorghum bioethanol-gasoline blends

4.6.3. Oxygen content of the bioethanol-gasoline blends

The presence of oxygen in bioethanol gasoline blends have contribute to leading enhanced oxidation stability, improved engine efficiency and faster flame speed (Larsen et al., 2009). The high content of oxygen in bioethanol gasoline blends enhances the combustion process is tuned to be better (Seggiani et al., 2012). Sasongko and Wijaya (2017) reported that bioethanol can be tread as a partially oxidized hydrocarbon due to oxygen atom contained in bioethanol and it could increase the number of oxygen atoms for the combustion process (leaning effect). In this study, elemental analyzer (CE 440, Exeter Analytical, Inc., USA) was employed to measure the oxygen content of the *Manihot glaziovii* and sweet sorghum bioethanol-gasoline blends. For the oxygen

content analysis, it is crucial to ensure that there are no fluorine, phosphorous, silicon, and most metals, which will lead to oxidation of the sample (removal of oxygen from the sample) and contaminate the catalyst inside the pyrolysis tube. The sample must be inserted into the silver capsules (without nickel sleeves) and the silver capsules need to be loosely crimped using a pair of tweezers to prevent the capsules from being stuck to the sample. Acetanilide/benzoic acid was used as the calibration standard for oxygen content analysis. The sample weight must be within a range of 1500–2500 µg. The results were recorded using the Windows®-based application software supplied with the elemental analyzer. The oxygen content values were found to be 6.35 and 7.13% for the blends containing 20% of *Manihot glaziovii* and sweet sorghum bioethanol, respectively, as shown in **Figure 4.20.** The findings were in line with the results by Schifter et al (2011), where the oxygen content is 7.36% for the blends containing 20% of bioethanol. The greater the content of oxygen in the fuel blends the more the oxidation tendency of CO, which will reduce CO emissions (Iodice et al., 2016).

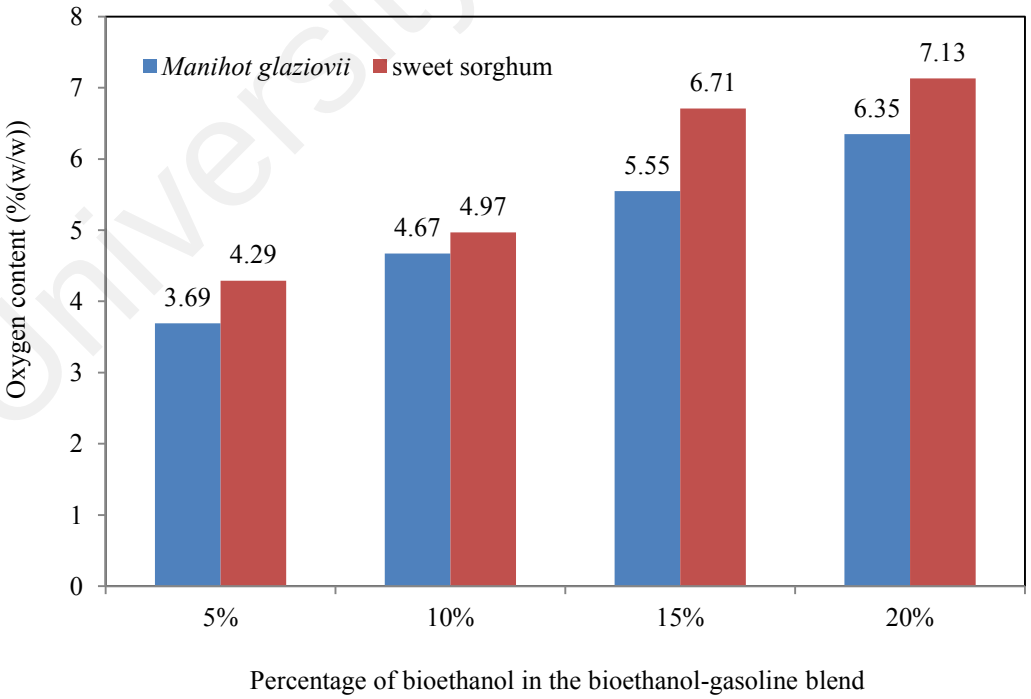

Figure 4.20: Oxygen content values of the *Manihot glaziovii* and sweet sorghum bioethanol-gasoline blends

4.6.4. Lower heating value of bioethanol-gasoline blends

The LHVs of the *Manihot glaziovii* bioethanol-gasoline and sweet sorghum bioethanol-gasoline blends are shown in **Figure 4.21**. It can be observed that the LHV decreased as the bioethanol content was increased in the bioethanol-gasoline fuel blends. Based on **Figure 4.21**, LHV of *Manihot glaziovi* and sweet sorghum bioethanol were decreased about 3.7 and 4.9%, respectively. The results are slightly better or similar to Yao and Chiang (2009), where LHV decreased by 4.9%. Instead, for pure bioethanol, the LHV is well defined. At ethanol content increasing, the LHV decreases, and therefore, a higher fuel flow rate, with respect to gasoline, is necessary at parity of engine load and efficiency. Instead, at ethanol content increasing in gasoline, the air mass required to burn the same mass of fuel in stoichiometric conditions decreases. The heat content of stoichiometric mixture takes into account both the LHV and the stoichiometric air fuel ratio. The fact that this value is similar for all the tested blends implies that the total mass flow rate (air + fuel) is only slightly reduced, at parity of engine load and efficiency and at ethanol content increasing. Therefore the same mass has to be aspirated by the engine. Anyway, a higher heat of vaporization of ethanol can reduce the mixture temperature, increasing the density and reducing the volume of the mixture to be aspirated (De Simio et al., 2012).

The highest LHVs were obtained for the blends with 5% of *Manihot glaziovii* and sweet sorghum bioethanols, with a value of 42.82 and 42.13 MJ/kg, respectively. In contrast, the lowest LHVs were obtained for the blends with 20% of *Manihot glaziovii* and sweet sorghum bioethanols, with a value of 41.28 and 40.14 MJ/kg, respectively. Decreasing LHV was followed by an increase in oxygen concentration in the blends with 20% of bioethanols. Indeed, Iodice et al.(2016) and Schifter et al. (2011) found that the higher oxygen content will improve the combustion characteristics and reduce

exhaust emissions, but this comes at the expense of a reduction in the heating value of the fuel.

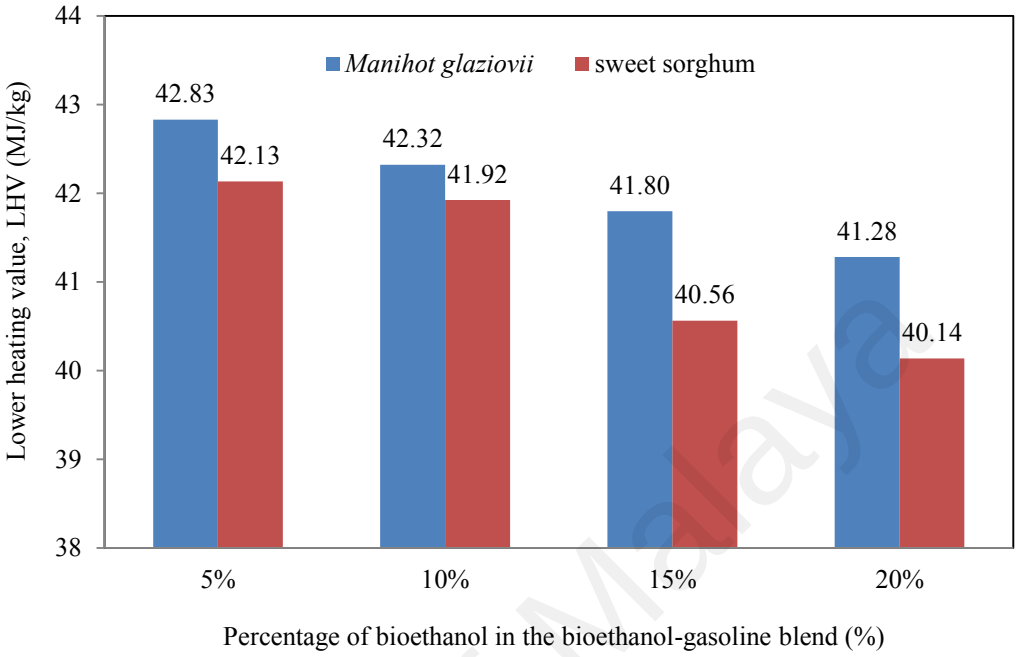

Figure 4.21: Lower heating values of the *Manihot glaziovii* and sweet sorghum bioethanol-gasoline blends

4.6.5. Research octane number of the bioethanol-gasoline blends

According to the SAE J1297 standard (SAE J1297, 2007) and Andrae (2008), the RONs of ethanol are 129 and 128, respectively. By definition, fuel octane rating in a spark ignition engine is a measure of the resistivity of a fuel to auto-ignition and prevent engine knocking (Anderson et al., 2012). In describing the RON of bioethanol-gasoline fuel blend mole basis interpretation is preferred since the air-fuel mixture chemical molar compositions corresponds to the scale of chemical reaction rates (Anderson et al., 2010). In this study, the RON of *Manihot glaziovii* and sweet sorghum bioethanol-gasoline blends increased with an increase in the percentage of bioethanol and the RONs of the blends were higher compared with that for gasoline. According to Aditiya et al. (2016), the high RON (108) of bioethanol is favorable to prevent engine knocking and early ignition in internal combustion engines. Because of the high RON for ethanol, compression ratio before the beginning of engine knocking for the fuel blends can be

higher than that by gasoline (Foong, 2013). Also, as reported by Kar et al. (2009), with every addition of 10% of ethanol in the blend ignition timing can be advanced by 5.6%, which they found the resistance to engine knocking was increased. Moreover, the addition of ethanol retards short ignition timing and improves engine performance owing to the improved combustion characteristics of the spark ignition engine (Masum et al., 2014). The RONs of the *Manihot glaziovii* and sweet sorghum bioethanol-gasoline blends are shown in **Figure 4.22**.

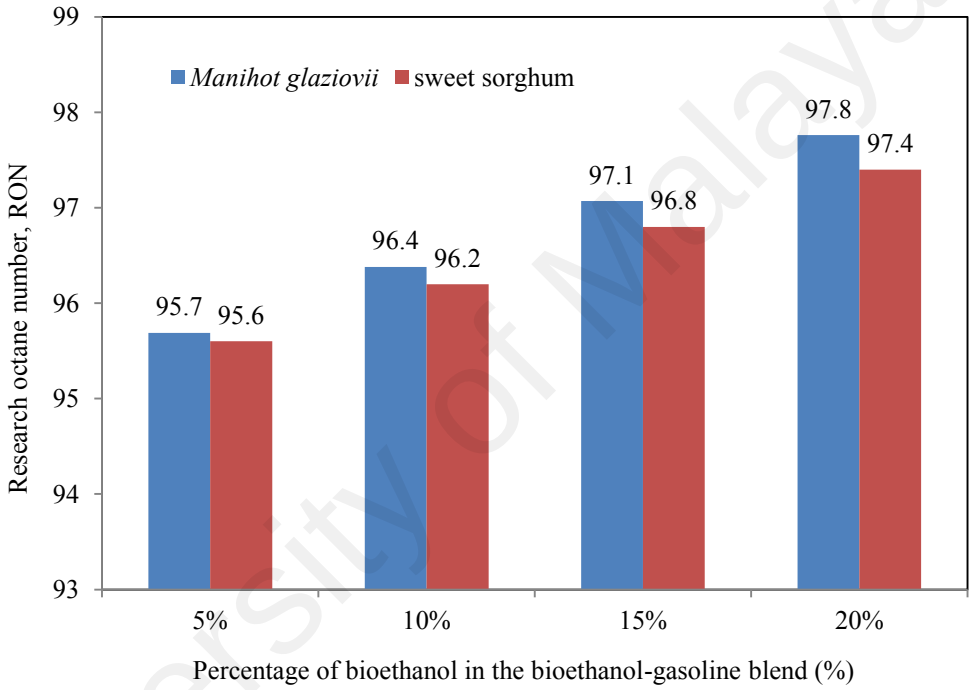

Figure 4.22: Research octane numbers of the *Manihot glaziovii* and sweet sorghum bioethanol-gasoline blends

4.6.6. Summary

Manihot glaziovii and sweet sorghum bioethanols were produced from enzymatic hydrolysis of *Manihot glaziovii* and sweet sorghum starches, respectively. For the enzymatic hydrolysis process, α-amylase from *Bacillus licheniformis* Type XII-A and amyloglucosidase from *Aspergillus niger* were used as the catalysts for liquefaction and saccharification. The yeast *Saccharomyces cerevisiae* was used for the fermentation process. The optimum values of the enzymatic hydrolysis process parameters for the *Manihot glaziovii* starch were as follows: (1) substrate loading: 19.99

%(w/v), (2) α-amylase concentration: 109.97 U/g, (3) amyloglucosidase concentration: 65.98 U/mL, and (4) stroke speed: 51.46 spm. For sweet sorghum starch, the optimum values of the enzymatic hydrolysis process parameters were as follows: (1) substrate loading: 19.99 %(w/v), (2) α-amylase concentration: 109.59 U/g, (3) amyloglucosidase concentration: 36 U/mL, and (4) stroke speed: 63.19 spm. The results showed that the substrate loading was the most important factor that influences the reducing sugar yield. The reducing sugar yields obtained from the optimum enzymatic hydrolysis process parameters were 196.15 and 170.26 g/L for *Manihot glaziovii* and sweet sorghum, respectively. For the fermentation process, the optimum yeast concentration, reaction temperature, and agitation speed were found to be 1.18 g/L, 36.48 °C, and 217 rpm, respectively, for *Manihot glaziovii* whereas the values were 1.29 g/L, 35.36°C, and 188.97 rpm, respectively, for sweet sorghum. The *Manihot glaziovii* and sweet sorghum bioethanol yields obtained from fermentation by yeast *Saccharomyces cerevisiae* at these optimum conditions were 94.45 and 82.13 g/L, respectively. The density and viscosity were found to be higher for the bioethanol-gasoline blends whereas the LHVs and RONs were found to be lower compared with those for gasoline.

4.7. Engine performance parameters

4.7.1. Air-fuel ratio

The mixture of air and fuel in an internal combustion motor is a crucial determinant of the combustion process in the cylinder. Therefore, the mixture of air and fuel must be as balanced as possible as it will affect the combustion efficiency, engine power, and emissions (Suiuay et al., 2020). Air-fuel ratio (lambda = λ) is a comparison $\frac{(AFR)_{act}}{(AFR)_{st}}$, where $(AFR)_{act}$ is the actual air-fuel ratio and $(AFR)_{st}$ is the stoichiometric air-fuel ratio of the test fuel (Yücesu et al., 2007). An ideal mixture of air and fuel promotes an optimal engine performance, by delivering an efficient fuel consumption and combustion. The air-fuel ratio theoretically has an important role in understanding how

a mixture burns, if the ratio of a mixture is lower than the theoretical ratio ($\lambda < 1$) then the mixture will become rich and combustion that occurs due to lack of oxygen. Conversely, if the mixture ratio is higher ($\lambda > 1$) than the theoretical ratio the mixture will become lean or too much oxygen in the combustion, while for stoichiometric mixtures is defined as $\lambda = 1$ (Schifter et al., 2011; Suiuay et al., 2020). From the results of the experiment, the value of λ obtained is greater than 1 so it is in lean region. **Table 4.17** shows the results of air-fuel ratio experiments.

Table 4.17: Air-fuel ratio (λ) values of the bioethanol-gasoline blends and gasoline

	λ (lambda) $= \frac{(AFR)_{act}}{(AFR)_{st}}$								
Rpm	Gasoline	ME5	ME10	ME15	ME20	SE5	SE10	SE15	SE20
1600	1.17	1.17	1.20	1.20	1.21	1.17	1.19	1.19	1.21
1800	1.19	1.17	1.16	1.17	1.18	1.20	1.16	1.19	1.20
2000	1.15	1.15	1.13	1.15	1.17	1.15	1.14	1.15	1.17
2200	1.16	1.16	1.12	1.13	1.16	1.15	1.15	1.15	1.16
2400	1.18	1.15	1.12	1.14	1.18	1.17	1.16	1.17	1.19
2600	1.17	1.16	1.16	1.18	1.20	1.18	1.18	1.17	1.20
2800	1.19	1.17	1.20	1.22	1.24	1.19	1.18	1.20	1.23
3000	1.15	1.16	1.19	1.19	1.21	1.16	1.16	1.18	1.20
3200	1.17	1.19	1.21	1.23	1.25	1.18	1.20	1.20	1.23
3400	1.14	1.19	1.24	1.26	1.27	1.16	1.18	1.21	1.25

4.7.2. Engine torque

Figure 4.23 displays engine torques (ET) resulted from gasoline and bioethanol-gasoline blends with respect to the engine speed. It shall be noted that ME and SE represent the *Manihot glaziovii* and sweet sorghum bioethanol-gasoline blends, respectively. As depicted in the **Figures**, ET increased following the increase of engine speed. At 3200 rpm, the ET was lower for gasoline (11.04 Nm) compared with that for the ME20 (11.51 Nm) and SE20 (11.30 Nm) blends. This was indeed expected due to the bioethanol-gasoline blends contained ~3−7% of oxygen and these blends had higher octane numbers compared with gasoline, which improved combustion. Even though the

addition of bioethanol into gasoline decreased its heating value, this was compensated by the improvement in engine power and torque. This can be attributed to the fact that bioethanols are oxygenated fuels, which will improve the combustion characteristics and increase the ET (Karaaslan et al., 2011). In addition, Hsieh et al. (2002) reported that the heating value of the ethanol/gasoline blends will reduce with the increase of the ethanol content in the mixtures. However, this consideration does not mean that the use of ethanol may led to a decreased power output of the engine. In fact, by focusing on the heating value of the stoichiometric air/fuel mixtures (that is the ratio between the heating value and stoichiometric air/fuel ratio), it is clear that this parameter represents the amount of energy introduced in the engine cylinder with the unity mass of stoichiometric mixture of air and fuel (Iodice et al., 2017). This result is also consistent with research by Elfasakhany (2015) using a spark-ignition engine, single cylinder, 4-strokes, and a carburetor fuel system. The study reported that the increase in the percentage of ethanol content increases engine torque, as the experiment resulted in engine torque of 3.7% increase at 3000 rpm from combusting E10 compared to using gasoline. Results from this study are in accordance with those by Najafi et al. (2009), who reported the combustion characteristics improvement from the increase of ethanol content in the fuel blend. The air-fuel ratios in this study are λ=1.25 and 1.23 for ME20 and SE20, respectively, at an engine speed of 3200, which indicates combustion conditions in the lean region. At the same air-fuel ratio, ET can also be improved by charge density increases and the addition of oxygenated alcohol into the fuel blend, producing a more efficient lean combustion (Masum et al., 2014).

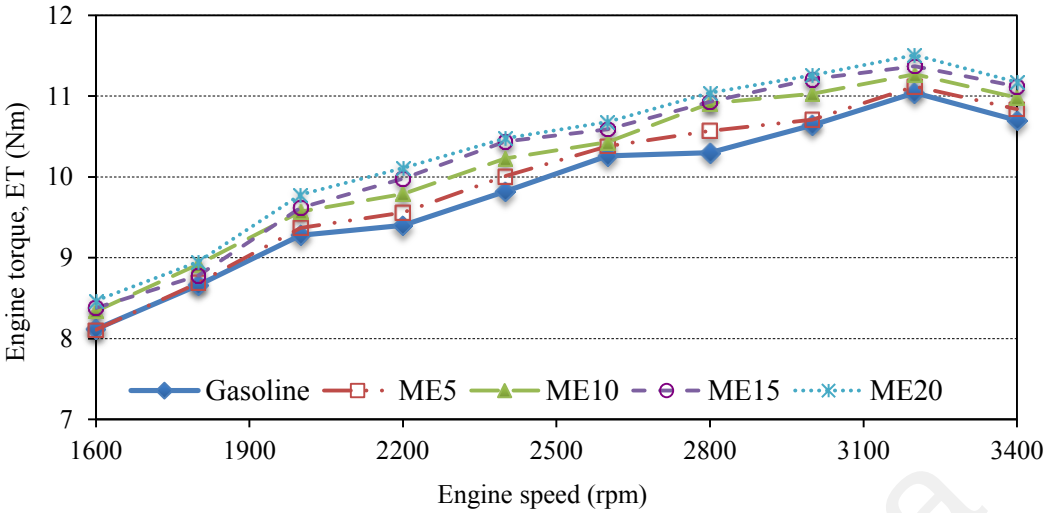

(a)

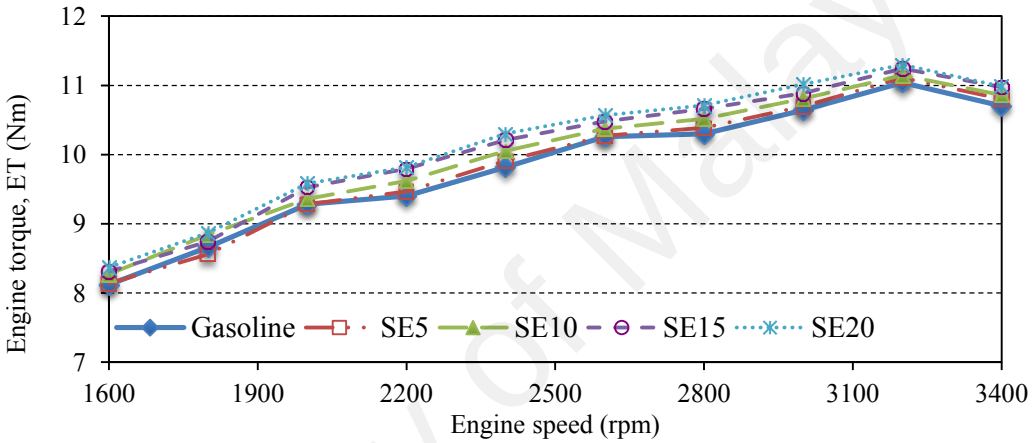

(b)

Figure 4.23: Effect of engine speed of bioethanol-gasoline blend and gasoline fuels on the engine torque at full throttle conditions (a) *Manihot glaziovii* (b) sweet sorghum

4.7.3. Brake power

The brake power (BP) produced plotted against engine speed from engine performance test by gasoline and bioethanol-gasoline blends is shown in **Figure 4.24**. In general, the BP was slightly higher for the ME20 (3.86 kW) and SE20 (3.78 kW) blends compared with that for gasoline (3.70 kW). The higher BP can be associated with the combustion improvement due to the ethanol addition in the blend. Furthermore, the *Manihot glaziovii* and sweet sorghum bioethanol-gasoline blends have higher oxygen content, which enhances the reaction between the air and fuel in the combustion. It was investigated by Al-Hasan (2003) using spark ignition engine (typeToyota-Tercel-3A) at the throttle opening position and variable engine speed operating conditions. The result

showed that increasing brake power continues until the percentage of ethanol reaches 20%. After this point, brake power starts to decrease by about 8.3%. Besides that, the air-fuel ratios that occur for ME20 and SE20 are λ=1.25 and 1.23, respectively, at given engine speed, and this suggests a lean region. The combustion of gasoline in the engine test is characterized as the fuel-lean region, which increases combustion performance. At the same engine speed, the use of bioethanol-gasoline blends enhances the combustion performance because of their higher oxygen content and this elevates the engine power (Al-Hasan, 2003; Park et al., 2014).

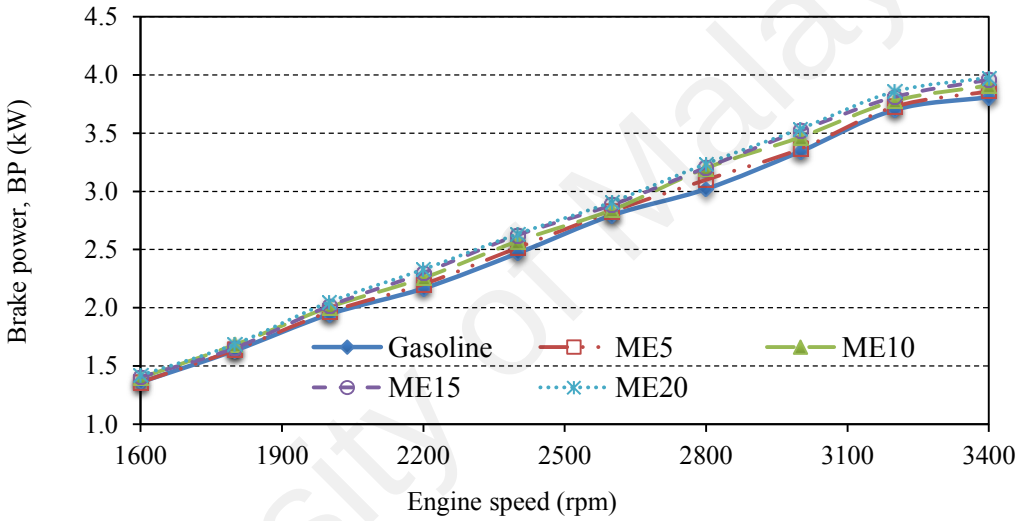

(a)

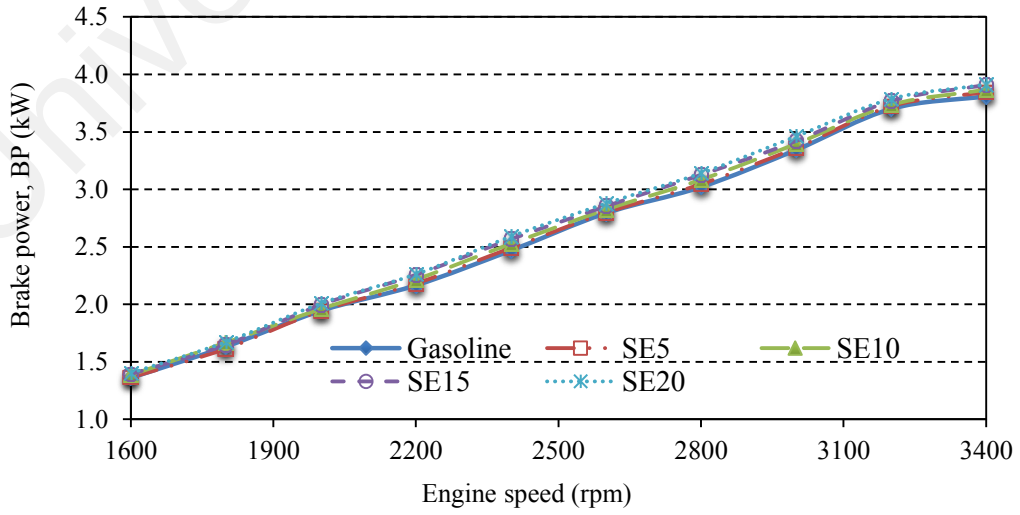

(b)

Figure 4.24: Effect of engine speed of bioethanol-gasoline blend and gasoline fuels on the brake power (BP) at full throttle conditions (a) *Manihot glaziovii* (b) sweet sorghum

4.7.4. Brake specific fuel consumption

Variation of brake specific fuel consumption (BSFC) of gasoline and bioethanol-gasoline blends over a range of engine speed is shown in **Figure 4.25**. The lowest BSFC was found at 3200 rpm, with the values of 270.74 and 279.42 g/kWh for the ME20 and SE20, respectively. At 3200 rpm engine speed, BSFC of gasoline was 288.8 g/kWh, which is higher than those for the bioethanol-gasoline blends investigated in this study. The high oxygen content (~3−7%) of the *Manihot glaziovii* and sweet sorghum bioethanols results in a lower BSFC value for bioethanol-gasoline blends than that of gasoline. This is the addition to the lean operation as indicated by the air-fuel ratios (λ) of 1.25 and 1.23 for ME20 and SE20, respectively, at 3200 rpm. Accordance with Yücesu et al. (2007), who reported minimum BSFC obtained at 1.05 AFR (λ) for all test fuels and rose up depending on ethanol content. Since no engine modifications were made in this study, the favorable engine performance can be attributed to the higher octane numbers of the *Manihot glaziovii* and sweet sorghum bioethanols, which improves the combustion characteristics. Najafi et al. (2009) found that the BSFC values are lower for E5-E20 fuels than that of gasoline due to the ethanol percentage increase, which improved the engine performance.

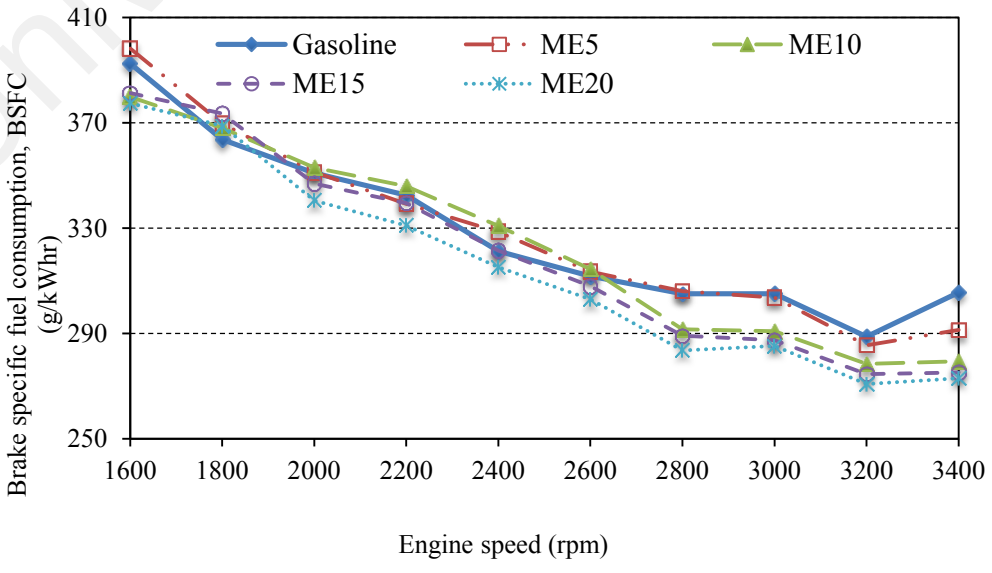

(a)

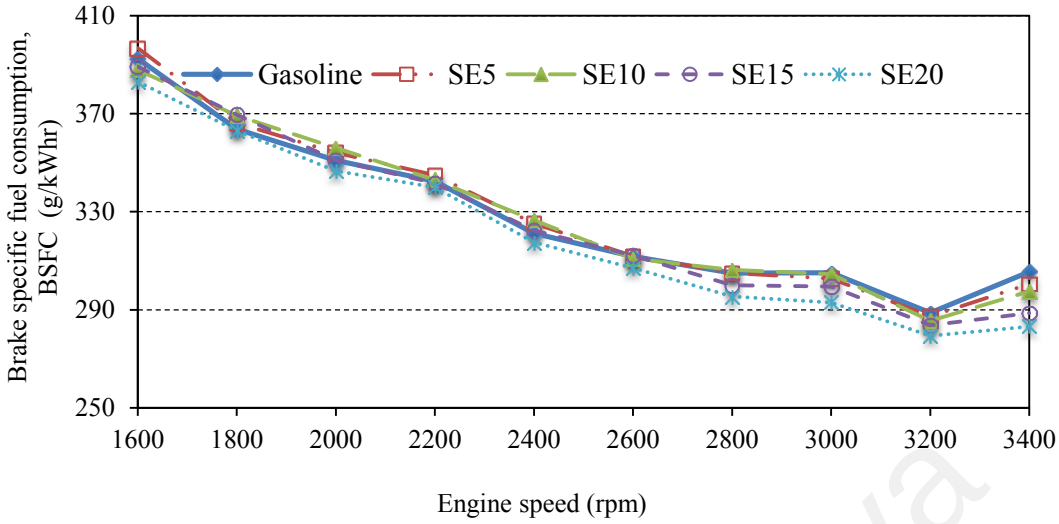

(b)

Figure 4.25: Effect of engine speed of bioethanol- gasoline blend and gasoline fuels on the brake specific fuel consumption (BSFC) at full throttle conditions (a) *Manihot glaziovii* (b) sweet sorghum

4.7.5. Brake thermal efficiency

Variation of brake thermal efficiency (BTE) from engine performance test using gasoline and bioethanol-gasoline blends over a range of engine speed is shown in **Figure 4.26**. The maximum BTE values were obtained for the ME20 and SE20 blends, with a value of 32.21 and 32.10%, respectively. The maximum BTE values for these blends are higher compared with that for gasoline (28.6%). In comparison with gasoline fuel, there is an increase in BTE by 11.21 and 10.90% for ME20 and SE20, respectively. The BTE increases with an increase in the percentage of bioethanol, which conforms well with the results of Anu Nair et al. (2018). In their experiment using a four-stroke engine, single cylinder, and a carburetor fuel system, BTE was found to increase by 10.37% when using bioethanol-gasoline fuel blends (E25). Similar results are reported by Najafi et al. (2009), who observed that the BTE of the bioethanol-gasoline blend of 20% ethanol is 5.8% higher compared with that of gasoline. As the ethanol content increases in the fuel blend, the indicated work increases (i.e., the indicated efficiency $_i$ increases). There is a relationship between the engine speed and the brake thermal

efficiency, as observed that the brake thermal efficiency reaches a maximum as the engine speed reaching 3000 rpm. Moreover, the added ethanol produces lean mixtures that increase the relative air–fuel ratio of 0.925 to a higher value and makes the burning more efficient. These results are also in accordance with study Datta et al. (2012), in which they reported an increase in BTE of 6% for E40 compared to gasoline. The results from this study can be attributed to the greater oxygen content of the *Manihot glaziovii* bioethanol-gasoline and sweet sorghum bioethanol-gasoline blends, in comparison with that of gasoline (Eyidogan et al., 2010). The excess oxygen results in a better combustion, which improves the BTE (Masum et al., 2015; Schifter et al., 2011). In addition, the air-fuel ratio (λ) that occurs in the lean region, as indicated by the value of 1.25 and 1.23 for ME20 and SE20, respectively, at 3200 rpm engine speed, and this is in accordance by Wu et al. (2016) research which reports an increased thermal efficiency at λ = 1.4. In general, the bioethanol-gasoline blends with the highest percentage of bioethanol (20%) had higher oxygen content, which enhanced the combustion characteristics, resulting in the highest BTE.

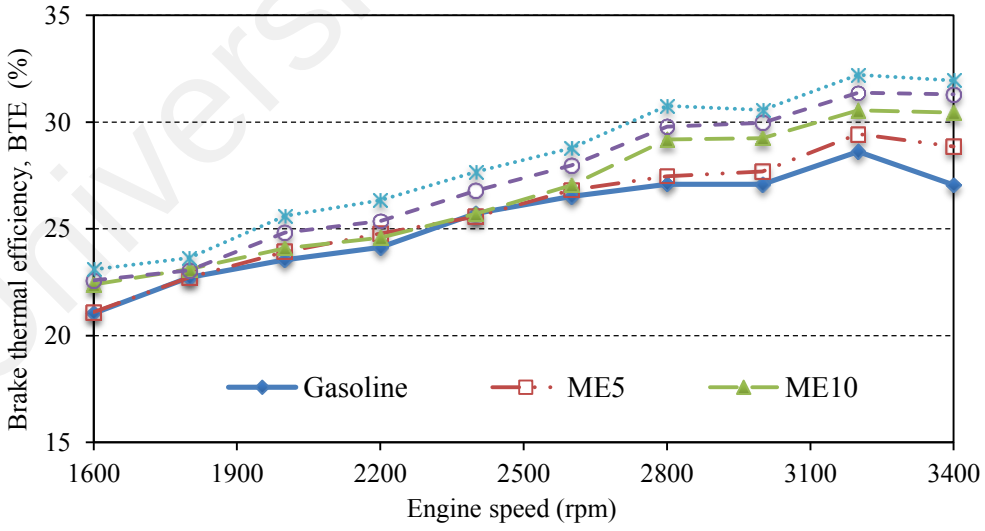

(a)

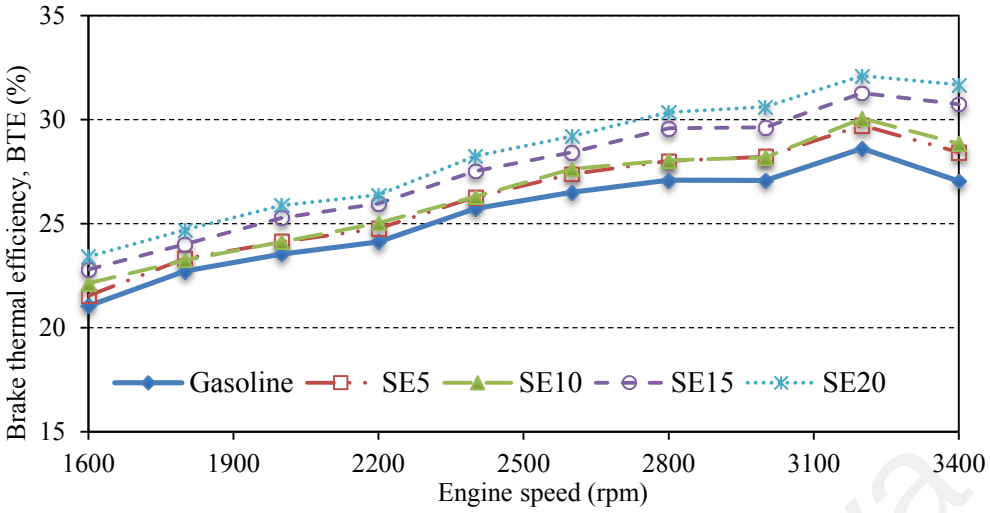

(b)

Figure 4.26: Effect of engine speed of bioethanol- gasoline blend and gasoline fuels on the brake thermal efficiency (BTE) at full throttle conditions (a) *Manihot glaziovii* (b) sweet sorghum

4.7.6. Summary

In general, the *Manihot glaziovii* and sweet sorghum bioethanol-gasoline blends improved the performance of the single-cylinder four-stroke spark ignition engine, as indicated by the higher ET, BP, and BTE, as well as lower BSFC. The highest BTE values were obtained for the ME20 and SE20 blends, with a value of 32.21 and 32.10%, respectively, which were higher than that for gasoline (28.61%). In addition, the BSFC was the lowest for the ME20 and SE20 blends at 3200 rpm, with a value of 270.74 and 279.42 g/kWh, respectively. In contrast, the BSFC was higher for gasoline (288.79 g/kWh) at this engine speed. Also, the air-fuel ratio (λ) shows a lean region of 1.25 and 1.23 for ME20 and SE20, respectively, at 3200 rpm engine speed.

4.8. Exhaust emission parameters

4.8.1. Carbon monoxide emissions

CO is a relatively unstable gas and tends to react with other compounds. **Figure 4.27** shows CO emissions resulted from engine test using gasoline and bioethanol-gasoline fuel blends over a range of engine speed. From this **Figure**, it can be observed

that the fuel blends resulted lower CO emissions than that by gasoline. At 3000 rpm ME20 and SE20 produced the lowest CO emissions with a value of 1.06 and 1.19 %(v/v), respectively. In contrast, the CO emissions obtained for gasoline were 1.59 %(v/v) at this engine speed, which were higher compared with the bioethanol-gasoline blends. As the bioethanol content increases, the CO emissions decrease. CO emissions were also observed decreased as the engine speed increased due to the higher air-fuel ratio (λ), which improved combustion (Canakci et al., 2013; Ozsezen & Canakci, 2011). The ratio air-fuel for ME20 and SE20 is λ = 1.21 and 1.20, respectively, at 3000 rpm engine speed and this condition is a lean region. This result is also in accordance with Wu et al. (2016), who reported a decrease in CO emissions at an air-fuel ratio (λ) of 1.2. In addition, according to Deng et al. (2019) in their research using a single-cylinder four-strokes motorcycle, they explained that CO emission drops sharply when the air-fuel ratio changed from rich to lean. Specifically, at full load, the CO emission decreases about 4 times when λ changes from 0.85 to 1.1 and continues to decrease until at λ = 1.2. Bioethanols have higher oxygen content compared with gasoline, and this essentially provides more oxygen during the combustion process. This oxygen excess in the fuel blend results in a ~~l~~leaning effect". In other words, as the ethanol content in the blend is increased the combustion is leaner, close to stoichiometric combustion and results in better combustion characteristics.

The high heat of vaporization results in a lower energy content, which reduces the adiabatic flame temperature (Canakci et al., 2013). As an oxygenated fuel, bioethanol-gasoline fuel blend carries a high oxygen content, which allows the engine to operate close to stoichiometric combustion. This increases the combustion temperature and therefore, most of the CO are oxidized into CO_2, such that a lower amount of CO emissions is detected in the exhaust (Alptekin et al., 2015). Charge cooling effect is possible with the fuel blend due to the high latent heat of vaporization, and this

decreases the temperature, which increases the volumetric efficiency. For this reason, the addition of bioethanol into gasoline promotes the combustion efficiency and boosts the engine power.

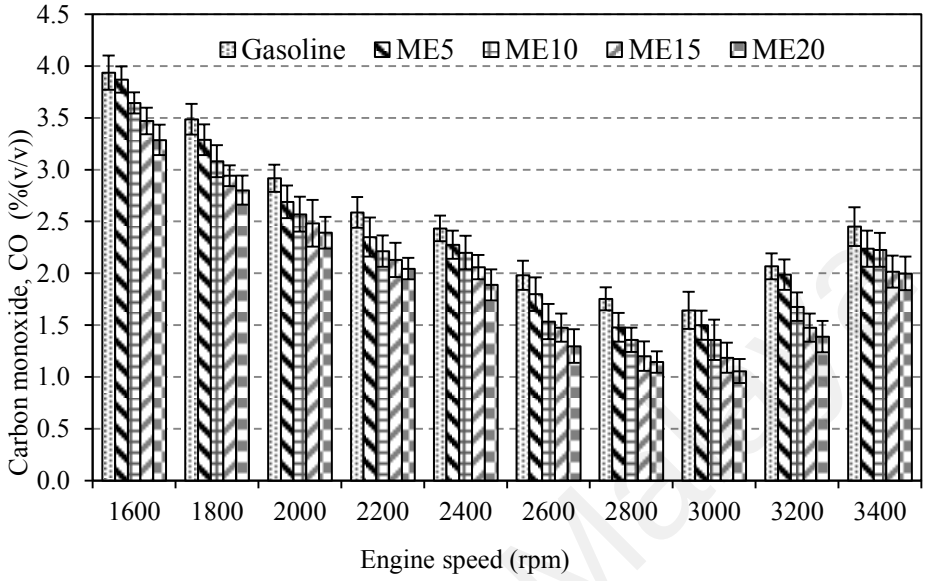

(a)

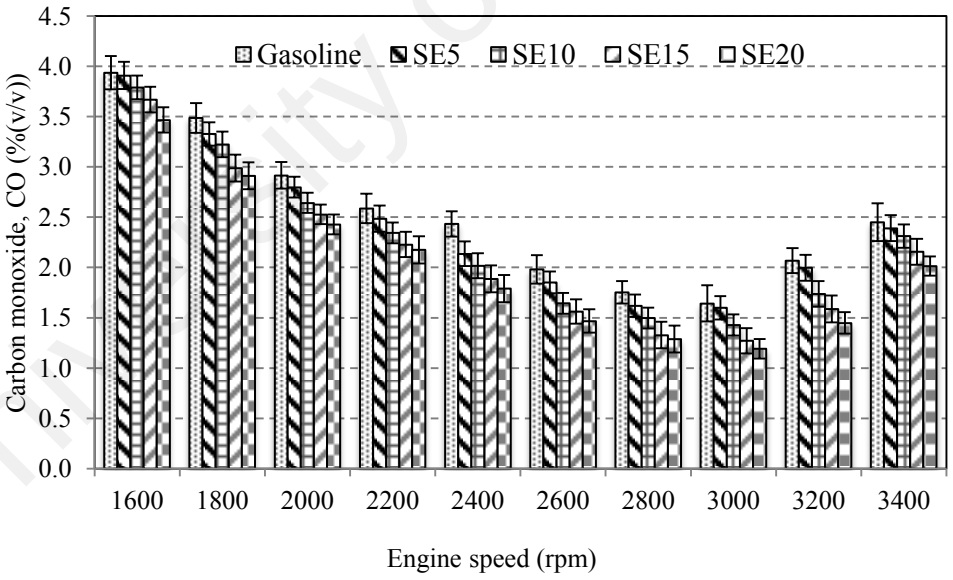

(b)

Figure 4.27: Effect of engine speed of bioethanol-gasoline blend and gasoline fuels on the carbon monoxide emissions (CO) at full throttle conditions (a) *Manihot glaziovii* (b) sweet sorghum

4.8.2. Unburned hydrocarbon emissions

Hydrocarbon (HC) emissions from engine performance test using gasoline and bioethanol-gasoline fuel blends over a range of engine speed is depicted in **Figure 4.28**. Overall, bioethanol-gasoline fuel blends produced lower HC emissions than that of gasoline. At 3000 rpm, ME20 and SE20 blends produced the lowest HC emissions of 31.46 and 32.75 ppm, respectively. However, the lowest HC emissions obtained for gasoline was 40.31 ppm at 3000 rpm, which was higher than those for the ME20 and SE20 blends. As the ethanol content in the fuel blend increases, the HC emissions decrease. These results are in accordance with study Schifter et al. (2011). They conducted an experiment using a single cylinder spark ignition engine and reported that a 19% reduction in HC emission when using fuels containing 20% ethanol.

In addition, the air-fuel ratio is $\lambda = 1.21$ and 1.20 for both ME20 and SE20 fuels, respectively, at 3000 rpm engine speed improves the HC emission. This is consistent with the research by Wu et al. (2016), who reported a decrease in HC emission resulted from combustion in lean areas with air fuel ratio range from $\lambda = 1$ to 1.2. This is mainly because of the appropriate lean burn condition ($\lambda = 1.2$) benefits more efficient combustion. The combustion gets leaner and approaches stoichiometric as the engine speed increases. Consequently, as the ethanol content increases the HC emissions decrease (Chansauria & Mandloi, 2018; Saikrishnan et al., 2018).

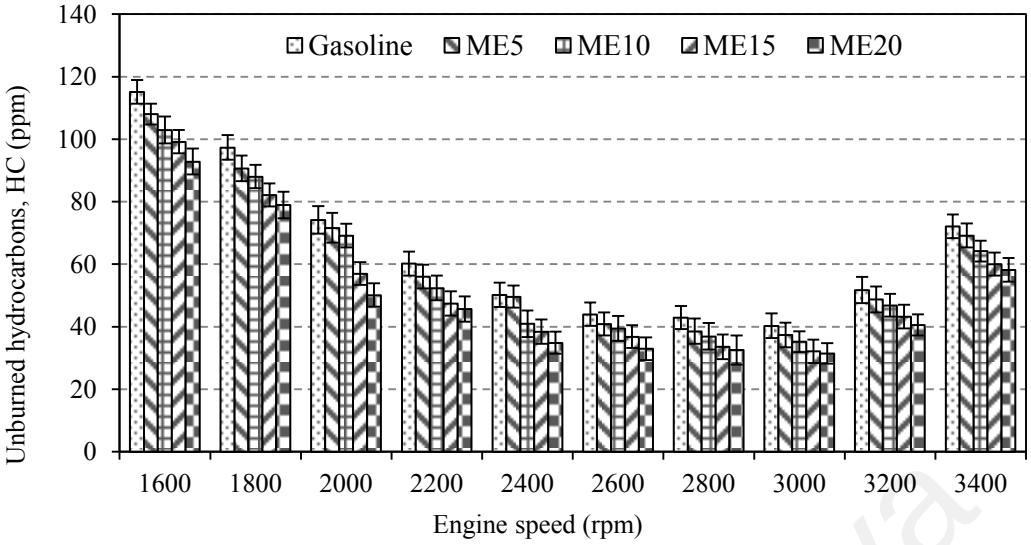

(a)

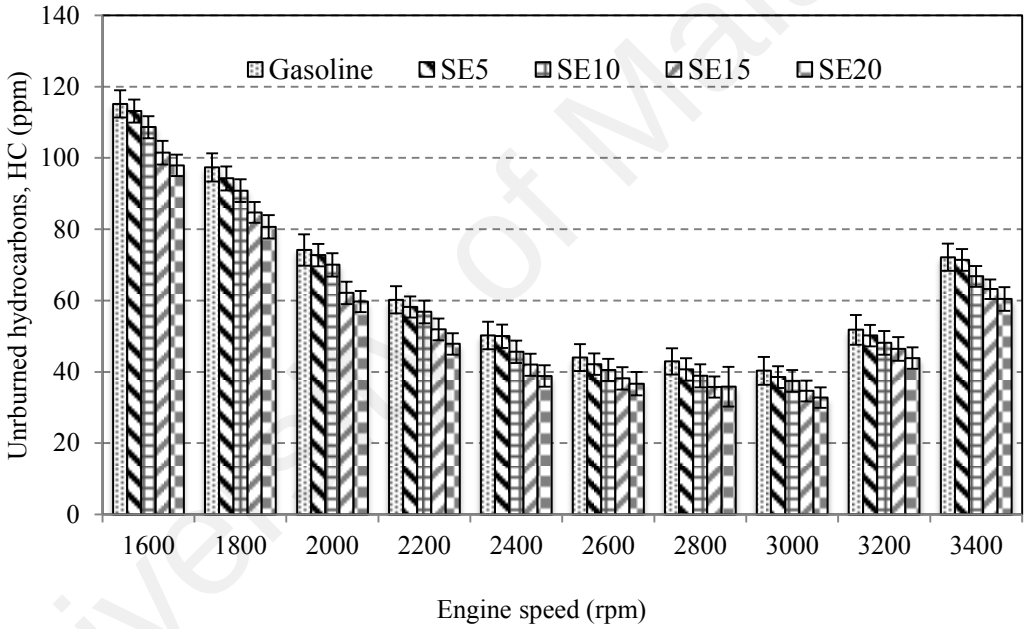

(b)

Figure 4.28: Effect of engine speed of bioethanol-gasoline blend and gasoline fuels on the unburned hydrocarbon emissions (HC) at full throttle conditions (a) *Manihot glaziovii* (b) sweet sorghum

4.8.3. Nitrogen oxide emissions

Figure 4.29 shows the NO_x emissions for the gasoline and bioethanol-gasoline blends. In general, the NO_x emissions of bioethanol-gasoline blends were higher than those of gasoline. The highest NO_x emissions were obtained for the ME20 and SE20

blends at 1600 rpm, with a value of 221.58 and 226.75 ppm, respectively. The lowest NO_x emissions were obtained for the ME05 and SE05 blends at 3000 rpm, with a value of 37.74 and 38.99 ppm, respectively. The NO_x emissions for gasoline were lowest (32.47 ppm) at 3000 rpm and highest (177.15 ppm) at 1600 rpm. The operating lambdas in this study for ME20 and SE20 of 1.21 and 1.20, respectively, also contribute to the NO_x emission. This is also agreed by the research of Deng et al. (2019), who experimented using a 4-stroke and single-cylinder motorcycle gasoline engine. They reported that the NO_x formation increases by a large margin when the air-fuel ratio changes from rich region to lean region, for instance, at $\lambda = 1.1$ and 100% engine load the NO_x value is about 2.4 times relative to that of $\lambda = 0.85$.

In general, NO_x are formed at higher combustion temperatures, and the adiabatic flame temperature (maximum temperature of the reactants in the combustion process) occurs when the combustion approaches stoichiometric conditions. The addition of bioethanol into gasoline results in a leaner air-fuel mixture, resulting in an almost stoichiometric conditions, which increases the combustion temperature. Consequently, bioethanol-gasoline fuel blends result greater NO_x emissions compared with those of gasoline, regardless of the engine speed. The higher cylinder temperatures at 3200 and 3400 rpm resulted in higher NO_x emissions, as shown in **Figure 4.29**. In general, the production of NO_x are highly reliant to the air-fuel ratio and combustion temperature.

Besides that, greater combustion temperature of bioethanol due to the high oxygen content from the bioethanol produces more NO_x emissions (Celik, 2008; Masum et al., 2013). NO_x emissions vary following the amount of ethanol content in the fuel blend and engine operation conditions.

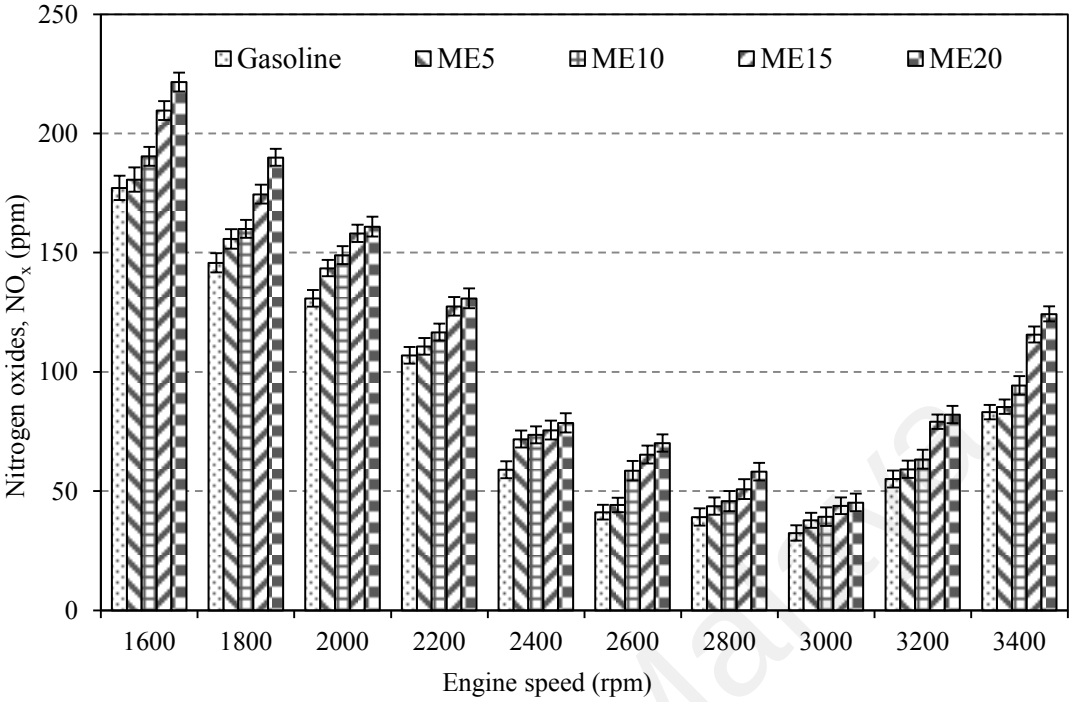

(a)

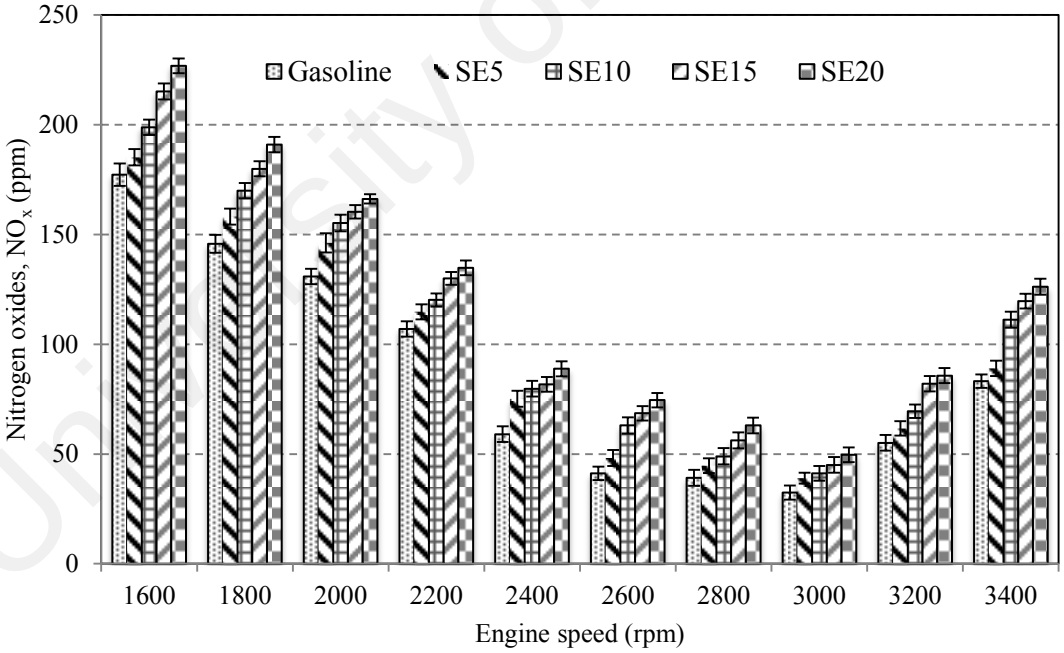

(b)

Figure 4.29: Effect of engine speed of bioethanol-gasoline blend and gasoline fuels on the nitrogen oxide emissions (NO_x) at full throttle conditions (a) *Manihot glaziovii* (b) sweet sorghum

4.8.4. Summary

The results showed that the CO and HC emissions were the lowest for the ME20 (1.06 %(v/v) and 31.46 ppm, respectively) and SE20 blends (1.19 %(v/v) and 32.75 ppm, respectively) among all of the fuels tested in this study. These emissions were higher for gasoline, with a value of 1.59 %(v/v) and 40.31 ppm, respectively. The NO_x emissions were the lowest for the ME05 and SE05 blends at 3000 rpm, with a value of 37.74 and 38.99 ppm, respectively. In contrast, the NO_x emissions were lower for gasoline (32.47 ppm) at this engine speed.

4.9. Corrosion of copper coupons immersed in the bioethanol-gasoline blends

4.9.1. Surface morphologies

Figure 4.30 shows the color changes of the copper coupons immersed in the gasoline and bioethanol-gasoline blends at different immersion times (800, 1600, and 2400 h) performed at room temperature (25–30°C). In general, the chosen immersion times were sufficient to achieve reaction equilibrium of copper-fuel the static immersion tests. Specimen‘s weight losses can be observed to analyze the timing variation to reach copper-fuel equilibrium. There was no significant change in the color of the copper coupons immersed in gasoline. In contrast, there were significant changes in the color of the copper coupons immersed in the bioethanol-gasoline blends. As the ethanol content in the blend and the immersion time increased, the color changes were apparent, where the copper coupons became more tarnished, as evidenced from the lack of metallic luster. The presence of tarnish was most apparent for the copper coupons immersed in the ME20 and SE20 blends for 2400 h, indicating the occurrence of corrosion.

(a)

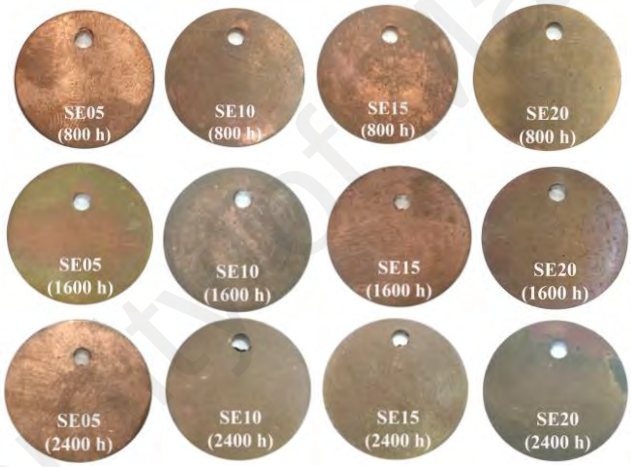

(b)

Figure 4.30: Photographs of the copper coupons immersed in the (a) *Manihot glaziovii* bioethanol-gasoline blends and (b) sweet sorghum bioethanol-gasoline blends for 0, 800, 1600, and 2400 h

The surface morphologies of the copper coupons immersed in the bioethanol-gasoline blends (ME05, ME10, ME15, ME20, SE05, SE10, SE15, and SE20) for 800 and 2400 h were examined by SEM. The SEM images (magnification: 7000×) of the copper coupons are shown in **Figures 4.31–4.34**. It can be seen that the copper coupons immersed in the ME20 and SE20 blends had higher localized pitting rates compared with those immersed in gasoline. In general, there was no severe corrosion and pitting damage in the copper coupons immersed in gasoline. However, pits were observed in

the copper coupons immersed in the bioethanol-gasoline blends, where the number and size of the pits became more pronounced as the ethanol content in the blend. This can be associated with the higher oxygen content of the *Manihot glaziovii* and sweet sorghum bioethanols. In addition, the surface morphologies of the copper coupons were influenced by the immersion time. The copper coupons immersed for 800 h showed small round pits on the surface whereas black pits were distributed on the surface of the copper coupons at 2400 h. The formation of pits and some damage on the copper surface was observed for copper coupons immersed in fuel blends with a higher percentage of bioethanol. The highest number of small pits was observed for copper coupons immersed in the ME20 and SE20 blends. Copper reacts with oxygen to form copper(II) oxide (CuO) and the reduction of CuO produces copper(I) oxide (Cu_2O). These are the main corrosion products observed for copper coupons immersed in bioethanol (Kannan et al., 2014). In this study, the ME20 and SE20 blends resulted in more severe corrosion compared with the other bioethanol-gasoline blends because of their higher oxidation products and water content. In addition, the hygroscopic nature of ethanol attracts water into the fuel, which leads to the formation of a mixture of water-ethanol and gasoline, or a two-phase mixture, from the single-phase ethanol-gasoline blend. With this phase separation, the metal immersed in the fuel is more susceptible to corrosion (Thangavelu et al., 2016b). The formation of pits on the metal surface as a result of corrosion can be reduced by using antioxidants at ambient temperature. The water presence in the conical flasks used for the static immersion tests is also another factor that contributes towards corrosion of the copper coupons. The pits on the surface of the copper coupons immersed in the ME20 and SE20 blends (**Figure 4.31**) appeared darker owing to the formation of CuO (Thangavelu et al., 2016a). The morphologies of the pits and mechanism of pitting corrosion are influenced by the negative and positive ion concentrations in the bioethanol-gasoline fuel blends. Study by Mankowski et al.

(1997) reported that the reaction of copper with oxygen forms an outer layer of an oxygen-rich $CuO/CuCO_3$, which then followed by an inner layer of Cu_2O. Through CuO layer eradication on copper surface, more pits are formed with the formation of Cu_2O. Studies by Lou et al. (2009) and Sridhar et al. (2006) agree with the results, as they found that oxygen had the most significant effect on corrosion. The SEM images indeed indicate the presence of oxide layers on the surface of the copper coupons. This is likely because the protective oxide layers dissolve at room temperature, which hinders passivation and keeps the metallic sites in the active state (Tabish, 2018). In general, the prolonged immersion of copper coupons in the bioethanol-gasoline blends can lead to corrosion, resulting in discoloration of the specimens.

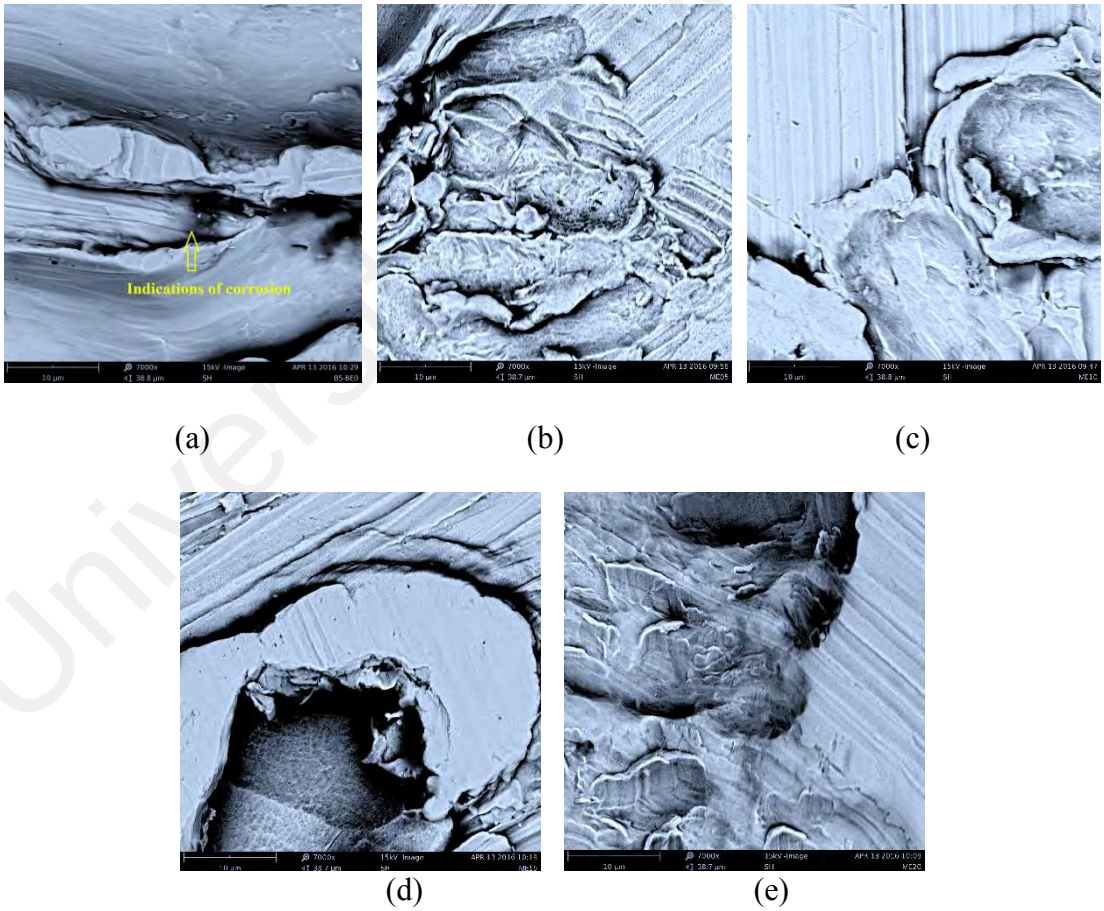

Figure 4.31: SEM images (magnification: 7000×) of the surface of the copper coupons immersed in (a) gasoline, (b) ME5, (c) ME10, (d) ME15, and (e) ME20 at room temperature (25–30°C) for 800 h

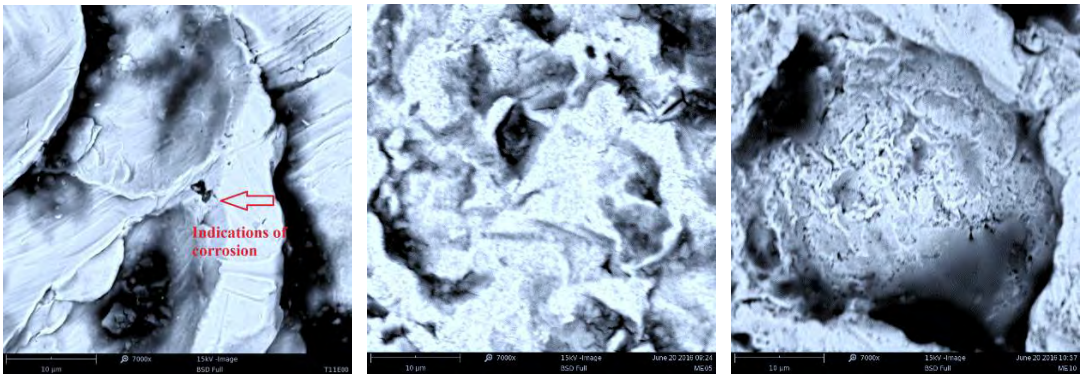

(a) (b) (c)

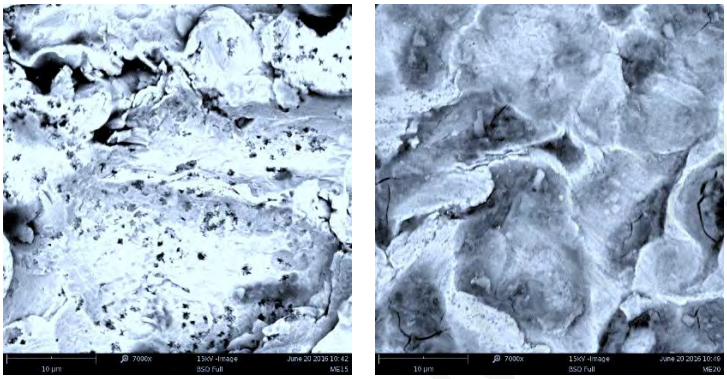

(d) (e)

Figure 4.32: SEM images (magnification: 7000×) of the surface of the copper coupons immersed in (a) gasoline, (b) ME5, (c) ME10, (d) ME15, and (e) ME20 at room temperature (25–30°C) for 2400 h

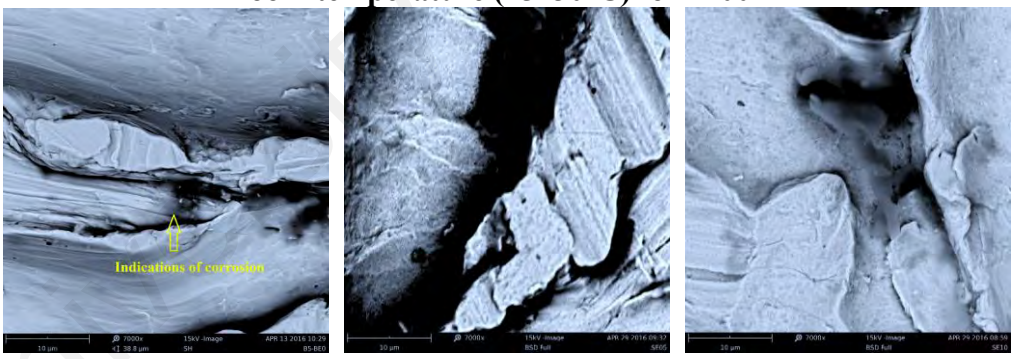

(a) (b) (c)

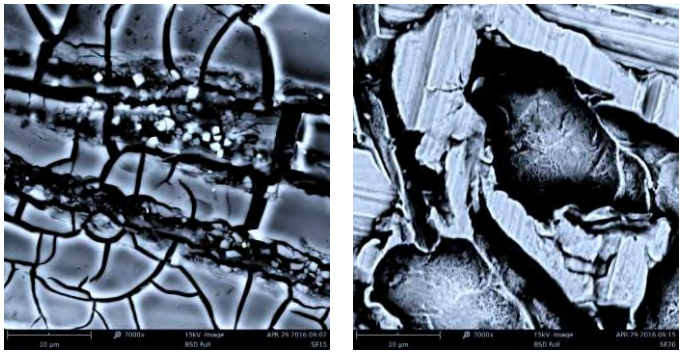

(d) (e)

Figure 4.33: SEM images (magnification: 7000×) of the surface of the copper coupons immersed in (a) gasoline, (b) SE5, (c) SE10, (d) SE15, and (e) SE20 at room temperature (25–30°C) for 800 h

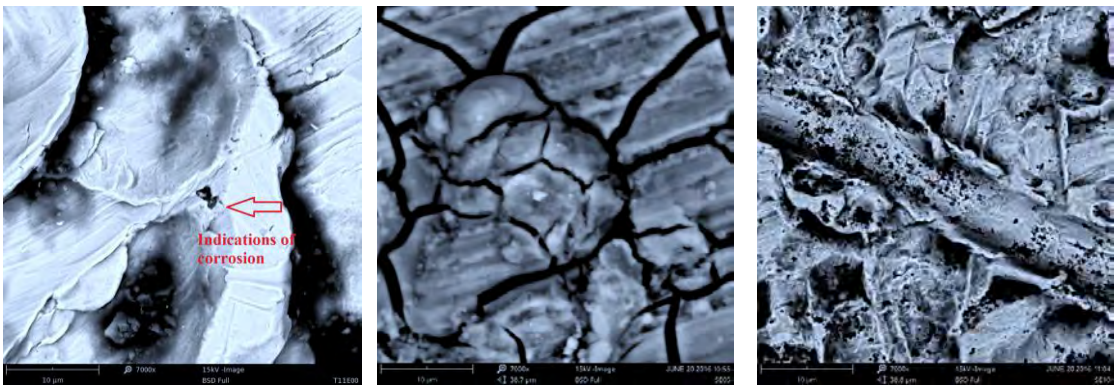

(a) (b) (c)

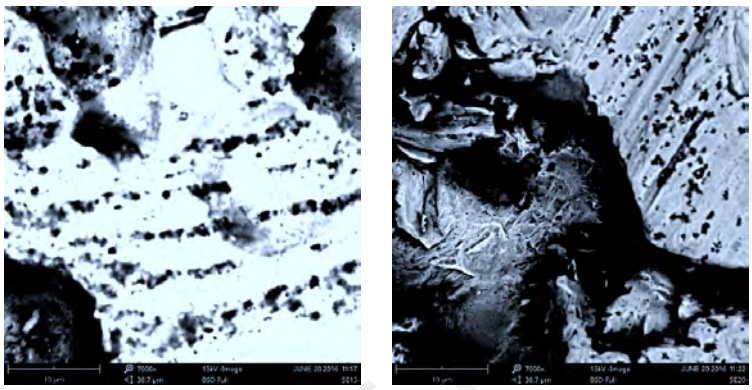

(d) (e)

Figure 4.34: SEM images (magnification: 7000×) of the surface of the copper coupons immersed in (a) gasoline, (b) SE5, (c) SE10, (d) SE15, and (e) SE20 at room temperature (25–30°C) for 2400 h

Figure 4.35 shows the EDX spectra of the corroded copper surfaces after immersion in the bioethanol-gasoline blends for 2400 h. Based on the results, it can be deduced that metal oxides composed of carbon and oxygen are present on the corroded surface of the copper coupons. This confirms the formation of copper oxides on the copper surfaces observed in the SEM images. The prolonged immersion time (2400 h) also resulted in a high concentration of oxygen on the copper surfaces. The oxygen concentration was 1.61 %(w/w) for the copper coupon immersed in gasoline whereas the oxygen concentrations were 15.57 and 19.66 %(w/w) for the copper coupons immersed in the ME20 and SE20 blends, respectively. The formation of copper oxides on the copper surfaces immersed in the ME20 and SE20 blends can be attributed to the hygroscopic nature of the bioethanols. Similar results are also studied by Thangavelu et al. (2016a). They reported that the corrosion potential of copper in the bioethanol

gasoline blends (E25) at room temperature for 1400 h is 0.285 mm/year. This is due to the faster formation of cuprite oxide in the aggressive environment, which provides anticorrosion protection to copper (Baena et al., 2012).

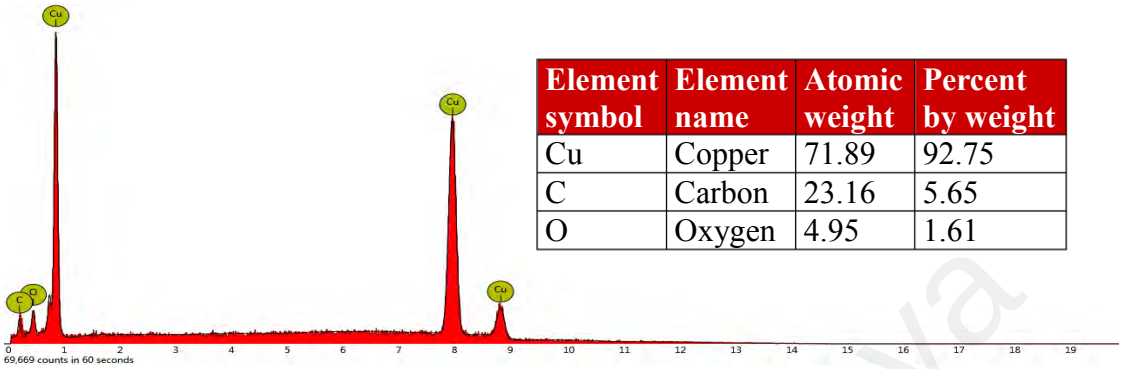

Element symbol	Element name	Atomic weight	Percent by weight
Cu	Copper	71.89	92.75
C	Carbon	23.16	5.65
O	Oxygen	4.95	1.61

(a)

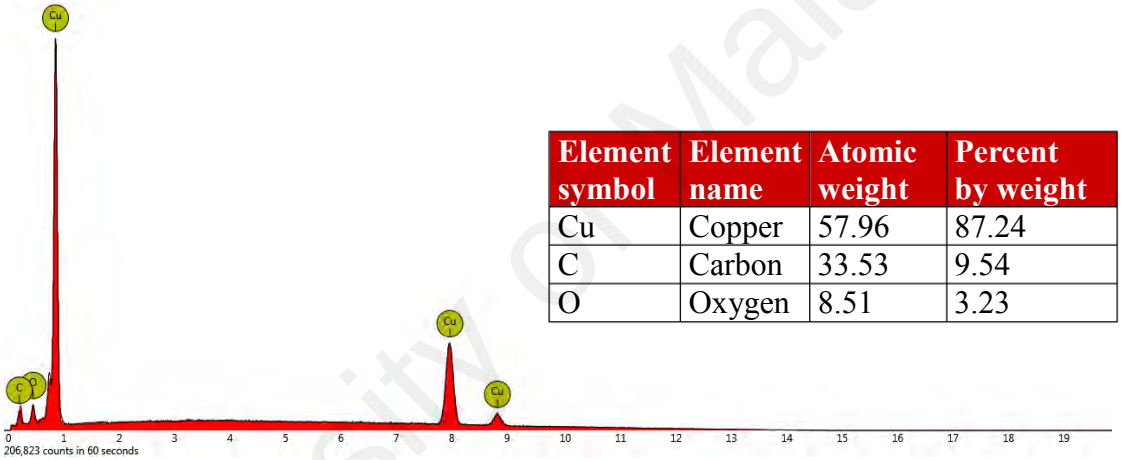

Element symbol	Element name	Atomic weight	Percent by weight
Cu	Copper	57.96	87.24
C	Carbon	33.53	9.54
O	Oxygen	8.51	3.23

(b)

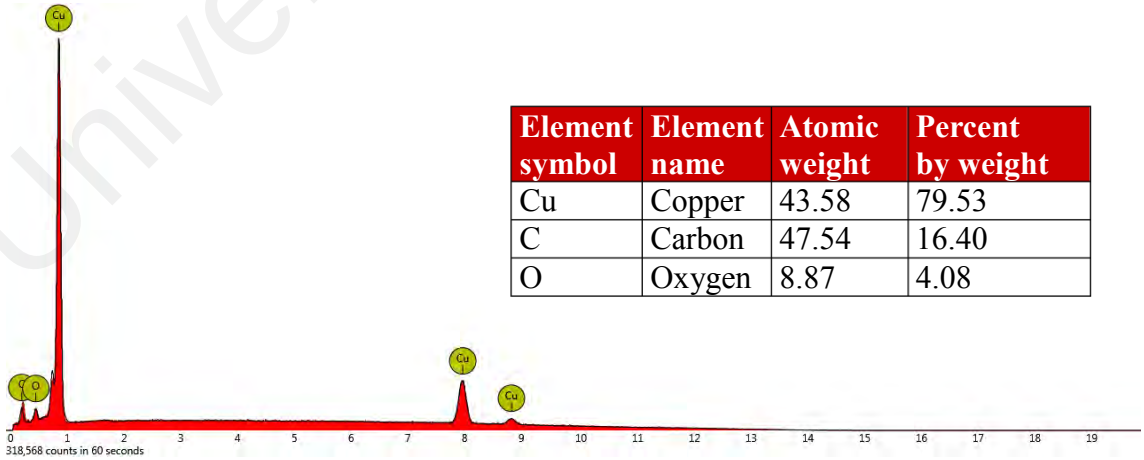

Element symbol	Element name	Atomic weight	Percent by weight
Cu	Copper	43.58	79.53
C	Carbon	47.54	16.40
O	Oxygen	8.87	4.08

(c)

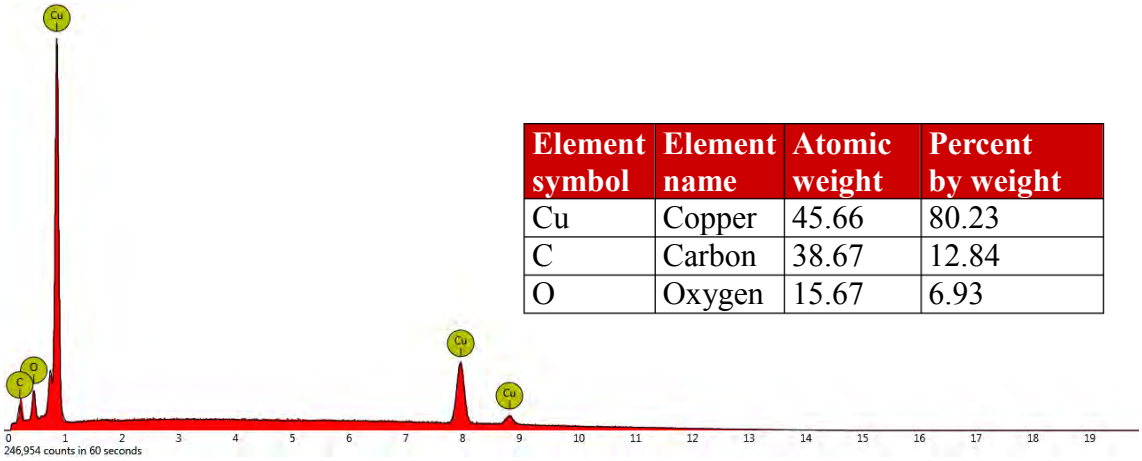

Element symbol	Element name	Atomic weight	Percent by weight
Cu	Copper	45.66	80.23
C	Carbon	38.67	12.84
O	Oxygen	15.67	6.93

(d)

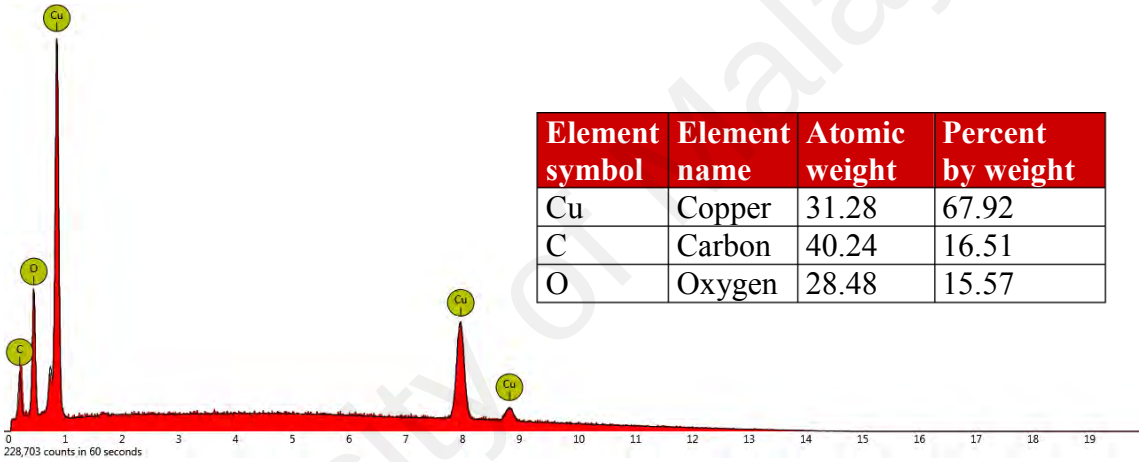

Element symbol	Element name	Atomic weight	Percent by weight
Cu	Copper	31.28	67.92
C	Carbon	40.24	16.51
O	Oxygen	28.48	15.57

(e)

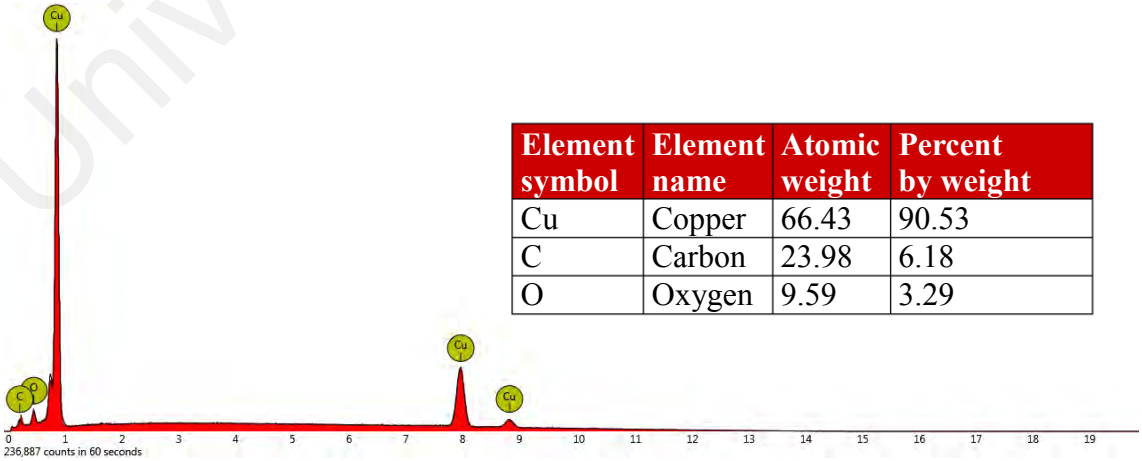

Element symbol	Element name	Atomic weight	Percent by weight
Cu	Copper	66.43	90.53
C	Carbon	23.98	6.18
O	Oxygen	9.59	3.29

(f)

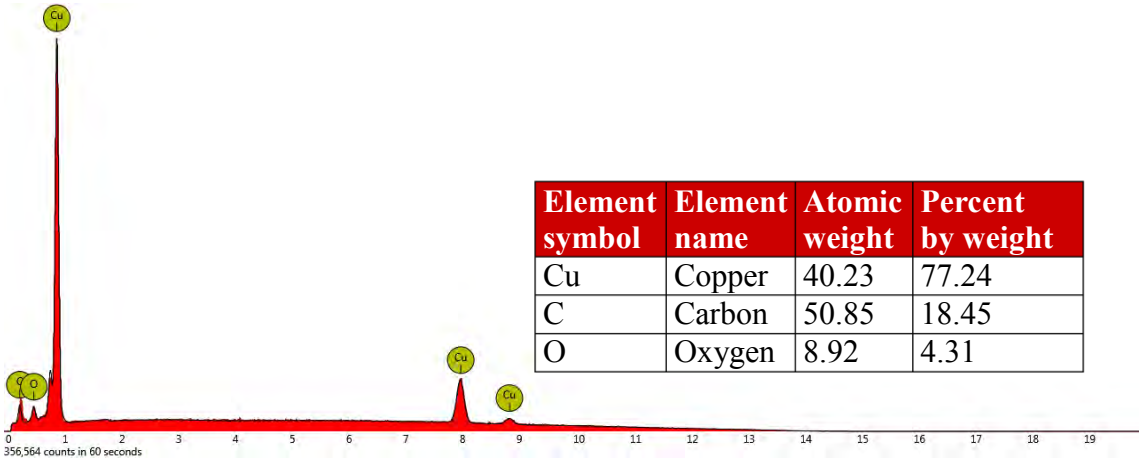

Element symbol	Element name	Atomic weight	Percent by weight
Cu	Copper	40.23	77.24
C	Carbon	50.85	18.45
O	Oxygen	8.92	4.31

(g)

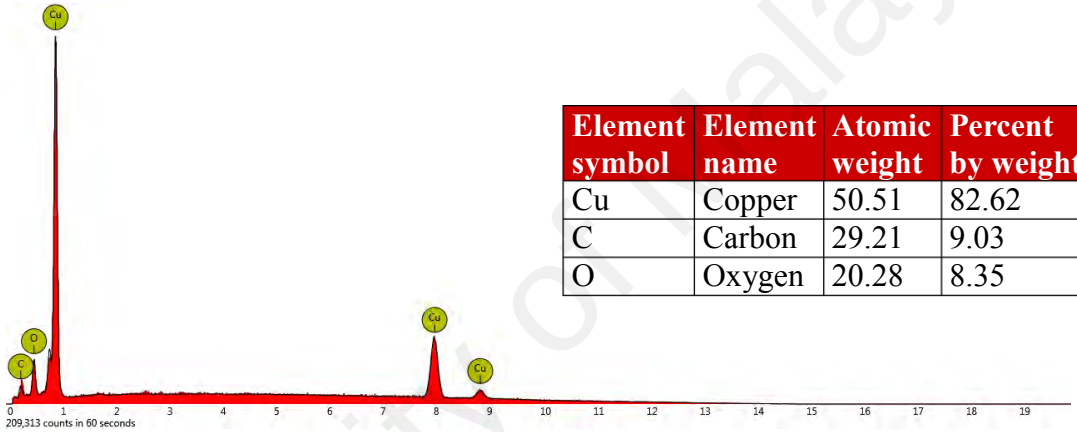

Element symbol	Element name	Atomic weight	Percent by weight
Cu	Copper	50.51	82.62
C	Carbon	29.21	9.03
O	Oxygen	20.28	8.35

(h)

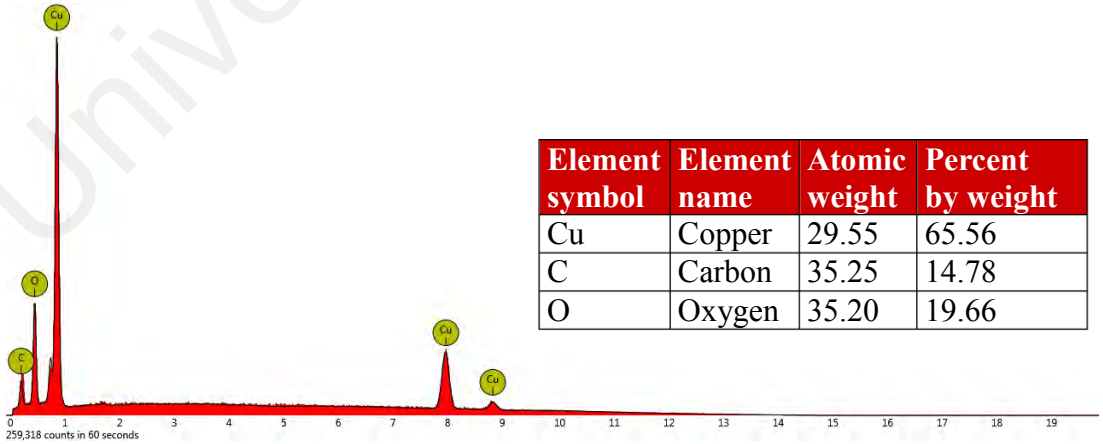

Element symbol	Element name	Atomic weight	Percent by weight
Cu	Copper	29.55	65.56
C	Carbon	35.25	14.78
O	Oxygen	35.20	19.66

(i)

Figure 4.35: Elemental compositions of the copper coupons immersed in (a) gasoline, (b) ME05, (c) ME10, (d) ME15, (e) ME20, (f) SE05, (g) SE10, (h) SE15, and (i) SE20 for 2400 h at ambient temperature

4.9.2. Corrosion rate

Figure 4.36 shows the corrosion rates of the copper coupons immersed in the gasoline and bioethanol-gasoline blends at different immersion times. It can be observed as ethanol content increased the corrosion rate increased accordingly. After immersion for 800 h, the corrosion rate was found to be lower for the copper coupon immersed in gasoline (0.00084 mm/year) compared with those for the copper coupons immersed in the ME5 (0.00132 mm/year), ME10 (0.00144 mm/year), ME15 (0.00252 mm/year), and ME20 (0.00286 mm/year) blends. The results conform well with those of Jafari et al. (2011) who reported that the corrosion rate increases accordingly as the ethanol content in the fuel blend increases. Jafari et al. (2011) researched the corrosion behavior of metal materials (copper) in a gasoline-ethanol blend. They reported an increase of corrosion rate by 2.11×10^{-5} mm/year in gasoline blended with 15% ethanol. Besides, Kannan at al. (2014) reported a higher corrosion rate with E85 than the corrosion rate due to E10 and E0. Copper corrosion rate after 1320 hours immersion is 0.720 mm/year for E85 mixed fuel, and this is similar to that reported by Thangavelu et al. (2016a). They observed 0.285 mm/year corrosion potential of copper in the bioethanol gasoline blends (E25) at room temperature for 1400 h.

This is also apparent for the copper coupons immersed in the sweet sorghum bioethanol-gasoline blends, where the corrosion rate was lower for the copper coupon immersed in gasoline (0.00084 mm/year) compared with those immersed in the SE5 (0.00142 mm/year), SE10 (0.00148 mm/year), SE15 (0.00284 mm/year), and SE20 (0.00299 mm/year) blends for 800 h. This increase is associated with the greater oxygen content of the sweet sorghum bioethanol compared with that for the *Manihot glaziovii* bioethanol. Also, the hygroscopic nature of bioethanol promotes corrosion (Singh et al., 2018). Matějovský et al. (2017) reported that as the content of ethanol in fuel increases more the conductivity and ability of the fuel to absorb water, hence the fuel is becoming

more corrosive. The corrosion rates of immersed copper are 0.0052, 0.0054, and 0.0072 mm/year for E40, E60, and E85, respectively. In addition, higher engine speeds can lead to mechanical wear and abrasive effects. The erosion of passive coatings on the surface can also increase the likelihood of corrosion. Copper reacts with oxygen to form the outer layer of an oxygen-rich $CuO/CuCO_3$ and an inner layer of Cu_2O. More pits are formed with the formation of the Cu_2O layer due to the CuO layer annihilation on the copper surface. Therefore, the changes in the fuel viscosity allows carbon to be transported to the metal surface and deposit in the active areas. Therefore, larger anodes and smaller cathodes result in a higher corrosion rate. A greater amount of bioethanol in the blend and a higher fuel viscosity can lead to the formation of more pits (pitting damage), which will alter the morphology of the copper surface.

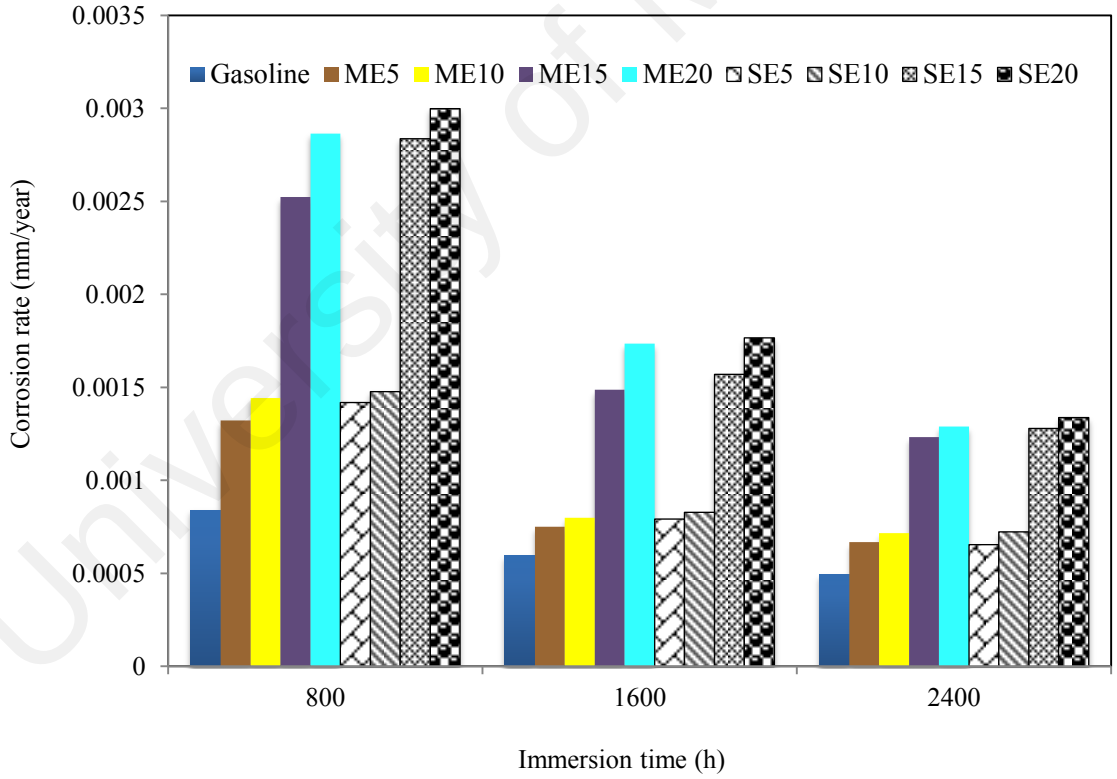

Figure 4.36: Corrosion rates of the copper coupons immersed in the gasoline and bioethanol-gasoline blends for 80, 1600, and 2400 h at room temperature

4.9.3. Effects of corrosion on the properties of the bioethanol-gasoline blends

4.8.3.1. Total acid number

In petrochemical substances, TAN represents the summation of acidic compounds in the samples, using acid-base titration method where KOH is used as the titrant. In expressing TAN, units milligrams of KOH per gram of sample is used. The tested samples are diluted with isopropyl alcohol since they are non-aqueous, and isopropyl alcohol is a solvent for KOH. The TAN is given by:

$$\text{TAN (mg KOH/g)} = \frac{C_{\text{titrant}}(\text{eq/L}) \times V_{\text{titrant}}(\text{mL})}{ne_{\text{titrant}} \times m_{\text{sample}}(\text{g})} \times M_{\text{KOH}}(\text{g/mol})$$

$$\text{TAN (mg KOH/g)} = \frac{0.1(\text{eq/L}) \times V_{\text{titrant}}(\text{mL})}{1 \times m_{\text{sample}}(\text{g})} \times 56.11(\text{g/mol}) \quad (4.2)$$

where V_{titrant} is the volume in milliliters (mL) of the NaOH solution, M_{KOH} is the exact concentration of the standard NaOH solution in grams per mole (g/mol), and m_{sample} is the mass of the test sample in grams (g).

The TAN values of the gasoline and bioethanol-gasoline blends were measured before and after the static immersion tests at different immersion times and the results are shown in **Figure 4.37.** After 2400 h of immersion, the TAN was slightly lower for gasoline (0.54 mg KOH/g) compared with those for the ME5 (0.55 mg KOH/g), ME10 (0.57 mg KOH/g), ME15 (0.60 mg KOH/g), and ME20 (0.62 mg KOH/g) blends. TAN values for the sweet sorghum bioethanol-gasoline blends were slightly higher, with values of 0.57, 0.60, 0.63, and 0.67 mg KOH/g for the SE5, SE10, SE15, and SE20 blends, respectively. The TAN is increased of 0.51 and 0.58 mg KOH/g for the *Manihot glaziovii* (ME20) and sweet sorghum (SE20) bioethanol-gasoline blends, respectively. These results are consistent with research conducted by Kannan (2014), who reported an increase in TAN by 0.133 mg KOH/g in the E85 fuel blend exposed to copper. The results indicate that the percentage of bioethanol and immersion time have a high

influence on TAN values of the bioethanol-gasoline blends. From the results, it can also be observed that copper is a strong catalyst for the oxidation of the bioethanol-gasoline blends, as indicated by the increase in the TAN values. The results from this study are in agreement with those by Thangavelu et al. (2016a). According to Kaul et al. (2007), even though TAN is not a measure of the oxidation rate, it provides an indication of the oxidation rate.

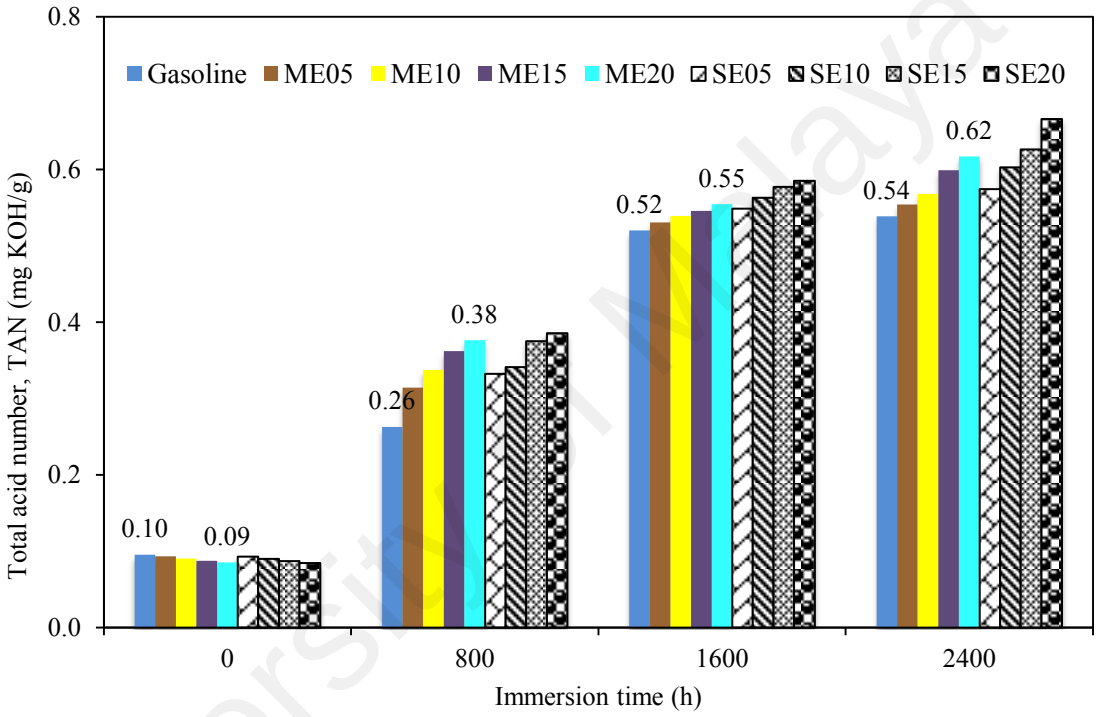

Figure 4.37: Total acid numbers (TANs) of the bioethanol-gasoline blends and gasoline when the copper coupons were immersed in these fuels for 0, 800, 1600, and 2400 h at room temperature

4.8.3.2. Density

Figure 4.38 shows the density values of the bioethanol-gasoline blends and gasoline when the copper coupons were immersed in these fuels at different immersion times at room temperature. After immersion for 2400 h, gasoline had the lowest density (758.64 kg/m^3) compared with the ME5 (765.05 kg/m^3), ME10 (768.72 kg/m^3), ME15 (771.85 kg/m^3), ME20 (775.67 kg/m^3), SE5 (762.84 kg/m^3), SE10 (770.68 kg/m^3), SE15 (773.68 kg/m^3), and SE20 (778.45 kg/m^3) blends. The results indicate that the

percentage of bioethanol in the fuel blends and the immersion time have a significant effect on the density of the fuels. Higher concentration of bioethanol will cause more corrosion spot on the metallic coupons. In addition, copper corrosion has a significant effect on the fuel density, regardless if it is gasoline or bioethanol-gasoline blends. The density increases by 1.45% for the *Manihot glaziovii* bioethanol-gasoline blends (ME20), and the value is slightly higher (1.74%) for the sweet sorghum bioethanol-gasoline blends (SE20) after immersed for 2400 h. In addition, the maximum acceptable limit for density of fuel grade ethanol is 791.5 kg/m3 (ASTM D4806) (Thangavelu et al., 2016a).

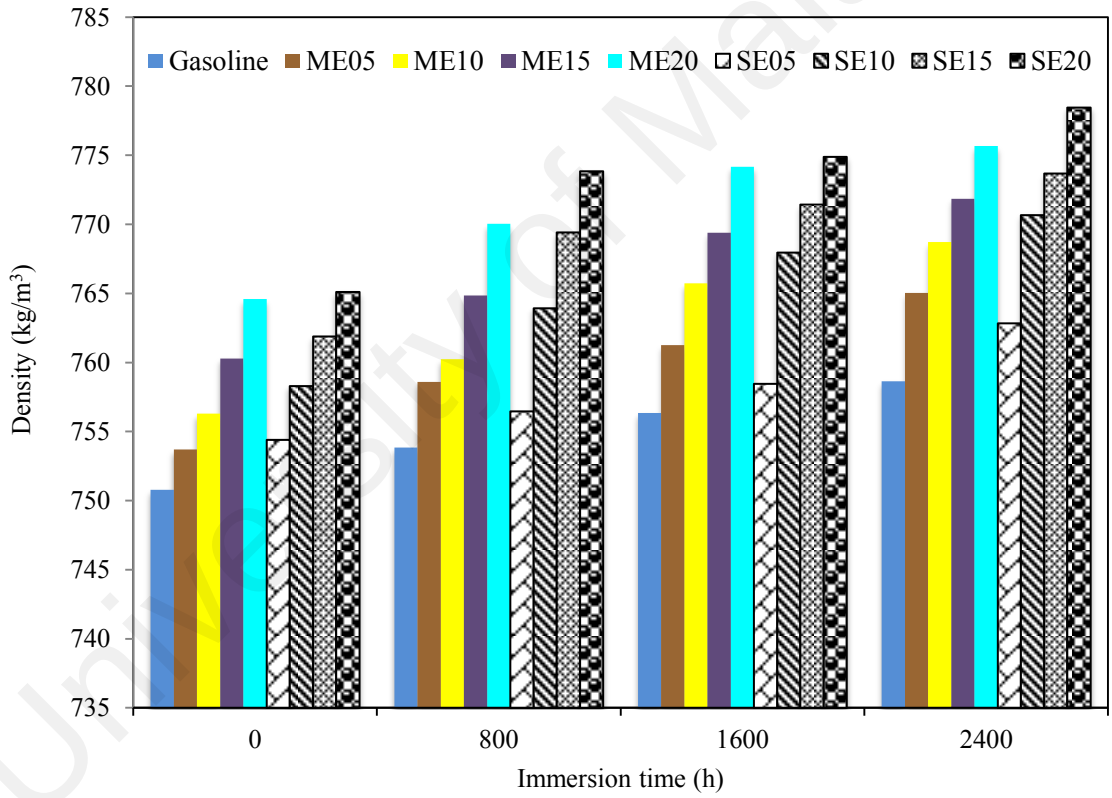

Figure 4.38: Density values of the bioethanol-gasoline blends and gasoline when the copper coupons were immersed in these fuels for 0, 800, 1600, and 2400 h at room temperature

4.8.3.3. Viscosity

Figure 4.39 shows the viscosity values for the gasoline and bioethanol-gasoline blends when the copper coupons were immersed in these fuels at different immersion

times at room temperature. In general, the viscosity values were higher for the sweet sorghum bioethanol-gasoline blends compared with the *Manihot glaziovii* bioethanol-gasoline blends and gasoline. As shown in **Figure 4.39**, the highest viscosity was obtained for the SE20 blend (0.8 mm^2/s), followed by the ME20 blend (0.78 mm^2/s) after 2400 h. In contrast, the viscosity of gasoline was 0.62 mm^2/s after 2400 h. The viscosity is increased of 6.53 and 8.26% for the *Manihot glaziovii* (ME-20) and sweet sorghum (SE-20) bioethanol-gasoline blends, respectively. The results indicate that the percentage of bioethanol and immersion time have a significant effect on the viscosity of the bioethanol-gasoline blends. Copper also has a pronounced effect on the fuel viscosity.

According to Thangavelu et al. (2016a) there is an increment in the viscosity of E25 and E50 in the bioethanol gasoline blends. Whereas the copper exposed to bioethanol fuel E50 shows a higher increment (20%) in viscosity compared with copper exposed to fuel blend E25. The increase in viscosity of bioethanol gasoline blends is due to the increment of oxidation products and the transformation of metal elements in the fuel blends in the presence of oxygen (Fazal et al., 2010). The increasing viscosity leads to the formation of products that are likely to cause changes in the quality of fuels (affecting their physical and chemical properties), and it may accelerate the oxidation of hydrocarbon ingredients of the fuel. This then leads to the development of gum and sludge in the fuel (Ziółkowska & Wardzińska, 2015).

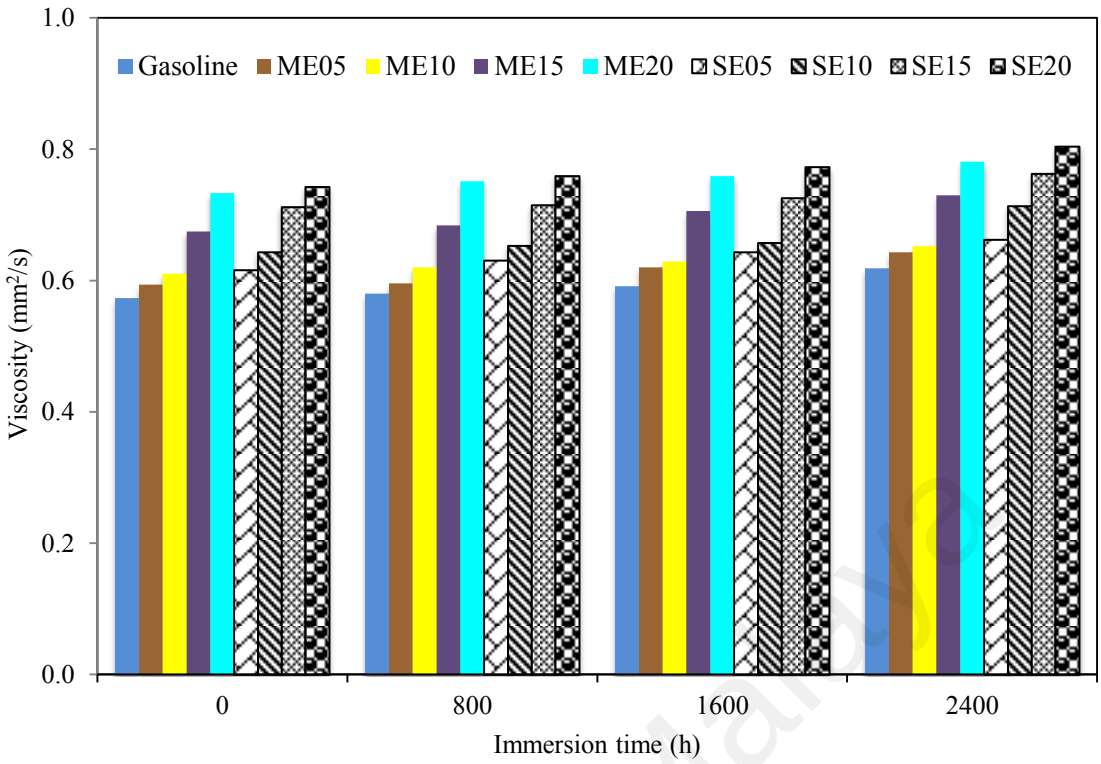

Figure 4.39: Viscosity values of the bioethanol-gasoline blends and gasoline when the copper coupons were immersed in these fuels for 0, 800, 1600, and 2400 h at room temperature

4.8.3.4. Fourier transform infrared spectra of the sediment formed on the surface of the copper coupons

FTIR spectroscopy is a well-established analytical technique to characterize materials. This characterization technique operates based on the principle of the vibrations and rotations of the bonds between the atoms or functional groups under exposure of a specific frequency, and this correlates to the chemical structure of the tested material (Linder, 2012). As the name implies, FTIR spectroscopy involves the use of the Fourier transform to analyze the spectroscopy results. This method utilizes the absorption differences of infrared radiation. The infrared region of the electromagnetic spectrum falls within a wavenumber range of 14000–10 cm^{-1}. Based on the wavenumber, the infrared region are categorized as: (1) near-infrared (14000–4000 cm^{-1}), which is sensitive to vibration overtones, (2) mid-infrared (4000–400 cm^{-1}) is related to the vibrational energy transition from the molecules, which provides

information on the group-group functions in the molecule, and (3) far-infrared (400–10 cm^{-1}), which is used to analyze molecules containing heavy atoms such as inorganic compounds. However, special technique is required for far-infrared FTIR spectroscopy (Griffiths & De Haseth, 2007). Mid-infrared region is commonly utilized for FTIR spectrometers, however the use of near- and far-infrared regions are also beneficial in providing further information about certain materials (Stuart, 2015). In this study, a FTIR spectrometer (Tensor 27, Bruker Optik GmbH, Germany) was used to obtain the mid-infrared region (wavenumber range: 4000–400 cm^{-1}) FTIR spectra and to determine the functional groups present in the sediment formed on the copper coupon surface in the immersion test in gasoline and bioethanol-gasoline blends for 2400 h.

Figure 4.40 shows the FTIR spectra of the sediment formed on copper coupon surface after 2400 h immersion test using gasoline and bioethanol-gasoline blends. Function group region is defined by the left region of 1500 cm^{-1}, while the right of this wavelength is called the fingerprint region. As shown in **Figure 4.40(a)**, O–H stretching vibrations can be indicated by the intense transmittance peak at 3035 cm^{-1}. C–H stretching is assigned at the transmittance peak of 2873 cm^{-1}. The transmittance peak at 1610 cm^{-1} indicates the presence of an alkene group with various C=C bonds. The transmittance peak at 1496 cm^{-1} with medium intensity indicates the presence of a alkane group ($–CH_3$) with C–H bonds. C–C stretching is ascribed by the intense transmittance peaks of 1461 and 1053 cm^{-1}, which indicate the presence of ether groups.

It can be seen from **Figure 4.40(b)** that the O–H asymmetric stretching vibrations is attributed by the intense transmittance peaks at 3027, 3028, and 3030 cm^{-1}. C–H asymmetric stretching vibrations is ascribed by the intense transmittance peaks of 2869 and 2874 cm^{-1}. C=C symmetric stretching vibrations and C–H stretching vibrations are ascribed by the transmittance peaks of 1608 and 1456 cm^{-1}, respectively.

C–C antisymmetric stretching vibrations is assigned by the transmittance peaks at 1051 and 1032 cm^{-1}.

The wavenumbers, band assignment, functional groups, and transmittance intensities of the peaks detected in the FTIR spectra are presented in **Table 4.18**.

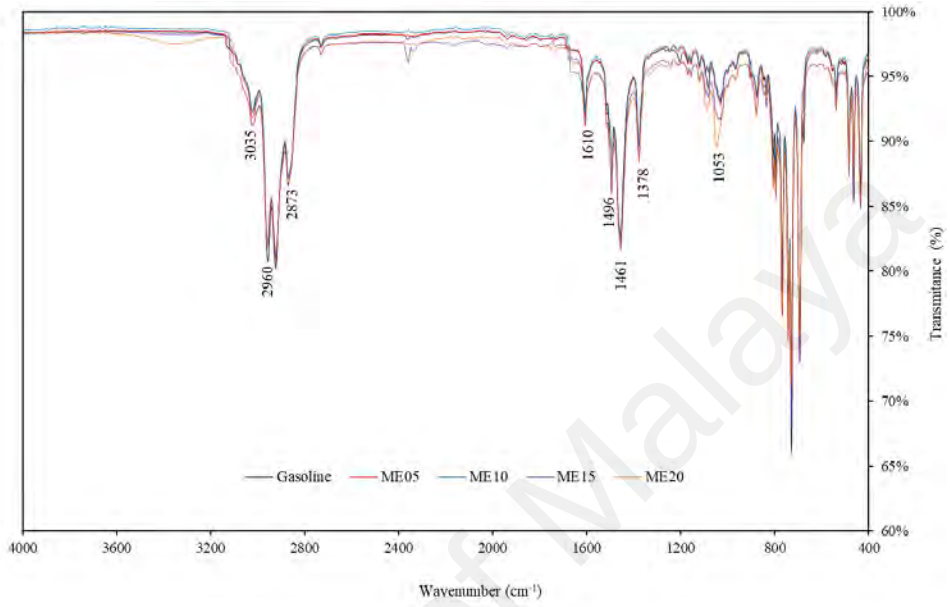

(a)

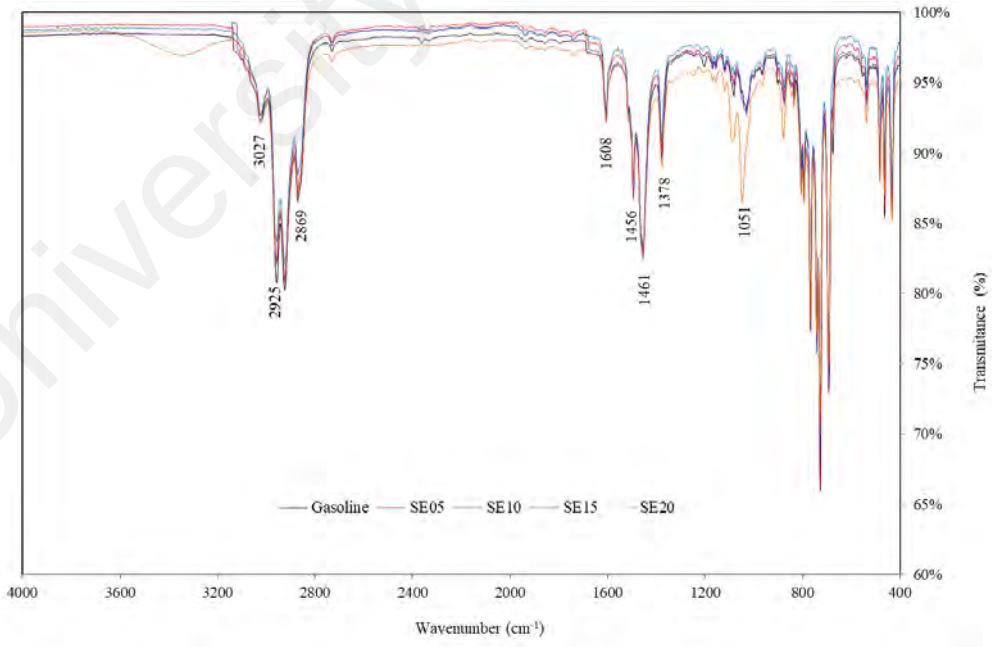

(b)

Figure 4.40: FTIR spectra of the sediment formed on the surface of the copper coupons after immersion in gasoline, (a) *Manihot glaziovii* bioethanol-gasoline blends and (b) sweet sorghum bioethanol-gasoline blends for 2400

Table 4.18: Wavenumbers, functional groups, band assignment, and transmittance intensities of the peaks detected in the FTIR spectra for the sediment formed on the surface of the copper coupons immersed in the gasoline and bioethanol-gasoline blends

Wavenumber (cm^{-1})									Functional group	Band assignment	Transmittance intensity
Gasoline	ME05	ME10	ME15	ME20	SE05	SE10	SE15	SE20			
3030	3028	3028	3028	3035	3030	3028	3028	3027	O–H	Asymmetric stretching vibration	Strong
2872	2872	2872	2874	2873	2874	2874	2874	2869	C–H	Asymmetric stretching vibration	Strong
1607	1607	1608	1608	1610	1608	1608	1608	1608	C=C	Symmetric stretching vibration	Strong
1456	1456	1456	1456	1496	1456	1456	1456	1461	C–H	stretching vibration	Weak
1032	1032	1032	1041	1053	1032	1032	1032	1051	C– C	Anti-symmetric stretching vibration	Middling

4.9.4. Summary

Gasoline containing higher amounts of bioethanol significantly influences the corrosion of ferrous and nonferrous metals. The highest corrosion rate was observed in copper in the contaminated ME5–ME20 and SE5–SE20 fuel. This can be related to the contents of water and acidic substances and the solubility of oxygen in the fuel, which are increased along with the increasing content of ethanol. Corrosion tests were carried out at room temperature by immersing copper coupons in bioethanol-gasoline blends at different immersion times (800, 1600, and 2400 h) and the corrosion rates and fuel properties were analyzed. The corrosion rate of metals in ME20 and SE20 are found high. The phenomenon is caused by the degradation of bioethanol fuel properties upon exposure to metals, and this is identified by TAN, acidity, density, viscosity, and color changes. Moreover, copper elements enhance the oxidation of bioethanol. Corrosion and degradation of fuel properties are **50%** high in higher ethanol blends (ME20 and SE20) compared with lower ethanol blends (ME5 and SE5). The results reveal that the low ethanol concentration (up to **E20**) is considered feasible in terms of material compatibility.

Presumably, hydrated copper oxide is formed on the copper surface during the tests at room temperatures, which copper reacts with oxygen and forming the red copper oxide according to the following reaction (equation 4.3):

$$6C_2H_5OH + 2Cu \rightarrow 3H_2 + 2Cu\,(C_2H_5O)_3 \qquad (4.3)$$

The reaction involves the substitution of the copper atom originating from the metal or from the oxide film with a hydrogen atom originating from bioethanol, which hydrogen and copper acetate are formed. The SEM images suggest that the copper coupons immersed in the ME20 and SE20 blends have a higher number of local pits compared with the copper coupon immersed in pure gasoline. The EDX spectra reveal

the presence of metal oxides (composed of carbon and oxygen) on the surface of the corroded copper coupons. The present results indicate that the test samples of bioethanol gasoline blends show a lower corrosive effect on the copper selected for the corrosion tests. This confirms literature reports relating to the adverse effect of the bio component on the durability of structural materials. Considering the duration of fuel immerse time and the corrosion rate for bioethanol gasoline test samples up to 2400 h which is a beneficial phenomenon such as impedance spectroscopy, techniques enabling a microscopic examination of the surface condition and composition, as well as measuring the rate of corrosion, initiated in the early immerse the copper in bioethanol gasoline blends.

CHAPTER 5: CONCLUSIONS AND RECOMMENDATIONS

5.1. Conclusions

The escalating demand for energy is a universal problem. The gradual depletion of fossil fuel reserves over the years and the growing concern over the environmental impact of fossil fuel combustion have led to a pressing need to search for alternative sources of energy that are both renewable and sustainable. One of the ways to fulfill this need is to produce bioethanols and their blends from non-edible feedstocks. This study explores the potential of producing bioethanols from *Manihot glaziovii* tubers and sweet sorghum grains, which are both non-edible feedstocks. Optimization was used to design the experiments for the enzymatic hydrolysis and fermentation processes and the ANN-GA models were used to optimize the parameters of these processes. Following this, the effect of bioethanol-gasoline blends on engine performance, exhaust emission and copper corrosion was also investigated. The following conclusions were drawn based on the findings:

1. *Manihot glaziovii* tubers and sweet sorghum grains were found to be potential feedstocks for bioethanol production because of their high starch content. Their wide availability in the tropical regions in South-East Asia makes these feedstocks a practical solution for bioethanol production in this region and help tackle the food versus fuel issue, considering that these feedstocks are non-edible and inexpensive. The carbohydrate content is above 70 %(w/w) for *Manihot glaziovii* and sweet sorghum starches, which carries great potential for bioethanol production.
2. The optimum substrate loading, α-amylase concentration, amyloglucosidase concentration, and stroke speed were determined for enzymatic hydrolysis of sweet sorghum starch were found to be 19.99 %(w/v), 109.59 U/g, 36 U/mL, and

63.19 spm, respectively. The corresponding reducing sugar yields for enzymatic hydrolysis of *Manihot glaziovii* and sweet sorghum starches were 196.15 and 170.26 g/L, respectively. The optimum yeast concentration, reaction temperature, and agitation speed were found to be 1.18 g/L, 36.48°C, and 217 rpm, respectively, and the corresponding *Manihot glaziovii* bioethanol yield was 94.45 g/L. The optimum yeast concentration, reaction temperature, and agitation speed were determined to be 1.29 g/L, 35.36°C, and 188.97 rpm, respectively, and the corresponding sweet sorghum bioethanol yield was 82.13 g/L.

Energy consumption from *Manihot glaziovii* and sweet sorghum from this study is summed to 103.95 kWh. It is obvious in bioethanol production that there have been many significant signs of progresses, including in renewable biomass pretreatment, reducing glucose production and fermentation of glucose (pentose and hexose) as well as bioethanol separation and purification in the recent decades. Therefore, the energy consumption concept is needed to utilize renewable feedstocks more comprehensively and to manufacture more value-added coproducts that would reduce the cost of bioethanol production, hence it can be viable with economically competitive prices.

3. The properties *Manihot glaziovii* and sweet sorghum bioethanols fulfilled the specifications ASTM D4806 standard. The density of *Manihot glaziovii* and sweet sorghum bioethanols were found to be 803.7 and 807.9 kg/m^3, respectively, which were within the range of 785–809.9 kg/m^3. The LHV of the *Manihot glaziovii* and sweet sorghum bioethanols were 27.3 and 26.9 MJ/kg which were close to ASTM D4806 standard (29.7 MJ/kg). Moreover, the density of bioethanol gasoline blends ME20 and SE20 are 764.6 and 765.1 kg/m^3 which are close to gasoline.
4. Based on the results of the engine tests, the ET was found to increase whereas the BSFC decreased with an increase in the engine speed up to 3400 rpm. This can be

attributed to the leaning effect as a result of blending gasoline with bioethanol. The BP and BTE were found to increase with an increase in the engine speed for the bioethanol-gasoline blends. In general, the ME20 and SE20 blends (percentage of bioethanol: 20%) produced the best engine performance (highest ET, BP, and BTE, and lowest BSFC) among all of the fuel blends tested in this study. Thus, these fuel blends appear to be a favorable substitute for gasoline without compromising the engine performance.

The bioethanol-gasoline blends resulted in lower CO and HC emissions compared with gasoline because of the leaning effect of the bioethanol-gasoline blends and the lower molar hydrogen/carbon ratios of the bioethanols. However, the NO_x emissions were higher for the bioethanol-gasoline blends, which is likely because the combustion regime shifts to stoichiometric combustion, which increases the combustion temperature, resulting in higher NO_x emissions. The highest NO_x emissions were produced for the ME20 and SE20 blends at 1600 rpm, with a value of 221.58 and 226.75 ppm, respectively. In contrast, the lowest NO_x emissions were produced for the ME05 and SE05 blends at 3000 rpm, with a value of 37.74 and 38.99 ppm, respectively.

5. The corrosion of copper coupons immersed in the bioethanol-gasoline blends increased with the percentage of bioethanol in the blend and immersion time. After 800 h of immersion, the corrosion rate was found to be 0.00286 and 0.00299 mm/year for the ME20 and SE20 blends, respectively. In contrast, the corrosion rate was lower for gasoline, with a value of 0.000841 mm/year. In addition, the degradation of the fuel properties indicates that the bioethanol-gasoline fuel blends cause more severe corrosion to copper compared with gasoline.

5.2. Recommendations for future work

In general, the objectives of this study are achieved. However, there are avenues for further research. Based on the findings of this study, the following recommendations are made:

- In this study, ANN modeling was selected because it is useful for virtual experimentations and therefore, it is suitable to optimize the parameters of the enzymatic hydrolysis and fermentation processes. In future work, other artificial intelligence techniques can be used to optimize the bioethanol production parameters. The ratio of bioethanol produced from the optimum process has the highest ethanol yield and content, and this is beneficial in the long run as it can compensate for the use of fossil fuels and less greenhouse gas emissions. Therefore, it can be further developed to contribute to energy and environmental goals such as energy return on investment (EROI) in the future. EROI analysis can be carried out using non-edible feedstock since it has a promising prospect as an eco-friendly and sustainable feedstock in bioethanol production.
- In this study, two non-edible feedstocks (*Manihot glaziovii* tubers and sweet sorghum grains) were used to produce bioethanol and their blends. The produced bioethanol was further tested through investigation of engine performance and exhaust emissions of a single-cylinder four-stroke spark ignition engine fueled with these reflected fuels. Future work can be carried out by exploring other non-edible feedstocks for bioethanol production and assess the physicochemical properties, engine performance, and exhaust emissions of the bioethanols and their blends.
- In this study, the bioethanols were blended with gasoline up to a percentage of 20%. In future work, experiments can be carried out to assess the engine performance and exhaust emissions of the spark ignition engine fueled with

Manihot glaziovii and sweet-sorghum bioethanol-gasoline blends with higher percentages of bioethanol. In addition, the optimum blend can be determined based on the following characteristics: minimum exhaust emissions, maximum engine performance, and maximum combustion efficiency.

- Future work can be carried out to investigate the effects of *Manihot glaziovii* bioethanol-gasoline and sweet-sorghum bioethanol-gasoline blends on soot and particular matter emissions and the results can be compared with the recommended values stipulated in bioethanol standards.
- This study can be extended to investigate the combustion characteristics (cylinder pressure and heat release rate as a function of the crank angle) of the single-cylinder four-stroke spark ignition engine fueled with the *Manihot glaziovii* bioethanol-gasoline and sweet-sorghum bioethanol-gasoline blends.
- The corrosion analysis of temperature effect on copper can be performed in the future study. The effect of temperature can be used for the storage stability of the blend fuels. This will provide a more in-depth study on the degradation of the engine components and fuel to investigate the impact and feasibility of using bioethanol-gasoline blend as the substitute fuels for spark ignition engine in the long run.

REFERENCES

(2013). Section 28 - Climate Change, in: Cleveland, C.J., Morris, C. (Eds.), Handbook of Energy. Elsevier, Amsterdam, pp. 903-933.

Abbi, M., Kuhad, R.C., & Singh, A. (1996). Bioconversion of pentose sugars to ethanol by free and immobilized cells of Candida shehatae (NCL-3501): Fermentation behaviour. *Process Biochem 31*, 555-560.

Abdel-Rahman, A., & Osman, M. (1997). Experimental investigation on varying the compression ratio of SI engine working under different ethanol–gasoline fuel blends. *International Journal of Energy Research 21*, 31-40.

Abel, J., & Virtanen, S. (2015). Corrosion of martensitic stainless steel in ethanol-containing gasoline: influence of contamination by chloride, H 2 O and acetic acid. *Corros Sci 98*, 318-326.

Adelekan, B. (2010). Investigation of ethanol productivity of cassava crop as a sustainable source of biofuel in tropical countries. *Afr. J. Biotechnol 9*.

Ademiluyi, F., & Mepba, H. (2013). Yield and properties of ethanol biofuel produced from different whole cassava flours. *ISRN Biotechnol 2013*.

Adewuyi, Y.G., & Deshmane, V.G. (2015). Intensification of enzymatic hydrolysis of cellulose using high-frequency ultrasound: An investigation of the effects of process parameters on glucose yield. *Energ Fuels 29*, 4998-5006.

Aditiya, H., Mahlia, T., Chong, W., Nur, H., & Sebayang, A. (2016). Second generation bioethanol production: A critical review. *Renew Sust Energ Rev 66*, 631-653.

Al-Baghdadi, M.A.R.S. (2008). Measurement and prediction study of the effect of ethanol blending on the performance and pollutants emission of a four-stroke spark ignition engine. *Proceedings of the Institution of Mechanical Engineers, Part D: Journal of Automobile Engineering 222*, 859-873.

Al-Hasan, M. (2003). Effect of ethanol–unleaded gasoline blends on engine performance and exhaust emission. *Energ Convers Manage 44*, 1547-1561.

Almodares, A., & Hadi, M. (2009). Production of bioethanol from sweet sorghum: A review. *African Journal of Agricultural Research 4*, 772-780.

Alonso-Gómez, L.A., Solarte-Toro, J.C., Bello-Pérez, L.A., & Cardona-Alzate, C.A. (2020). Performance evaluation and economic analysis of the bioethanol and flour production using rejected unripe plantain fruits (Musa paradisiaca L.) as raw material. *Food and Bioproducts Processing 121*, 29-42.

Alptekin, E., Canakci, M., Ozsezen, A.N., Turkcan, A., & Sanli, H. (2015). Using waste animal fat based biodiesels–bioethanol–diesel fuel blends in a DI diesel engine. *Fuel 157*, 245-254.

Alvira, P., Tomás-Pejó, E., Ballesteros, M., & Negro, M. (2010). Pretreatment technologies for an efficient bioethanol production process based on enzymatic hydrolysis: a review. *Bioresour Technol 101*, 4851-4861.

Ambrozin, A.R.P., Monteiro, M.R., Santos, A.O., & Kuri, S.E. (2010). Evaluation of galvanic corrosion of a Zn alloy in alcohol fuel. *Fuel Process Technol 91*, 1687-1690.

Anderson, J., DiCicco, D., Ginder, J., Kramer, U., Leone, T., Raney-Pablo, H., & Wallington, T. (2012). High octane number ethanol–gasoline blends: Quantifying the potential benefits in the United States. *Fuel 97*, 585-594.

Anderson, J.E., Kramer, U., Mueller, S.A., & Wallington, T.J. (2010). Octane Numbers of Ethanol− and Methanol−Gasoline Blends Estimated from Molar Concentrations. *Energy & Fuels 24*, 6576-6585.

Andrae, J.C.G. (2008). Development of a detailed kinetic model for gasoline surrogate fuels. *Fuel 87*, 2013-2022.

Anu Nair, P., Sarath, S., Kumar, A.S., George, A.J., & Das, A.G. 2018. Experimental Study on the Effects of Bio Ethanol Petrol Blends in a Spark Ignition Engine: Performance Analysis. Springer International Publishing, Cham, pp. 327-336.

Avilés Martínez, A., Saucedo-Luna, J., Segovia-Hernandez, J.G., Hernandez, S., Gomez-Castro, F.I., & Castro-Montoya, A.J. (2011). Dehydration of bioethanol by hybrid process liquid–liquid extraction/extractive distillation. *Ind Eng Chem Res 51*, 5847-5855.

Ayodele, B.V., & Cheng, C.K. (2015). Modelling and optimization of syngas production from methane dry reforming over ceria-supported cobalt catalyst using artificial neural networks and Box–Behnken design. *Journal of Industrial and Engineering Chemistry 32*, 246-258.

Badger, P. (2002). Ethanol from cellulose: a general review. *Trends in new crops and new uses 1*, 17-21.

Baena, L.M., Gómez, M., & Calderón, J.A. (2012). Aggressiveness of a 20% bioethanol–80% gasoline mixture on autoparts: I behavior of metallic materials and evaluation of their electrochemical properties. *Fuel 95*, 320-328.

Baeyens, J., Kang, Q., Appels, L., Dewil, R., Lv, Y., & Tan, T. (2015). Challenges and opportunities in improving the production of bio-ethanol. *Prog Energ Combust 47*, 60-88.

Bajpai, P. (2018). Chapter 17 - Carbohydrate Chemistry, in: Bajpai, P. (Ed.), Biermann's Handbook of Pulp and Paper (Third Edition). Elsevier, pp. 363-371.

Balat, M. (2011). Production of bioethanol from lignocellulosic materials via the biochemical pathway: a review. *Energ Convers Manage 52*, 858-875.

Balat, M., & Balat, H. (2009). Recent trends in global production and utilization of bio-ethanol fuel. *Appl Energ 86*, 2273-2282.

Balat, M., Balat, H., & Öz, C. (2008). Progress in bioethanol processing. *Prog Energ Combust 34*, 551-573.

Ballesteros, M., Oliva, J., Negro, M., Manzanares, P., & Ballesteros, I. (2004). Ethanol from lignocellulosic materials by a simultaneous saccharification and fermentation process (SFS) with Kluyveromyces marxianus CECT 10875. *Process Biochem 39*, 1843-1848.

Bansal, A., Illukpitiya, P., Tegegne, F., & Singh, S.P. (2016). Energy efficiency of ethanol production from cellulosic feedstock. *Renewable and Sustainable Energy Reviews 58*, 141-146.

Barcelos, C., Maeda, R., Betancur, G., & Pereira Jr, N. (2011). Ethanol production from sorghum grains [Sorghum bicolor (L.) Moench]: evaluation of the enzymatic hydrolysis and the hydrolysate fermentability. *Braz. J. Chem. Eng 28*, 597-604.

Başkan, K.S., Tütem, E., Akyüz, E., Özen, S., & Apak, R. (2016). Spectrophotometric total reducing sugars assay based on cupric reduction. *Talanta 147*, 162-168.

Bates, R.G., Pinching, G.D., & Smith, E.R. (1950). pH standards of high acidity and high alkalinity and the practical scale of pH. *J. Res. Nat. Bur. Stand 45*, 418-429.

Bayraktar, H. (2005). Experimental and theoretical investigation of using gasoline–ethanol blends in spark-ignition engines. *Renewable energy 30*, 1733-1747.

Belboom, S., Bodson, B., & Léonard, A. (2015). Does the production of Belgian bioethanol fit with European requirements on GHG emissions? Case of wheat. *Biomass and bioenergy 74*, 58-65.

Bensah, E.C., & Mensah, M. (2013). Chemical pretreatment methods for the production of cellulosic ethanol: technologies and innovations. *Int J Chemical Eng 2013*.

Berg, H.O. 2013. Comparison of conversion pathways for lignocellulosic biomass to biofuel in mid-Norway. Institutt for energi-og prosessteknikk.

Bergin, M.S., West, J.J., Keating, T.J., & Russell, A.G. (2005). Regional atmospheric pollution and transboundary air quality management. *Annu. Rev. Environ. Resour. 30*, 1-37.

Bessou, C., Ferchaud, F., Gabrielle, B., & Mary, B. (2011). Biofuels, Greenhouse Gases and Climate Change, in: Lichtfouse, E., Hamelin, M., Navarrete, M., Debaeke, P. (Eds.), Sustainable Agriculture Volume 2. Springer Netherlands, Dordrecht, pp. 365-468.

Biezma, M., & San Cristobal, J. (2005). Methodology to study cost of corrosion. *Corros Eng., Sci Technol 40*, 344-352.

Bjerre, A.B., Olesen, A.B., Fernqvist, T., Plöger, A., & Schmidt, A.S. (1996). Pretreatment of wheat straw using combined wet oxidation and alkaline hydrolysis resulting in convertible cellulose and hemicellulose. *Biotechnol Bioeng 49*, 568-577.

BP. (2019). British Petroleum Statistical review of world energy *Retrieved March 2020 from https://www.bp.com/content/dam/bp/business-sites/en/global/corporate/pdfs/energy-economics/statistical-review/bp-stats-review-2019-full-report.pdf*.

Brown, R.J., Keates, A.C., & Brewer, P.J. (2010). Sensitivities of a Standard Test Method for the Determination of the pHe of Bioethanol and Suggestions for Improvement. *Sensors 10*, 9982-9993.

Brownstein, A.M. (2014). Renewable motor fuels: the past, the present and the uncertain future. Butterworth-Heinemann.

Buruiana, C.-T., Garrote, G., & Vizireanu, C. (2013). Bioethanol production from residual lignocellulosic materials: A review-Part 2. *The Annals of the University of Dunarea de Jos of Galati. Fascicle VI. Food Technology 37*, 25.

Can, Ö., Çelikten, İ., & Usta, N. (2004). Effects of ethanol addition on performance and emissions of a turbocharged indirect injection Diesel engine running at different injection pressures. *Energy conversion and management 45*, 2429-2440.

Canakci, M., Ozsezen, A.N., Alptekin, E., & Eyidogan, M. (2013). Impact of alcohol–gasoline fuel blends on the exhaust emission of an SI engine. *Renewable energy 52*, 111-117.

Canilha, L., Chandel, A.K., Suzane dos Santos Milessi, T., Antunes, F.A.F., Luiz da Costa Freitas, W., das Graças Almeida Felipe, M., & da Silva, S.S. (2012). Bioconversion of sugarcane biomass into ethanol: an overview about composition, pretreatment methods, detoxification of hydrolysates, enzymatic saccharification, and ethanol fermentation. *BioMed Res Int 2012*, 15.

Cardona, C.A., & Sánchez, Ó.J. (2007). Fuel ethanol production: process design trends and integration opportunities. *Bioresour Technol 98*, 2415-2457.

Cavazzuti, M. (2012). Optimization methods: from theory to design scientific and technological aspects in mechanics. Springer Science & Business Media.

Celik, M.B. (2008). Experimental determination of suitable ethanol–gasoline blend rate at high compression ratio for gasoline engine. *Applied thermal engineering 28*, 396-404.

Cernat, A., & Elescu, Ş.V. (2013). Bioethanol available alternative fuel for SI engine. *Termotehnica 2*, 110-118.

Cerri, C., Galdos, M., Maia, S., Bernoux, M., Feigl, B., Powlson, D., & Cerri, C. (2011). Effect of sugarcane harvesting systems on soil carbon stocks in Brazil: an examination of existing data. *European Journal of Soil Science 62*, 23-28.

Ceviz, M.A., & Yüksel, F. (2005). Effects of ethanol–unleaded gasoline blends on cyclic variability and emissions in an SI engine. *Applied thermal engineering 25*, 917-925.

Chan, E., Rudravaram, R., Narasu, M.L., Rao, L.V., & Ravindra, P. (2007). Economics and environmental impact of bioethanol production technologies: an appraisal. *Biotechnol Mole Biology Rev 2*, 14-32.

Chang, S.K. (2010). Protein analysis, Food analysis. Springer, pp. 133-146.

Chang, V.S., & Holtzapple, M.T. (2000). Fundamental factors affecting biomass enzymatic reactivity. *Biotechnol Appl Biochem 84*, 5-37.

Chang, V.S., Nagwani, M., Kim, C.-H., & Holtzapple, M.T. (2001). Oxidative lime pretreatment of high-lignin biomass. *Biotechnol Appl Biochem 94*, 1-28.

Chansauria, P., & Mandloi, R.K. (2018). Effects of Ethanol Blends on Performance of Spark Ignition Engine-A Review. *Materials Today: Proceedings 5*, 4066-4077.

Chao, B., Liu, R., Zhang, X., Zhang, X., & Tan, T. (2017). Tannin extraction pretreatment and very high gravity fermentation of acorn starch for bioethanol production. *Bioresource technology 241*, 900-907.

Chen, H.-Z., & Liu, Z.-H. (2017). Enzymatic hydrolysis of lignocellulosic biomass from low to high solids loading. *Engineering in Life Sciences 17*, 489-499.

Chen, H., Liao, H., Tang, B.-J., & Wei, Y.-M. (2016). Impacts of OPEC's political risk on the international crude oil prices: An empirical analysis based on the SVAR models. *Energy Economics 57*, 42-49.

Cheng, M.H., Huang, H., Dien, B.S., & Singh, V. (2019). The costs of sugar production from different feedstocks and processing technologies. *Biofuels, Bioproducts and Biorefining 13*, 723-739.

Chiaramonti, D. (2007). Bioethanol: role and production technologies, Improvement of crop plants for industrial end uses. Springer, pp. 209-251.

Chohnan, S., Nakane, M., Rahman, M.H., Nitta, Y., Yoshiura, T., Ohta, H., & Kurusu, Y. (2011). Fuel ethanol production from sweet sorghum using repeated-batch fermentation. *J Biosci Bioeng 111*, 433-436.

Correa, D.F., Beyer, H.L., Possingham, H.P., Thomas-Hall, S.R., & Schenk, P.M. (2017). Biodiversity impacts of bioenergy production: Microalgae vs. first generation biofuels. *Renewable and Sustainable Energy Reviews 74*, 1131-1146.

Costa, R.C., & Sodré, J.R. (2010). Hydrous ethanol vs. gasoline-ethanol blend: Engine performance and emissions. *Fuel 89*, 287-293.

Costa, R.C., & Sodré, J.R. (2011). Compression ratio effects on an ethanol/gasoline fuelled engine performance. *Appl Thermal Eng 31*, 278-283.

Crutzen, P.J., Mosier, A.R., Smith, K.A., & Winiwarter, W. (2007). N 2 O release from agro-biofuel production negates global warming reduction by replacing fossil fuels.

Dai, D., Hu, Z., Pu, G., Li, H., & Wang, C. (2006). Energy efficiency and potentials of cassava fuel ethanol in Guangxi region of China. *Energy conversion and management 47*, 1686-1699.

Datta, A., Chowdhuri, A.K., & Mandal, B.K. (2012). Experimental Study on the Performances of Spark Ignition Engine with Alcohol-Gasoline Blends as Fuel. *International Journal of Energy Engineering 2*, 22-27.

De Baere, K., Verstraelen, H., Rigo, P., Van Passel, S., Lenaerts, S., & Potters, G. (2013). Reducing the cost of ballast tank corrosion: an economic modeling approach. *Mar Struct 32*, 136-152.

de Carvalho, A.L., Antunes, C.H., & Freire, F. (2016). Economic-energy-environment analysis of prospective sugarcane bioethanol production in Brazil. *Applied energy 181*, 514-526.

De Simio, L., Gambino, M., & Iannaccone, S. (2012). Effect of ethanol content on thermal efficiency of a spark-ignition light-duty engine. *ISRN Renewable Energy 2012*.

Deesuth, O., Laopaiboon, P., Klanrit, P., & Laopaiboon, L. (2015). Improvement of ethanol production from sweet sorghum juice under high gravity and very high gravity conditions: Effects of nutrient supplementation and aeration. *Ind Crops Prod 74*, 95-102.

Demirbas, A. (2008). The importance of bioethanol and biodiesel from biomass. *Energy Sources, Part B 3*, 177-185.

Demirbas, A. (2011). Competitive liquid biofuels from biomass. *Appl Energy 88*, 17-28.

Deng, B., Li, Q., Chen, Y., Li, M., Liu, A., Ran, J., Xu, Y., Liu, X., Fu, J., & Feng, R. (2019). The effect of air/fuel ratio on the CO and NOx emissions for a twin-spark motorcycle gasoline engine under wide range of operating conditions. *Energy 169*, 1202-1213.

Department of Agriculture, F.F. (2010). Cassava, production guideline. *Retrieved January, 2017*, from http://www.nda.agric.za/docs/Brochures/ProdGuideCassava.pdf.

Doğan, B., Erol, D., Yaman, H., & Kodanli, E. (2017). The effect of ethanol-gasoline blends on performance and exhaust emissions of a spark ignition engine through exergy analysis. *Applied thermal engineering 120*, 433-443.

Dominik, R., & Rainer, J. (2007). Biofuel technology handbook. *Renew Energ*, 1-149.

Dyartanti, E.R., Pranolo, S.H., Setiani, B., & Nurhayati, A. (2015). Bioethanol from sorghum grain (Sorghum bicolor) with SSF reaction using biocatalyst co-immobilization method of glucoamylase and yeast. *Energy Procedia 68*, 132-137.

Ebnesajjad, S. (2012). Handbook of biopolymers and biodegradable plastics: properties, processing and applications. William Andrew.

EIA. (2019a). Biofuels explained, Ethanol and the environment. *U.S. Energy Information Administration Retrieved March, 2020*, From https://www.eia.gov/energyexplained/biofuels/ethanol-and-the-environment.php.

EIA. (2019b). International Energy Outlook 2019. *U.S. Energy Information Administration Retrieved March, 2020*, from https://www.eia.gov/outlooks/ieo/pdf/ieo2019.pdf.

El-Faroug, M.O., Yan, F., Luo, M., & Fiifi Turkson, R. (2016). Spark Ignition Engine Combustion, Performance and Emission Products from Hydrous Ethanol and Its Blends with Gasoline. *Energies 9*, 984.

Elfasakhany, A. (2014). The Effects of Ethanol-Gasoline Blends on Performance and Exhaust Emission Characteristics of Spark Ignition Engines *International Journal of Automotive Engineering 4*, 609-620.

Elfasakhany, A. (2015). Investigations on the effects of ethanol–methanol–gasoline blends in a spark-ignition engine: Performance and emissions analysis. *Engineering Science and Technology, an International Journal 18*, 713-719.

Elhassan, M.S., Emmambux, M.N., Hays, D.B., Peterson, G.C., & Taylor, J.R. (2015). Novel biofortified sorghum lines with combined waxy (high amylopectin) starch and high protein digestibility traits: effects on endosperm and flour properties. *J Cereal Sci 65*, 132-139.

Emtiazi, G., Naghavi, N., & Bordbar, A. (2001). Biodegradation of lignocellulosic waste by Aspergillus terreus. *Biodegradation 12*, 257-261.

Eshton, B., & Katima, J.H. (2015). Carbon footprints of production and use of liquid biofuels in Tanzania. *Renewable and Sustainable Energy Reviews 42*, 672-680.

Eufrozina, N. (2009). Biotechnological production of bioethanol from different feedstocks: A review. *DOCT-US 1*, 85.

Eyidogan, M., Ozsezen, A.N., Canakci, M., & Turkcan, A. (2010). Impact of alcohol–gasoline fuel blends on the performance and combustion characteristics of an SI engine. *Fuel 89*, 2713-2720.

Farrell, A.E., Plevin, R.J., Turner, B.T., Jones, A.D., O'hare, M., & Kammen, D.M. (2006). Ethanol can contribute to energy and environmental goals. *Science 311*, 506-508.

Fazal, M., Haseeb, A., & Masjuki, H. (2010). Comparative corrosive characteristics of petroleum diesel and palm biodiesel for automotive materials. *Fuel Process Technol 91*, 1308-1315.

Fedenko, J.R., Erickson, J.E., & Singh, M.P. (2015). Root lodging affects biomass yield and carbohydrate composition in sweet sorghum. *Ind Crops Prod 74*, 933-938.

Ferreira, S.L.C., Bruns, R.E., Ferreira, H.S., Matos, G.D., David, J.M., Brandão, G.C., da Silva, E.G.P., Portugal, L.A., dos Reis, P.S., Souza, A.S., & dos Santos, W.N.L. (2007). Box-Behnken design: An alternative for the optimization of analytical methods. *Analytica Chimica Acta 597*, 179-186.

Foong, T.M. 2013. On the autoignition of ethanol/gasoline blends in spark-ignition engines.

Gabriel, K.J., & El-Halwagi, M.M. (2013). Modeling and optimization of a bioethanol production facility. *Clean Technol Envir Clean 15*, 931-944.

Ganesan, V. (2012). Internal combustion engines. McGraw Hill Education (India) Pvt Ltd.

Ge, J., & Lei, Y. (2017). Policy options for non-grain bioethanol in China: Insights from an economy-energy-environment CGE model. *Energy policy 105*, 502-511.

Ghanim, A. (2013). Bioethanol production from Iraqi date palm resources. *J. Babylon Univ. Eng. Sci 21*, 248-239.

Ghazikhani, M., Hatami, M., Safari, B., & Ganji, D.D. (2013). Experimental investigation of performance improving and emissions reducing in a two stroke SI engine by using ethanol additives. *Propulsion Power Research 2*, 276-283.

Girard, P., & Fallot, A. (2006). Review of existing and emerging technologies for the production of biofuels in developing countries. *Energy Sustain Dev 10*, 92-108.

Gnansounou, E. (2010). Production and use of lignocellulosic bioethanol in Europe: Current situation and perspectives. *Bioresour Technol 101*, 4842-4850.

Gnansounou, E., Vaskan, P., & Pachón, E.R. (2015). Comparative techno-economic assessment and LCA of selected integrated sugarcane-based biorefineries. *Bioresource technology 196*, 364-375.

Goel, A., Wati, L., & Hisar, C. (2013). Ethanol production from lignocellulosic materials. *Int J Innovations in Biosci 3*, 111-114.

González-García, S., Moreira, M.T., & Feijoo, G. (2010). Comparative environmental performance of lignocellulosic ethanol from different feedstocks. *Renew Sust Energ Rev 14*, 2077-2085.

Graf, A., & Koehler, T. (2000). Oregon cellulose-ethanol study. *Oregon Office of Energy. Salem OR USA*.

Grahovac, J., Jokić, A., Dodić, J., Vučurović, D., & Dodić, S. (2016). Modelling and prediction of bioethanol production from intermediates and byproduct of sugar beet processing using neural networks. *Renewable energy 85*, 953-958.

Grennfelt, P., Engleryd, A., Forsius, M., Hov, Ø., Rodhe, H., & Cowling, E. (2020). Acid rain and air pollution: 50 years of progress in environmental science and policy. *Ambio*, 1-16.

Griffiths, P.R., & De Haseth, J.A. (2007). Fourier Transform Infrared Spectrometry. Wiley.

Guido, C., Beatrice, C., & Napolitano, P. (2013). Application of bioethanol/RME/diesel blend in a Euro5 automotive diesel engine: potentiality of closed loop combustion control technology. *Appl Energ 102*, 13-23.

Gupta, A., & Verma, J.P. (2015). Sustainable bio-ethanol production from agro-residues: a review. *Renew Sust Energ Rev 41*, 550-567.

Gusakov, A.V., Salanovich, T.N., Antonov, A.I., Ustinov, B.B., Okunev, O.N., Burlingame, R., Emalfarb, M., Baez, M., & Sinitsyn, A.P. (2007). Design of highly efficient cellulase mixtures for enzymatic hydrolysis of cellulose. *Biotechnol Bioeng 97*, 1028-1038.

Hammond, G.P., & Seth, S.M. (2013). Carbon and environmental footprinting of global biofuel production. *Applied energy 112*, 547-559.

Han, K.J., Pitman, W.D., Kim, M., Day, D.F., Alison, M.W., McCormick, M.E., & Aita, G. (2013a). Ethanol production potential of sweet sorghum assessed using forage fiber analysis procedures. *Gcb Bioenergy 5*, 358-366.

Han, M., Kang, K.E., Kim, Y., & Choi, G.-W. (2013b). High efficiency bioethanol production from barley straw using a continuous pretreatment reactor. *Process Biochem 48*, 488-495.

Hanif, M., Mahlia, T.M.I., Aditiya, H.B., & Abu Bakar, M.S. (2017). Energy and environmental assessments of bioethanol production from Sri Kanji 1 cassava in Malaysia. *Biofuel Research Journal 4*, 537-544.

Hansdah, D., Murugan, S., & Das, L. (2013). Experimental studies on a DI diesel engine fueled with bioethanol-diesel emulsions. *Alexandria Engineering Journal 52*, 267-276.

Harmsen, P., Huijgen, W., Bermudez, L., & Bakker, R. 2010. Literature review of physical and chemical pretreatment processes for lignocellulosic biomass. Wageningen UR Food & Biobased Research.

Haseeb, A., Fazal, M., Jahirul, M., & Masjuki, H. (2011). Compatibility of automotive materials in biodiesel: a review. *Fuel 90*, 922-931.

Hassan, M.H., & Kalam, M.A. (2013). An overview of biofuel as a renewable energy source: development and challenges. *Procedia Eng 56*, 39-53.

Hermann, F., Zeuch, T., & Klingmann, J. 2004. The effect of diluents on the formation rate of nitrogen oxide in a premixed laminar flame, ASME Turbo Expo 2004: Power for Land, Sea, and Air. American Society of Mechanical Engineers Digital Collection, pp. 559-566.

Hill, J., Nelson, E., Tilman, D., Polasky, S., & Tiffany, D. (2006). Environmental, economic, and energetic costs and benefits of biodiesel and ethanol biofuels. *Proceedings of the National Academy of Sciences 103*, 11206-11210.

Hoai Vu, N.S., Hien, P.V., Mathesh, M., Hanh Thu, V.T., & Nam, N.D. (2019). Improved Corrosion Resistance of Steel in Ethanol Fuel Blend by Titania Nanoparticles and Aganonerion polymorphum Leaf Extract. *ACS omega 4*, 146-158.

Houx, J.H., & Fritschi, F.B. (2015). Influence of late planting on light interception, radiation use efficiency and biomass production of four sweet sorghum cultivars. *Ind Crops Prod 76*, 62-68.

Hsieh, W.-D., Chen, R.-H., Wu, T.-L., & Lin, T.-H. (2002). Engine performance and pollutant emission of an SI engine using ethanol–gasoline blended fuels. *Atmospheric Environment 36*, 403-410.

Hu, Z., Duan, D., Hou, S., Ding, X., & Li, S. (2015). Preliminary Study on Corrosion Behaviour of Carbon Steel in Oil–Water Two-Phase Fluids. *J Mater Sci Technol 31*, 1274-1281.

Huang, H.-J., Ramaswamy, S., Tschirner, U., & Ramarao, B. (2008). A review of separation technologies in current and future biorefineries. *Sep Purif Technol 62*, 1-21.

Iiyama, M., Neufeldt, H., Dobie, P., Njenga, M., Ndegwa, G., & Jamnadass, R. (2014). The potential of agroforestry in the provision of sustainable woodfuel in sub-Saharan Africa. *Current Opinion in Environmental Sustainability 6*, 138-147.

Iliev, S. (2018). Comparison of Ethanol and Methanol Blending with Gasoline Using Engine Simulation, Biofuels - Challenges and opportunities. IntechOpen, London.

International Standard Organization, I. (2001). Ethanol for industrial use methods of test part 2 detection of alkalinity or determination of acidity to phenolphthalein. *Retrieved Januari, 2017*, from : https://law.resource.org/pub/eac/ibr/eas.216.212.2001.pdf.

Iodice, P., Senatore, A., Langella, G., & Amoresano, A. (2016). Effect of ethanol–gasoline blends on CO and HC emissions in last generation SI engines within the cold-start transient: An experimental investigation. *Appl Energ 179*, 182-190.

Iodice, P., Senatore, A., Langella, G., & Amoresano, A. (2017). Advantages of ethanol–gasoline blends as fuel substitute for last generation Si engines. *Environmental Progress & Sustainable Energy 36*, 1173-1179.

Iranmahboob, J., Nadim, F., & Monemi, S. (2002). Optimizing acid-hydrolysis: a critical step for production of ethanol from mixed wood chips. *Biomass Bioenerg 22*, 401-404.

IRENA. (2012). The International Renewable Energy Agency. *Retrieved January, 2019 from https://www.irena.org/costs/Transportation/Bioethanol*.

Ismail, H.M., Ng, H.K., Queck, C.W., & Gan, S. (2012). Artificial neural networks modelling of engine-out responses for a light-duty diesel engine fuelled with biodiesel blends. *Applied energy 92*, 769-777.

Jafari, H., Idris, M.H., Ourdjini, A., Rahimi, H., & Ghobadian, B. (2011). EIS study of corrosion behavior of metallic materials in ethanol blended gasoline containing water as a contaminant. *Fuel 90*, 1181-1187.

Jain, A., & Chaurasia, S.P. (2014). Bioethanol production in membrane bioreactor (MBR) system: a review. *Int J Environ Res Dev 4*, 387-394.

Jambo, S.A., Abdulla, R., Azhar, S.H.M., Marbawi, H., Gansau, J.A., & Ravindra, P. (2016). A review on third generation bioethanol feedstock. *Renewable and Sustainable Energy Reviews 65*, 756-769.

Jiang, D., Hao, M., Fu, J., Liu, K., & Yan, X. (2019). Potential bioethanol production from sweet sorghum on marginal land in China. *Journal of Cleaner Production 220*, 225-234.

Joseph, T., Yeoh, H.-H., & Loh, C.-S. (2000). Somatic embryogenesis, plant regeneration and cyanogenesis in Manihot glaziovii Muell. Arg.(ceara rubber). *Plant Cell Rep 19*, 535-538.

Kalghatgi, G., & Stone, R. (2018). Fuel requirements of spark ignition engines. *Proceedings of the Institution of Mechanical Engineers, Part D: Journal of Automobile Engineering 232*, 22-35.

Kang, Q., Appels, L., Tan, T., & Dewil, R. (2014). Bioethanol from lignocellulosic biomass: current findings determine research priorities. *The Scientific World Journal 2014*.

Kannan, T.S., Piraiarasi, C., Ahmed, A.S., & Farid Nasir, A. 2014. Corrosion characteristics of copper in Malaysian bioethanol and gasoline blends, Applied Mechanics and Materials. Trans Tech Publ, pp. 122-126.

Kar, K., Cheng, W., & Ishii, K. (2009). Effects of Ethanol Content on Gasohol PFI Engine Wide-Open-Throttle Operation. *SAE International Journal of Fuels and Lubricants 2*, 895-901.

Karaaslan, S., Erman, C., Hepkaya, E., & Yücel, N. (2011). Numerical investigation of ethanol fuel blends on engine performance characteristics by using diesel-RK software. *International Scientific Journal*, 36-39.

Karagöz, P., Rocha, I.V., Özkan, M., & Angelidaki, I. (2012). Alkaline peroxide pretreatment of rapeseed straw for enhancing bioethanol production by same vessel saccharification and co-fermentation. *Bioresour Technol 104*, 349-357.

Kaul, S., Saxena, R., Kumar, A., Negi, M., Bhatnagar, A., Goyal, H., & Gupta, A. (2007). Corrosion behavior of biodiesel from seed oils of Indian origin on diesel engine parts. *Fuel Process Technol 88*, 303-307.

Kheiralla, A.F., El-Awad, M., Hassan, M.Y., Hussen, M., & Osman, H.I. (2011). Effect of Ethanol-Gasoline Blends on Fuel Properties Characteristics of Spark Ignition Engines. *University Of Khartoum Engineering Journal 1*.

Kiani, M.K.D., Ghobadian, B., Tavakoli, T., Nikbakht, A.M., & Najafi, G. (2010). Application of artificial neural networks for the prediction of performance and exhaust emissions in SI engine using ethanol- gasoline blends. *Energy 35*, 65-69.

Kim, S., & Dale, B. (2006). Ethanol Fuels: E10 or E85 – Life Cycle Perspectives (5 pp). *The International Journal of Life Cycle Assessment 11*, 117-121.

Kim, T.H., Taylor, F., & Hicks, K.B. (2008). Bioethanol production from barley hull using SAA (soaking in aqueous ammonia) pretreatment. *Bioresour Technol 99*, 5694-5702.

Kiss, A.A., David, J., & Suszwalak, P. (2012). Enhanced bioethanol dehydration by extractive and azeotropic distillation in dividing-wall columns. *Sep Purif Technol 86*, 70-78.

Koç, M., Sekmen, Y., Topgül, T., & Yücesu, H.S. (2009). The effects of ethanol–unleaded gasoline blends on engine performance and exhaust emissions in a spark-ignition engine. *Renew Energ 34*, 2101-2106.

Koizumi, T. (2015). Biofuels and food security. *Renewable and Sustainable Energy Reviews 52*, 829-841.

Korzen, L., Pulidindi, I.N., Israel, A., Abelson, A., & Gedanken, A. (2015). Single step production of bioethanol from the seaweed Ulva rigida using sonication. *RSC Adv 5*, 16223-16229.

Kucharczyk, K., & Tuszyński, T. (2018). The effect of temperature on fermentation and beer volatiles at an industrial scale. *Journal of the Institute of Brewing 124*, 230-235.

Kumar, D., & Singh, V. (2016). Dry-grind processing using amylase corn and superior yeast to reduce the exogenous enzyme requirements in bioethanol production. *Biotechnol Biofuels 9*, 228.

Kumar, R., & Wyman, C.E. (2009). Does change in accessibility with conversion depend on both the substrate and pretreatment technology? *Bioresour Technol 100*, 4193-4202.

Kumbhar, V.S., Mali, D.G., Pandhare, P.H., & Mane, R.M. (2012). Effect of lower ethanol gasoline blends on performance and emission characteristics of the single cylinder SI engine. *International Journal of Instrumentation, Control and Automation 1*, 51-54.

Kundu, P., Paul, V., Kumar, V., & Mishra, I.M. (2015). Formulation development, modeling and optimization of emulsification process using evolving RSM coupled hybrid ANN-GA framework. *Chem Eng Res Des 104*, 773-790.

Kura, A. (2014). An overview of bioethanol production from cassava feedstock in Nigeria. *J Biol Sci Bioconserv 6*, 59-72.

Küüt, A., Ritslaid, K., & Olt, J. (2011). Study of potential uses for farmstead ethanol as motor fuel. *Agron Res 9*, 125-134.

Lapuerta, M., Armas, O., & Garcia-Contreras, R. (2007). Stability of diesel–bioethanol blends for use in diesel engines. *Fuel 86*, 1351-1357.

Larsen, U., Johansen, T., & Schramm, J. 2009. Ethanol as a future fuel for road transportation: Main report. DTU Mekanik.

Leng, R., Wang, C., Zhang, C., Dai, D., & Pu, G. (2008). Life cycle inventory and energy analysis of cassava-based Fuel ethanol in China. *Journal of Cleaner Production 16*, 374-384.

Liang, C., Ji, C., Gao, B., Liu, X., & Zhu, Y. (2012). Investigation on the performance of a spark-ignited ethanol engine with DME enrichment. *Energy conversion and management 58*, 19-25.

Limayem, A., & Ricke, S.C. (2012). Lignocellulosic biomass for bioethanol production: current perspectives, potential issues and future prospects. *Prog Energ Combust 38*, 449-467.

Linder, J. 2012. Alcoholate corrosion of aluminium in ethanol blends-the effects of water content, surface treatments, temperature, time and pressure.

Liu, H., Xu, D., Dao, A.Q., Zhang, G., Lv, Y., & Liu, H. (2015). Study of corrosion behavior and mechanism of carbon steel in the presence of Chlorella vulgaris. *Corros Sci 101*, 84-93.

Liu, Z.-H., Qin, L., Zhu, J.-Q., Li, B.-Z., & Yuan, Y.-J. (2014). Simultaneous saccharification and fermentation of steam-exploded corn stover at high glucan loading and high temperature. *Biotechnol Biofuels 7*, 167.

Lou, X., Yang, D., & Singh, P.M. (2009). Effect of ethanol chemistry on stress corrosion cracking of carbon steel in fuel-grade ethanol. *Corrosion 65*, 785-797.

Luo, L. (2010). Biomass refining for sustainable development: analysis and directions. Department of Industrial Ecology, Institute of Environmental Sciences, Faculty of Science, Leiden University.

Machado, K.S., Seleme, R., Maceno, M.M., & Zattar, I.C. (2017). Carbon footprint in the ethanol feedstocks cultivation–Agricultural CO2 emission assessment. *Agricultural systems 157*, 140-145.

Mączyńska, J., Krzywonos, M., Kupczyk, A., Tucki, K., Sikora, M., Pińkowska, H., Bączyk, A., & Wielewska, I. (2019). Production and use of biofuels for transport in Poland and Brazil – The case of bioethanol. *Fuel 241*, 989-996.

Madson, P., & Monceaux, D. (1995). Fuel ethanol production. *The Alcohol Textbook 3*.

Mahalaxmi, S., & Williford, C. (2012). Biochemical conversion of biomass to fuels, Handbook of Climate Change Mitigation. Springer, pp. 965-999.

Mankowski, G., Duthil, J., & Giusti, A. (1997). The pit morphology on copper in chloride-and sulphate-containing solutions. *Corros Sci 39*, 27-42.

Manzetti, S., & Andersen, O. (2015). A review of emission products from bioethanol and its blends with gasoline. Background for new guidelines for emission control. *Fuel 140*, 293-301.

Maran, J.P., & Manikandan, S. (2012). Response surface modeling and optimization of process parameters for aqueous extraction of pigments from prickly pear (Opuntia ficus-indica) fruit. *Dyes and Pigments 95*, 465-472.

Maran, J.P., Manikandan, S., Thirugnanasambandham, K., Vigna Nivetha, C., & Dinesh, R. (2013). Box–Behnken design based statistical modeling for ultrasound-assisted extraction of corn silk polysaccharide. *Carbohydrate Polymers 92*, 604-611.

Martin, C., Klinke, H.B., & Thomsen, A.B. (2007). Wet oxidation as a pretreatment method for enhancing the enzymatic convertibility of sugarcane bagasse. *Enzyme and Microbial Technology 40*, 426-432.

Marx, S., Ndaba, B., Chiyanzu, I., & Schabort, C. (2014). Fuel ethanol production from sweet sorghum bagasse using microwave irradiation. *Biomass Bioenerg 65*, 145-150.

Marzialetti, T., Valenzuela Olarte, M.B., Sievers, C., Hoskins, T.J., Agrawal, P.K., & Jones, C.W. (2008). Dilute acid hydrolysis of Loblolly pine: A comprehensive approach. *Ind Eng Chem Res 47*, 7131-7140.

Maslova, O., Stepanov, N., Senko, O., & Efremenko, E. (2019). Production of various organic acids from different renewable sources by immobilized cells in the regimes of separate hydrolysis and fermentation (SHF) and simultaneous saccharification and fermentation (SFF). *Bioresource technology 272*, 1-9.

Masum, B., Kalam, M., Masjuki, H., Palash, S., & Fattah, I.R. (2014). Performance and emission analysis of a multi cylinder gasoline engine operating at different alcohol–gasoline blends. *RSC Adv 4*, 27898-27904.

Masum, B., Masjuki, H., Kalam, M., Fattah, I.R., Palash, S., & Abedin, M. (2013). Effect of ethanol–gasoline blend on NOx emission in SI engine. *Renew Sust Energ Rev 24*, 209-222.

Masum, B., Masjuki, H., Kalam, M.A., Palash, S., & Habibullah, M. (2015). Effect of alcohol–gasoline blends optimization on fuel properties, performance and emissions of a SI engine. *J Clean Prod 86*, 230-237.

Matějovský, L., Macák, J., Pospíšil, M., Baroš, P., Staš, M., & Krausová, A. (2017). Study of Corrosion of Metallic Materials in Ethanol–Gasoline Blends: Application of Electrochemical Methods. *Energy & Fuels 31*, 10880-10889.

Matsakas, L., & Christakopoulos, P. (2013). Optimization of ethanol production from high dry matter liquefied dry sweet sorghum stalks. *Biomass Bioenerg 51*, 91-98.

Matuszewska, A., Odziemkowska, M., & Czarnocka, J. (2013). Properties of bioethanol diesel oil mixtures. *Mater Process Energ 1*, 352-359.

McAloon, A., Taylor, F., Yee, W., Ibsen, K., & Wooley, R. 2000. Determining the cost of producing ethanol from corn starch and lignocellulosic feedstocks. National Renewable Energy Lab., Golden, CO (US).

McCormick, R.L., & Parish, R. (2001). Advanced petroleum based fuels program and renewable diesel program. *NREL/MP*, 540-32674.

McLaughlin, S.B., & Walsh, M. (1998). Evaluating environmental consequences of producing herbaceous crops for bioenergy. *Biomass and bioenergy 14*, 317-324.

Mehboob, S., Ali, T.M., Alam, F., & Hasnain, A. (2015). Dual modification of native white sorghum (Sorghum bicolor) starch via acid hydrolysis and succinylation. *LWT-Food Sci Technol 64*, 459-467.

Merrill, A., & Watt, B. (1973). Energy Value of Foods—Basis and Derivation. US Dept. of Agrie, Agrie Handb. No. 74, 105 pp. *SI. Rev*.

Miller, G.L. (1959). Use of dinitrosalicylic acid reagent for determination of reducing sugar. *Anal Chem 31*, 426-428.

Mood, S., Golfeshan, A., Tabatabaei, M., Jouzani, G., Najafi, G., Gholam, M., & Ardjmand, M. (2013). Lignocellulosic biomass to bioethanol, a comprehensive review with a focus on pretreatment. *Renewable and Sustainable Energy Reviews 27*, 77-93.

Moradi, G.R., Dehghani, S., Khosravian, F., & Arjmandzadeh, A. (2013). The optimized operational conditions for biodiesel production from soybean oil and application of artificial neural networks for estimation of the biodiesel yield. *Renewable energy 50*, 915-920.

Morikawa, Y., Zhao, X., & Liu, D. (2014). Biological co-production of ethanol and biodiesel from wheat straw: a case of dilute acid pretreatment. *RSC Adv 4*, 37878-37888.

Moshi, A.P., Crespo, C.F., Badshah, M., Hosea, K.M., Mshandete, A.M., & Mattiasson, B. (2014). High bioethanol titre from Manihot glaziovii through fed-batch simultaneous saccharification and fermentation in Automatic Gas Potential Test System. *Bioresour Technol 156*, 348-356.

Mosier, N., Wyman, C., Dale, B., Elander, R., Lee, Y., Holtzapple, M., & Ladisch, M. (2005). Features of promising technologies for pretreatment of lignocellulosic biomass. *Bioresour Technol 96*, 673-686.

Mosier, N.S., Ladisch, C.M., & Ladisch, M.R. (2002). Characterization of acid catalytic domains for cellulose hydrolysis and glucose degradation. *Biotechnol Bioeng 79*, 610-618.

Muktham, R., Bhargava, S.K., Bankupalli, S., & Ball, A.S. (2016). A Review on 1st and 2nd Generation Bioethanol Production-Recent Progress. *Journal of Sustainable Bioenergy Systems 6*, 72-92.

Muñoz, I., Flury, K., Jungbluth, N., Rigarlsford, G., i Canals, L.M., & King, H. (2014). Life cycle assessment of bio-based ethanol produced from different agricultural feedstocks. *The International Journal of Life Cycle Assessment 19*, 109-119.

Nabi, M.N. (2010). Theoretical investigation of engine thermal efficiency, adiabatic flame temperature, NOx emission and combustion-related parameters for different oxygenated fuels. *Applied thermal engineering 30*, 839-844.

Naik, S.N., Goud, V.V., Rout, P.K., & Dalai, A.K. (2010). Production of first and second generation biofuels: a comprehensive review. *Renew Sust Energ Rev 14*, 578-597.

Najafi, G., Ghobadian, B., Tavakoli, T., Buttsworth, D., Yusaf, T., & Faizollahnejad, M. (2009). Performance and exhaust emissions of a gasoline engine with ethanol blended gasoline fuels using artificial neural network. *Appl Energy 86*, 630-639.

Najafi, G., Ghobadian, B., Yusaf, T., Safieddin Ardebili, S.M., & Mamat, R. (2015). Optimization of performance and exhaust emission parameters of a SI (spark ignition) engine with gasoline–ethanol blended fuels using response surface methodology. *Energy 90*, 1815-1829.

Nassar, N.M. (2007). Wild and indigenous cassava, Manihot esculenta Crantz diversity: An untapped genetic resource. *Genet Resour Crop Ev 54*, 1523-1530.

Nguyen, T.L.T., Gheewala, S.H., & Garivait, S. (2007). Full chain energy analysis of fuel ethanol from cassava in Thailand. *Environ Sci Technol 41*, 4135-4142.

Numjuncharoen, T., Papong, S., Malakul, P., & Mungcharoen, T. (2015). Life-Cycle GHG Emissions of Cassava-Based Bioethanol Production. *Energy Procedia 79*, 265-271.

Olofsson, K., Bertilsson, M., & Lidén, G. (2008). A short review on SSF–an interesting process option for ethanol production from lignocellulosic feedstocks. *Biotechnol Biofuels 1*, 7.

Onuki, S. (2006). Bioethanol: Industrial production process and recent studies. *J Chem Technol Biotechnol 5*, 1Ã12.

Osei, G., Arthur, R., Afrane, G., & Agyemang, E.O. (2013). Potential feedstocks for bioethanol production as a substitute for gasoline in Ghana. *Renew Energ 55*, 12-17.

Özsezen, A.N. (2016). Evaluating Environmental Effects of Bioethanol-Gasoline Blends in Use a SI Engine. *Uluslararası Yakıtlar, Yanma Ve Yangın Dergisi*, 36-41.

Ozsezen, A.N., & Canakci, M. (2011). Performance and combustion characteristics of alcohol–gasoline blends at wide-open throttle. *Energy 36*, 2747-2752.

Pan, X., Arato, C., Gilkes, N., Gregg, D., Mabee, W., Pye, K., Xiao, Z., Zhang, X., & Saddler, J. (2005). Biorefining of softwoods using ethanol organosolv pulping: Preliminary evaluation of process streams for manufacture of fuel-grade ethanol and co-products. *Biotechnol Bioeng 90*, 473-481.

Pang, X., Mu, Y., Yuan, J., & He, H. (2008). Carbonyls emission from ethanol-blended gasoline and biodiesel-ethanol-diesel used in engines. *Atmospheric Environment 42*, 1349-1358.

Park, C., Choi, Y., Kim, C., Oh, S., Lim, G., & Moriyoshi, Y. (2010a). Performance and exhaust emission characteristics of a spark ignition engine using ethanol and ethanol-reformed gas. *Fuel 89*, 2118-2125.

Park, G.-Y., Kang, S.-H., & Lee, S.-W. (2016). An experimental study on spray and combustion characteristics based on fuel temperature of direct injection bio-ethanol-gasoline blending fuel. *Journal of Mechanical Science and Technology 30*, 5239-5246.

Park, J.-y., Shiroma, R., Al-Haq, M.I., Zhang, Y., Ike, M., Arai-Sanoh, Y., Ida, A., Kondo, M., & Tokuyasu, K. (2010b). A novel lime pretreatment for subsequent bioethanol production from rice straw–calcium capturing by carbonation (CaCCO) process. *Bioresource Technol 101*, 6805-6811.

Park, S.H., Yoon, S.H., & Lee, C.S. (2014). Bioethanol and gasoline premixing effect on combustion and emission characteristics in biodiesel dual-fuel combustion engine. *Appl Energy 135*, 286-298.

Pelletier, F., Masson, C., & Tahan, A. (2016). Wind turbine power curve modelling using artificial neural network. *Renewable energy 89*, 207-214.

Peng, J., Fan, Z., & Chen, G. 2011. Thermochemical Conversion Technology on Lignocellulosic Biomass to Liquid Fuel: A Critical Review, Power and Energy Engineering Conference (APPEEC), 2011 Asia-Pacific. IEEE, pp. 1-6.

Pérez, J., Munoz-Dorado, J., de la Rubia, T., & Martinez, J. (2002). Biodegradation and biological treatments of cellulose, hemicellulose and lignin: an overview. *Int Microbiol 5*, 53-63.

Phambu, N., Meya, A.S., Djantou, E.B., Phambu, E.N., Kita-Phambu, P., & Anovitz, L.M. (2007). Direct detection of residual cyanide in cassava using spectroscopic techniques. *J Agri Food Chem 55*, 10135-10140.

Pikunas, A., Pukalskas, S., & Grabys, J. (2003). Influence of composition of gasoline - ethanol blends on parameters of internal combustion engines. *Journal of KONES. 2003*, 205-211.

Pimentel, D., & Patzek, T.W. (2005). Ethanol Production Using Corn, Switchgrass, and Wood; Biodiesel Production Using Soybean and Sunflower. *Natural resources research 14*, 65-76.

Prakash, R., Henham, A., & Bhat, I.K. (1998). Net energy and gross pollution from bioethanol production in India. *Fuel 77*, 1629-1633.

Prasad, S., Singh, A., Jain, N., & Joshi, H. (2007). Ethanol production from sweet sorghum syrup for utilization as automotive fuel in India. *Energ Fuels 21*, 2415-2420.

Prices, G.P. (2020). Global Petrol Prices. *Retrieved March 2020 https://www.globalpetrolprices.com/ethanol_prices/*.

Raja, A.S., Arasu, A.V., & Sornakumar, T. (2015). Effect Of Gasoline-Ethanol Blends On Performance And Emission Characteristics Of A Single Cylinder Air Cooled Motor Bike Si Engine. *Journal of Engineering Science and Technology 10*, 3.

Rao, R.S., Jyothi, C.P., Prakasham, R., Sarma, P., & Rao, L.V. (2006). Xylitol production from corn fiber and sugarcane bagasse hydrolysates by Candida tropicalis. *Bioresour Technol 97*, 1974-1978.

Refaat, A. (2012). Biofuels from waste materials. *Compr Renew Energ 5*, 217-262.

Renzi, M., Bietresato, M., & Mazzetto, F. (2016). An experimental evaluation of the performance of a SI internal combustion engine for agricultural purposes fuelled with different bioethanol blends. *Energy 115*, 1069-1080.

Reynolds, R.E. (2002). Fuel specifications and fuel property issues and their potential impact on the use of ethanol as a transportation fuel. *Oak Ridge National Laboratory, Oak Ridge TN USA*.

RFA. (2018). FUEL ETHANOL Industry Guidelines, Specifications And Procedures. *Retrieved March 2020 https://ethanolrfa.org/wp-content/uploads/2018/07/Fuel-Ethanol-Industry-Guidelines-Specifications-2018.pdf*.

RFA. (2020). Renewable Fuels Association *Industry Statistics Retrieved March, 2020*, from https://ethanolrfa.org/statistics/annual-ethanol-production/.

Robak, K., & Balcerek, M. (2018). Review of second generation bioethanol production from residual biomass. *Food technology and biotechnology 56*, 174-187.

Ruan, R., Zhang, Y., Chen, P., Liu, S., Fan, L., Zhou, N., Ding, K., Peng, P., Addy, M., & Cheng, Y. (2019). Biofuels: Introduction, Biofuels: Alternative Feedstocks and Conversion Processes for the Production of Liquid and Gaseous Biofuels. Elsevier, pp. 3-43.

Ruhul, A., Kalam, M., Masjuki, H., Alabdulkarem, A., Atabani, A., Fattah, I.R., & Abedin, M. (2016). Production, characterization, engine performance and emission characteristics of Croton megalocarpus and Ceiba pentandra complementary blends in a single-cylinder diesel engine. *RSC Advances 6*, 24584-24595.

Rupar, K., & Sanati, M. (2005). The release of terpenes during storage of biomass. *Biomass Bioenerg 28*, 29-34.

Sadeghinezhad, E., Kazi, S., Sadeghinejad, F., Badarudin, A., Mehrali, M., Sadri, R., & Safaei, M.R. (2014a). A comprehensive literature review of bio-fuel performance in internal combustion engine and relevant costs involvement. *Renew Sust Energ Rev 30*, 29-44.

Sadeghinezhad, E., Kazi, S.N., Badarudin, A., Togun, H., Zubir, M.N., Oon, C.S., & Gharehkhani, S. (2014b). Sustainability and environmental impact of ethanol as a biofuel. *Rev Chem Eng 30*, 51-72.

Saga, K., Imou, K., Yokoyama, S., & Minowa, T. (2010). Net energy analysis of bioethanol production system from high-yield rice plant in Japan. *Applied energy 87*, 2164-2168.

Saha, B.C., & Cotta, M.A. (2006). Ethanol production from alkaline peroxide pretreated enzymatically saccharified wheat straw. *Biotechnol Prog 22*, 449-453.

Saikrishnan, V., Karthikeyan, A., & Jayaprabakar, J. (2018). Analysis of ethanol blends on spark ignition engines. *International Journal of Ambient Energy 39*, 103-107.

Saini, J.K., Saini, R., & Tewari, L. (2015). Lignocellulosic agriculture wastes as biomass feedstocks for second-generation bioethanol production: concepts and recent developments. *3 Biotech 5*, 337-353.

Saleh, A.M., & Al-Zubaidi, D.S.M. (2018). Engine Performance and Emission Fueled With Blends of Bioethanol-Gasoline *World Wide Journal 4*, 95-101.

Saravanan, A.P., Mathimani, T., Deviram, G., Rajendran, K., & Pugazhendhi, A. (2018). Biofuel policy in India: A review of policy barriers in sustainable marketing of biofuel. *Journal of Cleaner Production 193*, 734-747.

Sarkar, N., Ghosh, S.K., Bannerjee, S., & Aikat, K. (2012). Bioethanol production from agricultural wastes: an overview. *Renew Energ 37*, 19-27.

Sasongko, M.N., & Wijayanti, W. (2017). Effect of ethanol addition on the performance and exhaust emissions of a spark ignition engine. *Journal of Mechanical Engineering and Sciences 11*, 2734-2742.

Schifter, I., Diaz, L., Rodriguez, R., Gómez, J., & Gonzalez, U. (2011). Combustion and emissions behavior for ethanol–gasoline blends in a single cylinder engine. *Fuel 90*, 3586-3592.

Schifter, I., Dıaz, L., Vera, M., Guzmán, E., & López-Salinas, E. (2004). Fuel formulation and vehicle exhaust emissions in Mexico. *Fuel 83*, 2065-2074.

Schmer, M.R., Vogel, K.P., Mitchell, R.B., & Perrin, R.K. (2008). Net energy of cellulosic ethanol from switchgrass. *Proceedings of the National Academy of Sciences 105*, 464-469.

Seggiani, M., Prati, M.V., Costagliola, M.A., Puccini, M., & Vitolo, S. (2012). Bioethanol–gasoline fuel blends: exhaust emissions and morphological characterization of particulate from a moped engine. *Journal of the Air & Waste Management Association 62*, 888-897.

Seshaiah, N. (2010). Efficiency and exhaust gas analysis of variable compression ratio spark ignition engine fuelled with alternative fuel. *International Journal of Energy and Environment 1*, 861-870.

Shapouri, H. (2004). The 2001 net energy balance of corn-ethanol.

Shide, E., Wuyep, P., & Nok, A. (2004). Studies on the degraduation of wood sawdust by Lentinus squarrosulus (Mont.) Singer. *Afr J Biotechnol 3*, 395-398.

Siddegowda, K., & Venkatesh, J. (2013). Performance and emission characteristics of MPFI engine by using gasoline ethanol blends. *Int J Innov Res Sci 2*, 4891-4897.

Sindhu, R., Binod, P., & Pandey, A. (2016). Biological pretreatment of lignocellulosic biomass–An overview. *Bioresource technology 199*, 76-82.

Singh, S., Chakravarty, I., Pandey, K.D., & Kundu, S. (2018). Development of a process model for simultaneous saccharification and fermentation (SSF) of algal starch to third-generation bioethanol. *Biofuels*, 1-9.

Siswantoro, J., Prabuwono, A.S., Abdullah, A., & Idrus, B. (2016). A linear model based on Kalman filter for improving neural network classification performance. *Expert Systems with Applications 49*, 112-122.

Sjöblom, M., Matsakas, L., Christakopoulos, P., & Rova, U. (2015). Production of butyric acid by Clostridium tyrobutyricum (ATCC25755) using sweet sorghum stalks and beet molasses. *Ind Crops Prod 74*, 535-544.

Soccol, C.R., de Souza Vandenberghe, L.P., Medeiros, A.B.P., Karp, S.G., Buckeridge, M., Ramos, L.P., Pitarelo, A.P., Ferreira-Leitão, V., Gottschalk, L.M.F., & Ferrara, M.A. (2010). Bioethanol from lignocelluloses: status and perspectives in Brazil. *Bioresour Technol 101*, 4820-4825.

Soccol, C.R., Faraco, V., Karp, S., Vandenberghe, L., Thomaz-Soccol, V., Woiciechowski, A., & Pandey, A. (2011). Lignocellulosic bioethanol: current status and future perspectives. *Biofuels: alternative feedstocks and conversion processes*, 101-122.

Social, B.N.d.D.E.e., & Estratégicos, C.d.G.e.E. (2008). Sugarcane-based bioethanol: energy for sustainable development. BNDES.

Spitzer, P., Fisicaro, P., Seitz, S., & Champion, R. (2009). pH and electrolytic conductivity as parameters to characterize bioethanol. *Accredit Qual Assur 14*, 671.

Sridhar, N., Price, K., Buckingham, J., & Dante, J. (2006). Stress corrosion cracking of carbon steel in ethanol. *Corrosion 62*, 687-702.

Srinivasan, C.A., & Saravanan, C. (2010). Study of combustion characteristics of an SI engine fuelled with ethanol and oxygenated fuel additives. *J Sustain Energ Environ 1*, 85-91.

Srinivasan, C.A., & Saravanan, C.G. (2013). Emission Reduction on Ethanol–Gasoline Blend Using Fuel Additives for an SI Engine. *Energy Sources, Part A: Recovery, Utilization, and Environmental Effects 35*, 1093-1101.

Stamenković, O.S., Rajković, K., Veličković, A.V., Milić, P.S., & Veljković, V.B. (2013). Optimization of base-catalyzed ethanolysis of sunflower oil by regression and artificial neural network models. *Fuel Process Technol 114*, 101-108.

Statista. (2020a). Statistics. *Retrieved March 2020 https://www.statista.com/statistics/281606/ethanol-production-in-selected-countries/*.

Statista. (2020b). Statistics. *Retrieved March, 2020 from https://www.statista.com/statistics/262858/change-in-opec-crude-oil-prices-since-1960/*.

Stein, R.A., Anderson, J.E., & Wallington, T.J. (2013). An Overview of the Effects of Ethanol-Gasoline Blends on SI Engine Performance, Fuel Efficiency, and Emissions. *SAE International Journal of Engines 6*, 470-487.

Stuart, B. (2015). Infrared Spectroscopy, In Kirk-Othmer Encyclopedia of Chemical Technology, Inc (Ed.). ed. John Wiley & Sons.

Sudiyani, Y., Sembiring, K.C., & Adilina, I.B. (2014). Bioethanol G2: Production process and recent studies, Biomass and bioenergy. Springer, pp. 345-364.

Suiuay, C., Laloon, K., Katekaew, S., Senawong, K., Noisuwan, P., & Sudajan, S. (2020). Effect of gasoline-like fuel obtained from hard-resin of Yang (Dipterocarpus alatus) on single cylinder gasoline engine performance and exhaust emissions. *Renewable energy 153*, 634-645.

Sun, X., Sun, R., Fowler, P., & Baird, M. (2004). Isolation and characterisation of cellulose obtained by a two-stage treatment with organosolv and cyanamide activated hydrogen peroxide from wheat straw. *Carbohyd Polym 55*, 379-391.

Sun, Y. (2002). Enzymatic hydrolysis of rye straw and bermudagrass for ethanol production.

Sun, Y., & Cheng, J. (2002). Hydrolysis of lignocellulosic materials for ethanol production: a review. *Bioresour Technol 83*, 1-11.

Swana, J., Yang, Y., Behnam, M., & Thompson, R. (2011). An analysis of net energy production and feedstock availability for biobutanol and bioethanol. *Bioresource technology 102*, 2112-2117.

Szczepanski, D. 1998. factors influencing NOx emissions at Tarong and Stanwell power stations. Ph. D. thesis, The University of Queensland, Australia.

Tabish, A. (2018). Corrosion Behaviour of Biofuel. *Petroleum and Chemical Industry International 1*, 1-19.

Taherzadeh, M.J., & Karimi, K. (2008). Pretreatment of lignocellulosic wastes to improve ethanol and biogas production: a review. *Int J Molecul Sci 9*, 1621-1651.

Tan, I.S., & Lee, K.T. (2014). Enzymatic hydrolysis and fermentation of seaweed solid wastes for bioethanol production: An optimization study. *Energy 78*, 53-62.

Tang, J., Chen, K., Huang, F., & Li, J. (2013). Characterization of the pretreatment liquor of biomass from the perennial grass, Eulaliopsis binata, for the production of dissolving pulp. *Bioresour Technol 129*, 548-552.

Tanthapanichakoon, W., & Jian, S.W. (2012). Bioethanol Production from Cellulose and Biomass-Derived Syngas. *Eng J 16*.

Tavva, S.S.M.D., Deshpande, A., Durbha, S.R., Palakollu, V.A.R., Goparaju, A.U., Yechuri, V.R., Bandaru, V.R., & Muktinutalapati, V.S.R. (2016). Bioethanol production through separate hydrolysis and fermentation of Parthenium hysterophorus biomass. *Renewable energy 86*, 1317-1323.

Taylor, A.B., Moran, D.P., Bell, A.J., Hodgson, N.G., Myburgh, I.S., & Botha, J.J. 1996. Gasoline/alcohol blends: exhaust emissions, performance and burn-rate in a multi-valve production engine. SAE Technical Paper.

Thakur, A.K., Kaviti, A.K., Mehra, R., & Mer, K. (2017). Performance analysis of ethanol–gasoline blends on a spark ignition engine: a review. *Biofuels 8*, 91-112.

Thangavelu, S.K., Ahmed, A.S., & Ani, F.N. (2016a). Corrosive characteristics of bioethanol and gasoline blends for metals. *International Journal of Energy Research 40*, 1704-1711.

Thangavelu, S.K., Ahmed, A.S., & Ani, F.N. (2016b). Impact of metals on corrosive behavior of biodiesel–diesel–ethanol (BDE) alternative fuel. *Renewable energy 94*, 1-9.

Thompson, W., & Meyer, S. (2013). Second generation biofuels and food crops: co-products or competitors? *Global Food Security 2*, 89-96.

Tibaquirá, J.E., Huertas, J.I., Ospina, S., Quirama, L.F., & Niño, J.E. (2018). The Effect of Using Ethanol-Gasoline Blends on the Mechanical, Energy and Environmental Performance of In-Use Vehicles. *Energies 11*, 221.

TNB. (2020). Tenaga Nasional Berhad - Tariffs. *Retrieved March 2020 https://www.tnb.com.my/commercial-industrial/pricing-tariffs1/*.

Topgül, T., Yücesu, H.S., Çinar, C., & Koca, A. (2006). The effects of ethanol–unleaded gasoline blends and ignition timing on engine performance and exhaust emissions. *Renewable energy 31*, 2534-2542.

Trajer, J., Golisz, E., & Wojdalski, J. (2015). Analysis of Energy-consumption of Bioethanol Production in Agricultural Distilleries in Poland. *Agriculture and Agricultural Science Procedia 7*, 265-271.

Türköz, N., Erkuş, B., İhsan Karamangil, M., Sürmen, A., & Arslanoğlu, N. (2014). Experimental investigation of the effect of E85 on engine performance and emissions under various ignition timings. *Fuel 115*, 826-832.

Turner, D., Xu, H., Cracknell, R.F., Natarajan, V., & Chen, X. (2011). Combustion performance of bio-ethanol at various blend ratios in a gasoline direct injection engine. *Fuel 90*, 1999-2006.

Tutunea, D., Dima, A., & Bica, M. (2014). Experimental investigation on emissions and performance of a spark ignition engine fueled with gasoline ethanol blends. *Carbon 1*, 285-288.

Tutunea, D., & Dumitru, I. (2017). Experimental study on the effect of adding bioethanol in spark ignition engine. *Scientific Bulletin*, 8-20.

Tye, Y.Y., Lee, K.T., Abdullah, W.N.W., & Leh, C.P. (2012). Potential of Ceiba pentandra (L.) Gaertn.(kapok fiber) as a resource for second generation bioethanol: Effect of various simple pretreatment methods on sugar production. *Bioresour Technol 116*, 536-539.

Tye, Y.Y., Lee, K.T., Wan Abdullah, W.N., & Leh, C.P. (2011). Second-generation bioethanol as a sustainable energy source in Malaysia transportation sector: Status, potential and future prospects. *Renewable and Sustainable Energy Reviews 15*, 4521-4536.

USDA. (2017). USDA Report – Corn ethanol significantly reduces greenhouse gas emissions. *Retrieved March 2020 https://growthenergy.org/2017/01/12/usda-report-corn-ethanol-significantly-reduces-greenhouse-gas-emissions/*.

Vohra, M., Manwar, J., Manmode, R., Padgilwar, S., & Patil, S. (2014). Bioethanol production: feedstock and current technologies. *J Env Chem Eng 2*, 573-584.

Wang, C., Zeraati-Rezaei, S., Xiang, L., & Xu, H. (2017). Ethanol blends in spark ignition engines: RON, octane-added value, cooling effect, compression ratio, and potential engine efficiency gain. *Applied energy 191*, 603-619.

Wang, Y., Wang, M., Cai, D., Wang, B., Wang, Z., Qin, P., & Tan, T. (2016). Efficient L-lactic acid production from sweet sorghum bagasse by open simultaneous saccharification and fermentation. *RSC Adv 6*, 35771-35777.

Wingren, A., Galbe, M., & Zacchi, G. (2003). Techno-economic evaluation of producing ethanol from softwood: Comparison of SSF and SHF and identification of bottlenecks. *Biotechnol Prog 19*, 1109-1117.

Woodson, M., & Jablonowski, C. (2008). An economic assessment of traditional and cellulosic ethanol technologies. *Energ Source 3*, 372-383.

Wooley, R., Ruth, M., Sheehan, J., Ibsen, K., Majdeski, H., & Galvez, A. 1999. Lignocellulosic biomass to ethanol process design and economics utilizing co-current dilute acid prehydrolysis and enzymatic hydrolysis current and futuristic scenarios. NATIONAL RENEWABLE ENERGY LAB GOLDEN CO.

Wu, B., Wang, L., Shen, X., Yan, R., & Dong, P. (2016). Comparison of lean burn characteristics of an SI engine fueled with methanol and gasoline under idle condition. *Applied thermal engineering 95*, 264-270.

Wu, C.-W., Chen, R.-H., Pu, J.-Y., & Lin, T.-H. (2004). The influence of air–fuel ratio on engine performance and pollutant emission of an SI engine using ethanol–gasoline-blended fuels. *Atmos Environ 38*, 7093-7100.

Wu, Y., Zhao, F., Liu, S., Wang, L., Qiu, L., Alexandrov, G., & Jothiprakash, V. (2018). Bioenergy production and environmental impacts. *Geoscience Letters 5*, 14.

Wyman, C., & Yang, B. (2009). Cellulosic biomass could help meet California's transportation fuel needs. *Calif Agr 63*, 185-190.

Yao, Y.-C., Tsai, J.-H., & Chiang, H.-L. (2009). Effects of ethanol-blended gasoline on air pollutant emissions from motorcycle. *Sci Total Environ 407*, 5257-5262.

Yücesu, H.S., Sozen, A., Topgül, T., & Arcaklioğlu, E. (2007). Comparative study of mathematical and experimental analysis of spark ignition engine performance used ethanol–gasoline blend fuel. *Applied thermal engineering 27*, 358-368.

Yücesu, H.S., Topgül, T., Cinar, C., & Okur, M. (2006). Effect of ethanol–gasoline blends on engine performance and exhaust emissions in different compression ratios. *Appl Therm Eng 26*, 2272-2278.

Yue, L. (2009). Analysis of acidity in oil based matrices by infrared spectroscopy. *Food Sci Agric Chem*, 1-84.

Yüksel, F., & Yüksel, B. (2004). The use of ethanol–gasoline blend as a fuel in an SI engine. *Renewable energy 29*, 1181-1191.

Yusaf, T., Buttsworth, D., & Najafi, G. 2009. Theoretical and experimental investigation of SI engine performance and exhaust emissions using ethanol-gasoline blended fuels, 2009 3rd International Conference on Energy and Environment (ICEE), pp. 195-201.

Zhai, Y., Yu, D., Tafreshi, R., & Al-Hamidi, Y. (2011). Fast predictive control for air-fuel ratio of SI engines using a nonlinear internal model. *International Journal of Engineering, Science and Technology 3*, 1-17.

Zhang, C., Xie, G., Li, S., Ge, L., & He, T. (2010). The productive potentials of sweet sorghum ethanol in China. *Appl Energ 87*, 2360-2368.

Zhang, Y. (1999). Thermochemical conversion of swine manure to produce fuel and reduce waste. *Urbana 51*, 61801.

Zhao, X.-Q., Zi, L.-H., Bai, F.-W., Lin, H.-L., Hao, X.-M., Yue, G.-J., & Ho, N.W. (2011). Bioethanol from lignocellulosic biomass, Biotechnology in China III: Biofuels and Bioenergy. Springer, pp. 25-51.

Zheng, J.J., Wang, J.H., Wang, B., & Huang, Z.H. (2009a). Effect of the compression ratio on the performance and combustion of a natural-gas direct-injection engine. *Proceedings of the Institution of Mechanical Engineers, Part D: Journal of Automobile Engineering 223*, 85-98.

Zheng, Y., Pan, Z., & Zhang, R. (2009b). Overview of biomass pretreatment for cellulosic ethanol production. *Int J Agr Bio Eng 2*, 51-68.

Zhuang, Y., & Hong, G. (2013). Primary investigation to leveraging effect of using ethanol fuel on reducing gasoline fuel consumption. *Fuel 105*, 425-431.

Ziółkowska, M., & Wardzińska, D. (2015). Chapter 5 - Corrosiveness of fuels during storage processes, Storage Stability of Fuels. In Tech, Croatia, pp. 131-156.

List of Publications and Papers Presented

1. **Sebayang, A. H.**, Hassan, M. H. Ong, H. C., Dharma, S., Bahar, A. H., Silitonga, A. S., & Kusumo, F. (2017). Enzymatic hydrolysis using ultrasound for bioethanol production from durian (*Durio zibethinus*) seeds as potential biofuel. *Chemical Engineering Transactions, 56,* 553–558. https://doi.org/10.3303/CET1756093
2. **Sebayang, A. H.,** Hassan, M. H. Ong, H. C., Dharma, S., Silitonga, A. S., Kusumo, F., Mahlia, T. M. I., & Bahar, A. H. (2017). Optimization of reducing sugar production from *Manihot glaziovii* starch using response surface methodology. *Energies, 10*(1). https://doi.org/10.3390/en10010035
3. **Sebayang A. H.**, Masjuki, H. H., Ong, H. C., Dharma, S., Silitonga A. S., Kusumo, F., & Milano, J. (2017). Prediction of engine performance and emissions with *Manihot Glaziovii* bioethanol−gasoline blended using extreme learning machine. *Fuel*, *210,* 914–921. https://doi.org/10.1016/j.fuel.2017.08.102
4. **Sebayang, A. H.**, Masjuki, H. H., Ong, H. C., Dharma S., Silitonga A. S., Kusumo, F., & Milano, J. (2017). Optimization of bioethanol production from sorghum grains using artificial neural networks integrated with ant colony. *Industrial Crops and Products*, *97*, 146–155. https://doi.org/10.1016/j.indcrop.2016.11.064
5. **Sebayang, A. H.**, Masjuki, H. H., Ong, H. C., Dharma, S., Silitonga, A. S., Mahlia, T., M. I., & Aditiya, H. B. (2016). A perspective on bioethanol production from biomass as alternative fuel for spark ignition engine. *RSC Advances, 6*(18), 14964–14992. https://doi.org/10.1039/C5RA24983J